Universidad de Huelva

Departamento de Ciencias Integradas

Characterisation and valorisation of materials from a copper metallurgical complex

Memoria para optar al grado de doctora
presentada por:

Daniela Carolina Paz Gómez

Fecha de lectura: 17 de febrero de 2022

Bajo la dirección de los doctores:

Juan Pedro Bolívar Raya

Silvia Pérez Moreno

Huelva, 2022

CC BY NC ND

CHARACTERISATION AND VALORISATION OF MATERIALS FROM A COPPER METALLURGICAL COMPLEX

DANIELA CAROLINA PAZ GÓMEZ

University of Huelva

Doctoral Thesis 2021

CHARACTERISATION AND VALORISATION OF MATERIALS FROM A COPPER METALLURGICAL COMPLEX

Conducted by:

DANIELA CAROLINA PAZ GÓMEZ

University of Huelva

Doctoral Thesis 2022

Supervised by:

DR. JUAN PEDRO BOLÍVAR RAYA

DRA. SILVIA PÉREZ MORENO

This Thesis is presented to fulfil the requirements of the Official PhD programme in Industrial and Environmental Science and Technology of the University of Huelva and to obtain the title of DOCTOR.

JUAN PEDRO BOLÍVAR RAYA, Professor of the Department of Integrated Sciences of the University of Huelva, and

SILVIA PÉREZ MORENO, Post-doctoral researcher of the Department of Integrated Sciences of the University of Huelva.

DECLARE: that the Doctoral Thesis titled "**Characterisation and valorisation of materials from a copper metallurgy complex**" has been conducted by Mrs DANIELA CAROLINA PAZ GÓMEZ in the Department of Integrated Sciences of the University of Huelva under their supervision, to obtain the title of Doctor of the University of Huelva

Huelva, December 2021

BOLIVAR RAYA JUAN PEDRO - 30451377K

Firmado digitalmente por BOLIVAR RAYA JUAN PEDRO - 30451377K
Fecha: 2021.12.20 16:24:04 +01'00'

Signed: Dr. Juan Pedro Bolívar Raya

PEREZ MORENO SILVIA MARIA - 44203353K

Firmado digitalmente por PEREZ MORENO SILVIA MARIA - 44203353K
Fecha: 2021.12.20 14:14:42 +01'00'

Signed: Dra. Silvia Pérez Moreno

FUNDING

This research was supported by two Atlantic Copper company projects: “Characterization of wastes from copper smelting and evaluation of potential applications” (Ref.: 3-2017); and “Copper recovery and arsenic removal from electrolytic sludge generated in the electrolytic treatment plant” (Ref.: 36-2016). Furthermore, this study was also supported by other funding sources: the Spanish Ministry of Economy and Competitiveness (MINECO), through the project ‘‘Fluxes of radionuclides emitted by the phosphogypsum piles located at Huelva; assessment of the dispersion, radiological risks and remediation proposals” (Ref.: CTM2015-68628-R); and the of the Regional Government of Andalusia project entitled “Basic processes regulating the fractionations and enrichments of natural radionuclides under acid mine drainage conditions” (Ref.: UHU-1255876).

A mi familia, Dora, José Francisco, Gabriela y Mary

A mi pareja José Ramón

AGRADECIMIENTOS

Estas son las últimas líneas que escribo de mi Tesis a la que me he dedicado en cuerpo y alma durante cuatro años. Ha sido una etapa llena de altibajos con mucho trabajo y en la que he superado y aprendido un sinfín de cosas. Durante esta experiencia son muchas las personas que me han acompañado y han aportado su granito de arena. A ellos, dedico estas últimas líneas agradeciendo todas y cada una sus contribuciones. A sabiendas de que es imposible agradecerles a todos en este breve escrito, me gustaría comenzar por agradecer de forma general a todas aquellas personas que han colaborado de forma directa e indirecta en la elaboración de esta Tesis.

En primer lugar, quiero expresar mi más sincero agradecimiento a mi director de tesis, el Dr. Juan Pedro Bolívar Raya, por confiar en mí, por darme la oportunidad de trabajar con él, y de realizar mi Tesis Doctoral algo que veía como un sueño. Gracias por tú apoyo incondicional, motivación y paciencia. En definitiva, gracias por la ayuda brindada y por el conocimiento aportado durante estos años. Espero y deseo que con la defensa de esta Tesis veas cumplidas tus expectativas.

En segundo lugar, quiero agradecer a mi codirectora de Tesis, la Dra. Silvia Pérez Moreno, por su trabajo, asesoramiento, paciencia y por todo ese tiempo que me ha dedicado. Hemos compartido mucho tiempo juntas, en el laboratorio, en el despacho, en la cafetería… Aunque por norma general siempre hemos tenido la misma visión del trabajo, no siempre hemos estado de acuerdo en los detalles, lo cual ha conducido a no pocos enfrentamientos y choques de ideas que pese a parecer trabas en el camino, han resultado ser la verdadera clave para realizar un trabajo del cual creo que podemos sentirnos orgullosas. Muchas gracias por aportarme otra perspectiva.

A Atlantic Copper y más concretamente a Guillermo Ríos e Irene Ruiz, por su amabilidad y predisposición a colaborar con este trabajo, el cual no hubiera sido posible sin su ayuda. También me gustaría animarlos a continuar con esa política ejemplar de sostenibilidad y respeto al medioambiente. Muchas gracias.

Agradecer a todos miembros del grupo de investigación “FRYMA” de cual formo parte por su ayuda incondicional en especial a:

Antonio Padilla (Padi), una de las piezas fundamentales de este grupo de investigación. Gracias por tu disponibilidad para todo aquello que necesitaba, gracias por poner mi idea de un borboteador en algo físico y sobre todo gracias por tu amabilidad y predisposición. Además, y como dice la canción “Daniela por dentro está llena de puertas unas cerradas, otras abiertas” pues mi puerta siempre estará abierta para todo aquello que necesites.

A mis compañeros y/o amigos de viajes José Luis e Isidoro, aunque habéis acabado antes esta aventura, hemos compartido buenos y malos momentos, y habéis sido mi paño de lágrimas en más ocasiones de las que me hubiera gustado. En fin, muchas gracias por vuestro apoyo incondicional.

A Fernando por la confianza depositada en mí, por los buenos momentos que hemos pasado yendo a muestrear y por esas muestras tan complicadas que siempre me traías.

Angie (hija adoptiva de FRYMA), por sus consejos y sugerencias. A pesar de que ya no estas en el escritorio del lado se te echa mucho de menos.

A mi nuevo compañero, Alejando Barba, no dudo que conseguirás la tesis, pero el mundo es algo más que la Física.

A Manuel Gázquez que desde la distancia y siempre con una sonrisa me ha prestado su ayuda y apoyo en el desarrollo de esta Tesis

Por supuesto, también quiero agradecer a todas las personas que me acogieron como una más de la familia durante mi estancia en Dpto. de Ingeniería de Materiales y Cerámicas de la Universidad de Aveiro, en el especial a el Dr. João Labrincha, gracias por darme la oportunidad de conocer y aprender lo que hacéis en vuestro grupo de investigación. Gracias, por su tiempo, por sus consejos y por su ayuda. Ha sido una experiencia inolvidable. También me gustaría agradecer a Inês Vilarinho y João Carvalheiras por su haberme enseñado lo que hacéis, por vuestra disposición incondicional a ayudarme y por resolver todas mis dudas. Por supuesto agradecer también Rui Novais y Paula Seabra por vuestro recomendaciones y sugerencias. A los técnicos Ana Ribeiro y Artur Sarabando por la ayuda prestada. También a Gonçalo, hemos pasado muy buenos momento haciendo ensayos mecánicos, es broma, gracias por arrimar el hombro conmigo.

También me gustaría agradecer a mis compañeras de piso en Portugal Marta, María, Luciane y Gabriela gracias por hacerme sentir como en casa. Espero volver a veros pronto.

Y por último y no por ello menos importante me gustaría agradecer a mis hermanos (José Francisco, Gabriela y Mary) y a mi madre (Dora). Por confiar en mi cuando ni siquiera yo creía en mí, por no dejar que me rinda y por estar siempre conmigo a pesar de la distancia. Mama te admiro eres mi mayor ejemplo y supongo que también lo eres para mis hermanos, me he convertido en la persona que soy ahora gracias a tu esfuerzo, trabajo y sacrificio. Para mi eres todo un ejemplo a seguir. GRACIAS. Por supuesto a José Ramon (mi feo) mi más sincero agradecimiento por la paciencia que has tenido conmigo en este tiempo, por ser mi apoyo, mi fuerza cuando no la tenía, por confiar en mí, por no dejar que me rinda, en definitiva simplemente GRACIAS. Y no podía olvidarme de darle

la gracias a la familia de mi pareja que siempre me han acogido como una más de la familia brindando su apoyo y preocupándose por mí en todo momento. Finalizo diciendo Gracias Familia.

Daniela Carolina Paz Gómez

RESUMEN

Atlantic Copper es una empresa española cuyo complejo metalúrgico se encuentra en Huelva. Es uno de los mayores fabricantes de cátodos de cobre de Europa y representa el 8.5 % del PIB de la provincia. Utilizando las tecnologías más avanzadas, producen cátodos de alta pureza (> 99.99 %). Esta empresa se enmarca en la estrategia de economía circular llevando a cabo la gestión de subproductos, materiales intermedios y residuos de forma que se reduzca el impacto ambiental de su actividad lo máximo posible, y a su vez se reduzcan los costes asociados.

El objetivo principal de esta tesis doctoral ha sido evaluar y desarrollar posibles líneas de valorización de diferentes residuos y/o materiales generados en la fabricación de cátodos cobre de alta pureza. Los materiales estudiados fueron: torta del lavado de gases (TLG), finos de convertidores (FC), torta del electrolito (TE), y lodos de la planta de tratamiento de efluentes líquidos (LPTEL).

Para ello, en primer lugar, se realizó una caracterización exhaustiva de los materiales con el fin de determinar la composición química, las fases minerales, el tamaño de las partículas, microestructura y la movilidad de los contaminantes. Teniendo en cuenta los resultados obtenidos en la caracterización y la literatura consultada se identificaron y evaluaron las posibles aplicaciones. Posteriormente, se seleccionaron distintas líneas de valorización en función de las características y propiedades de cada material estudiado.

Los estudios realizados a TLG y FC mostraron que ambos residuos estaban compuestos principalmente por Pb (> 20 % p/p) principalmente en forma de anglesita, y la TLG además contenía una alta concentración de Se (> 30 % p/p) en forma metálica. Por lo tanto, estos residuos podrían ser una importante fuente secundaria de Se y Pb. Por ello, se propuso la recuperación de Se por un proceso de tostado y la recuperación de Pb por un proceso hidrometalúrgico. La recuperación de Se-Pb podría suponer beneficios ambientales notables en contraste con su disposición en vertedero, así como también una reducción en sus costes de gestión.

Por otra parte, la TE presentaba una alta concentración de Cu (≈ 50 % p/p) como domeiquita (Cu_3As), cuprita (Cu_2O), Cu metálico y sulfato de cobre hidratado ($CuSO_4 \cdot xH_2O$), y además una alta concentración de As (≈ 10 % p/p), principalmente como Cu_3As. Por lo tanto, dicho material podría ser una importante fuente secundaria de Cu. Sin embargo, el contenido de As debería ser eliminado para evitar problemas durante su reprocesamiento o valorización. Para la recuperación de Cu se optó por la disolución de la TE, la cual se logró usando un medio ácido, H_2SO_4 (1.4 M)/HNO_3 (1.8 M), y una relación sólido-líquido 1:20 g/mL. Posteriormente, se llevaron a cabo dos líneas de investigación: a) Eliminar el As de la disolución de TE mediante una precipitación con hierro y luego recuperar el

Cu de disolución libre de As; y b) Recuperar el cobre de la disolución de TE mediante una cristalización evaporativa y luego precipitar el arsénico.

En la primera línea de investigación, el As se eliminó de la disolución de TE mediante su precipitación como arseniato de hierro (III), obteniéndose una alta eficiencia (> 70 %). Sin embargo, alrededor del 50 % del Cu también co-precipitó junto al As, sugiriendo que el cobre debería recuperarse previamente. En la segunda línea de investigación, más del 90 % del Cu contenido en TE se recuperó como sulfato de cobre pentahidratado, con una alta pureza (≥ 99.5 % p/p), mediante un proceso de cristalización evaporativa. Además, alrededor del 70 % del As se eliminó durante dicho proceso, en forma de As_2O_3 (> 99 % p/p). Por tanto, se consideró que este proceso es una forma eficaz tanto de recuperar Cu como de eliminar el As contenido en la TE.

Por otro lado, el LPTEL presentaba una alta concentración de CaO (≈ 70 % p/p) y en menor proporción contenía SiO_2, Fe_2O_3, MgO, SO_3 (15–1 % p/p) y Al_2O_3 (≈ 0.4 % p/p). Además, presentaba As (≈ 3.4 % p/p) y otros elementos como Ba, Cu, Pb, Sb, Sr y Zn en concentraciones traza (< 1 % p/p). Este material contenía varias fases minerales: calcita ($CaCO_3$), yeso ($CaSO_4 \cdot 2H_2O$), y portlandita ($Ca(OH)_2$) y oxihidróxido de hierro (III) ($Fe_{21}O_{31}(OH)$). Para LPTEL, la línea de valorización y/o inmovilización propuesta fue usarlo como materia prima en la fabricación de geopolímeros.

Los geopolímeros obtenidos tuvieron una excelente resistencia a la compresión (50–20 Mpa), estos valores se consideraron admisibles para aplicaciones de construcción. Sólo la pasta más compacta (CSWs10) lixivió 2 mg/kg de As, valor que se encuentra en el límite establecido para la admisión de materiales en vertederos de residuos no peligrosos.

ABSTRACT

Atlantic Copper is a Spanish company whose metallurgical complex is in Huelva. It is one of the biggest manufacturers of copper cathodes in Europe and accounts for 8.5 % of the province's GDP. Using the most advanced technologies, they produce high-purity copper cathode (> 99.99 %). This company is framed within a circular economy strategy carrying out the management of by-products, intermediate materials, and waste to reduce the environmental impact of its operations as much as possible and, turn in, reduce the associated costs.

The central goal of this doctoral thesis has been to evaluate and develop possible valorisation lines for different wastes and secondary materials generated in the manufacture of high-purity cathodes. The studied materials were sludge scrubber (SS), sludge from converters (SC), electrolyte sludge (ES), and copper wastewater sludge (CWS).

For that purpose, first, an exhaustive characterisation was carried out to determine chemical composition, mineral phases, particle sizes, microstructure, and pollutants' mobility. Considering the characterisation results and the literature consulted, potential applications were identified and evaluated. After, different valorisation lines were selected for each studied material based on its characteristics and properties.

The studies carried out to SS and SC showed that both sludges were mainly composed of Pb (> 20 % w/w) mainly as anglesite, and the SS also contained a high concentration of Se (> 30 % w/w) as metallic selenium. Therefore, these wastes could be an important secondary source of Se and Pb. Thus, Se recovery by roasting process and Pb recovery by hydrometallurgy process were proposed. Se-Pb recovery could have remarkable environmental benefits in contrast to its disposal in landfill, as well as a reduction in its management cost.

On the other hand, ES presented a high Cu concentration (≈ 50 % w/w) as domeykite (Cu_3As), cuprite (Cu_2O), Cu metal and copper sulphate hydrate ($CuSO_4 \cdot xH_2O$) and also a high As concentration (≈ 10 % w/w), mainly as Cu_3As. Therefore, this material could be an important secondary source of Cu. However, As content should be removed for avoiding problems in reprocessing or valorisation. For the Cu recovery, ES dissolution was chosen, which was achieved using an acid medium, H_2SO_4 (1.4 M)/HNO_3 (1.8 M), and a solid-to-liquid ratio of 1:20 g/mL. Subsequently, two lines of research were carried out: a) Arsenic removal from the ES solution by precipitation with iron, and then copper recovery from the arsenic-free solution; b) Copper recovery from the ES solution by an evaporative crystallisation, and then arsenic precipitation.

In the first line of research, As was removed from ES solution by precipitation as iron (III) arsenate, with high efficiency (> 70 %). However, about 50 % of Cu was also co-precipitated with the As, suggesting copper should previously recover. In the second line of research, more than 90 % of the Cu contained in the sludge was recovered as very pure copper sulphate (≥ 99.5 % w/w) by an evaporative crystallization process. Moreover, around 70 % of the As was removed during this process as As_2O_3 (> 99 % w/w). Therefore, this process was considered an effective way to recover Cu and remove the As contained in ES.

On the other hand, CWS presented a high concentration of CaO (≈ 70 % w/w) and, in a minor proportion, contained SiO_2, Fe_2O_3, MgO, SO_3 (15–1 % w/w) and Al_2O_3 (≈ 0.4 % w/w). In addition, CWS presented As (≈ 3.4 % w/w) and other elements such as Ba, Cu, Pb, Sb, Sr, and Zn in traces concentration (< 1 % w/w). This material contained several mineral phases: calcite ($CaCO_3$), gypsum ($CaSO_4 \cdot 2H_2O$), portlandite ($Ca(OH)_2$), and iron oxide hydroxide ($Fe_{21}O_{31}(OH)$). For CWS, the proposed valorisation and/or immobilisation line was to use it as raw material in geopolymer materials.

The geopolymers obtained had an excellent compressive strength (50–20 Mpa), these values were considered admissible for construction applications. Only the highest compact paste (CWSs10) leached 2 mg/kg of As, this value coincides with the threshold limit established for the admission of non-hazardous waste landfills.

TABLE OF CONTEND

CHAPTER 1.
INTRODUCTION

1.1 BACKGROUND

1.1.1 State of art

The copper was one the first metal used by the human and was known at least 10000 years ago. Its early uses were in jewellery, ornaments, utensils, tools, coins, and weapons. Its use increased gradually until the discoveries and inventions relating to electricity and magnetism of the late 18th and early 19th centuries and the products manufactured from copper, helped launch the Industrial Revolution. The mass adoption of electricity increased dramatically its demand in the 20th century. The dramatic copper demand growth continues in the 21st century due mainly to the rapid industrialization of China, consuming more than 50 % of copper demand (Schlesinger et al., 2011; Statista, 2019). Furthermore, copper is estimated to be even more crucial for society in the future, due to the expected increase in copper-intensive low-carbon energy and the electrification of transportation technologies (Auping et al., 2012; Schipper et al., 2018a; Wang et al., 2021).

Copper is unique electricity conducting properties, which makes it difficult to replace. It is excellent thermal conductivity as well as being corrosion resistant and antimicrobial. In addition, it is ductile and malleable therefore it is easily fabricated into wire, pipe, and other forms, and easily joined. These properties give it a wide range of applications in several sectors such as the manufacture of electrical and electronic products, building construction, the manufacture of industrial machinery and equipment, transport, and consumer products (Schlesinger et al., 2011; Seetharaman et al., 2014).

According to the International Copper Study Group (ICSG), world refined copper production reached 24 Mt in 2019 (ICSG: International Copper Study Group, 2020), which accompanies a significant amount of solid wastes in the form of waste rock, dusts, sludges and slags, wastewater, and gaseous emission. Therefore, copper industry represents a risk to environmental and human health (Csavina et al., 2011; Izydorczyk et al., 2021; Rzymski et al., 2017). However, the copper industry has been improving its waste management for recent years, following the regulations in force at each moment.

In recent decades, the copper manufacturing industries have been focusing on the implementation of systems to improve the recycling and valorisation rate of their by-product and wastes as an economic and environmental advantageous alternative to the increase in disposal costs. The implementation of the new waste EU Directive (Directive 2008/98/EC, 2008) is more in line with the growing sensitivity towards the preservation of the environment, and the big problem of waste disposal. This Directive on waste gives measures to protect the environment and human health by preventing or reducing the adverse impacts of the generation and management of waste and by reducing overall impacts of resource use and improving the efficiency of such use.

The current EU strategy, named Circular Economy, has an ambitious goal of "zero waste". Waste management plays a central role, determining how the European Union waste hierarchy is put into practice. This hierarchy establishes a priority order from prevention (reduce), reuse, recycling, recovery (valorisation) and disposal (Deselnicu et al., 2018; EEA: European Environment Agency, 2016; European Commission, 2015). For this, manufacturing industries have introduced effective resource management consisting of recycling, reusing, and valorisation of these ones, reducing the production cost and decreasing risks for the environment and human health (Khan et al., 2021, 2020).

The copper industry is at the forefront of the industries committed to reducing the environmental impact of its operations. The modern European copper industries invest millions of euros each year on improving their processes as well as research and innovation, to reduce the environmental footprint. For this, it is carried out environmental infrastructure projects, sensors, instrumentation and measurement projects, copper metals recycling, cleaning, treatment, and waste management projects. For instance, the modern European copper industries employ the third of energy consumption in environmental protection measures.

Copper is one of the few materials that can be repeatedly recycled without losing its chemical or physical properties. Recycling requires up to 85 % less energy than primary extraction, emitting around 40 Mt fewer CO_2 per year. According to ICSG, about 50 % of the copper demand in Europe comes from recycling (secondary production). However, recycled copper alone cannot meet the needs of society, thus we also depend on copper primary production (European Copper Institute, 2018; ICSG: International Copper Study Group, 2020). Furthermore, copper mining and metallurgy offers many useful by-products and wastes that contain valuable components such as gold, silver, zinc, lead, cobalt, molybdenum, rhenium, tellurium, and other rare earth that are profitable to recover. In other cases, treatment of these is needed to prevent the release of toxic or hazardous chemicals. Consequently, an evaluation of the physicochemical properties of the by-products and wastes is needed to select the most appropriate management (reuse, recycling, or recovery) before their disposal. This evaluation and diagnosis are pivotal to building a circular economy.

1.1.2 Industrial process production of Cu at Huelva

Copper presents naturally in the Earth's crust in a wide variety of minerals. The most commonly occurs as copper-iron-sulphide and copper sulphide minerals, such as chalcopyrite ($CuFeS_2$) and chalcocite (Cu_2S). Also, copper can be found as copper oxidized minerals (carbonates, oxides, hydroxide-silicates, and sulphates) or as "native" copper. The content of these minerals in an ore body is low. Copper ores normally contain from 0.5 % Cu (open pit mines) to 2 % Cu (underground mines). These copper minerals are almost always accompanied by iron sulphide as pyrite (FeS_2) and pyrrhotite (FeS). Furthermore, copper ores contain other sulphide such as molybdenite (MoS_2), sphalerite (ZnS), and galena (PbS) (ICSG: International Copper Study Group, 2020; Schlesinger et al., 2011; Seetharaman et al., 2014).

About 80 % of high-purity copper cathodes are produced from these ores by concentration, smelting and refining (pyrometallurgical process), while another 20 % is obtained by hydrometallurgical processes. Copper ores are initially crushed and ground into small particles (around 50 μm), and then undergo concentration by froth flotation. During the flotation process, reagents are added that make the Cu minerals water repellent while leaving waste minerals wetted. This water repellency causes Cu minerals to float on rising bubbles while other minerals remain un-floating. The floated Cu-mineral particles overflow the flotation cell to become the copper concentrate containing about 30 % Cu. The main components of copper concentrated, apart from copper, are iron and sulphur (Cu-Fe-S) (Schlesinger et al., 2011; Seetharaman et al., 2014). The mineral composition of the concentrates used in Huelva is very varied because they come from mines on several continents. According to a recent study with various copper concentrates(Bacedoni et al., 2020)a, the most copper concentrates presented chalcopyrite ($CuFeS_2$) and pyrite (FeS_2) as the main mineral phases. However, some copper concentrates also contained chalcocite (Cu_2S), covelline (CuS), bornite (Cu_5FeS_4) as main mineral phases. In addition, galena (PbS), sphalerite (ZnS), tennantite ($Cu_{11}FeAs_4S_{13}$), stannite (Cu_2FeSnS_4), tetrahedrite ($Cu_9Fe_3Sb_4S_{13}$) or pyrrhotite (FeS) was identified as the minority mineral phases.

Atlantic Copper is a Spanish company whose metallurgical complex is in Huelva (south-western Spain). It is one of the biggest manufacturers of copper cathodes in Europe, which produces about $2.9 \cdot 10^5$ t/y of ultrapure copper (> 99.99 % Cu). They manage several by-products, intermediate materials, and wastes. The industrial process is shown in Figure 1.1 and is described below.

The industrial process begins with the reception of the copper ore concentrates. Copper concentrates arrive by ship at the outer harbour of Huelva, are unloaded, and are carried to the plant in lorries, where they are stored. The copper concentrate is mixed with a silica flux (SiO_2) and recycled

materials coming from the industrial process, and then are introduced into Flash Smelting Furnace (FSF) at 1250 ºC (Figure 1.1). The objective of the smelting is oxide S and Fe from copper concentrate to produce a Cu-enriched molten sulphide phases "matte", following the Eq. 1.1. The oxidant is generally O_2-enriched air. Simultaneously, the oxidised iron reacts with the silica to form molten slag or fayalite slag (Fe_2SiO_4), according to Eq. 1.2. The incorporation of silica flux promotes the immiscibility of the matte and slag and decreases the amount of Cu in the slag. The amount of SiO_2 depends on the slag having a low solubility for Cu and a sufficient fluidity to facilitate bleeding and separation between matte and slag. SiO_2/Fe mass ratio between 0.7–1.0 is normally used(Atlantic Copper, 2017; Schlesinger et al., 2011). Also, flash smelting produces gases by the oxidation of the sulphur present in the concentrate, SO_2 content ranges between 30–34 % (Pérez et al., 2018b). These gases are at high temperatures (around 1350 ºC) are sent to the Power Plant (Figure 1.1) where the gases are used to produce a high-pressure stream and generate electrical energy. After, the cold gases are sent into the Acid Plant to produce commercial sulphuric acid (about 10^6 t/y of 98.5 %-pure).

$$2CuFeS_{2(s)} + 3.25O_{2(g)} \rightarrow Cu_2S_{(l)} + 0.5FeS_{(l)} + 1.5FeO_{(s)} + 2.5SO_{2(g)} \qquad \textit{Eq. 1.1}$$

$$2FeO_{(s)} + SiO_{2(s)} \rightarrow Fe_2SiO_{4(l)} \qquad \textit{Eq. 1.2}$$

The "matte" contains around 60 % copper, the rest is sulphur, iron, and other metals. The matte (mainly Cu_2S and FeS) and slag are immiscible phases, enabling their separation by decantation. The matte is transferred to the Peirce-Smith converters (PS), where Fe and S are removed to produce blister copper (99 % Cu) by blowing the bath with O_2-enriched air through tuyeres. The converting is carried out in two steps. In the first step (slag blow), the FeS is oxidized to SO_2 and FeO, according to Eq. 1.3. The FeO combines with silica to form slag molten (Eq. 1.2). This step is ended when there is about 1 % Fe in the matte. In the second step (copper blow), the remaining Cu_2S, named white metal, is refined into blister copper, following the Eq. 1.4. The copper blow is finished when oxide copper begins to appear in the copper molten. Both converting reactions are formed SO_2-enriched off-gases (5–10 %), which is combined with FSF gas and sent to the acid plant (Pérez et al., 2018b; Schlesinger et al., 2011; Seetharaman et al., 2014).

$$2FeS_{(l)} + 3O_{2(g)} + SiO_{2(s)} \rightarrow Fe_2SiO_{4(l)} + 2SO_{2(g)} \qquad \textit{Eq. 1.3}$$

$$Cu_2S_{(l)} + O_{2(g)} \rightarrow 2Cu_{(l)} + SO_{2(g)} \qquad \textit{Eq. 1.4}$$

The slag generated in the smelting and conversion process is treated in the Electric Furnace (EF) to recover the remaining copper in the slags (1 and 5 %, respectively), leaving the final copper content

at below 1 % (S.M. Pérez-Moreno et al., 2018; Pérez et al., 2018a). The final slag is cooled and granulated with water to obtain an industrial product called iron silicate (about $6.5 \cdot 10^5$ t/y).

The copper blister contains residual S and O (about 0.02 % and 0.5% O), which are eliminated by oxidation in the Fire-Refining Furnace (FRF). The final product of FRF is a copper molten (0.003 % S and 0.16 % O), which is cast into pieces about a meter square and 320 kg of weight, called "anodes" on casting wheels, producing about $3.3 \cdot 10^5$ t/y of copper anodes with 99.7 % Cu (Atlantic Copper, 2017).

Copper anodes are converted to commercial copper cathodes (> 99.99 % Cu) by electrolysis in the electrorefining plant, Figure 1.1. In the electrolysis process, copper is electrochemically dissolved from the anodes into the "electrolyte", following Eq. 1.5, and then electrodeposited on the stainless-steel cathodes (1 m^2), where the electrons and Cu^{2+} ions recombine to form copper metal (without the anode impurities), according to Eq. 1.6. The copper metal formed is named copper cathode. The electrolysis process carries out at about an overvoltage of 0.3 V and an electrolyte temperature of about 65 ºC, which improve the conductivity and mass transfer. The electrolyte is a solution of copper sulphate and sulphuric acid with around 45 g/L of Cu and 1.8 M g/L of H_2SO_4. Also, some additives, such as chloride (20–50 ppm), organic levelling, and grain-refining agents (1–10 ppm), are added in very low concentrations to improve the morphology and purity of the copper cathode (Atlantic Copper, 2017; Schlesinger et al., 2011).

$$Cu^0_{anode} \rightarrow Cu^{2+} + 2e^- \qquad E° = -0.34\,V \qquad \textit{Eq. 1.5}$$

$$Cu^{2+} + 2e^- \rightarrow Cu^0_{cathode} \qquad E° = +0.34\,V \qquad \textit{Eq. 1.6}$$

In the electrochemical process, the impurities from anodes such as Ag, Au, Se and Te, being more noble than copper (higher redox potential than copper), remain undissolved in the electrolyte and are deposited on the bottom of the cells, forming the "anode slime". The anode slime is a marketable product (10^3 t/y), and the impurities less noble than copper, such as, Bi, Fe, Ni and Sb, remain dissolved in the electrolyte. The concentration of these impurities gradually increases in the electrolyte negatively affecting the copper cathodic quality. To control the impurities levels is carried an electrolyte purge and new clean electrolyte is added. The purge is sent to the Electrolyte Treatment Plant (ETP), where copper is recovered by electrowinning. The final solution contains 1–2 g/L Cu and a part is returned to the refining process, and another part is sent to the Nickel Plant (Figure 1.1)where this element is recovered as marketable nickel carbonate ($1.4 \cdot 10^3$ t/y). The resulting effluent is sent to the Gypsum Plant (GP) where it is mixed with a weak acid from the acid plant for manufacturing marketable artificial gypsum.

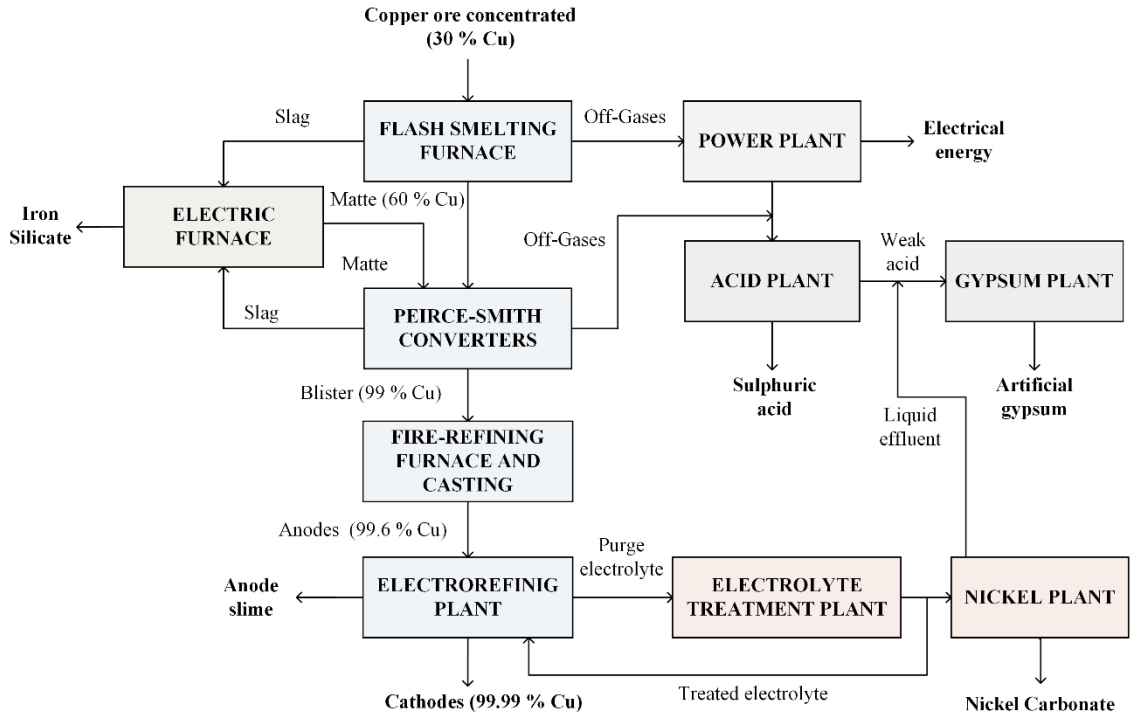

Figure 1.1. *Overview of main materials flows and processes from the copper metallurgical complex.*

1.1.2.1 Off-gases treatment from smelting and converting processes

Off-gases from FSF mainly contain SO_2 (30–35 %) and other impurities such as As, Bi, Cd, Cu, Pb, Sb, Se, Te and Zn, which can be as dust and/or gas (vapor). Off-gases are cooled from 1350 ºC to 400 ºC in a heat recovery boiler where high-pressure steam is produced to generate electricity (around 20–25 % of the total power consumed by the complex), reducing electricity consumption from off-site power plants. Afterwards, the outgoing gases are dedusted in the hot electrostatic filters. The dusts are collected and are recycled to Flash Smelting Furnace FSF (Figure 1.1). On the other hand, the dedusted gases from the smelting and converting process are mixed and pumped to the scrubbing section, where the finest particles are removed, and the gas temperature is reduced. The gases around 350 ºC are passed through Radical Flow Scrubber (RFS) where adiabatic cooling and particles removal are done by using water/weak acid in a closed circuit. After, the gases are cooled in the cooling tower, are passed through wet electrofilters, and transferred to the acid plant. Finally, the precipitated solids, named **sludge scrubber (SS),** are collected in a decanter (Figure 1.2). About 40 t/y of this hazardous residue (EWC 100607) are produced, stored, and transported to a controlled landfill 70 km from Huelva city (Atlantic Copper, 2017). A fraction of weak acid produced, is bled off to the gypsum plant to produce the artificial gypsum (about $3.5 \cdot 10^4$ t/y), see Figure 1.1.

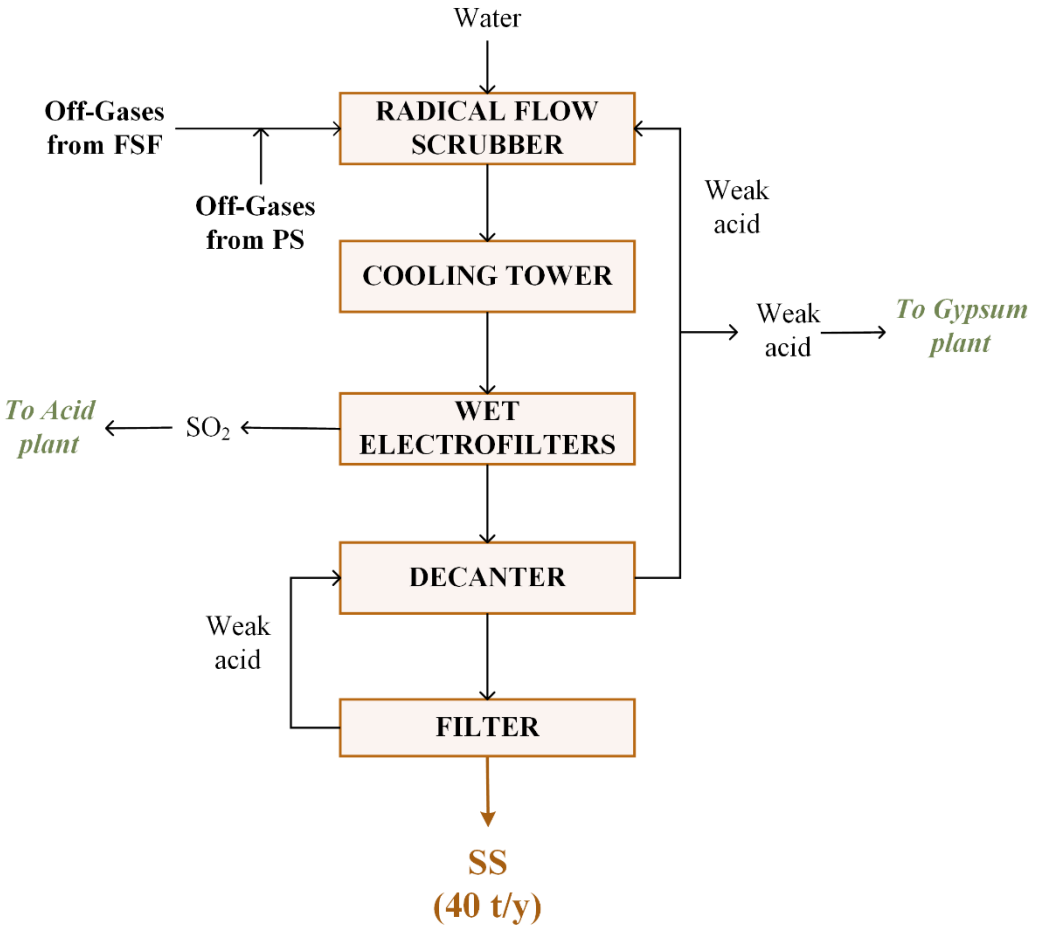

Figure 1.2. *Flowchart of the scrubbing section.*

Off-gases from the Peirce-Smith converters (PS)contain between a 5–10 % SO_2 and other impurities such as As, Bi, Cu, Pb, Sb, Se and Zn, which are dusted off in the hot electrostatic filters, mixed with off-gases from FSF, and are sent to the scrubbing section (Figure 1.2). The converter dust (oxysulphates) is collected in these filters and stored. About 70 % of these dusts are returned to FSF, while rest 30 % (around 1100 t/y) are sent to the repulp tank where are combined with water to form a slurry (Figure 1.3). This slurry is pumped to hydro-cyclone, where the coarse particles are separated from fines particles (< 15 µm). Previous studies found that valuable metals (Cu and Au) are contained in the coarse particles. These are collected to the cyclone underflow, pumped to the pressure filters, and then recycled to the FSF. Whereas the impurities such as arsenic, bismuth, antimony, lead, and zinc presented in the fine particles are reported the cyclone overflow, gone to thickener, and then pumped to pressure filters (Figure 1.3). The sludge is composed of fine dust of converters**, named sludge from converters (SC)**. About 430 t/y of SC are produced and managed as hazardous residue (EWC 100606), disposing of by controlled landfills (Atlantic Copper, 2017).

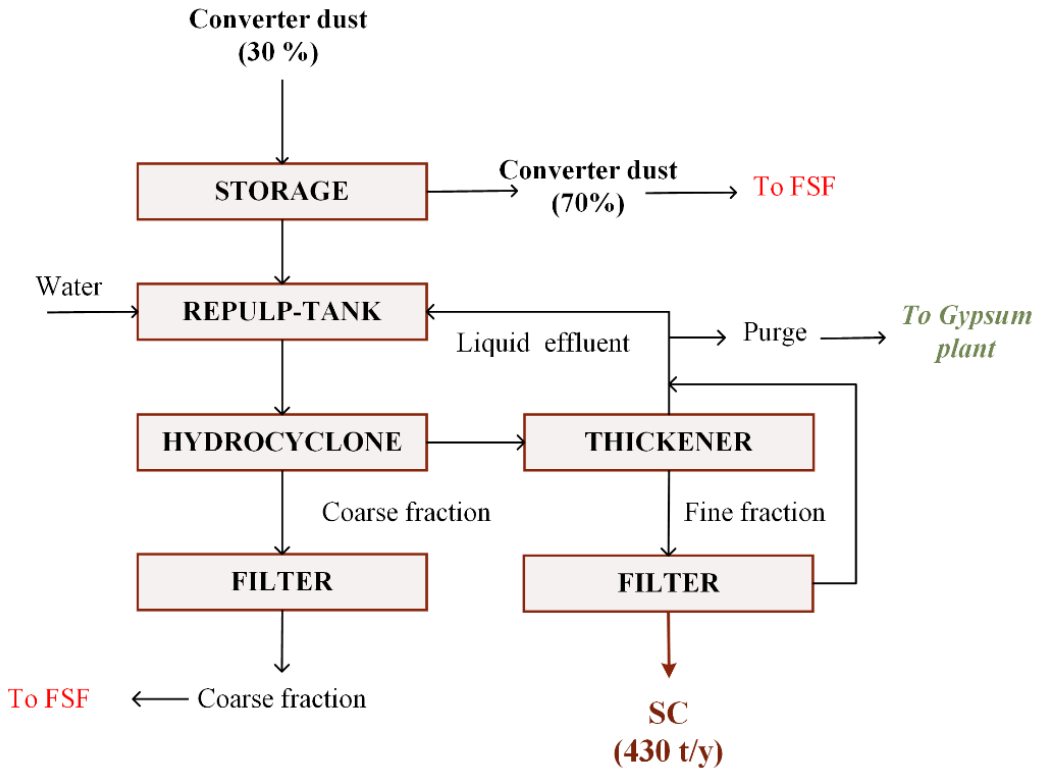

Figure 1.3. *Flowchart of the converter dust treatment plant*

Figure 1.4 shows the FSF and PS off-gases treatment overview and where the studied sludges are generated. Today both sludges (SS and SC) are disposed of in a controlled landfill for hazardous wastes, where they are treated for their stabilization, in order to reduce the mobility of pollutants contained in them and do not exceed the thresholds established in the Royal Decree (RD)1481/2001 regulation based on the Directive 1999/31/EC on landfills (Directive 1999/31/EC, 1999; RD 1481/2001, 2013). The management of both wastes implies high transport and storage costs, and a potential environmental impact. For these reasons, this practice must be substituted by the valorisation of these wastes.

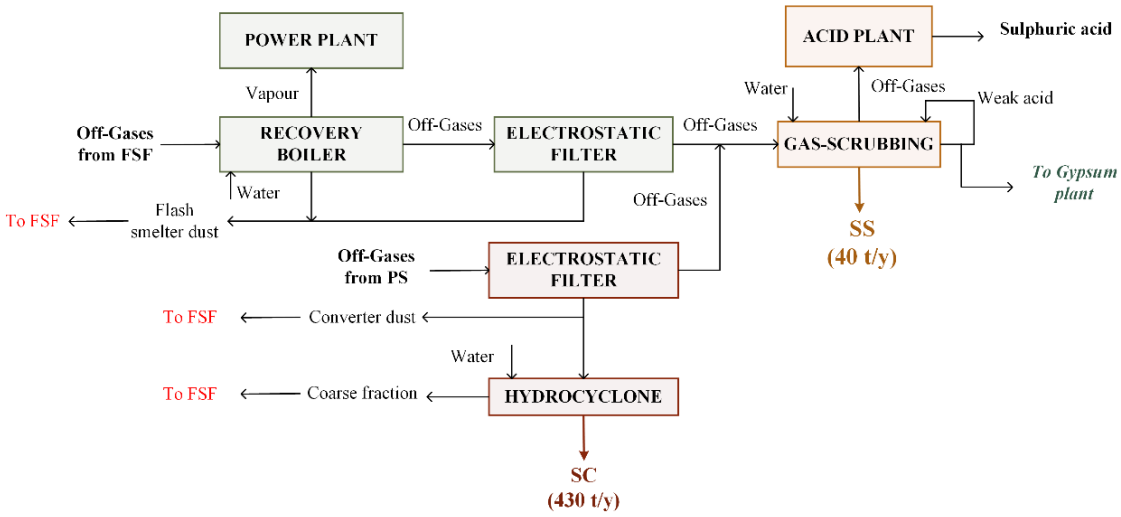

Figure 1.4. *Flowchart of the off-gases treatment from smelting and converting processes*

1.1.2.2 Electrolyte Treatment Plant (ETP)

During the copper electro-refining process, elements with a lower redox potential than copper (less noble) such as As, Bi, Ni, Sb, etc., remain in solution, while Cu self-deposits on the cathode. The concentration of these impurities gradually increases in the electrolyte, producing undesirable phenomena that negatively affect the quality of the copper cathode. Therefore, to control the concentration of impurities a volume of electrolyte must be bled to ETP (Artzer et al., 2018; Wesstrom and Araujo, 2012).

Electrolyte treatment involves three stages of "decopperrizing" which is done in a set of electrowinning cells named "liberator cells", where the copper concentration in the electrolyte is decreased. In the first stage, the copper from the electrolyte is electrodeposited onto the stainless-steel cathodes by applying a current of 2 V using lead (Sn + Ca) anodes. B-grade copper cathode (> 99.7 % Cu, 10^3 t/y) is produced, which is employed to make wire rods, tubes, foils, copper-based alloyed products, and chemicals (Atlantic Copper, 2017), and consequently, the copper content is reduced from about 45 g/L to 25 g/L.

In the second stage, the anode scrap from the electro-refining process is used as cathodes, where the copper present in the electrolyte solution is deposited. Cu concentration at the outlet decreases up to about 10 g/L. Cu-enrich scrap is remelted in the PS converters.

In the third, the arsenic is removed from the solution by electrowinning onto the lead (Sn + Ca) cathode, forming a black sludge known as liberator cell sludge or **electrolyte sludge (ES)**. The treated electrolyte contained 1–2 g/L Cu, which prevents the formation of arsine gas. If the copper

concentration in the discharge is less than 500 ppm, arsine is produced due to the overvoltage necessary to form arsine gas (Artzer et al., 2018; Wesstrom and Araujo, 2012). A fraction of the treated electrolyte is bled off to the nickel plant and the rest sent back to the electrolyte tank house for reuse (Figure 1.5).

Today, around $1.3 \cdot 10^3$ t/y of ES are produced and transferred to a Nutch filter to remove the electrolyte before returning to FSF. ES is recycled to recover its copper content (around 60 % Cu), but its recirculation implies serious problems of arsenic accumulation in the industrial process. Therefore, it is necessary to study others copper recovery alternatives (arsenic-free) from ES.

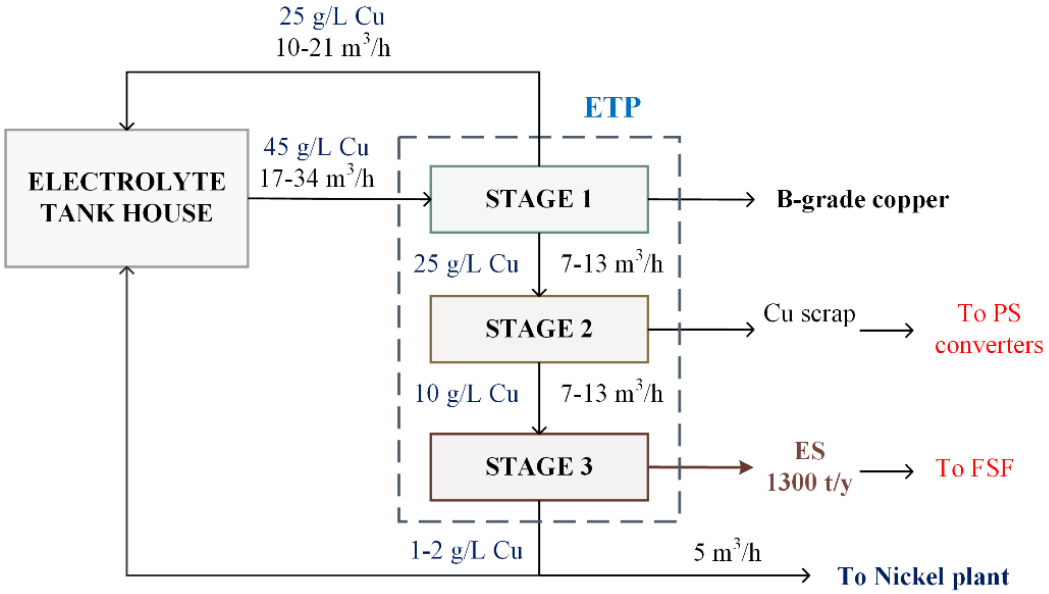

Figure 1.5. *Flowchart of electrolyte treatment plant (ETP)*

1.1.2.3 Liquid Effluent Treatment Plant (LETP)

The liquid effluent treatment plant (LETP) treats several streams produced during the copper manufacturing process. The main streams are a slag granulation purge, a gas scrubbing purge, final effluent from gypsum plant, and other effluents from the laboratory, boilers, cleaning, rainwater, etc. In this plant, physicochemical methods are applied to remove metals. The liquid effluent treatment is carried in four steps: homogenization, pre-treatment, polishing and ultrafiltration.

Homogenization is done to control the composition and flow that feeds the system. For this, the effluents are received and homogenized in two tanks, one for acid/neutral effluents (1400 m^3) and a much smaller one for alkaline effluents (500 m^3). In the pre-treatment, both effluents are mixed in a first lamellar decanter where the iron coagulants ($FeCl_3$ and/or $FeSO_4 \cdot 7H_2O$), a flocculant and an oxidizing agent (H_2O_2) are also added. Moreover, the pH is adjusted until 10.5–11.5 using a lime

slurry. Two outlet streams are obtained, one solid stream is sent to thickener and the liquid stream is passed through a sand filter, and then sent to the polishing. In this step, the arsenic is reduced using the polishing treatment which consist of adding CO_2 to adjust the pH between 8–9. After, the liquid stream is transferred to a second lamellar decanter where iron coagulant, a flocculant, and other reactants are added. Two outlet streams are formed, and solid stream is sent to thickener and liquid stream is sent to an ultrafiltration (UF) system where fine particles that remain in the liquid effluent are eliminated by the UF membrane. A fraction of the final effluent is recycled for reuse (cleaning of sand filters and UF membrane, CO_2 dilution, process water, etc.) and the rest is discharged to the Huelva estuary. UF system also produce a solid stream composed of fine particles, which is sent to the thickener.

During the pre-treatment and the polishing step are produced solid due to metals precipitation. Both solids are collected in the underflow of the decanters, mixed in the thickener together the fine particles collected in the UF system, and then sent to pressure filters. The resulting solid is named **copper wastewater sludge (CWS).** About $2 \cdot 10^3$ t/y of CWS (EWC 190813) are produced, stored, and carried to a controlled landfill 70 km from Huelva city. This management involves high transport and storage costs, and a potential environmental impact. For these reasons, this practice must substitute by a valorisation of CWS.

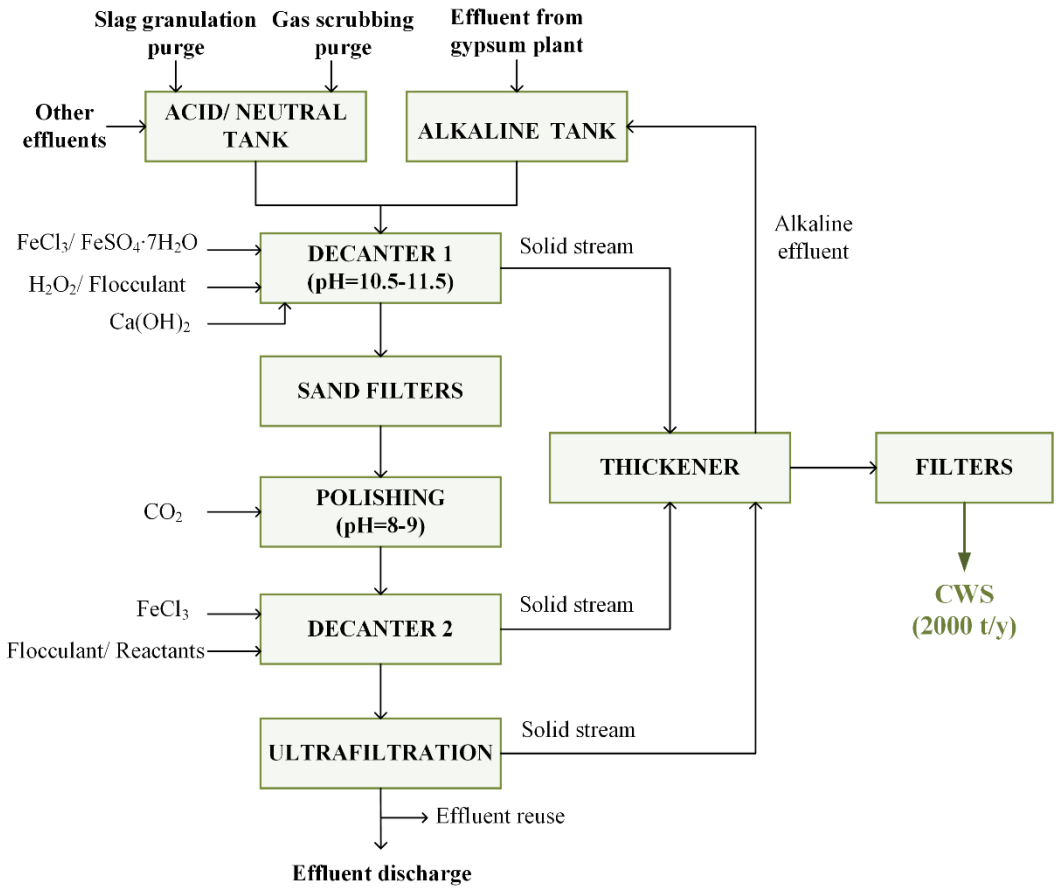

Figure 1.6. *Flowchart of liquid effluent treatment plant (LETP)*

1.2 OBJECTIVES

Considering the problems exposed in the previous section, the main objective of this thesis has been to evaluate and develop possible valorisation lines for different wastes and/or secondary materials generated in the manufacture of high-purity copper cathodes.

To achieve the main objective, the following specific objectives were established:

1. To carry out a physical, chemical, mineralogical and microstructure characterization of the waste and/or secondary materials as well as evaluate the mobility of pollutants.

2. To identify and evaluate the potential applications as well as the potential pollutants. Considering the characterization results and conducted a literature search.

3. To establish a valuation line for waste and/or secondary materials under study, considering current regulations and available technology.

4. To develop at least one of the proposed valorisation procedures of the wastes and/or materials under study.

5. To determine the physicochemical properties and the environmental impact of new materials. In addition, perform the required tests for future application, following the regulation in force.

1.3 OUTLINE

This document is organized into four chapters. The first chapter presents the study developed in this doctoral thesis, providing some useful background for the reader. A description of the state of the art on the topic of the copper industry has been included, as well as a description of the waste generation processes and/or secondary materials. In addition, the main objectives, and a short description of the structure of the thesis are presented.

The second chapter details the materials and methods applied in this research work. First, the wastes and secondary materials sampling are described as well as the pre-treatments that have been subjected. Then, the proposed experimental procedures are developed. Finally, the characterization techniques and technological test used for determination of physicochemical properties of waste, secondary materials and new materials have been summarised.

The third chapter presents the results and discussions of the data collection, divided into four subchapters. Each one of these subchapters corresponds to a complete copy of the published scientific paper, in accordance with the Regulation of PhD studies from the University of Huelva, article 35, 2nd section, chapter IV. The four subchapters are:

- **Subchapter 3.1.** Characterization of two sludges from a pyrometallurgical copper smelting complex for designing a Se and Pb recovery proposal. This section shows an exhaustive characterization of two sludges generated in the off-gas cleaning system smelting and converting processes from copper metallurgy. In addition, a diagnosis to select the most appropriate treatment for their valorisation is presented, and a proposal for the recovery of Se and Pb is shown. This manuscript was published in Waste and Biomass Valorization (Paz-Gómez et al., 2020).
- **Subchapter 3.2.** Arsenic removal procedure for the electrolyte from a hydro-pyrometallurgical complex. The section reports a procedure for arsenic removal from electrolyte sludge from the electrolyte treatment plant. Firstly, dissolution tests are shows, and then arsenic removal tests by precipitation with Fe are presented, as well as a physicochemical characterization of the formed solids in these studies. This work was published in Chemosphere (Paz-Gómez et al., 2021a).
- **Subchapter 3.3.** Copper recovery from sludges generated in the electrolyte treatment plant of a pyrometallurgical complex. This section focuses on a procedure for the copper recovery (arsenic-free) from electrolytic sludge from the electrolyte treatment plant for its return to the industrial process and/or commercialization. In this work, copper recovery experiments as copper (II) sulphate pentahydrate ($CuSO_4 \cdot 5H_2O$) using evaporative crystallization are

presented. In addition, the physicochemical characterization of the solids obtained is shown, as well as the precipitation efficiency and the possible practical implications of the proposed procedure. This manuscript was published in Hydrometallurgy (Paz-Gómez et al., 2021b).

- **Subchapter 3.4**. Immobilization of hazardous wastes in geopolymer materials. This section reports the immobilisation of the copper wastewater sludge, including the possibility of its valorisation as potential building materials. This work is evaluated, the incorporation of a certain amount of the sludge into the geopolymer materials using the one-part method, making a comparison with a material of references and other residue (phosphogypsum). For this, physicochemical characterization and technological tests of new materials are carried. This work has been sent for publication in Sustainability (under review).

Finally, the fourth chapter develops the main conclusions of this thesis, as well as the future lines of research. Additionally, a complete list of all references used in the study are included at the end of this chapter.

CHAPTER 2.

MATERIALS AND METHODS

2.1 SAMPLINGS AND PRE-TREATMENTS

This section describes the samplings and pre-treatments carried out for each of the wastes and/or secondary materials studied.

2.1.1 Samplings

The samplings were done in different periods over the last five years, which were carried out by the Atlantic Cooper's personnel. About 4–5 kg for each sample were collected in each sampling.

- For the sludge scrubber (SS) and sludge of converters (SC), four sampling campaigns were performed for one month, i.e., one for each week of March 2015. Four sample of each sludge were collected to analyse their homogeneity.
- For electrolytic sludge (ES), several sampling campaigns were carried out over three months in spring 2017. A sample was collected every eight days to verify the homogeneity of the ES. Ten samples were collected.
- For copper wastewater sludge (CWS), two sampling campaigns were carried out for one week in May 2019, in which two composed samples were collected.

2.1.2 Pre-treatments

The samples were stored in airtight containers after collection. In the laboratory, the samples were dried at 60 ºC to constant weight and homogenized by manual agitation for carefully to break the clods of the samples. For some analysis (DRX, ICP-MS, etc.), the samples were milled on a mill ring (Retsch, RS 100) and sieved at 63 μm mesh.

The experiments to which the samples have been subjected are shown in the next sections, as well as the different characterization techniques and technological tests used.

2.2 EXPERIMENTS

This section summarizes the experiments performed, which will be explained in more detail in Chapter 3.

2.2.1 Dissolution of the electrolyte sludge (ES)

The dissolution of the electrolyte sludge (ES) was carried out in acid medium by using sulphuric acid solution (H_2SO_4). The influence of temperature, solid-to-liquid ratio, and the type of oxidising agent (air, oxygen, and nitric acid) were studied. Firstly, ES dissolution was done by applying different sulphuric (H_2SO_4) and nitric acids (HNO_3 as oxidising agent) solutions, where different conditions were simulated: 1) two solid-to-liquid ratios, of 1:10 to 1:20 g/mL were employed; 2) sulfuric acid and nitric acid concentrations used ranged from 0.9 to 2.7 M and between 1.0 and 1.8 M, respectively; 3) the temperature and reaction time were: 24 h / 20 ºC, and 2.5 h / 50 ºC. During the experiments, the solution was stirred. Secondly, ES dissolution was performed applying a constant airflow (2 L/min) as oxidising agent and several concentrations of H_2SO_4 solution (2, 4, 6 and 10 M). Finally, ES dissolution was done using O_2 (purity > 99.5 %) as oxidising agent, this experiment was carried out under optimal concentrations of H_2SO_4 solution (2 M) and a O_2 constant flow of 8 L/min at a pressure of 1 atm. In the experiments with air or oxygen the solution was stirred at 500 rpm and heated at 80 ºC for 2.5 h. Finally, the blue solution formed by complete dissolution of the ES was named electrolyte sludge solution (ES solution).

The equipment used for these experiments is shown in Figure 2.1. A reaction vessel (1 L beaker) without a lid, a magnetic stirrer with a heating plate, and a thermocouple were used for the HNO_3 experiments (Figure 2.1a). A beaker (1 L) equipped with a bubbler system consists of a lid with holes through which 16 equidistant glass tubes are inserted for a homogeneous distribution of the air/O_2, was used for the air or O_2 experiments. Additionally, a flowmeter, a thermal jacket and air pump were also used. The O_2 is injected from oxygen bottles (Figure 2.1b).

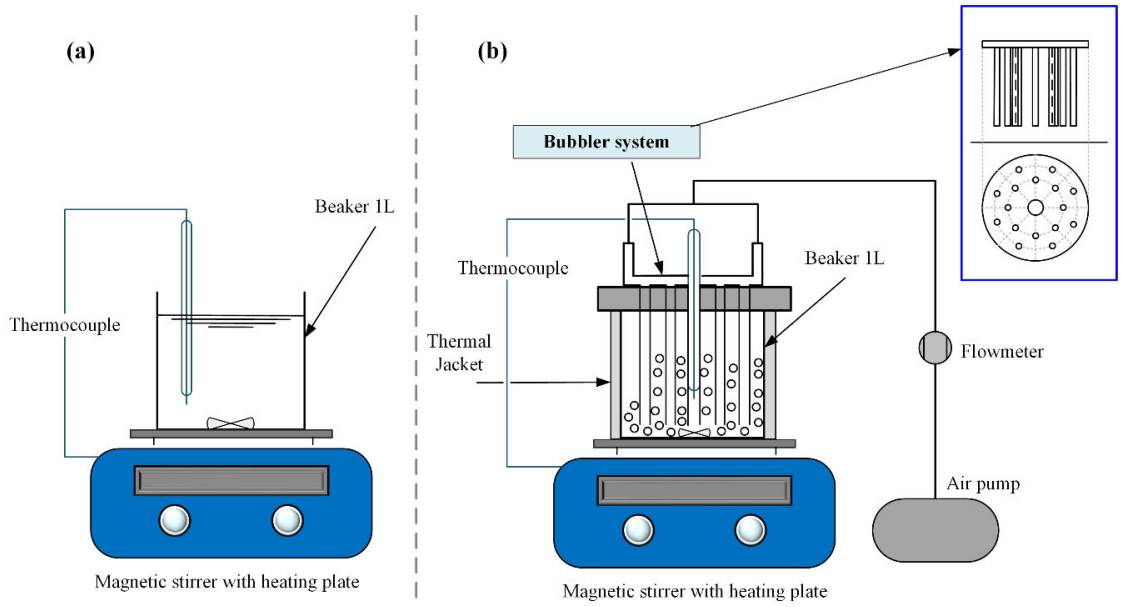

Figure 2.1. *Experimental equipment using dissolution of ES. (a) With HNO_3 and (b) with Air or O_2.*

2.2.2 Arsenic Removal

Arsenic removal experiments were carried out using two solutions. The first solution, called "artificial solution", was prepared by dissolving hydrated arsenic (V) oxide ($As_2O_5 \cdot 3H_2O$) with distilled water and heating to 60 ºC in the laboratory, whose As concentration were 10 g/L. The second solution was obtained by complete dissolution of the ES, named "ES solution". The arsenic removal was carried by precipitation with ferric ions through the formation of scorodite ($FeAsO_4 \cdot 2H_2O$), following the reaction 2.1.

$$4H_3AsO_{4(aq)} + 4FeSO_{4(aq)} + O_{2(g)} + 6H_2O_{(aq)} \leftrightarrow 4FeAsO_4 \cdot 2H_2O_{(s)} + 4H_2SO_{4\ (aq)} \qquad \textit{Eq. 2.1}$$

According to the literature consulted (Demopoulos, 2014; Droppert, 1996; Fujita et al., 2009a, 2008a), the scorodite formation can carry out using Fe^{2+} or Fe^{3+} sources, when using ferrous ions, air or oxygen is added to oxidize the ferrous ions to ferric, which induces the precipitation of arsenic (Eq. 2.1). In addition, the precipitation of scorodite occurs at pH between 1.5 and 3.0. However, the induction of pH must carry out by sequential neutralization stages to control the scorodite formation. The synthesis is normally performed in three stages of pH adjustment. In step I (pH 1.5), the Fe source is added, and the reaction continues for 3 h. The As precipitation reaction reaches equilibrium at a final pH lower than the initial pH. To induce the precipitation of As, the equilibrium (Eq. 2.1) must move to the right by decreasing the acidity. This achieves by adding an alkaline agent until a pH around 2.0 (stage II), which reach the equilibrium again (pH ≈ 1.5) after about 3 h. Then the pH

is increased between 2.5–3.0 by another alkali addition (step III), reaching a final pH of around 2.0 after equilibrium.

The experiments for arsenic removal carried out with the artificial solution were focused on looking for the method optimization of $FeAsO_4 \cdot 2H_2O$ formation. In these experiments, several conditions were simulated: 1) two Fe^{3+} sources ($FeCl_3$, $Fe_2(SO_4)_3 \cdot 7H_2O$); 2) One Fe^{2+} source ($FeSO_4 \cdot 7H_2O$), and air was injected at a rate of 1–2 L/min to oxidise the Fe^{2+} to Fe^{3+}. Both simulations were done at an As/Fe molar ratio of 1.5, without pH adjustment and under continuous stirring at 85 ºC for 6 h; 3) the precipitation was carried out in three stages of pH adjustment using $Ca(OH)_2$ or $Mg(OH)_2$, ferrous sulphate, and air. The experimental conditions were the same as those used in previous experiments (As/Fe molar = 1.5; T= 85 ºC), except the reaction time was 3 h for each stage. The pH was adjusted to 1.5, 2.0 and 2.5 in steps I, stage II, and III, respectively.

The arsenic removal experiments with the ES solution were carried out under the optimal conditions found in the previous experiments (As/Fe molar= 1.5; T= 85 ºC; Reaction time for stage = 3 h). Thus, these experiments were performed in three stages of pH adjustments using $Ca(OH)_2$ or $Mg(OH)_2$ as alkali reagents for pH control. The procedure was the same as the previous experiments. However, in this case, an initial stage was included since ES solution pH was below 0.5. The initial stage consisted of increase the pH until 1.5 to achieve the ferric arsenate precipitation subsequently in the others three stages.

The equipment used in the As removal experiments consisted of a beaker with a lid used as the reaction vessel equipped with, a heating plate with thermocouple, a thermal jacket, a mechanical stirrer, an air pump, and flowmeter (Figure 2.2).

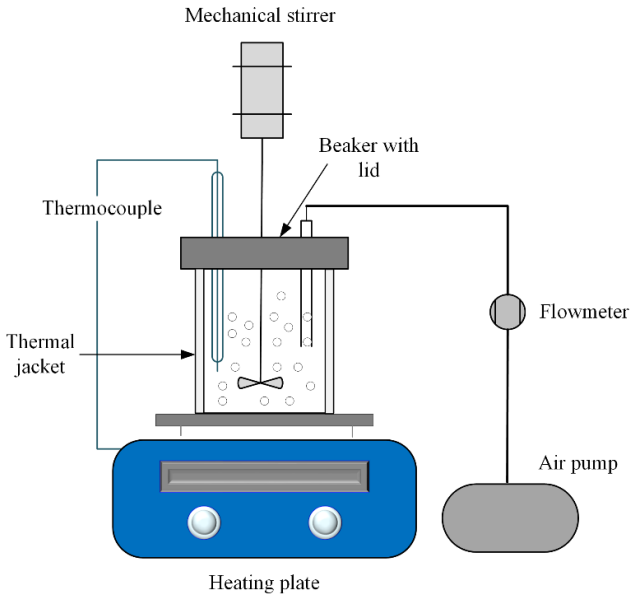

***Figure 2.2**. Experimental equipment for arsenic removal.*

2.2.3 Copper recovery

Copper recovery experiments were carried out by an evaporative crystallization process to produce copper (II) sulphate pentahydrate ($CuSO_4 \cdot 5H_2O$). The electrolyte sludge solution (ES solution) was evaporated with continuous stirring (450 rpm) at 80 ± 5 ºC and using different concentration factors *(CF = V_0/ V_i*, where V_0 is the initial volume of the solution, and V_i is the final volume of the obtained solution at each evaporation step). After, the temperature was reduced at a cooling rate of 0.5 ºC/min until reaching room temperature (~ 20 ºC). The ES solution remained immobilized for 24 h, being the crystal growth stage. Then the solution was filtered to collect the $CuSO_4 \cdot 5H_2O$ crystals, which were rinsed with ethanol and dried at 50 ºC until reaching a constant weight. The copper recovery experiments were carried out by two methods: sequential and non-sequential evaporation. The sequential method consisted of a crystallization process done in five sequential evaporation stages, i.e., the initial solution used in stage II is the final solution of stage I after having collected the $CuSO_4 \cdot 5H_2O$ crystals. At each stage, approximately the same amount of solution was evaporated. On the other hand, in the non-sequential experiments, three crystallization processes were carried, evaporating different amounts of solution at each of them and starting from the ES solution in each case.

The equipment used in the Cu recovery experiments consisted of a 250 mL reaction vessel with (250 mL graduated beaker) without a lid, a magnetic stirrer with a heating plate, a thermocouple, and a thermal jacket (Figure 2.3).

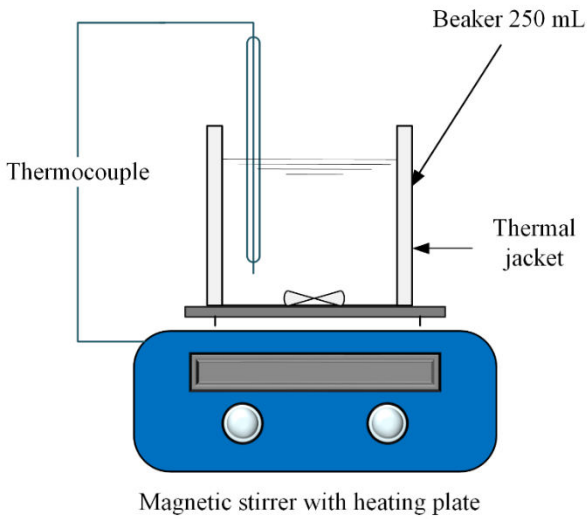

***Figure 2.3**. Experimental equipment for copper recovery.*

2.2.4 Preparation of geopolymer materials

The geopolymer materials were manufactured using the one-component or "just add water" method, which consists of mixing a solid alkaline activator and a solid aluminosilicate precursor with or without aggregates (alumina, sand, fibres, etc.) in dry and then the water is added to initiate the reaction. This process is analogous to preparing ordinary Portland cement-based materials (Hajimohammadi and van Deventer, 2017; Luukkonen et al., 2018a). Most studied precursor consists of a CaO-MgO-Al_2O_3-SiO_2 system which forms calcium-aluminium-silicate-hydrate gel (C-A-S-H in cement chemist notation) as the result of alkali activation. This gel phase is highly reactive and induce the silicate and polysialate network formation and hardening throughout the geopolymer matrix (Komnitsas and Zaharaki, 2007; Luukkonen et al., 2018b).

In these experiments, blast furnace slag (BFS) was used as solid aluminosilicate precursor. In the preparation, a fraction solid precursor is substituted by two hazardous wastes, namely phosphogypsum (PG) and copper wastewater sludge (CWS). Granulated sodium metasilicate anhydrous (Na_2O= 47–49.5 %, SiO_2= 50.5–53 %) from Sigma-Aldrich was used as solid alkali activator and, for the mortars (M), commercial natural sand from Weber Saint-Gobaing, Aveiro, Portugal, was used as aggregate. In this study, the geopolymer materials with sand were called mortars.

Geopolymer pastes and mortars were prepared for the experiments. The reference geopolymer paste was prepared only with BFS. The other geopolymer pastes were prepared by substituting a certain

amount of the precursor for the PG and CWS residues. The mechanical properties were studied in function of particle size distribution of the wastes. Thus, the CWS sample was sieved at 63 µm and then the geopolymer was prepared with that fraction. The mortar specimens were prepared for the sand-to-binder ratio of 4:1 (g/g), the mass of the binder is the mass of precursor and residue. For the reference geopolymer mortar, the BFS was mixed with sand. Then, the other mortar specimens were prepared, replacing a certain amount of the BFS with PG or CWS. In section 3.4.2.2 are shown the mixtures performed with each residue.

The equipment used for the preparation of pastes and mortars is shown in Figure 2.4. The procedure consists of weighing and manually mixing the solid precursor, activator, and sand only in the case of mortars in a plastic bag. When the mixture was completely homogeneous, mixed with water in the mechanical mixer for 1 min. Then, the slurry was manually mixed with a palette for 1 min. After, this is again mechanically mixed for 1.5 min. Finally, the sample is cast into 40×40×40 mm metallic moulds.

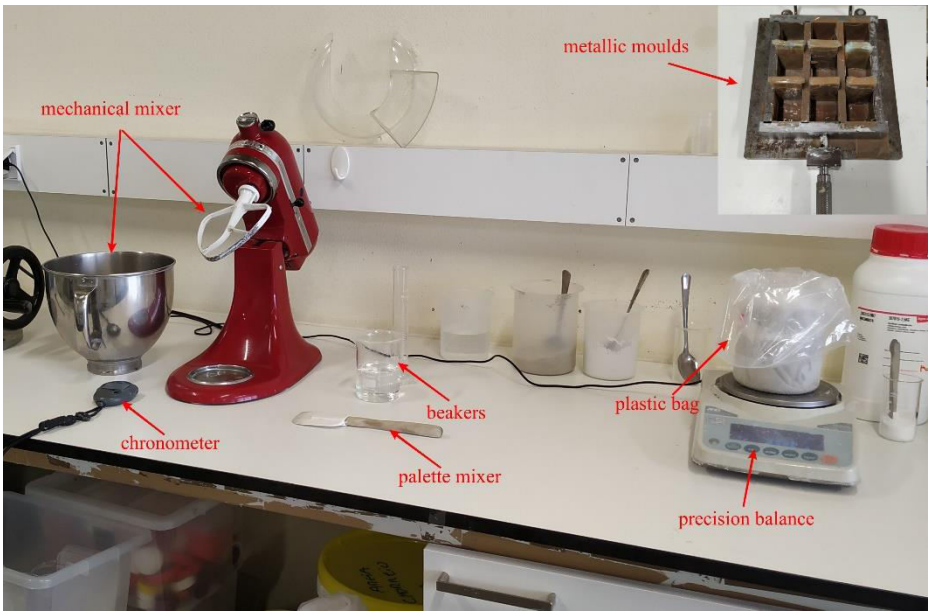

***Figure 2.4**. Experimental equipment for the preparation of geopolymer materials.*

2.3 CHARACTERIZATION TECHNIQUES

This section describes the techniques used in the physic-chemical characterization of the collected sludges and the new material produced in the experiments.

Granulometry

The particle size distribution of the samples was determined with a modular analyser, Mastersizer 2000-Malvern equipped with 52 detectors, a wet sample dispersion unit Hydro 2000MU, and He-Ne lamp as light source at a wavelength of 632.8 nm, property of the Central Research Services at the University of Huelva (Spain). The laser analyser provides the primary size information for particles in the 0.02 to 2000 μm range. For this, a representative amount of each sample (20–30 mg) is placed in 50 mL ethanol (dispersant) and subjected to ultrasound for 10 min at room temperature, followed by magnetic stirring (700 rpm) in a flask for 30 min to ensure the homogeneous distribution of the particles. Aliquots are then collected for granulometric analysis. The calibration method is carried out with several certified reference materials (CRMs) were employed to calibrate the method: LTX3300C Nanosphere Size Standards, 2009A and 2009B Duke Polymer Microsphere Uniform Standards, 4009, 4009A and 4009B Duke Standards Microsphere Size Standards. Before each run, it is verified that the device parameters are within the measurement range.

For some samples, the wet particles size distribution was determined using an analyser HORIBA Scientific Partica LA-960V2 equipped with, a fraction cell accessory, and red solid-state 5 mW laser diode (650 nm) and blue solid-state 3 mW LED (405 nm) as light sources, property of the department of materials and ceramic engineering of University of Aveiro, Portugal. The laser analyser provides the primary size information for particles between 10 nm a 3000 μm. For this, about 10–100 mg of sample is place in fraction cell with 5–10 mL of ethanol. The wet system of equipment includes a fill pump, liquid level sensor, circulation pump, 30 W in-line ultrasonic probe, and drain valve. It is all software-controlled, and measurement takes 60 s at the push of a button.

X-Ray diffraction (XRD)

The mineralogy of the samples was performed using a Panalytical X'Pert Pro diffractometer, equipped with the Cu X-ray source and X'celerator detector, operating under the following conditions: voltage 40 kV; current 10 mA; range 5–70° 2θ; step size 0.017° 2θ; time per step 50.165 s; divergence slit fixed and angle 0.5°. The crystalline mineral fractions were identified using a X'Pert High- Score Plus software, along with the PDF-4 Minerals 2013 ICDD (International Centre for Diffraction Data) database. The quantification of the mineral phases was performed using the

Rietveld method, which employs corundum (Standard Reference Materials: SRM 1976a) as an internal standard to determine the amount of amorphous material. The X-ray diffraction analysis was carried out in accredited Activation Laboratories (Actlabs) from Canada.

For some samples was performed with a Bruker D8-Advance diffractometer equipped with Göebel mirror (non-planar samples), a high temperature chamber (up to 900 ºC), a KRISTALLOFLEX K 760-80F x-ray generator, (power: 3000 W, voltage: 20–60kV and current: 5–80 mA) and an X-ray tube with a copper anode, installed in Research Technical Services (SSTTI) of the University of Alicante. The crystalline mineral phases were identified with the software Match! (Phase Identification from Powder Diffraction) of Crystal Impact using the COD database (Crystallography Open Database). In this case, zincite (ZnO) was added prior to the analysis as an internal standard to determine amorphous material and quantify the mineral phases.

During the doctoral stay in the department of materials and ceramic engineering of University of Aveiro (Portugal). It was employed to identify crystalline phases a Panalytical X'Pert PRO^3 diffractometer, equipped with the Cu X-ray source, graphite monochromator, grazing angle XRD, and temperature chamber with "in situ" measurements up to 1300 ºC, proper of this department. The operating conditions were voltage 45 kV; current 40 mA; range 10–80° 2θ; step size 0.026° 2θ; time per step 497 s; divergence slit fixed and angle 0.43°. The crystalline mineral fractions were identified using a X'Pert High- Score Plus software, along with the PDF-4 Minerals 2013 ICDD.

X-Ray fluorescence (XRF)

The major elements were measured by XRF employing a Panalytical AXIOS model sequential spectrometer, in the Central Research Services of the University of Seville (Spain). This is equipped with an X-ray tube of 4 kW, a front window, and an anode of Rh, five analysing crystals (PX1, PE 002, LIF 200, Ge 111, and LIF 220), and two detectors (flow and scintillation). Prior to the analysis, the samples were prepared as pressed discs of 40 mm in diameter and 25 mm in thickness. This is equipped with an X-ray tube of 4 kW, a front window, and an anode of Rh, five analysing crystals (PX1, PE 002, LIF 200, Ge 111, and LIF 220), and two detectors (flow and scintillation). Prior to the analysis, the samples were prepared as pressed discs of 40 mm in diameter and 25 mm in thickness. Additionally, a Philips X'Pert PRO MPD spectrometer was used, installed in the CICECO - Aveiro Materials Institute of the University of Aveiro (Portugal).

For the calibration, a standard MAC 80090-20 X-ray Fluorescence Universal Set for 20 elements (Na, Mg, Al, Si, P, S, Cl, Ca, Ti, Cr, Mn, Fe, Ni, Cu, Zn, Nb, Sn, Ba, W, Pb) was used. To verify

the quality of the result, several CRMs (GBW 07238 (NCS DC 70006), SX18-04, and BIR-1a) were used.

Inductively Coupled Plasma Optical Emission Spectrometry (ICP-OES)

The determination of trace elements was carried out in inductively coupled plasma optical emission spectrometry (ICP-OES), Varian 735ES. This analysis was carried out in Activation Laboratories (Actlabs) from Canada.

Prior to the analysis, the samples were digested by mixing four acids (hydrochloric, nitric, perchloric and hydrofluoric acid), named the "near-total dissolution method". For the digestion, 0.25 g samples were taken and added HF, followed by a mix of HNO_3 and $HClO_4$. After, the mix is heated using a programmer controlled in several ramping and holding cycles which takes the samples to dryness. Once dryness is achieved, the samples are dissolved in aqua regia, then diluted and analysed.

For some aliquots were dissolved by "peroxide total fusion method". This assay method is ideal for base metals such as Cu, Pb, Zn, Ni, and refractory elements such as Mo, Nb, Ta, As, Cr, Ti as well as a range of other elements. This method involves a mixing solid sample with an alkali fusion flux inside a nickel crucible, heated to about 600–800 ºC with agitation until complete reaction and dissolution of the sample in the flux. The mixture is cooled in situ to produce a vitreous mass and is easily soluble in dilute acids.

Quality control (QC) included the use of blanks, replicates, and several CRMs (CZN-4, OREAS 45d, OREAS-97, OREAS-98, OREAS-101a and RGTH, etc.).

Inductively Coupled Plasma Mass Spectrometry (ICP- MS)

The inductively coupled plasma mass spectrometer (ICP-MS) was also used for the determination of traces elements. This measurement was carried out in Actlabs (Canada). This laboratory used Perkin Elmer Sciex ELAN 9000 spectrometer. Quality control (QC) included the use of blanks, replicates, and several CRMs (GRX-1, GXR-4, GXR-6, MP-1b, SAR-M, SBC-1, etc.).

Scanning Electron Microscope with Energy Dispersive Spectrometer (SEM-EDS)

The morphology and microstructure of the samples were studied using an environmental scanning electron microscope (SEM) QUANTA-Fei 200, installed Central Research Services at the University of Huelva (Spain) and Hitachi S4100, property of the department of materials and ceramic engineering of University of Aveiro (Portugal). Both were equipped with an energy dispersive

spectrometer (EDS) which enables multi-elemental semi-quantitative analysis. A database was used to determine the mineralogical composition (Mineralogy Database, 2012a).

A scanning electron probe microanalyzer (EPMA) JEOL JXA-8200 model with four wavelength dispersive X-ray spectrometers and energy dispersive X-ray spectrometers (EDS) was used to obtain the spatial distribution of several elements. This analysis was carried out Central Research Services at the University of Huelva (Spain).

Prior to the analysis, the samples were inserted in the epoxy resin (Araldite®), then grinded with silicon carbide paper (SIC paper) and polished with 6, 3 and 1 μm diamond paste. Afterwards, the samples were covered with a thin layer of Au–Pd, in a Spark Blazer SCD 050, which made them conductive for electrons, thus facilitating their observation in the microscope.

Thermal Analysis

Thermogravimetric analysis (TGA), differential thermal analysis (DTA) and differential scanning calorimetry (DSC) were used to study the thermal behaviour of the samples. TGA-DTA analysis was carried out by Scientific and Technical Services of the University of Oviedo (Spain) using a Mettler-Toledo TG-SDTA 851E thermobalance and for TGA-DSC analysis was performed by the Research Technical Services of the University of Alicante using a Mettler-Toledo TG/DSC2 thermobalance. Both thermobalances are coupled to the ICP-MS (Pffeifer ThermoStar) equipment to determine the composition of the residual gases. For the operating conditions used were 25–1000 °C with a heating rate of 10 °C/min and an inert N_2 atmosphere with a flow rate of 50 mL/min. Before analysis, the samples were finely ground and homogenized.

Fourier transform infrared spectroscopy (FTIR)

Fourier transform infrared spectroscopy (FTIR) analysis, in attenuated total reflection (ATR) mode was used to determine the vibrational bonds formed (functional groups) in the geopolymer. This analysis was performed using the Perkin Elmer Spectrum BX FT-IR spectrophotometer (Figure 2.8), equipped with the single horizontal Golden Gate ATR cell, property of the CICECO – Aveiro Institute of Materials of the University of Aveiro (Portugal). The operating conditions used to obtain the spectra were a wavenumber range of 4000–400 cm^{-1}, with a resolution of 8 cm^{-1} and 128 scans.

Leaching test

To evaluate the mobility of the pollutants in the samples, a leaching test protocol based on the EN 12457-4 test (CEN: European Committee for Standardization, 2002a) was applied, according to the

RD 1481/2001 of 27 December, which regulates the disposal of waste by landfill, in agreement with the provisions of Directive 1999/31/EC on landfill. RD-1481/2001* establishes the waste acceptance criteria for each type of landfill, which are classified as inert, non-hazardous, and hazardous. In addition, this regulation shows the threshold level established for each type of waste (inert, non-hazardous, and hazardous).

The leaching test set out in the norm EN 12457-4 was adopted in this experiment, where the extraction fluid used was distilled water at a liquid/solid ratio of 10 L/kg (± 2%). Polyethylene bottles were employed as extraction vessels, which were subjected to rotation with agitation equipment with Teflon-coated rod at 5–10 rpm during 24 ± 0.5 h. Then, the solution was vacuum filtered using membrane filters of 0.45 μm pore size, in agreement with the EN 12457-4. Finally, the solutions were preserved for analysis by ICP-OES and ICP-MS.

To evaluate the immobilization of the pollutants in the geopolymer materials, leaching tests were carried out following the EN 12457-2 (CEN: European Committee for Standardization, 2002b). The extraction fluid used was distilled water at a liquid/solid ratio of 10 L/kg (± 2%). The geopolymer specimen was submerged in distilled water without agitation during 24 ± 0.5 h. Then, the solution was collected and measured in total reflection x-ray fluorescence spectrometer (TXRF – S2 PICOFOX 50 keV), with detection limit raging in the ppb. This leaching test was carried in the University of Aveiro, Portugal. Quality control for both leaching tests included the use of blanks and replicates.

* RD 1481/2001 of December 27 has been repealed by RD 646/2020 of July 7, which regulates waste disposal by depositing it in a landfill.

2.4 GEOPOLYMER TECHNOLOGICAL TESTS

This section describes the technological tests carried out on geopolymers, which are the same as those applied to cement and mortar for masonry. These tests were carried out department of materials and ceramic engineering of University of Aveiro (Portugal). In all tests the above tests, three replicates were used, and their respective standard uncertainty was calculated.

Determination of consistence of fresh mortar

Flow table test was used to assess the consistence of the paste, in agreement with the EN 1015-3 (CEN: European Committee for Standardization, 1998). The consistence is a measure of the fluidity and/or wetness of the fresh mortar and gives a measure of the deformability of the fresh mortar when subjected to a certain type of stress.

Flow table test was performed by the procedure described below. First, the mould was placed in the centre of the disk of the flow table. After, the mortar was introduced into two layers. Each layer is compacted by at least ten short strokes of the tamper to ensure uniform filling of the mould (Figure 2.5). Next, the excess mortar is shimmed off with a palette and wiped the free area of the disc clean and dry, being especially careful to remove any water from around the bottom edge of the mould. After around 15 s, slowly, the mould is raised vertically and measured of initial diameter (Figure 2.5). Then, the mortar was spread out on the disk by jolting the flow table 15 times at the constant frequency of about one per second and measured of final diameter (Figure 2.5). The diameter measurement of the mortar was carried in two directions at right angles to one another using a calliper.

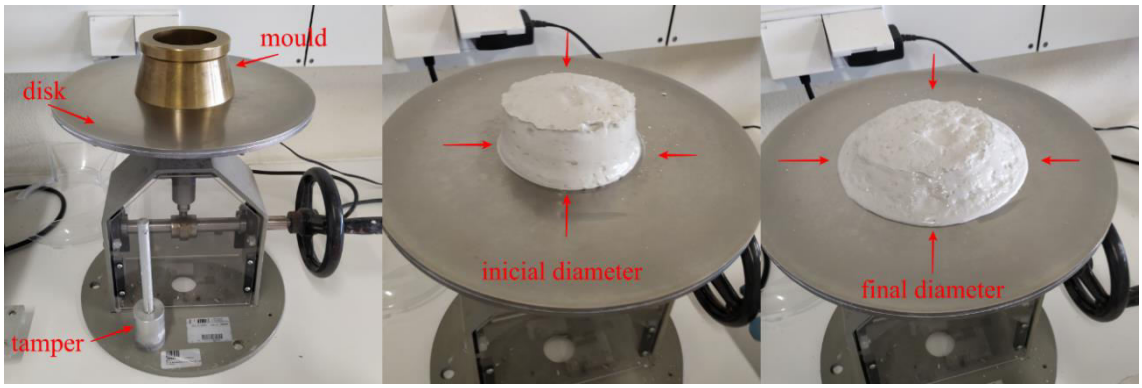

Figure 2.5. *Flow table test*

Setting time of cement: Vicat apparatus

Setting time (initial and final) was determined using the Vicat apparatus, according to European norm EN 196-3 (CEN: European Committee for Standardization, 2005). The setting times of cement give an indication of how long the cement will remain workable when used in a concrete mix. If the cement has deteriorated or was originally defective, it may take an excessive time to set.

The standard Vicat apparatus is shown in Figure 2.6. The setting time test procedure consisted of placing a fresh cement paste sample in the mould and levelling it with a palette. After, the initial needle was fitted to apparatus, brought into contact with the cement paste surface and released. Initially, the needle penetrated entirely through the paste to the base of the mould. These steps were repeated at regular intervals (10 min) at different points on the surface until the needle only penetrates around 5 ± 1 mm of the mould base. The time from initial mixing the cement with water until the desired penetration was achieved is the initial setting time. Then, the initial needle was changed to a cylindrical blunt-ended needle hollowed to determine the final setting time. The needle was brought gently into contact with the surface of the paste and released, leaving a 5 mm mark of diameter in the paste. This operation was repeated every 10 min until the edge did not mark the paste. Thus, the time passed from the initial mixing until this moment is the final setting time.

***Figure 2.6**. Vicat apparatus*

Calorimetric measurements

Calorimetry test measures the heat generated from the early reactions of the cement materials. The heat outflow tracks the reactions of the mixture, which gives visibility into the behaviour of concrete/mortar in a way that a setting time test or compressive strength test could not. The time and shape of the temperature curve obtained through calorimetry is an indicator of the relative performance of the mixture.

This test consisted of placing a fresh paste sample in a vessel with a lid through which a thermocouple passed. First, the thermocouple was dipped into the paste to monitor the temperature. After the vessel was placed in the quasi-adiabatic calorimeter, the chamber was closed and then started the temperature and time measurement. Next, the thermocouple was connected to the data acquisition device (Data Logger Switch Unit34970A from Agilent). The calorimetry test was performed during the first 24 h of curing in a climatic chamber (Fitoclima 300 EP10 from Aralab) at relative humidity (RH) of 65 % and a temperature of 20 ºC. These conditions were selected to represent the conditions present in the plastic bag during the first 24 h of curing.

Before the test (about 24 h), the quasi-adiabatic calorimeter, the vessel with lid, thermocouple and raw materials were placed in the chamber at 65 % of RH and 20 ºC.

Compressive strength

The compressive strength was determined using a Universal Testing Machine (UTM, Shimadzu AG-25TA), according to EN- 1015-11 (CEN: European Committee for Standardization, 1999). The UTM used is shown in the Figure 2.7.

The compressive strength test of the specimen was carried out after 7 and 28 days of curing. First, the specimen was filed, removing any loose grit or other material from the sides of the specimen. Then, the length, width and height of the cube were measured using a calliper. Next, the platens of the testing machine, with a clean cloth, were wiped. After, the specimen was placed between the compressive platens at its centre position. The specimen must be carefully aligned to load applied to the whole width of the faces in contact with the platens. The test was conducted using a load displacement of 0.5 mm/min. Finally, the compressive strength test ends after the maximum load are recorded (the specimen breaks down).

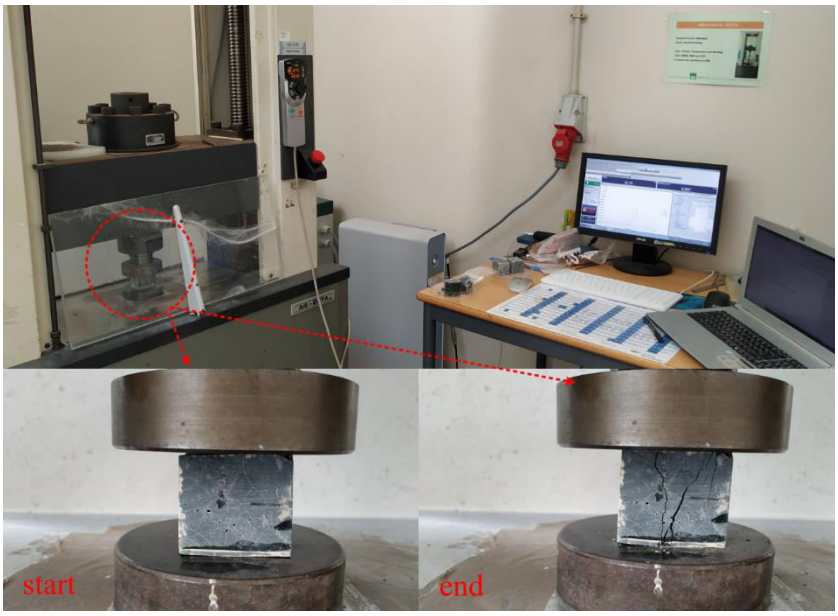

Figure 2.7. *Universal Testing Machine (Shimadzu AG-25TA). The images of the start and end of the test are shown at the bottom of the figure.*

Water absorption

The water absorption of specimens was measured by total immersion in water. After 28 days of curing, the specimen was weighed and placed in the tray (Figure 2.8). Water distilled was added until the specimen was completely immersed. After 24 h, the specimen was removed, wiped off surface water with a dampened cloth, and weighed. The percentage of water absorption calculated following Eq. 2.2, where *"M_0"* is the initial mass, *"M_{24}"* and the mass measured after 24 h.

$$Water\ absortion\ (\%) = = \frac{(M_0 - M_{24})}{M_0} \times 100 \qquad \textbf{Eq. 2.2}$$

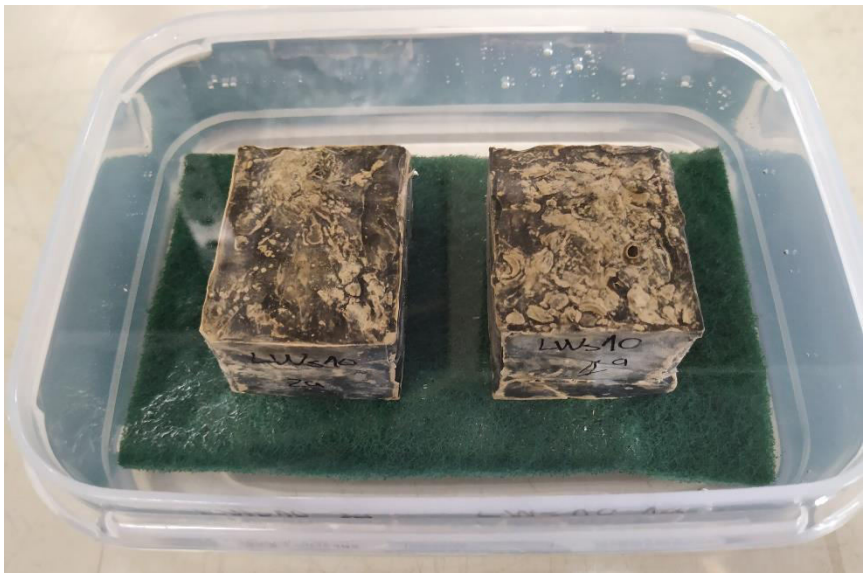

Figure 2.8. *Water absorption test*

Capillarity

The water absorption coefficient due to capillary action, named capillary coefficient, of specimens was determined by immersing one of faces of the specimen, following EN 1015-18 (CEN: European Committee for Standardization, 2002c).

After 28 days of curing, the specimen was weighed and placed in the tray. Water distilled was added until a depth of 5–10 mm was reached (Figure 2.9). The chronometer was activated. Then every 10 min, the specimen was removed from the tray, quickly wiped off surface water with a dampened cloth, weighed and replaced immediately into the tray. This procedure was repeated for 90 min. The sample was kept submerged for 24 and then weighed. Finally, the specimen's capillary coefficient (C in kg/m^2 min$^{0.5}$) was determined through the straight-line slope linking the representative points of the measurement carried out at 10 min and 90 min. According to Eq. 2.3, where *"ΔM"* is the difference between the initial mass "M_0" and the mass measured every 10 min *"M_i", "A"* is the submerged surface, and "t" is the elapsed time.

$$C\left(\frac{kg}{m^2\ min^{0.5}}\right) = \frac{\Delta M}{A\sqrt{t}} = \frac{(M_0 - M_i)}{A\sqrt{t}} \qquad \textbf{Eq. 2.3}$$

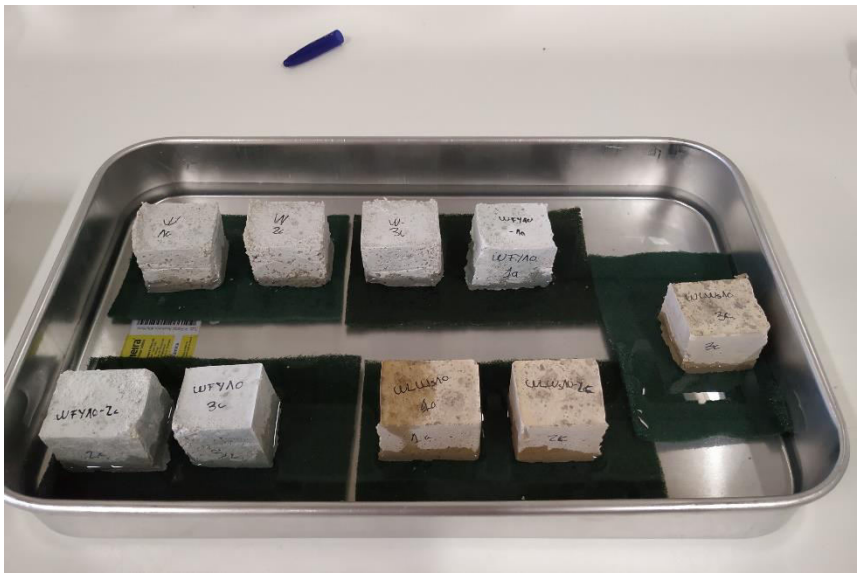

***Figure 2.9**. Capillary test*

CHAPTER 3.

RESULTS AND DISCUSSIONS

SUBCHAPTER 3.1

CHARACTERIZATION OF TWO SLUDGES FROM A PYROMETALLURGICAL COPPER SMELTING COMPLEX FOR DESIGNING A SE AND PB RECOVERY PROPOSAL

3.1 CHARACTERIZATION OF TWO SLUDGES FROM A PYROMETALLURGICAL COPPER SMELTING COMPLEX FOR DESIGNING A Se AND Pb RECOVERY PROPOSAL

D.C. Paz-Gómez[1], S.M. Pérez-Moreno[1], I. Ruiz-Oria[2], G. Ríos[2] and J.P. Bolívar[1]

Waste and Biomass Valorization 12 (2021) 2739-2755

Abstract

Gas scrubbing sludge (SS) and fine dust of converters (SC) are wastes generated in the off-gas cleaning system of smelting and converting processes. Both wastes are considered hazardous materials due to their high metal contents and leaching characteristics. The main purpose of this study was to gain essential knowledge on the recovery of valuable elements contained in these wastes. Thus, an exhaustive characterization was carried out to determine the composition, mineral phases, particle size, and leachability of both wastes (SS and SC) as a preliminary step to select the most appropriate applications and treatment for them. These wastes are composed of fine particles (~ 95 % < 63 μm), mainly containing Pb (> 20 %) as anglesite ($PbSO_4$), while SS presents a high concentration of Se (34 %), which is mainly identified as metallic selenium. Therefore, these residues could be used as secondary sources of Pb and Se. The recovery of Se by roasting process and Pb recovery by hydrometallurgical route seem to be the best options for the management of these wastes.

Graphical abstract

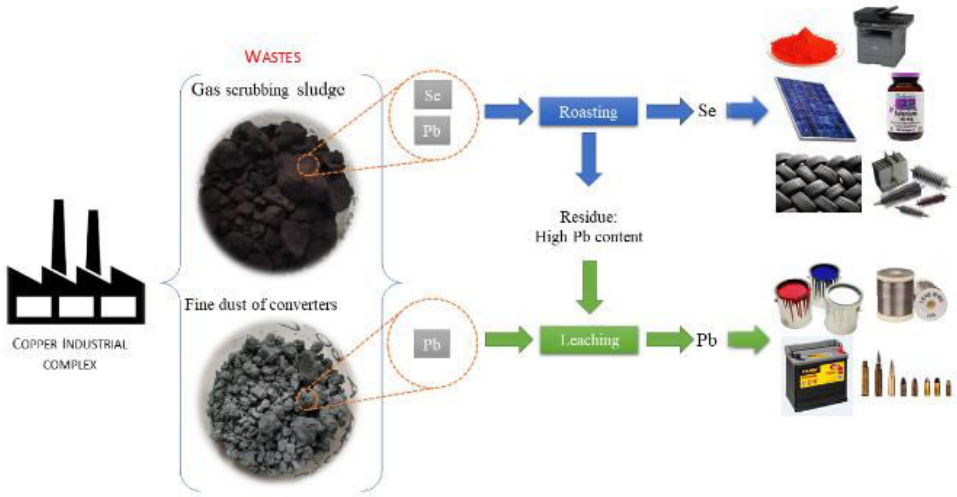

Keywords: Converter dust, Gas scrubbing sludge, Selenium recovery, Copper smelting, sludge characterization.

Statement of Novelty

This study is new to Waste & Biomass Valorization because it is the first time that these two wastes from copper smelting are deeply characterized and proposed a viable pathway for their valorization.

3.1.1 Introduction

The global demand for copper has increased in the last 50 years due to expanding sectors such as electrical and electronic components, building construction, manufacture of industrial machinery and equipment, transport, and consumer products. Refined copper production worldwide reached 23.5 million tonnes in 2017 (ICSC: International Copper Study Group, 2018), which accompanies a huge amount of dust, sludge, slag and wastewater (Csavina et al., 2014; Newhook et al., 2003). In the last decades, the recycling and valorisation increase of the industrial wastes has reduced disposal costs and prevented risks for the environment and human health (EEA: European Environment Agency, 2017; European Commission, 2015).

A big hydro-pyrometallurgical copper industrial complex is located in Huelva (Spain), which is one of the biggest manufacturers of copper cathodes in Europe, which produces around $2.9 \cdot 10^5$ t/y of high purity copper (99.99 % Cu). The industrial process (Fig. 3.1) begins with the smelting of copper concentrate (around 30 % Cu), in the Flash Furnace (FF), in which the “matte” with 64 % Cu is obtained. Then, the matte is introduced into the Converter Furnaces (CF), where it becomes “blister copper” (> 99 % Cu). The slag generated in the FF and CF is treated in an Electric Furnace (EF) to recover the remaining copper in the slags (1.5 % and 5 %, respectively), leaving the final copper content below 1 % in the obtained slag from the EF, which is mainly formed by iron silicates (Fig. 3.1). The blister copper is transformed into “copper anodes” (99.6 % Cu, $3.3 \cdot 10^5$ t/y) in the Refining Furnaces (RF). Finally, the anodes are subjected to the electro-refining step, in which “copper cathodes” are obtained (> 99.99 % Cu).

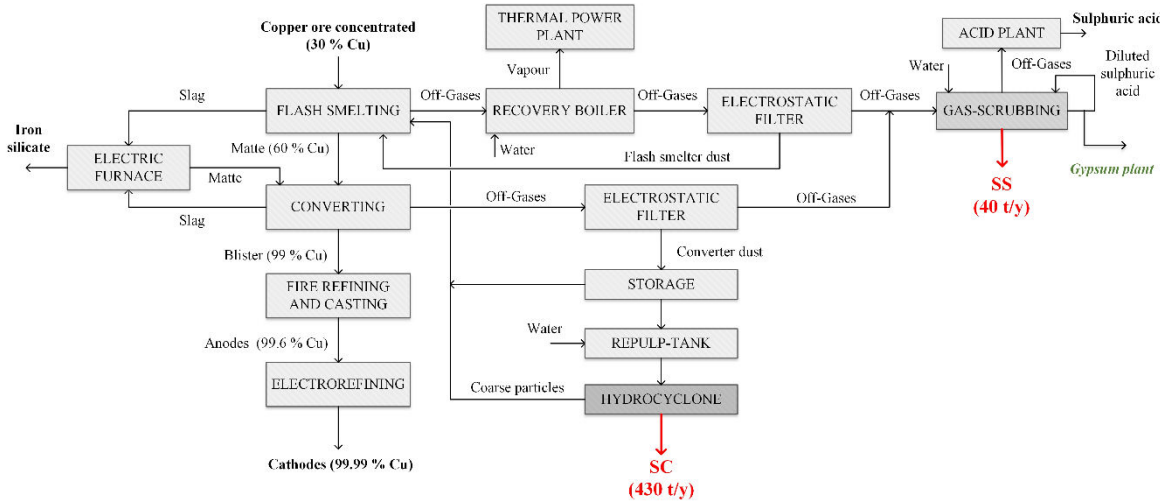

Figure 3.1. *Overview of material flows and process.*

Smelting copper concentrate in the FF is a continuous process in which O_2-enriched air is blown and dried concentrate, flux agent (SiO_2) and recycled materials come from different steps of the process at 1250 ºC. The copper concentrate (raw material with about 30% in Cu) reacts with O_2 to form molten iron-silicate (slag) and Cu-enriched molten sulphide phase (matte, in which the copper content is still rather low, about 60%), is a solution composed mainly by Cu_2S and FeS. And then the slag and matte are separated due to their different densities. In addition, most of the sulphur contained in the raw material goes out as SO_2-rich off-gas (Pérez et al., 2018b; Schlesinger et al., 2011).

The SO_2-rich gases from FF are cooled in a heat recovery boiler (Fig. 3.1), where a high-pressure steam is produced, which generates electricity. Then, the outgoing gases from the boiler are dedusted in electrostatic filters, and the collected dusts are returned to FF. On the other hand, the dedusted gases coming from both FF and CF electrofilters are mixed and introduced into the scrubber section, where the smallest particles and some soluble gases are removed by using diluted acid. And finally, the precipitated solids (Sludge Scrubber = SS) are collected in a decanter. About 40 t/y of SS are produced and stored in a controlled landfill located 70 km from Huelva city (Atlantic Copper, 2017; Schlesinger et al., 2011).

On the other hand, the matte is oxidized using O_2-enriched air, in the CF. This conversion is a batch process in two stages: the slag and copper blows. The first stage is the slag blow, in which FeS is oxidized to produce slag. This stage is ended when there is about 1 % Fe in the matte; then, the slag is removed, producing a matte with a low S content (white metal), which is oxidized to blister copper. The converting process is finished when oxide copper begins to appear in the copper sample. Both stages generate SO_2-enriched off-gases (Schlesinger et al., 2011).

Off-gases from CF are dusted off in electrostatic filters (see figure 3.1), and purified gases, previously mixed with off-gases from FF, are sent to the scrubber section. About 70 % of the converter dust collected in these filters is sent to FF, whereas the remaining 30 % of this dust (around 1100 t/y) is sent to hydro-cyclones, where the coarse particles are separated from fine particles (< 15 μm). Previous studies indicated that the valuable metals (copper and gold) are found in the coarse particles, which are recycled into FF, whereas the impurities (As, Bi, Sb, Pb and Zn), are contained in the fine particles, forming a final sludge composed of fine dust of converters (SC), which are disposed by landfill at around 430 t/y (Atlantic Copper, 2017). Both wastes are currently disposed in a controlled landfill for hazardous wastes, where they are managed by applying a stabilization process to reduce the mobility of pollutants contained in them, and do not exceed the thresholds established in the Royal Decree (RD)1481/2001, regulation based on the Directive 1999/31/EC on landfills (Directive 1999/31/EC, 1999; RD 1481/2001, 2013). The management of both wastes implies high transport and storage costs, in addition to a potential environmental impact. For these reasons, this practice must be replaced by the valorisation of these wastes.

There are few studies in the literature about the characterization and valorisation of these wastes. Some authors report on the recovery of Cu and other marketable elements, such as Ag, Bi, Co and Zn (Lastra-Quintero et al., 2014; Nuñez et al., 1985; Yang et al., 2010). Moreover, other authors have studied the removal/stabilization of hazardous elements, such As and Cd (Morales et al., 2010; Vircikova and Havlik, 1999; Vítková et al., 2011). Other works suggest the recovery of high added-value elements, such as Ge and Se (Font et al., 2011; González et al., 2017; Xing et al., 2018).

The properties of this type of residues depend not only on the composition of the concentrate fed into the FF, but also on temperature, oxidation conditions, which are determined by the furnace type, and the off-gas cleaning system employed (Ha et al., 2015; Morales et al., 2010; Schlesinger et al., 2011). For these reasons, it is necessary to characterize these residues before deciding the most suitable treatment, in order to recover the valuable elements (Balladares et al., 2014; Okanigbe et al., 2017; S.M. Pérez-Moreno et al., 2018).

Taking into account the previous facts, the main objective of this work was to propose an alternative process for the recovery of valuable elements contained in two wastes of a copper smelting plant (SC and SS), based on a thorough characterization.

3.1.2 Materials and methods

3.1.2.1 Materials

Four sampling campaigns were performed over a period of one month in March 2015. Four samples were collected for each of the previously commented wastes, i.e., sludges from scrubber (SS) and sludges from hydro-cyclones from CF off-gases (SC). At each sampling, about 4–5 kg for each sample was collected, and then they were dried at 60 °C and homogenized by manual agitation trying to break the clods but avoiding the breakage of particles the make up the sample. To verify the homogenization degree in some samples four aliquots were taken and measured by ICP-MS, finding that dispersion of the obtained concentrations was comparable to the RSD (Relative Standard Deviation) of the individual measurements. Moreover, some elements were measured by two different analytical techniques (ICP-MS and XRF), and the concentrations measured by both techniques were analogous. In addition, the SS samples were washed with distilled water to remove the remaining sulphuric acid, and it was verified that in the washing waters there was a negligible amount of the rest of the elements from the solid waste.

3.1.2.2 Characterization techniques

3.1.2.2.1 Granulometry

The particle size range of the samples was determined through a granulometric analysis using a modular analyser, Mastersizer 2000, with He-Ne laser diffraction technology at a wavelength of 632.8 nm. A representative amount of each sample was placed in ethanol and subjected to ultrasound for 10 minutes, followed by magnetic stirring for around 30 minutes. In addition, several certified reference materials were employed to calibrate the method: LTX3300C Nanosphere Size Standards, 2009A and 2009B Duke Polymer Microsphere Uniform Standards, 4009, 4009A and 4009B Duke Standards Microsphere Size Standards.

3.1.2.2.2 Mineralogy and Chemical composition

The study of the mineral phases present in the samples was performed using a Panalytical X'Pert Pro diffractometer, equipped with the Cu X-ray source and X'celerator detector, operating under the following conditions: voltage 40 kV; current 10 mA; range 5–70 deg 2Θ; step size 0.017 deg 2Θ; time per step 50.165 s; divergence slit fixed, angle 0.5˚. The crystalline mineral fractions were identified using a X'Pert HighScore Plus software, along with the PDF-4 Minerals 2013 ICDD database. The quantification of the mineral phases was performed using the Rietveld method, which employs corundum as an internal standard to determine the amount of amorphous material. The X-ray diffraction analysis was carried out in Activation Laboratories (Actlabs) from Canada.

The major elements were identified and quantified by an X-ray fluorescence (XRF) analysis using a Panalytical (AXIOS model) sequential spectrometer. This system is equipped with an X-ray tube of 4 kW, Rh from window and anode, five analysing crystals (PX1, PE 002, LIF 200, Ge 111, and LIF 220) and two detectors (flow and scintillation). Previously, the samples were prepared as pressed discs of 40 mm in diameter and 25 mm in thickness.

The determination of trace elements was carried out by two measurement techniques: Inductively Coupled Plasma Mass Spectrometer (ICP-MS), Perkin Elmer Sciex ELAN 9000, and Inductively Coupled Plasma Optical Emission Spectrometry (ICP-OES), Varian 735 ES. Prior to the analysis, the samples were digested by mixing four acids (hydrochloric, nitric, perchloric and hydrofluoric acid). Moreover, some aliquots were dissolved by fusion with sodium peroxide.

3.1.2.2.3 Thermal Analysis

The thermal behaviour of the samples was studied by two methods: Thermogravimetric analysis (TGA) and Differential Thermal analysis (DTA). A TG-85E 11 SDTA Mettler thermobalance was employed, coupled to an ICP-MS equipment (Pffeifer ThermoStar) to determine the composition of off-gasses. The operating conditions used were 25 – 1000 ˚C with a heating rate of 10 ˚C/min and an inert atmosphere of N_2 with a flow of 50 mL/min.

3.1.2.2.4 Scanning electron microscopy (SEM)

The morphology and microstructure of the samples were studied using an environmental scanning electron microscope QUANTA-Fei 200. This was equipped with an Energy Dispersive Spectrometer (EDS) which enables multi-elemental semi-quantitative analysis. Then, a database was used to determine the mineralogical composition (Mineralogy Database, 2012a).

A scanning electron microprobe (EPMA) JEOL JXA-820 model with four wavelength-dispersive X-ray spectrometers and energy dispersive X-ray spectrometers (EDS) was used to obtain the spatial distribution of several elements.

Prior to the analysis, the samples were inserted in the epoxy resin (Araldite®), then grinded with silicon carbide paper (SIC paper) and polished with 6, 3 and 1 μm diamond paste. Afterwards, the samples were covered with a thin layer of Au-Pd, in a Spark Blazer SCD 050, which made them conductive for electrons, thus facilitating their observation in the microscope.

3.1.2.2.5 Leaching test

To evaluate the mobility of the pollutants, the UNE[2] leaching test (CEN: European Committee for Standardization, 2002a), from Directive 1999/31/EC, was applied. This directive regulates the disposal of waste by landfill. The waste acceptance criteria are established for each type of landfill in this norm. The leaching test set out in the norm was adopted in this experiment. The extraction fluid used was distilled water at a liquid/solid ratio of 10 L/kg (± 2%). Polyethylene bottles were employed as extraction vessels, which were subjected to rotation with agitation equipment with Teflon-coated rod at 5-10 rpm during 24 ± 0.5 h. Then, the solution was vacuum filtered using membrane filters of 0.45 μm pore size, in agreement with the UNE-EN 12457-4.

3.1.3 Results and discussion

3.1.3.1 Physical-chemical characterization

3.1.3.1.1 SS characterization

Granulometry

The particle grain-size distribution is very useful to decide the possible applications and treatments of a specific inorganic waste. The granulometry obtained for SS waste is summarised in Table S3.1, in supplementary material (Annex I.1). It is characterised by a high proportion of "silt" (87 ± 8 %), and low contents of "clay" (11 ± 4 %) and "sand" particles (2.4 ± 1.3 %), presenting a monomodal distribution, as it is expected from a wet precipitation process, with a maximum of 8 μm (Fig. 3.2a).

In the Fig. 3.2b the cumulative volume particles distribution curve is shown, where the percentiles can be easily seen, obtaining that the median of the particles size distribution (d_{50}) is around 8 μm, and the d_{90} on 19 μm. This particle size distribution presents a high proportion of fine particles, which is highly beneficial in the manufacturing of construction materials (Al-Jabri et al., 2011; Murari et al., 2014; Wang et al., 2005; Zhao et al., 2014), or for improving the reactivity of the waste during leaching processes (Hansen et al., 2005; Khalid et al., 2019a).

[2]Spanish acronym for "Una Norma Española"

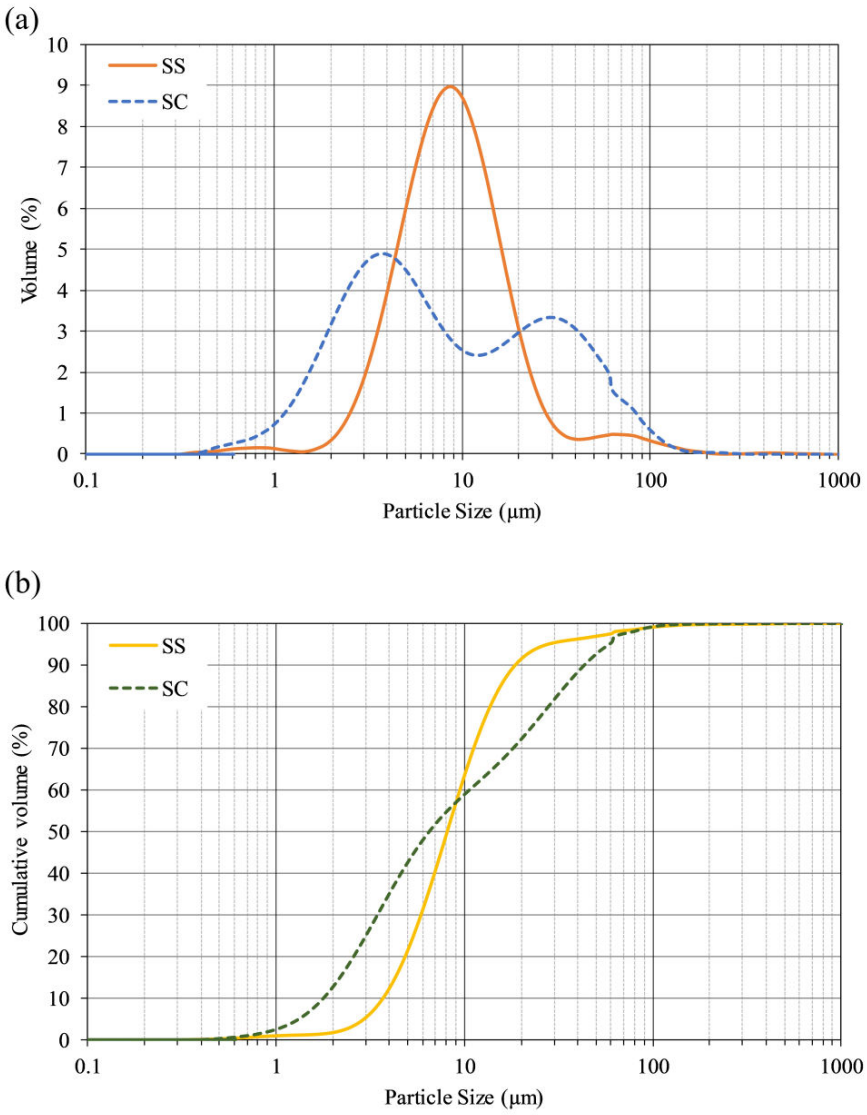

Figure 3.2. *Particle size distribution in % volume (a) and % cumulative volume (b) of the samples.*

Elemental composition

The average concentration of the major and trace elements for the SS samples, measured by XRF and ICP-MS, are shown in Figure 3.3. This information is essential to identify the potential elements to be recovered and the pollutants that should be removed or reduced for their valorisation.

SS contains very high concentrations of Se (34.6 ± 0.4 %) and Pb (20.8 ± 0.3 %), whereas Hg (8.0 ± 0.1 %), S (6.3 ± 0.1 %), Sn (3.5 ± 0.1 %), Ge (2.0 ± 0.2 %) and I (1.4 ± 0.1 %) are in proportions less than 10 %. Other elements, such as, Bi, Cu, Fe and Zn, were found in concentrations below 1 %, and Cr, Sb, Te, Cd and Ni were found in trace concentrations (10–100 ppm). The high content of metals, such as Se, Pb, and Hg, could be due to the fact that they can be fully volatilized during smelting

processes, after which they can either solidify as the gas cools down or form solid particles in the scrubber (Montenegro et al., 2013; Schlesinger et al., 2011).

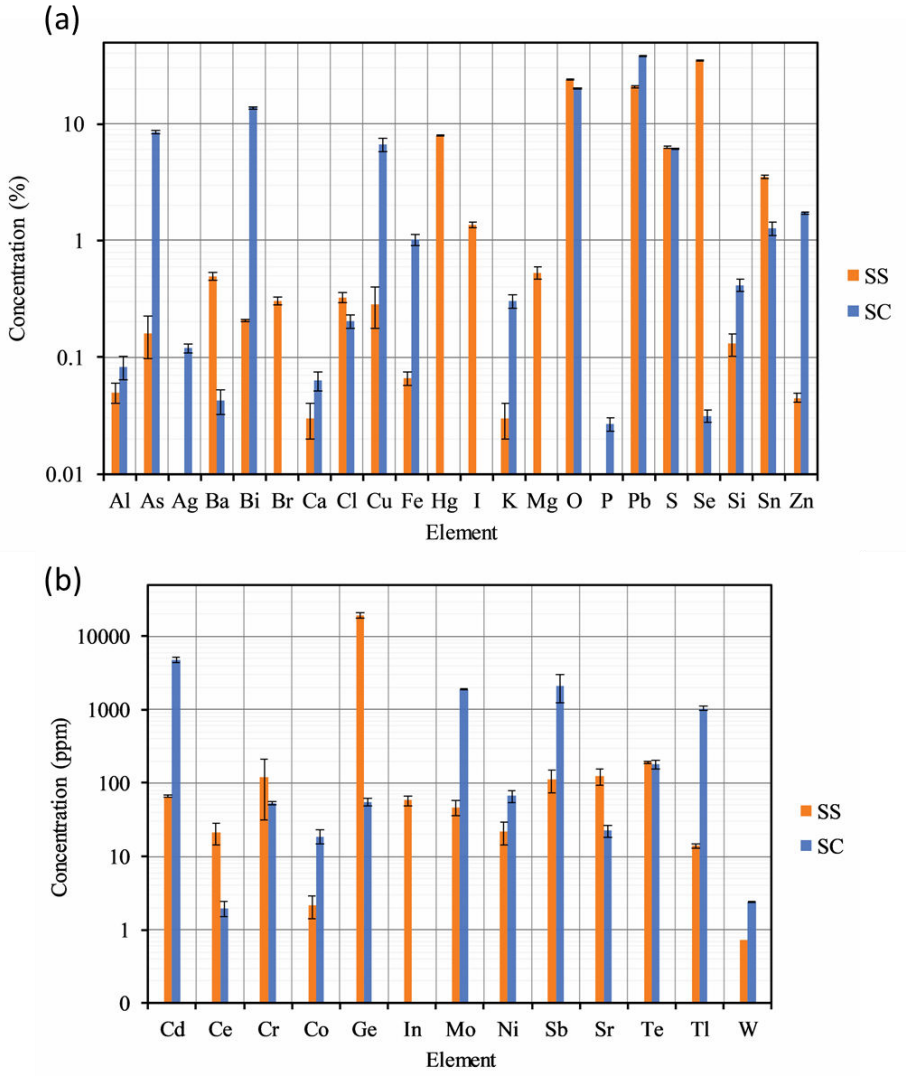

Figure 3.3. *Concentration of major elements (a) and trace elements (b) in the samples. The standard uncertainty (1 σ) was calculated as the standard deviation of the mean* $\sigma = S_x/(n)^{1/2}$*, where "n=3" is number of the samples.*

Mineralogy

The Figure S3.1 shows the diffraction pattern (see, supplementary material Annex I.1). The main mineral phases were metallic selenium (34 % Se) and anglesite (27 % $PbSO_4$). According to the XRF results, the calculated $PbSO_4$ concentration (around 30%) is in agreement with the XRD one (experimental uncertainties ≤ 10 %). Therefore, both results agree with the content of Pb and Se obtained by XRF.

The metallic Se probably came from the reaction of SO_2 in the off-gas with SeO_2 volatized in the smelting process and the water added in the gas scrubber system, as shown in reaction 3.1 (Ramachandra Rao, 2006).

$$SeO_{2\ (g)} + 2SO_{2(g)} + 2H_2O_{(l)} \rightarrow Se_{\ (s)} + 2H_2SO_{4(l)} \qquad \textit{Eq. 3.1}$$

On the other hand, the $PbSO_4$ was probably formed during the cooling down of the off-gases, when the solidified PbO reacts with SO_2 and O_2, according to reaction 3.2 (Balladares et al., 2014; S.M. Pérez-Moreno et al., 2018; Pérez et al., 2019)

$$PbO_{(s)} + SO_{2(g)} + 1/2\,O_{2\ (g)} \rightarrow PbSO_{4(s)} \qquad \textit{Eq. 3.2}$$

In addition, SS had a high content of XRD-amorphous phase (around 40 %). The XRF analysis showed high concentrations of other elements such as Hg, Sn and Ge, but no mineral phase was found associated to them. Therefore, these elements have to be considered forming part of the XRD-amorphous phase, which is formed by either no crystalline phases or microcrystalline phases, they cannot be detected by the XRD. The formation of a high amorphous fraction can be due to the fast cooling produced in the gas scrubbing (Balladares et al., 2014; González et al., 2017).

Thermogravimetric analysis

A TGA analysis was conducted to determine the thermal behaviour of the sludge (SS), contributing to the identification of some chemical compounds that were present in the sample. The results can be seen in Fig. 3.4. It is observed that SS had three thermal events, which occurred at 310 ºC, 562 ºC and 730 ºC. SO_2 was detected in the last two events, thus the mass losses were probably due to the decomposition of metal sulphates. The sulphates decomposition is usually determined from the liberation of SO_3 but is decomposed autocatalytically into $SO_2 + O_2$ in the plasma, being detected in the ICP-MS the m/z= 64 and m/z =32, respectively.

The DTA curve shows a thermal event at 200 ºC, associated with the selenium melting. Then, it evaporated at around 600 ºC (Hoffmann and King, 2000; Olin et al., 2010). It can also be assumed that part of the mass loss (about 35 %) at 562ºC was due to this evaporation. The transition temperatures obtained are slightly different than the average ones obtained under ideal conditions for the transitions of Se (around 220°C and 685 °C), a fact being produced by the interactions between the different substances that compose the real matrix.

The first thermal event at 310 ºC (DTG curve) corresponds to the decomposition of Hg_2SO_4 via the chemical reaction 3.3 (Rumayor et al., 2013), which is in a proportion of 9 % in the sample taking into account the mass loss at this peak. According to the stoichiometry of eq. 3.3, the reaction produces about 5 % of $HgSO_4$ that decompose at 562 ºC with other species ($Sn(SO_4)_2$, and Se volatilization) in accordance with reaction 3.4. In this point, the mass loss identified is about 44 %, being the remain loss mass about 7 % (from the total mass lost at 562 ºC, 51 %). This mass loss suggests that probably the sample also contains about 7 % $HgSO_4$, being in agreement to the Hg concentration measured by XRF.

$$Hg_2SO_{4(s)} \rightarrow HgSO_{4(s)} + Hg_{(g)} \qquad \textit{Eq. 3.3}$$

$$HgSO_{4(s)} \rightarrow Hg_{(g)} + SO_{2(g)} + O_{2(g)} \qquad \textit{Eq. 3.4}$$

In agreement with the XRF data the SS sample contains about 3.5 % Sn, which could be as $Sn(SO_4)_2$. The decomposition of $Sn(SO_4)_2$ occurred at around 580 °C, according to reaction 3.5 (Ali and Sajadi, 2011; Kolta and Askar, 1975). It can also be assumed that part of the mass loss (about 5 %) at 562 °C was due to this decomposition, corresponding 9 % this compound in SS sample.

$$Sn(SO_4)_{2(s)} \rightarrow SnO_{2(s)} + 2SO_{3(g)} \qquad \textit{Eq. 3.5}$$

The decomposition of $PbSO_4$ took place at probably 730 ºC, according to reaction 3.6 (Ali and Sajadi, 2011; Kolta and Askar, 1975). In agreement with the mass loss, it is estimated that the sample contained around 23 % of this compound. This datum confirms the result obtained in the XRD analysis and the Pb obtained in the XRF analysis.

$$PbSO_{4(s)} \rightarrow PbO_{(s)} + SO_{3(g)} \qquad \textit{Eq. 3.6}$$

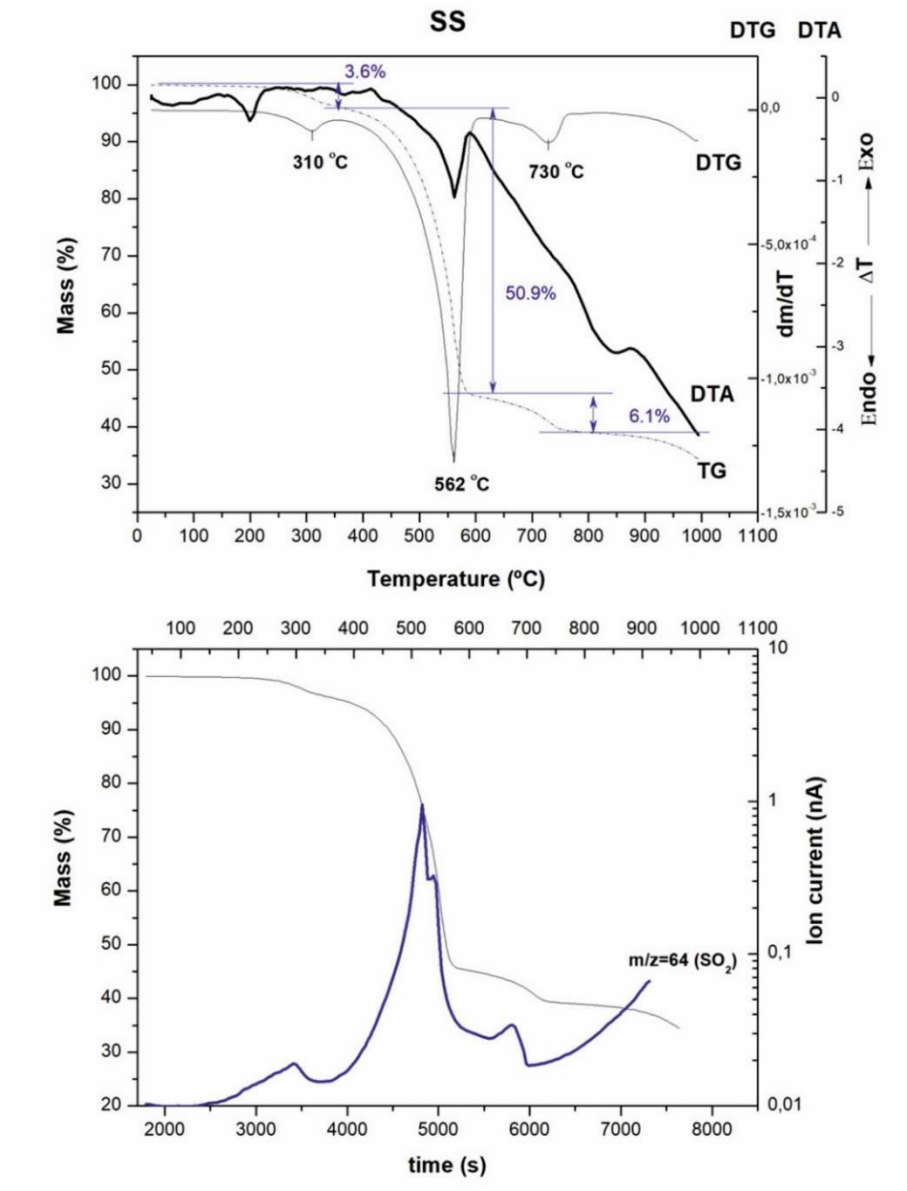

Figure 3.4. *TG-DTG-DTA curve and gases detected in the SS.*

Scanning electron microscopy (SEM)

The SEM analysis performs a visual study of the surface of the residue, which can help to the identify pollutant or unknown particles, thus providing information about the interactions between the phases present in the material. In addition, this technique is used for the determination of the size, texture, and morphology of the particles in order to understand the micro-properties of the material. The data obtained in the SEM and EDS analyses of the SS sample are shown in Fig. 3.5.

The sample presents an agglomerated morphology formed by fine particles, according to the granulometric analysis. The main composition determined by EDS is similar to that obtained in the

XRF results, in which the sample was mainly composed of Se, Pb, Hg and S. Due to their amorphous morphology, it was difficult to identify the compounds that are presented in the fine fraction. However, it was possible to identify large particles (point 1, Fig. 3.5), which had a high content of Pb, S and O, in agreement with the EDS spectra. Their composition and prismatic habit suggest that these particles are composed of lead sulphate (anglesite), with a size between 1 and 50 μm. Furthermore, the experimental mass ratio Pb/S is 6.17, which is in agreement with the theoretical ratio of anglesite (Pb/S = 6.18), within of experimental uncertainties (≤ 10 %). This result agrees with the previous results that one of the mineral phases found in the sample was anglesite ($PbSO_4$).

Dark grey particles were also detected (point 2, Fig. 3.5), with a Si/O mass ratio analogous to quartz (SiO_2), but its characteristic crystalline habit was not observed. The sample present around 0.2 % of this compound, proving the presence of Si in the sample.

In addition, it was identified small particles of metallic Se (point 3, Fig. 3.5), which presented a granular shape with a size between 2 and 5 μm. These results are in line with those obtained in the XRD analysis. Moreover, medium-sized particles were found (point 4, Fig. 3.5), whose S and Cu proportion was like that of covellite (CuS). The sample contained less than 1 % of this compound. It can also be seen that its texture was granular, with a size of around 20 μm. This result confirms the presence of Cu in the sample, in agreement with the data obtained in the XRF analysis.

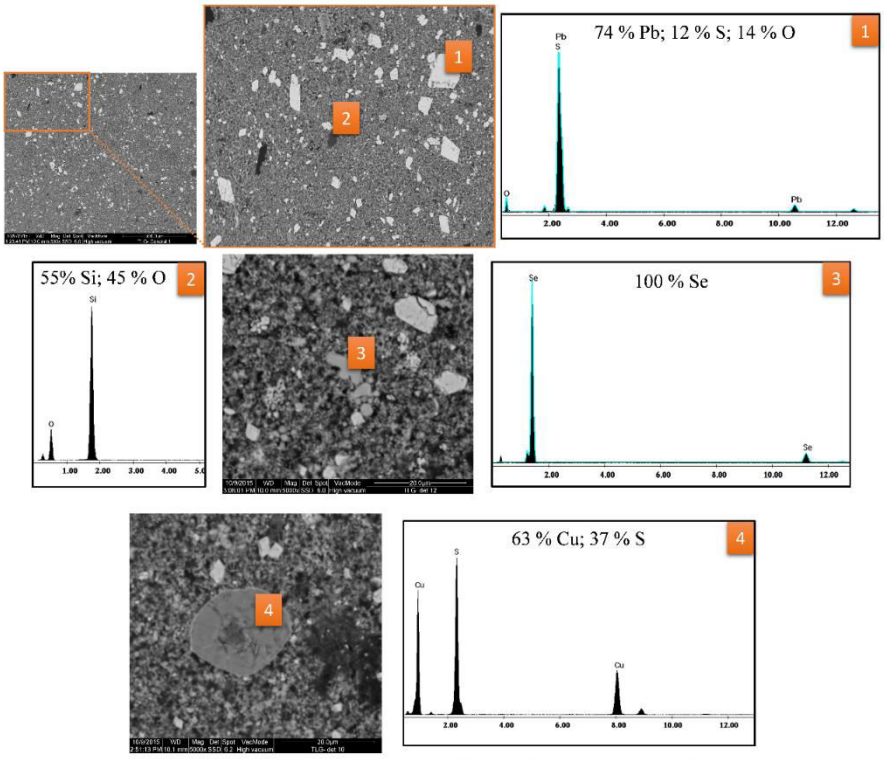

Elements	Cl	Cu	Ge	Hg	I	O	Pb	S	Se
% Wt	0.9	0.7	0.5	11	2.4	10	22	7.4	45

Figure 3.5. *Scanning electron micrograph of SS particles. The table also shows the general composition determined by EDS from the image located at the top left.*

The secondary electron image of the SS region and X-ray mapping of principal elements (Se, Pb, S, Hg, As, Cu, Sn and Cd) present in the sample are shown in Fig S3.2 (see, supplementary material Annex I.1). Se, Hg, As, Sn and Cd were distributed throughout the matrix. It is observed that there are regions in which Pb, and S are coincident, proving the existence of a $PbSO_4$ phase. Moreover, there were areas identified in which Cu and S were coincident, confirming the presence of CuS previously found in the SEM analysis.

Leaching test

A UNE leaching test (CEN: European Committee for Standardization, 2002a) was carried out, according to the RD 1481/2001 of 27 December, which regulates the disposal of waste by landfill, in agreement with the provisions of Directive 1999/31/EC on landfills. Table 3.1 shows the results obtained and the threshold concentration for non-hazardous material and hazardous material, expressed in mg of element leached per kg of original material. The transfer coefficients (η) are also shown, which represent the fraction of an element (%) that has been transferred into the liquid.

The SS leached a concentration (C_{SS}) of As, Cd, Cu, S, Pb, Sb and Zn that exceeded the thresholds established for their disposal as non-hazardous material in a controlled landfill. Moreover, the SS matrix leached 99 % As, 96 % S, 63 % Cd, 53 % Cu and 43 % Zn, whereas the Pb leached was below 0.01. The transfer into the solution of sulphur (as anion SO_4^{2-}) is much higher than some heavy metals (e.g., Pb presents a transfer very low, around 0.01%). This is due to metals such as Pb, Sn, Fe, etc., which form very "reactive" chemical species with a high tendency to be bound onto the solid material. The amount of each metal precipitated will depend on its mobility into the leaching solution. These results are in line with other studies where metals, such as Pb, present a low mobility in water (Caruso et al., 2008; Król et al., 2020; S.M. Pérez-Moreno et al., 2018).

A leaching test determined that this waste is likely to produce leachates with high contents of pollutants, which could be harmful to human health and the environment in the case of their disposal by landfill. Therefore, other alternatives must be sought, which focus on obtaining not only health and environmental benefits, but also economic solutions.

***Table 3.1**. UNE test results for the samples.*

Element	C_{SS} (mg/kg)	η_{SS} (%)	C_{SC} (mg/kg)	η_{SC} (%)	Threshold Level Non-Hazardous Material (mg/kg)	Threshold Level Hazardous Material (mg/kg)
As	1579	99	222	$2.6 \cdot 10^{-1}$	2	25
Ba	< 0.02	-	< 0.02	-	100	300
Cd	41.7	63	1410	29	1	5
Co	0.19	10	1.2	6	-	-
Cr	2.3	1.9	< 0.02	-	10	70
Cu	1525	53	11093	16	50	100
Fe	295	44	0.4	$3.9 \cdot 10^{-3}$	-	-
Mo	2.93	6.2	1.1	$5.6 \cdot 10^{-2}$	10	30
Ni	4.39	20	7.1	11	10	40
Pb	19	$9.1 \cdot 10^{-3}$	20	$5.2 \cdot 10^{-3}$	10	50
S	60160	96	12880	21	20000	50000
Sb	2.7	2.4	5.7	$2.7 \cdot 10^{-1}$	0.7	5
Se	< 0.02	-	0.4	$1.3 \cdot 10^{-1}$	0.5	7
Sn	12.4	$3.5 \cdot 10^{-2}$	< 0.01	-	-	-
Tl	2.4	17	114	11	-	-
Zn	205	43	14594	85	50	200

3.1.3.1.2 SC characterization

Granulometry

The particle size distribution (% volume) obtained for SC is compiled in Table S3.1. The SC sample is composed of a high concentration of "silt" particles (62 ± 3 %), followed by a proportion of "clay"

particles (34 ± 3 %) and a low content of "sand" particles (4.6 ± 1.5 %), presenting a multimodal size distribution with two maximums at 4 and 30 μm (Fig. 3.2a). The second maximum could be also linked to the hydro-cyclones efficiency, which could not be 100 %, thus coarse particles may be found in this waste.

The Fig. 3.2b shows the cumulative volume particles size distribution obtained for SC, in which is observed that the median particles size distribution (d_{50}) is about 6.5 μm and d_{90} on 42 μm. As was previously mentioned, the fine particles (especially those between 8–40 μm), are very beneficial for construction materials manufacturing, since by controlling the size particle of the cement components can be also optimized some of its properties related to the setting, hardening and curing, as the compressive strength or permeability (Al-Jabri et al., 2011; Hu and Gao, 2008; Murari et al., 2014; Wang et al., 2005). In addition, the recovery by hydrometallurgy route can be also favoured due to the high reactivity of fine particles, lower than 40 μm (greater specific area) (Hansen et al., 2005; Khalid et al., 2019a).

Elemental composition

The average composition of the major and trace elements for SC is shown in Fig. 3.3. The SC sample contained Pb (38 ± 1 %) as the major element, and in lower proportion Bi (13.6 ± 0.4 %), As (8.5 ± 0.3 %), Cu (6.7 ± 0.9 %), S (6.1 ± 0.1 %), Zn (1.7 ± 0.1 %) and Sn (1.3 ± 0.2 %). Other elements, such as Ag, K, Fe and Si, were found in a proportion below 1 %. Furthermore, the sample presented Cd, Mo, Sb and Tl (5000–2000 ppm), and Te, Ni, Ge, and Cr (200–50 ppm) as their main trace elements.

The Cu present in this waste came from the converter furnace's off-gases, which carry substantial levels of dust, composing particles of unreacted concentrate and droplets of matte/slag. These dusts generally contain 20–40 % mass Cu at the converters output (Schlesinger et al., 2011). Consequently, most of these dusts were recovered in the electrostatic filters and the hydro-cyclones and then they were recycled in the FF, returning around 80 % Cu. On the other hand, the fine dust (SC) contained a low Cu concentration and was rich in impurities, such as Pb, As, Bi and Zn, which were volatilized in the smelting process and precipitated as the gases cool down (Montenegro et al., 2013; Morales et al., 2010), in agreement with the results obtained.

Mineralogy

From the SC diffractogram (Fig. S3.1, Annex I.1), the anglesite (32 % $PbSO_4$) was the only mineral phase identified. Lead sulphate was formed during the condensation of Pb volatilized with $SO_2 + O_2$ by reaction 3.2 (Balladares et al., 2014; S.M. Pérez-Moreno et al., 2018; Pérez et al., 2019). In

agreement with the literature consulted (Balladares et al., 2014; Montenegro et al., 2013; Schlesinger et al., 2011) and the XRF analysis, other crystalline phases should be identified, but it should be noted the waste is a sludge composed of fine particles of converted dust come from hydro-cyclones, in which the most oxides react with diluted sulphuric acid solution becoming in sulphates, that they are not detected by XRD.

Furthermore, SC had a high content of XRD-amorphous phase (about 68 %). The XRF analysis showed a high concentration of As, Bi, Cu and Sn, but no mineral phases of these were identified by XRD, suggesting this fact that they are found in the called amorphous phase, which could contain these elements either as a poorly crystalline phase or other microcrystalline phases, which cannot be detected by the equipment. The formation of a large amorphous fraction can be due to a short cooling time in the gas cleaning system (Balladares et al., 2014; González et al., 2017).

Thermogravimetric analysis

In Fig. 3.6, the DTA curve reveals that the most thermal events were endothermic and indicated the decomposition of chemical species contained in the matrix. The SC sample had seven thermal events, which occurred at 108 ºC, 290 ºC, 415 ºC, 446 ºC, 563 ºC, 660 ºC and 782 ºC. Water was detected in the first and second events, which were due to a loss of crystallised water of some hydrated compound. The third thermal event was exothermic, which are probably associated with some chemical and physical thermal reaction types (Földvári, 2011). The other thermal events were due to the decomposition of sulphates, corroborated by the detection of SO_2 in the ICP-MS system.

According to the decomposition temperature and the total loss of water, the hydrated compound could be a copper (II) sulphate pentahydrate ($CuSO_4 \cdot 5H_2O$) which is dehydrated at 108 ºC and 290 ºC, according to reaction 3.7 and 3.8, and then is decomposed at 446 ºC, following reactions 3.9. The literature consulted (Földvári, 2011; Martínez Roca, 2007; Mu and Perlmutter, 1981; Tagawa, 1984)

confirms that the dehydrated copper sulphate gives three thermal events, which were detected around 75 °C, 110 °C and 250 °C, however, the water loss was detected in the first two thermal events in the range 50–300 ºC, which can be due to the interactions between the different substances that compose the matrix and/or experimental conditions (heating rate). Considering the mass loss, it is estimated that the sample contained around 6 % of this compound. However, Cu concentration in the matrix was much higher (about 7 %), meaning that Cu was forming other compounds.

$$CuSO_4 \cdot 5H_2O_{(s)} \rightarrow CuSO_4 \cdot H_2O_{(s)} + 4H_2O_{(g)} \quad (108\ ºC) \qquad \textit{Eq. 3.7}$$

$$CuSO_4 \cdot H_2O_{(s)} \rightarrow CuSO_{4(s)} + H_2O_{(g)} \quad (290\ ºC) \qquad \textit{Eq. 3.8}$$

$$CuSO_{4(s)} \rightarrow CuO_{(s)} + SO_{3(g)} \quad (446\ ºC) \qquad \textit{Eq. 3.9}$$

The thermal event at 415 ºC probably corresponds to thermal oxidation of CuS to Cu_2S, according to reaction 3.10 (Dunn and Muzenda, 2001; Földvári, 2011). However, it was not possible to calculate the CuS concentration in the sample due to SO_2 liberated in this event detected together with the SO_2 generated in the $CuSO_4$ decomposition. Moreover, the loss mass was not significant (see curve TG, Fig 3.6).

$$2CuS_{(s)} + O_{2(g)} \rightarrow Cu_2S_{(s)} + SO_{2(g)} \qquad \textit{Eq. 3.10}$$

The decomposition of iron (II) sulphate ($FeSO_4$) occurred at 563ºC (Földvári, 2011; Siriwardane et al., 1999). According to the amount of mass lost, it was calculated that the sample contained around 3 % of this compound. This result confirms that the Fe concentration obtained in the XRF analysis (around 1 %) is in line with the content of $FeSO_4$ in the sample.

$$FeSO_{4(s)} \rightarrow FeO_{(s)} + SO_{3(g)} \qquad \textit{Eq. 3.11}$$

The mass loss at 660 ºC corresponds to the decomposition of $ZnSO_4$, according to reaction 3.12 (Kolta and Askar, 1975; Mu and Perlmutter, 1981; Siriwardane et al., 1999). Considering the mass loss, it is estimated that the sample had about 5 % $ZnSO_4$. This datum is in line with the percentage of Zn found in the XRF analysis (around 2 %).

$$ZnSO_{4(s)} \rightarrow ZnO_{(s)} + SO_{3(g)} \qquad \textit{Eq. 3.12}$$

The mass loss produced at 782 ºC is associated with the thermal decomposition of anglesite ($PbSO_4$), according to reaction 3.6 (Ali and Sajadi, 2011; Kolta and Askar, 1975). The percent mass loss, about 8 %, suggests that the sample contained 30 % anglesite. This result is in line with those obtained in the XRD and XRF analyses.

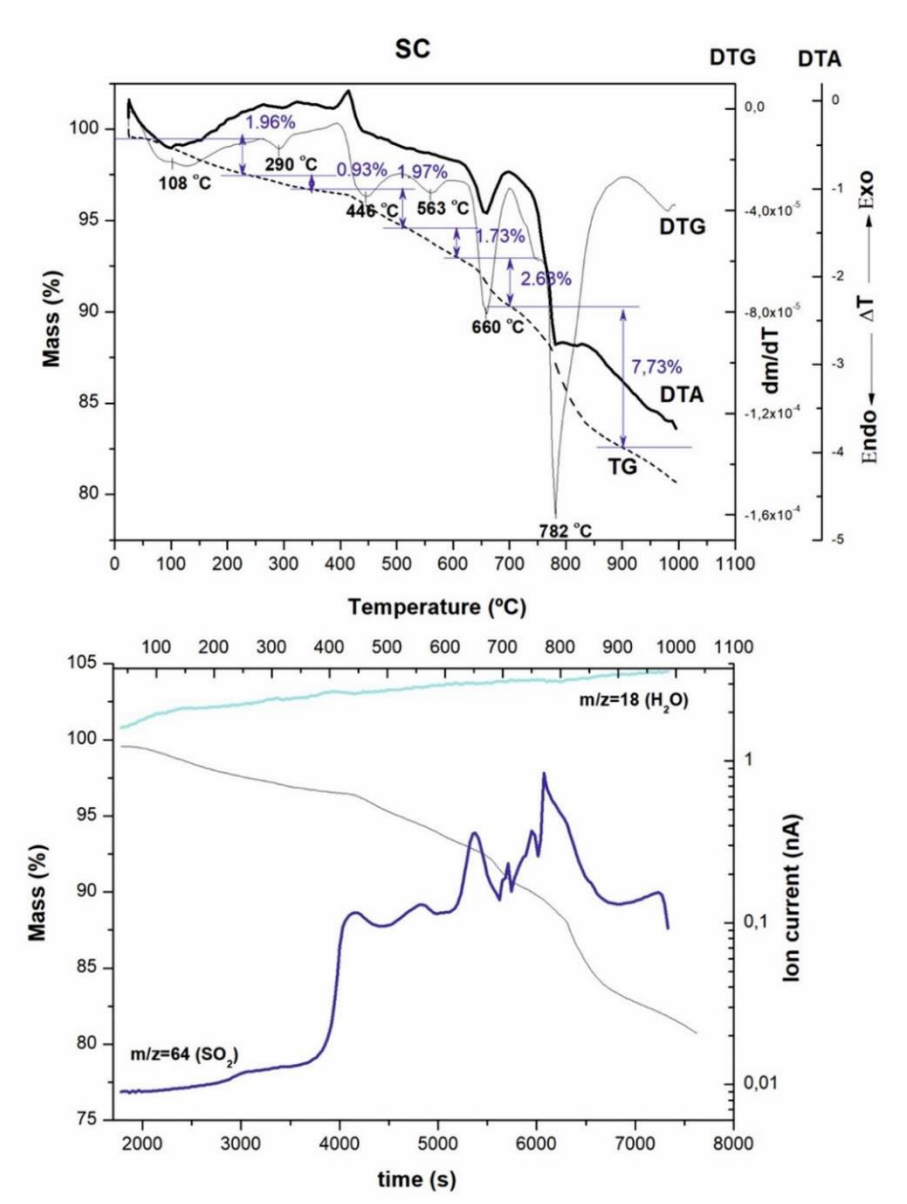

Figure 3.6. *TG-DTG-DTA curve and gases detected in the SC.*

Scanning electron microscopy

The SEM and EDS analyses of SC determined that sample was composed of agglomerates of very fine particles with the inclusion of spherical particles with size between 20–50 μm (see, Fig. 3.7), in agreement with the granulometry results. These spherical particles (point 1, Fig. 3.7) had a high concentration of Cu and S (around 74 % and 23 %, respectively) according to the EDS spectra. Their composition and morphology suggest that these particles are similar to chalcocite in composition (Cu_2S). This chemical species was not detected in the thermal analysis since the decomposition of Cu_2S occurs at a higher temperature (> 1100 ºC). Moreover, the presence of these particles and the

CuS, detected in the thermal analysis, confirm that Cu was found as sulphides and sulphates in this sludge (Balladares et al., 2014; González et al., 2017). According to the results obtained in the TGA analysis, and considering the Cu concentration, it is estimated that the SC contained about 4 % of this compound. Moreover, it was proved that bright particles (point 2, Fig. 3.7) were composed by Pb, S and O in the same proportion that to the one found in lead sulphates (anglesite). This mineral phase was also identified in the XRD and TGA analyses. This mineral showed several crystalline habits; in this case, it can be observed that a small crystal with a laminar texture is involved. The composition of the grey areas (area 3, Fig. 3.7) was analogous to the general composition determined by the EDS and XRF analyses (table, Fig. 3.7), thus that it can be asserted that the matrix was composed of fine particle aggregates.

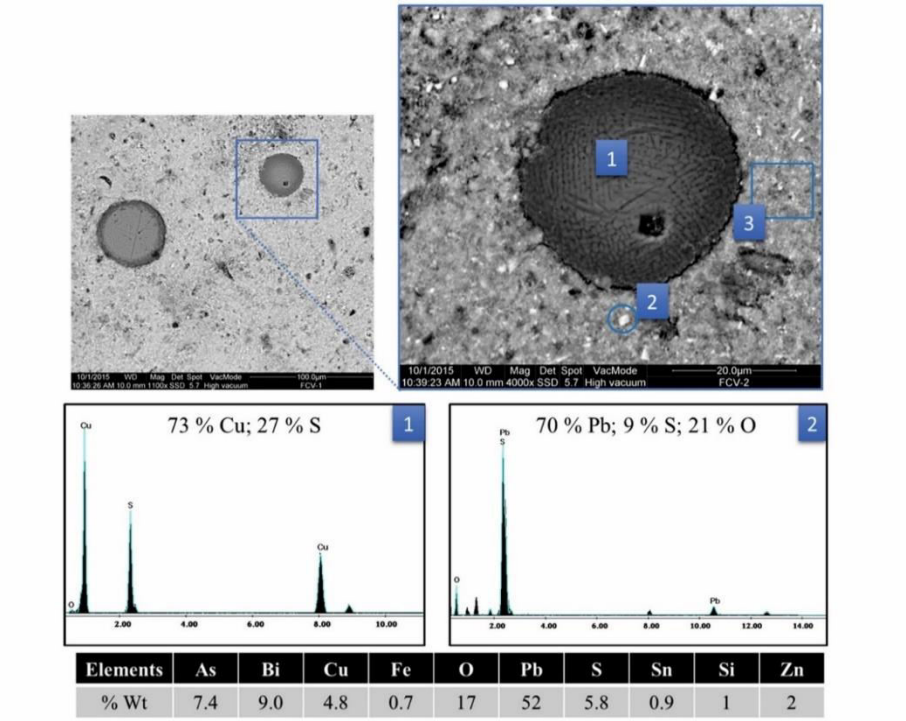

Elements	As	Bi	Cu	Fe	O	Pb	S	Sn	Si	Zn
% Wt	7.4	9.0	4.8	0.7	17	52	5.8	0.9	1	2

Figure 3.7. *Scanning electron micrograph of SC particles and general composition determined by EDS.*

The distribution of principal elements (Pb, Bi, As, Cu, S, Zn, Sn and Fe) present in the sample is shown in Fig. S3.3, Annex I.1, which includes a secondary electron image and X-ray mapping of a SC region. As can be observed, Pb, Bi, As, S, and Sn are uniformly distributed in the sample. Moreover, this image confirms the presence of As and Bi in the amorphous phase, which was not detected in the XRD or SEM analyses. Both elements could be present as oxide (Balladares et al., 2014; Chen et al., 2012; Morales et al., 2010)

The mapping reveals regions with a high content of sulphur and copper, which corresponds to the spherical particles previously identified as Cu_2S in the SEM analysis. Moreover, there were sections in which sulphur and zinc coincided, confirming the presence of $ZnSO_4$, previously found in the results of the TGA analysis. Likewise, there were also areas where iron and sulphur were coincident, confirming the presence of $FeSO_4$, which was also identified in the TGA analysis.

Leaching

The SC sample leached a concentration (C_{SC}) of As, Cd, Cu, Pb, Sb and Zn above the limit established for its landfill disposal as a non-hazardous material (Table 3.1). This matrix leached 85 % Zn, 29 % Cd, 21 % S and 16 % Cu, whereas the amount of Sb and Pb leached were below 1 % and 0.01 %, respectively. This waste tends to produce leachates with a high content of pollutants, consequently the residue must be stabilized prior to its disposal by landfill or its new application, suggesting the study of alternative treatments to develop health, environmental and economic benefits.

3.1.3.2 Discussion

These wastes (SS and SC) presented particles size with a median (d_{50}) around 10 µm, which can be highly beneficial in the manufacturing of construction materials (Al-Jabri et al., 2011; Murari et al., 2014; Zhao et al., 2014)and can also favour the recovery of some metals during the hydrometallurgy route due to the high reactivity of the fine particles in view of their greater specific area (Khalid et al., 2019b; Wang et al., 2005).

The elemental composition confirms that both residues are different even though both contain Pb as one of their major elements. The high Pb concentration is due to the fact that around 50 % of Pb, which is present in copper ore concentrate, is volatilized during the FF and CF processes (Schlesinger et al., 2011; Wang et al., 2017). Anglesite ($PbSO_4$) is the dominant mineral phase present in both wastes (see, Fig. S3.1 Annex I), at 27 % and 33 % for SS and SC, respectively, in agreement with the high contents of lead in these samples. The SEM images (see, Fig. 5 and 7) reveal that the size particle of $PbSO_4$ (anglesite) is different, which is probably associated with different formation mechanisms. The size of $PbSO_4$ particles in SS is larger than in SC. The small lead sulphate particles are apparently formed throughout the fast cooling from CF off-gases. On the other hand, the large particles are probably formed when the remaining particles of PbO from off-gases of FF and CF react with sulphuric acid diluted in the scrubber section.

The main difference between the two wastes is the high content of metallic selenium (around 35 % Se) in SS, which probably comes from CF gases, since around 25 % of Se is volatilized in CF, whereas 5 % is volatilized in FF (Montenegro et al., 2013; Schlesinger et al., 2011).

Both wastes contain high concentrations of XRD-amorphous phase, approximately 40 % in SS and 68 % in SC. Some compounds present in the XRD-amorphous phase of SS and SC were identified by thermogravimetric and SEM-EDS analysis. SC contains copper, iron, lead and zinc sulphates ($CuSO_4 \cdot 5H_2O$, $FeSO_4$, and $ZnSO_4$) formed from the oxides during the cooling and cleaning steps of the gas. Copper sulphurs (CuS and Cu_2S), were also found, probably coming from droplets of matte carried in the off-gas that solidified unreacted during cooling gas. The high Cu concentration in SC samples demonstrates that 80 % of the Cu present in the converter dusts is recovered by the hydro-cyclones. In addition, the amorphous material of SS is composed of mercury and tin sulphates (Hg_2SO_4, $HgSO_4$ and $Sn(SO_4)_2$), which probably is produced the reaction of both Sn and Hg oxides with diluted sulphuric acid in the scrubber section. Finally, the fine particles of CuS found in SEM-EDS analysis have the same origin as mentioned above. The SiO_2 was also found in the SS sample, which likely comes from small particles of unreacted flux.

Another difference between these two residues is the concentration of impurities such as As, Bi, Cd, Sb and Zn. The low concentration of impurities such as As, Bi and Sb in SS was found due to the most of them are removed in the electrostatic filters before the gases are sent to the scrubbing section. On the other hand, SC has a high content of As, Bi, Cd, Sb and Zn, since this residue is formed by fine particles coming from converters dust, since it contains the major impurities levels. The SC sample contains a high concentration of As and Bi (around 10 %), however, no compound these elements were found neither by XRD, SEM or thermal analysis. Considering the consulted literature, these elements could be as oxides (As_2O_3 and Bi_2O_3) (Chen et al., 2012; Lucheva et al., 2017; Montenegro et al., 2013; Okanigbe et al., 2017; Schlesinger et al., 2011). Furthermore, the SS sample present around 2 % Ge which could be as GeO and/or GeS_2 (Font et al., 2011), but these compounds were also not detected by the previous characterization techniques.

A summary of the physicochemical characterization performed in both wastes (SS and SC) is shown in Table 3.2.

Table 3.2 *Summary of the components found in the SS and SC samples and the granulometry analysis. N.I= Not Identified.*

	SS			***SC***		
Granulometry	clay 11 Element (%)	silt 87 Compound	sand 2 Mineral	clay 34 Element (%)	silt 62 Compound	sand 4 Mineral
As	0.16	N.I	N.I	8.5	N.I	N.I
Bi	0.21	N.I	N.I	14	N.I	N.I
Cu	0.30	CuS (0.5 %)	N.I	7.0	$CuSO_4 \cdot 5H_2O$ (6 %) CuS* Cu_2S (4 %)	N.I
Fe	0.07	N.I	N.I	1.0	$FeSO_4$ (3 %)	N.I
Hg	8.0	Hg_2SO_4 (5%) $HgSO_4$ (7%)	N.I	< 0.01	N.I	N.I
Pb	21	N.I	$PbSO_4$ (27 %)	38	N.I	$PbSO_4$ (32 %)
Se	35	N.I	Se (34 %)	0.03	N.I	N.I
Si	0.13	SiO_2 (0.2 %)	N.I	0.42	N.I	N.I
Sn	3.5	$Sn(SO_4)_2$ (9%)	N.I	1.3	N.I	N.I
Zn	0.05	N.I	N.I	1.7	$ZnSO_4$ (5 %)	N.I

**No possible to calculate the CuS concentration in SS due to SO_2 liberated in this event is detected together with the SO_2 generated in the $CuSO_4$ decomposition.*

The content of valuable metals in both wastes (SC and SS) along with the increasing cost of waste disposal on controlled landfill, increasingly restrictive legislation and their potential risk to human health and the environment, suggest that efforts should be focused on valorising these wastes. Taking into account the physical, chemical and mineralogy characterization and the consulted bibliographic, these residues could be an important secondary source of Se and Pb (Hait et al., 2009; Kilic et al., 2013; Montenegro et al., 2013; Morales et al., 2010; Wang et al., 2016; Xing et al., 2018). The recovery of these as metals with 99.99 % purity is proposed, in order to make higher profits and thus contributing to the circular economy of these elements in the copper production process.

3.1.3.3 Proposal for their valorisation

Currently, there are not any companies which use these kinds of wastes as a secondary source of Se and Pb. Copper anode slime is the main source of selenium since there are no mineral reserves. There are several processes that nowadays are being applied at copper refineries whose advantages and disadvantages are summarised in Table S3.2, Annex I.1 (Hait et al., 2009; Hoffmann, 1989; Hoffmann and King, 2000; Kilic et al., 2013; Wang et al., 2016; Xiao et al., 2019). On the other hand, Pb is usually extracted together with Zn from the dust generated in an electric furnace, which

is one of the main secondary sources of Pb (Lin et al., 2017; Mocellin et al., 2017; Pérez-Moreno, 2018; Ruşen et al., 2008; Shen and Forssberg, 2003).

The metal global demand will increase in the next decades, including Pb and Se, due to using wind, solar, and energy storage batteries and new technologies (Öhrlund, 2012; The World Bank, 2017). Nowadays, selenium is marketed as selenium metal, with different refined grades, or selenium dioxide. The metal Se price is around $4.4 \cdot 10^4$ \$/t (U.S. Geological Survey, 2019), being above the copper ($6.2 \cdot 10^3$ \$/t). The Pb is consumed as lead metal with a price around $1.9 \cdot 10^3$ \$/t, depending of refined grade (LME: London Metal Exchange, 2019; U.S. Geological Survey, 2019). Therefore, the recovery of Se and Pb involves an associated value, which can contribute considerably to the economic viability of the activity which will mainly depend on manufacturing cost.

There are different routes for the metal recovery, as such pyrometallurgy, hydrometallurgy or a combination of both. The recovery path will depend on many factors, such as the physical, chemical, and mineralogical characteristics of wastes, their quantity generated (40 t/y of SS and 430 t/y of SC), the production costs and potential environmental impacts. In the present study, it has been proposed to apply the pyro-hydrometallurgical route for recovery Se and Pb, based on the chemical composition and physicochemical properties of the wastes, which could satisfy the requirements of smelting for the suitable use of these residues as a secondary source in the appropriate environmental conditions.

The process would begin with the recovery of selenium from SS using a roasting process (Hait et al., 2009; Hoffmann, 1989; Hoffmann and King, 2000; Svens, 1985), being separated due to the existence of different boiling points in relation to the other components of the waste, as was verified by the TGA analysis. The process involves the roasting of SS at 700 ºC and then, a cooling process in two steps. In the first cooling step, the mercury species would be removed from the off-gases using a condenser (Lee et al., 2017), in which the gases are cooled down to around 300 ºC (below to evaporation point of Hg), obtaining a solid residue from the process. In the second step, the metallic Se is recovered at a lower temperature; lower to Se melting point, 221 ºC, as indicated in DTA curve. The flowchart proposed for the valorisation of these wastes is shown in Fig 3.8.

The process would continue with the blending of the calcined Pb-rich residue with SC to recover lead by hydrometallurgical route (González et al., 2017; Orhan, 2005; Ruşen et al., 2008; Xing et al., 2018). The stages would begin with Pb extraction using a sodium hydroxide solution (NaOH), since sulphate lead is dissolved easily and selectively in that leaching media (BăDănoiu et al., 2014; Şahin and Erdem, 2015). Then, the obtained solution would be separate from the solid residue, which would be mainly compose of Cu, As, Bi, and other elements, for instance, Ge. Afterwards, it is proposed

the recovery of metallic Pb from the solution through a cementation process, by adding Zn powder, and the final solution could be recycled to the leaching process. This practice is widely used in another industrial hydrometallurgy processes (Angelov and Groudev, 2002; Gouvea and Morais, 2007; Şahin and Erdem, 2015).

Currently, the generation of these two wastes imply the management of a total of 450 t/y of hazardous material. The proposed process could produce about 13.6 t/y of metallic Se and around 171 t/y of metallic Pb with high purity, minimizing one half the amount of these wastes. This fact would reduce the management waste costs and, in addition, could result in a significant revenue gain, as a result of the sale of these metals that it could reach more than $9.0 \cdot 10^5$ *$/y*. This proposal could be feasible, however, provided it is thoroughly studied and quantified, with the aim of evaluating their technical, environmental, and economic viability.

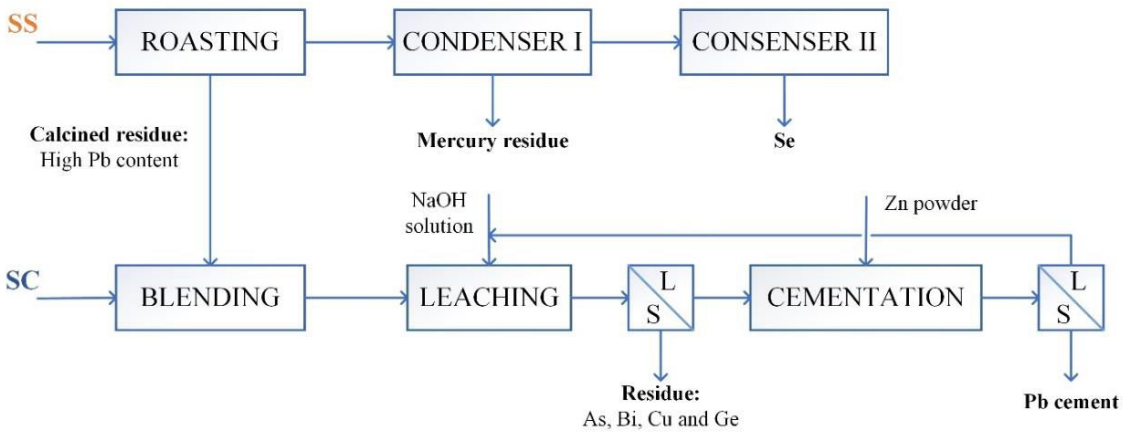

Figure 3.8. *Flowchart of the SS and SC treatment proposed.*

3.1.4 Conclusions

The present work is focused on finding and designing the most appropriate application and treatment for the valorisation of two wastes coming from the gas cleaning system of the smelting and converting furnaces belonging to a pyrometallurgical plant. For that, a deep physicochemical characterization of them was previously carried out. From this study, it is concluded that:

a. Both wastes are mainly composed of fine particles (< 10 μm), which is highly beneficial in the proposed hydrometallurgy process.
b. SS and SC wastes have a high Pb content, around 21 % and 38 %, respectively, which is mainly present as anglesite ($PbSO_4$).

c. SS also contains a high Se concentration (~ 34 %) as metallic selenium, and, in addition, this sludge presents high levels of Hg (~ 8 %) and Sn (~ 4 %) as sulphates (Hg_2SO_4, $HgSO_4$ and $Sn(SO_4)_2$, respectively).
d. SC contains Cu (~ 7 %), which is found as CuS, Cu_2S and $CuSO_4{\cdot}5H_2O$. Moreover, SC presents a high content of As and Bi (~ 10 %), but no compounds of these elements were identified.
e. Both wastes are considered hazardous materials, since they can produce leachates with high concentrations of metals (As, Cd, Cu, S and Zn).
f. According to the consulted literature, and composition and physicochemical properties found for these wastes, the SS could be an important secondary source of selenium, while both sludges could be used as a significant secondary source of lead. Se-Pb recovery can have remarkable economic and environmental benefits in contrast to their disposal in landfill.
g. The proposal for Se-Pb recovery consist in Se extraction from SS by using a roasting process, and then the calcined Pb-rich residue is blended with SC to recover Pb by hydrometallurgical route. The roasting process proposal could be an attractive option for Se recovery since roasting processes are widely used in primary copper refineries. On the other hand, Pb recovery by hydrometallurgy route would be the best option, considering that is one of the best alternative technology environmentally friendly.
h. In this sense, more researches are needed in order to evaluate the proposes alternative process to reuse these residues as a secondary source of Se and Pb.

SUBCHAPTER 3.2

ARSENIC REMOVAL PROCEDURE FOR THE ELECTROLYTE FROM A HYDRO-PYROMETALLURGICAL COMPLEX

3.2 ARSENIC REMOVAL PROCEDURE FOR THE ELECTROLYTE FROM A HYDRO-PYROMETALLURGICAL COMPLEX

D.C. Paz-Gómez, S.M. Pérez-Moreno, M.J. Gázquez, J.L. Guerrero, I. Ruiz-Oria, G. Ríos, J.P. Bolívar.

Chemosphere 281 (2021) 130651

Abstract

Commercial copper (Cu) is obtained by a hydro-pyrometallurgical process, where the Cu anodes obtained in the furnaces (Cu > 99.5%) are enriched up to 99.99 % in "cathodes" by electrorefining at an electrolysis plant. During this process, some impurities accumulate in the electrolyte, mainly arsenic (As), which decrease the quality of the Cu cathode. For this reason, the electrolyte is sent to an electrolyte cleaning plant (ECP) for its purification. Electrolyte sludge (ES) is produced in the last stage of purification and is recirculated back to the furnace due to the high Cu content. This recirculation involves a severe problem of As accumulation in the industrial process. The objective of this work was to develop a procedure to fully dissolve the ES, removing the As and recovering its Cu content. The ES dissolution process was optimised (dissolution efficiency > 99%) in H_2SO_4 (1.4 M)/HNO3 (1.8 M) medium using a 1:20 g mL^{-1} solid-to-liquid ratio. As was removed from the ES solution by its precipitation as iron (III) arsenate, with high efficiency (more than 70%). After As removal, the Cu can be precipitated as copper sulphate, which is used in several applications.

Graphical abstract

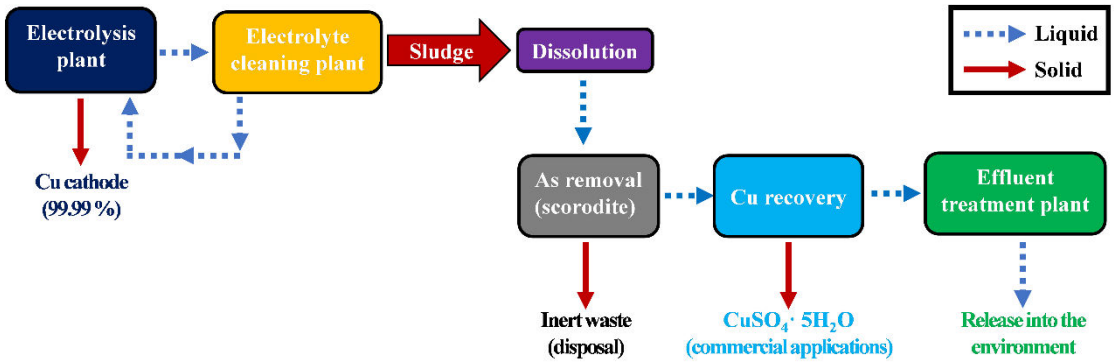

Keywords: Electrolyte sludge; Ferric arsenate; Scorodite; Arsenic removal; Copper–arsenic solution

3.2.1 Introduction

The demand for copper (Cu) minerals has increased quickly over the last 50 years, and it is expected to keep growing due to the essential role of Cu in modern technologies. Worldwide refined Cu production reached 24 Mt in 2019, and it involves a large amount of waste and wastewater generation (ICSG: International Copper Study Group, 2020). In recent decades, the manufacturing industry has tried to develop policies to reduce the environmental impact and to achieve sustained economic growth, following the current strategic lines aimed at ensuring the implementation and development of the "Circular Economy" through the efficient use of raw materials and residues. Therefore, policies on waste management must be directed apply the hierarchy established by normative: prevention, reduction, reuse, and recycle. A proper waste valorisation represents an excellent management alternative producing economic and environmental benefits. For this, industries have introduced effective resource management consisting of recycling, reusing, and valorisation of these ones, reducing the production cost and decreasing risks for the environment and human health (Khan et al., 2021, 2020; Liao et al., 2019).

Atlantic Copper S.L.U, located in Huelva (Spain), is one of the biggest manufacturers of ultrapure Cu cathodes (> 99.99% Cu) in Europe, producing more than $3 \cdot 10^5$ t y^{-1} (Atlantic Copper, 2017). During Cu electrorefining, the concentrations of the raw material impurities, such as As, Sb, Bi, Ni, etc., gradually increase in the electrolyte, which negatively affects the quality of the Cu cathode; therefore, the impurities must be removed. For this, a fraction of the electrolyte is continuously sent to an electrolyte cleaning plant (ECP) to reduce the level of impurities, especially As, and to recover a significant fraction of the Cu that is not electrodeposited in the cathode ("decopperising").

The electrolyte cleaning process involves three stages by electrowinning in liberator cells (Artzer et al., 2018; Wesstrom and Araujo, 2012). Firstly, the Cu concentration is reduced from 45 g L^{-1} to 25 g L^{-1}, providing a B-grade Cu cathode (> 99.97% Cu), which is commercialised. Secondly, the Cu concentration is further reduced to around 10 g L^{-1}. Finally, in the third step, the remaining Cu, and most of the As, is removed from the solution in the electrolyte sludge (ES). In the Huelva factory, about 1300 t of ES are produced annually. The final treated electrolyte is returned to the electrolyte tank for reuse.

Currently, the ES is sent to a flash smelting furnace (FSF) to recover its Cu content (≈ 60%), but this causes the accumulation of As during the industrial process, generating problems during liquid effluent treatment. Fig. 3.9 shows the procedure developed in this work for As-free Cu recovery, which consists of dissolving the ES by acid digestion, and then the As removal from the obtained dissolution (ES wastewater) by precipitation with iron as ferric arsenate. Finally, the As-free solution

may be used in two different ways: Cu is recovered as copper (II) sulphate pentahydrate ($CuSO_4 \cdot 5H_2O$) and returned to the industrial process or it is valorised in commercial applications, such as agriculture. On the other hand, the resulting industrial wastewater stream, with low pollutant content, can be sent to an effluent treatment plant (ETP) for final treatment before it is released into the environment. The novelty of the proposed procedure is the combination of different chemical processes (digestion, precipitation, and crystallisation) applied to the ES to achieve As removal and Cu recovery. Currently, this waste is a recirculating waste of the Cu metallurgy process, of which no treatment is known for the separation of both elements.

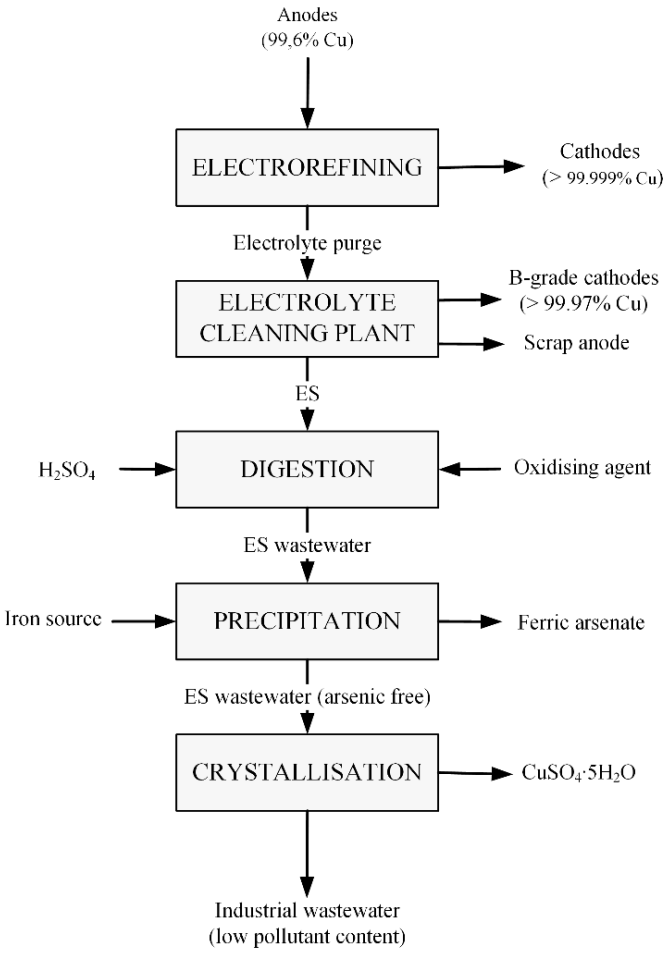

Figure 3.9. *Flowchart of the electrolyte sludge (ES) and the proposed treatment.*

There have been no previous studies describing As removal from ES. Most research has been focused on other co-products, such as slag, dust, or anode slime (Demopoulos, 2014; Min et al., 2015; Schwartz et al., 2017). In addition, there have been some investigations of As removal from waters for human consumption and/or industrial wastewater (Jain and Singh, 2012; Litter et al., 2010), and the methods used to reduce the As concentration in the solutions were precipitation, adsorption (Cao

et al., 2021; Chen et al., 2015; Hao et al., 2018), the use of ion exchange resins (Balaji et al., 2005; Lenoble et al., 2004), and the use of newly developed methods, such as electrocoagulation or membrane treatment (Nidheesh and Singh, 2017; Song et al., 2017; Zouboulis and Katsoyiannis, 2018). Nevertheless, the United States Environmental Protection Agency (EPA) designated As removal by co-precipitation with ferric ions in a liquid effluent as "the best demonstrated available technology (BDAT)" for As disposal (Rosengrant and Fargo, 1990). For that reason, this method has been the most researched in the last decades (Demopoulos, 2014; Fujita et al., 2008b; Le Berre et al., 2007; Schwartz et al., 2017; Zhang et al., 2019). The precipitation reaction can be expressed as the following:

$$4H_3AsO_{4(aq)} + 4FeSO_{4(aq)} + O_{2(g)} + 6H_2O_{(aq)} \leftrightarrow 4FeAsO_4 \cdot 2H_2O_{(s)} + 4H_2SO_{4\ (aq)} \qquad \textit{Eq. 3.13}$$

Considering the above facts, the central objective of this study was to remove the As from the dissolution of ES coming from the ECP, generating a final solution more suitable for recovering the dissolved copper sulphate. Firstly, ES dissolution tests were carried out. Then, the removal of As by precipitation with Fe was studied. The final solutions were analysed using various analytical techniques to determine the precipitation efficiency (PE) of the main elements, especially As and Cu, and the physical–chemical characteristics of the formed solids were studied.

3.2.2 Materials and methods

3.2.2.1 Materials

The ES employed in this research was collected from Atlantic Copper S.L.U in 2017. Six sampling campaigns were organised (one per week) with the aim of analysing the possible temporal variability in the characteristics of the ES. After collection, the samples were dried at 60 ºC to constant weight.

All iron reagents [$FeCl_3$, $Fe_2(SO_4)_3 \cdot 7H_2O$, $FeSO_4 \cdot 7H_2O$], arsenic reagent [$As_2O_5 \cdot 3H_2O$] and alkaline agents [$Ca(OH)_2$ and $Mg(OH)_2$] employed in this work were of analytical grade (purity > 95 %) and from Merck Company. The concentrations of the acids used were the following: 96 % H_2SO_4 and 65 % HNO_3. In addition, the oxygen used had a purity of > 99.5 %.

3.2.2.2 Experiments

3.2.2.2.1 Dissolution of the electrolyte sludge (ES)

The dissolution of the ES was performed in acid medium by using sulphuric acid (H_2SO_4). The influence of temperature, the solid-to-liquid ratio, and the type of oxidising agents (air, oxygen and

HNO_3) were studied. Firstly, the dissolution of ES was done applying a mixture of sulphuric acid (H_2SO_4) and nitric acid (HNO_3) solution, in which the solid-to-liquid ratio, molar concentration, temperature and reaction time, were changed and then the influence of using other oxidising agents (air and oxygen) was investigated.

The ES dissolution experiments with H_2SO_4 and HNO_3 were carried out in an uncovered reaction vessel with a volume of 1 L (see Fig. S3.4a). These experiments simulated different conditions: 1) solid-to-liquid ratios of 1:10 and 1:20 g mL^{-1} were used; 2) the H_2SO_4 and HNO_3 concentrations used ranged from 0.9 to 2.7 M and from 1.0 to 1.8 M, respectively; 3) the temperature and reaction time were 24, 50, and 80 ºC and 12 and 2.5 h, respectively. A summary of these experiments is shown in Table S3.3 of the supplementary material (Annex I.2), to note that the experiments with a solid-to-liquid ratio of 1:10 g mL^{-1} were not included in this table because the results obtained were not relevant. The solution was continuously agitated with a magnetic stirrer (500 rpm). Finally, the experimental solution was filtered to separate the obtained phases. The solid was rinsed with water and dried until a constant weight was obtained.

The experiments with air or O_2 were carried out in a 1 L reaction vessel (1 L beaker) covered with a lid with holes through which a thermocouple and air/O_2 channels were introduced (2 L min^{-1} and 8 L min^{-1}, respectively) (see Fig. S3.4b, Annex I.2). In the experiment with air, different concentrations (2, 4, 6, and 10 M) of a H_2SO_4 solution were used (see Table S3.3). When O_2 was used, the experiment was performed with a 2 M H_2SO_4 solution. In both experiments, the solution was heated to 80 ºC and continuously agitated with a magnetic stirrer at 500 rpm. Finally, the solution was filtered to separate the solid from the liquid phase. The solid phase was rinsed with water and dried at 60 ºC to constant weight.

The tests were codified as “X-Y-Z-W-R”, where “X” is the oxidising agent used to dissolve the sludge (N is nitric acid, O is oxygen, and A is air), “Y” represents the concentration of HNO_3 (M) or the gas flow of air or oxygen (in L min^{-1}), “Z” is the concentration of H_2SO_4 used, “W” is the time (h) and temperature (ºC) of the experiment (where A is 12 h and 24 ºC, B is 2.5 h and 50 ºC, and C is 2.5 h and 80 ºC), and “R” indicates if the sample was a replica. For example, N-1.6-1.8-A is a sample with HNO_3 as the oxidising agent (1.6 M) and the use of 1.8 M of H_2SO_4, with an experimental time of 12 h at 24 ºC, and A-2-4-C-R is a sample using air as the oxidising agent (2 L min^{-1}) and 4 M of H_2SO_4, with an experimental time of 2.5 h at 80 ºC, and it is a replicated sample.

3.2.2.2.2 .Arsenic removal

To study the elimination of As, two solutions were used for the experiments. One solution, named the artificial solution, contained 10 g L^{-1} of the As prepared in the laboratory using arsenic (V) oxide hydrate ($As_2O_5 \cdot 3H_2O$), and the second solution was obtained by fully dissolving the ES. In Table S3.4 of the supplementary material (Annex I.2), a summary of the experimental conditions for As removal is shown.

The experiments for As precipitation were carried out in three stages by gradually increasing the pH since protons are released during the formation of $FeAsO_4 \cdot 2H_2O$, which then decreases the pH and inhibits scorodite formation (see Eq. 3.13).The precipitation of $FeAsO_4 \cdot 2H_2O$ occurs at a pH of between 1.5 and 3.0, according to the literature consulted.(Droppert et al., 1996; Fujita et al., 2009a). In stage I, the Fe source was added, and the reaction proceeded for 3 h. The As precipitation reaction reaches equilibrium at a final pH that is lower than the initial pH. To favour the precipitation of As, the equilibrium (Eq. 3.13) should be moved to the right by decreasing the acidity (stage II). This is achieved by adding an alkaline agent up to a pH around 2.5, reaching newly the equilibrium (pH ≈ 1.5) after around 3 h. Then, the pH is increased to around 3 by another alkali addition (stage III), reaching a final pH of around 2 after equilibrium.

Arsenic removal using an artificial solution

Experiments with artificial solution focused on looking for the most suitable method for the synthesis of $FeAsO_4 \cdot 2H_2O$. In experiment E1-A, As removal with two compounds as Fe^{3+} sources [$FeCl_3$ and $Fe_2(SO_4)_3 \cdot 7H_2O$] and a As/Fe molar ratio of 1.5 without pH adjustment was carried out. The As precipitation experiments were done under continuous stirring (400 rpm) at 85 ºC for 6 h. In experiment E1-B, $FeSO_4 \cdot 7H_2O$ was employed as the Fe^{2+} source. In this experiment, air was injected at a rate of 1–2 L min^{-1} to oxidise the Fe^{2+} into Fe^{3+} under similar experimental conditions as experiment E1-A.

In experiments E2 and E3, the precipitation was performed through three stages of pH adjustment using $Ca(OH)_2$ or $Mg(OH)_2$, respectively. Ferrous sulphate was used in both experiments as the Fe source, with air used as the oxidising agent. The experimental conditions were the same as those used in experiment E1-B, except the reaction time that in E2 and E3 was 3 h for each stage. In stage I, pH adjustment was not necessary because the solution pH was around 1.5, but in stages II and III, the pH was adjusted to around 2 and 2.5, respectively. These experimental conditions are summarised in Table S3.4 of the supplementary material, Annex I.2. The equipment used in the As removal

experiments consisted of an air pump, a flowmeter, a mechanical stirrer, a heating plate with temperature control, a beaker with a lid used as the reaction vessel, and a thermal jacket.

Arsenic removal from the ES solution

Experiments E4 and E5 for As removal were carried out in three stages of pH adjustment using $Ca(OH)_2$ and $Mg(OH)_2$ as alkali reagents, respectively, following the same methodology of previous experiments (E2 and E3) (see Table S3.4). However, in both experiments, an initial stage was performed in which the pH was increased from an initial value of less than 0.5 (pH of the ES solution) to 1.5 to achieve the ferric arsenate precipitation (Droppert et al., 1996; Fujita et al., 2009a).

3.2.2.2.3 Analytical techniques of characterisation

The solids obtained from both ES dissolution and As removal experiments were subjected to different analytical techniques for their physicochemical characterisation. 1) X-ray fluorescence (XRF) (Panalytical sequential spectrometer, AXIOS model) was used to determine the major elements. 2) X-ray diffraction (XRD) with a Panalytical X'Pert Pro diffractometer and X'Pert HighScore Plus software was used to identify the mineral phases. 3) Thermogravimetric analysis (TGA) and differential scanning calorimetry (DSC) were used to study the thermal behaviour of the samples using a METTLER-TOLEDO TG/DSC2 thermobalance coupled to an inductively coupled plasma mass spectrometer (ICP-MS) (NETZSCH QMS-403 Aëolos Quadro) to determine the composition of the residual gases. 4) Scanning electron microscopy (SEM) (QUANTA-Fei 200) equipped with an energy dispersive spectrometer (EDS) was employed to study the morphology and microstructure of the solids. 5) The trace elements were analysed by ICP-MS (Perkin Elmer Sciex ELAN 9000) and inductively coupled plasma optical emission spectroscopy (ICP-OES) (Varian 735-ES) in the Activation Laboratories (Actlabs) from Canada, accredited in the norm ISO/IEC 17025:2017.

To ensure the repeatability of the experiments, two replicates of each were performed. When required, quality control (QC) of the analytical techniques was performed by measuring several certified reference materials (CRMs), duplicates, and blanks.

3.2.3 Results and discussion

3.2.3.1 ES dissolution

The ES sample used in the experiments contained a high Cu concentration (54 ±1 %), but it also had As (10 ± 1 %) and S (7 ± 1%) in minor proportions. Copper was present mainly as Cu metal (Cu) and cuprite (Cu_2O). In addition, another significant Cu fraction was associated with As, forming

domeykite (Cu_3As). The S content was also associated with Cu as poitevinite ($CuSO_4 \cdot H_2O$), see Fig. 3.10. Other elements, such as Bi, Fe, Ni, Pb, Sb, and Zn, were found at concentrations below 1 %.

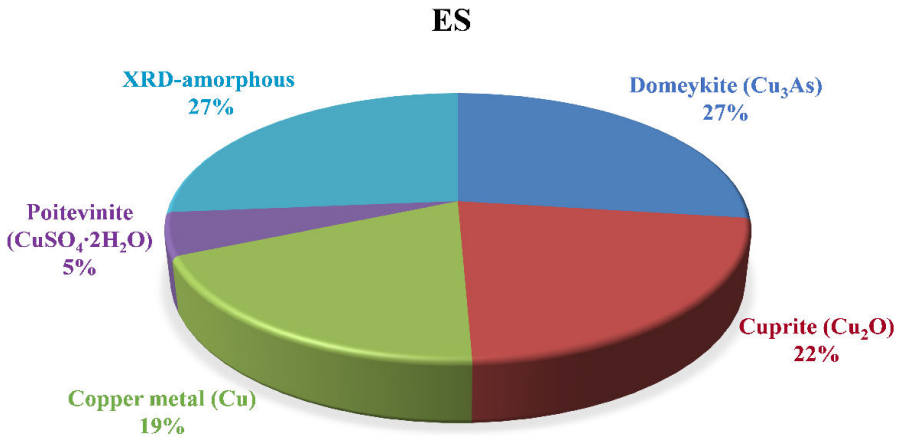

Figure 3.10. *Mineral phases of the ES.*

The dissolution percentage of the components present in the ES, focusing on Cu and As, was studied through several experiments described in the materials and methods section. The results are presented in Fig. 3.11. In addition, the chemical composition of the obtained solution can be seen in Fig. S3.5 of supplementary material, Annex I.2.

Similar results were obtained in the starting batch experiments and their replicates; therefore, only one of them are shown in Fig. 3.11a. The ES was not completely dissolved when air or O_2 was used (A-2-2-C and O-8-2-C, respectively). The dissolution efficiency, in mass, of the whole ES sample in these experiments was 32 % and 65 %, respectively, when 2 M H_2SO_4 was used. By using air, the Cu and As dissolved fractions were about 30 % and 5 %, respectively, while about 75 % of Cu and 33 % of As was reached with oxygen. The dissolution efficiency for the rest of the elements depends on the chemical solubility of each metal. For example, about 60 % of Ni was dissolved in both experiments. To point out that S was fully dissolved in the three experiments (see Fig. 3.11a), and this can be explained by considering that S is in the ES as poitevinite ($CuSO_4 \cdot H_2O$), see Fig. 3.11b.

On the contrary, the ES was fully dissolved in a solution of 1.4 M H_2SO_4 and 1.8 M HNO_3 for 2.5 h at 50 ºC (N-1.8-1.4-B) (see Table S3.3 of the supplementary material), achieving a dissolution efficiency of the ES of around 99.95 %. Fig. 3.11a shows that the dissolution efficiency of almost all major elements was about 100 %, while the dissolution efficiency of Ni was around 80 %. Therefore, this dissolution method was employed to obtain the ES solution used in the As removal experiments.

The ES solution obtained in experiment N-1.8-1.4-B was mainly composed of S (≈ 46 g L^{-1}), Cu (≈ 36 g L^{-1}), and As (≈ 5.2 g L^{-1}). Furthermore, the solutions presented concentrations of Bi, Sb, Ni, and P (100–250 ppm) and Fe, Pb, Te, and Zn (< 20 ppm) as trace elements (see Fig. S3.5 of the supplementary material).

To analyse the relationship between the elements with higher concentrations and the undissolved minerals from the ES, the mineralogy of the ES and the obtained final solids after acid attack was determined by XRD. In Fig. 3.11c, the proportion of undissolved mineral phases for A-2-2-C and O-8-2-C is shown. In experiment A-2-2-C, the dissolution of cuprite, copper metal, and domeykite was around 23 %, 63 %, and less than 1%, respectively, whereas in O-8-2-C, more than 90 % of Cu_2O and Cu and around 80 % of Cu_3As were dissolved. In both experiments, $CuSO_4 \cdot H_2O$ was completely dissolved.

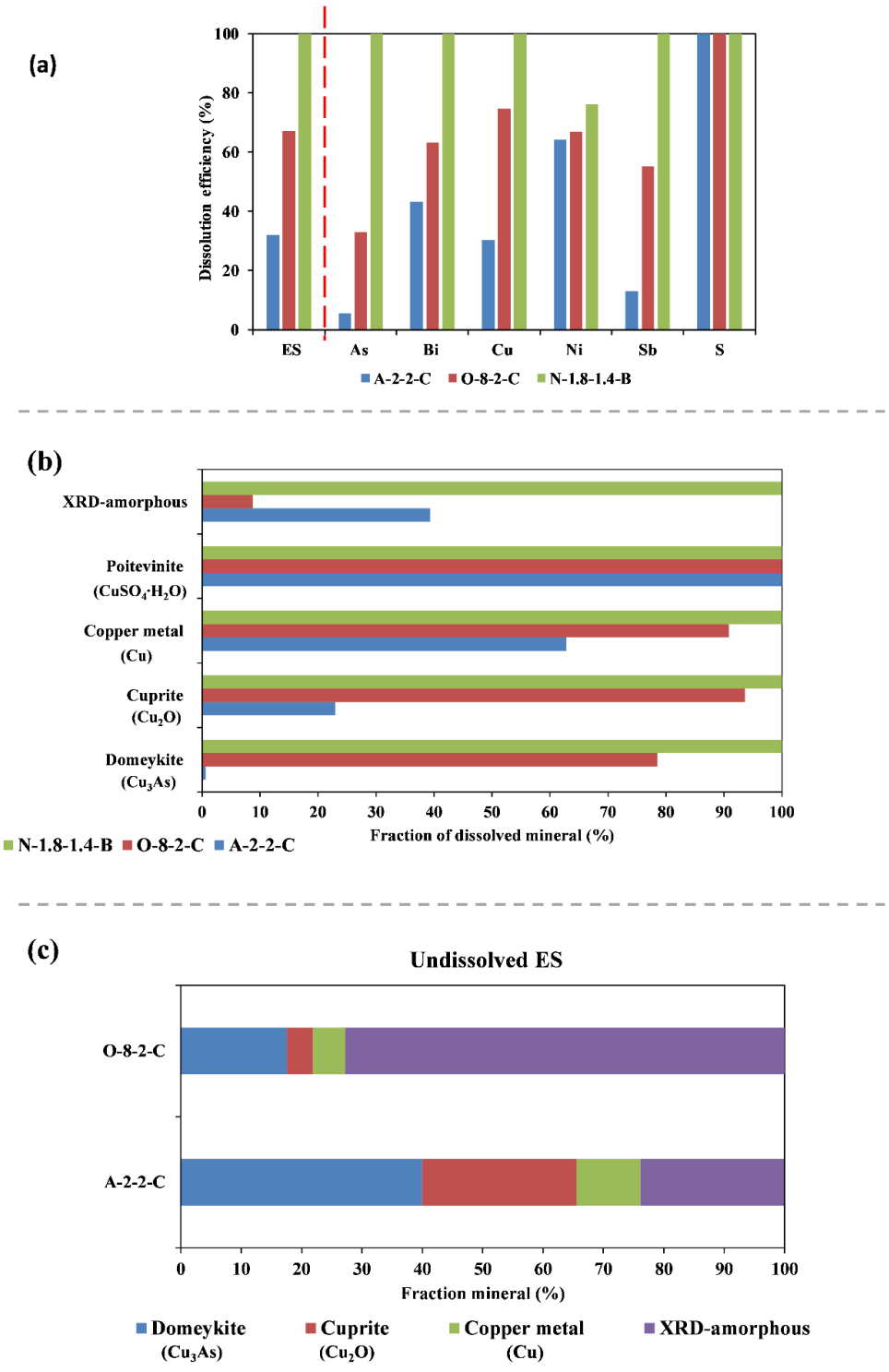

Figure 3.11. *Dissolution efficiency (%) of the major elements contained in the ES matrix by using different dissolution methods. (a). Fraction of dissolved mineral (%) in the experiments (b). Mineral phases presented in the undissolved ES (c).*

3.2.3.2 Time evolution of the experiments

The evolution of the experiments over time was evaluated by measuring the pH and oxidation–reduction potentials (ORPs). Fig. 3.12a shows the evolution of pH versus time, while Fig. 3.12b presents the correlation between pH and ORPs. In experiments E2 and E5, $Ca(OH)_2$ was used as neutralising to increase the pH, while $Mg(OH)_2$ was added in experiments E3 and E4 (see Table S3.4, Annex I.2).

For experiments E3 and E4, the pH decreased in the first 60 min (stage I), and after that no significant changes were observed (Fig. 3.12a). In stage II, alkali was added until obtaining a pH of around 2.3, and then the pH continuously decreased for 180 min. In stage III, the pH increased to around 2.9, and from this time the same trend as in the previous stages was observed. As can be seen, the pH changes are similar in both solutions when $Mg(OH)_2$ was used as the basic agent (Fig. 3.12a) since $Mg(OH)_2$ does not interfere with the formation of ferric arsenate (solid).

On the other hand, experiments E2 and E5, in which $Ca(OH)_2$ was used to increase the pH, did not show the same patterns as experiments E3 and E4 due to in E2 and E5 experiments, a secondary reaction between Ca and SO_4 ions is produced forming calcium sulphate which precipitates simultaneously with ferric arsenate (Demopoulos, 2014; Zhang et al., 2019). The possible differences in the pH behaviour with time in experiments E2 and E5 are due to the lower sulphate concentration in the used artificial solution in E2. In stage I, pH slowly decreases until the end of the stage in E2, while for E5 pH decreases during 120 min, and then no significant change was observed (see Fig. 3.12a). For stage II, the pH decreased faster in experiment E5 than in experiment E2. In the last stage of experiment E5, the pH rapidly decreased in the first 120 min, and then no significant changes were observed, while a continuous decrease was observed in experiment E2 (Dabekaussen et al., 2001; Fujita et al., 2009b).

A good linear relationship between the ORP and pH was observed (Fig. 4b), as would be expected considering the Nernst equation, which sets up the logarithmic relationships between the ORP and H^+ concentration, suggesting a linear correlation between both parameters. This phenomenon was observed during the experiments (Fig. 3.12b), where the ORP increased with decreasing pH value.

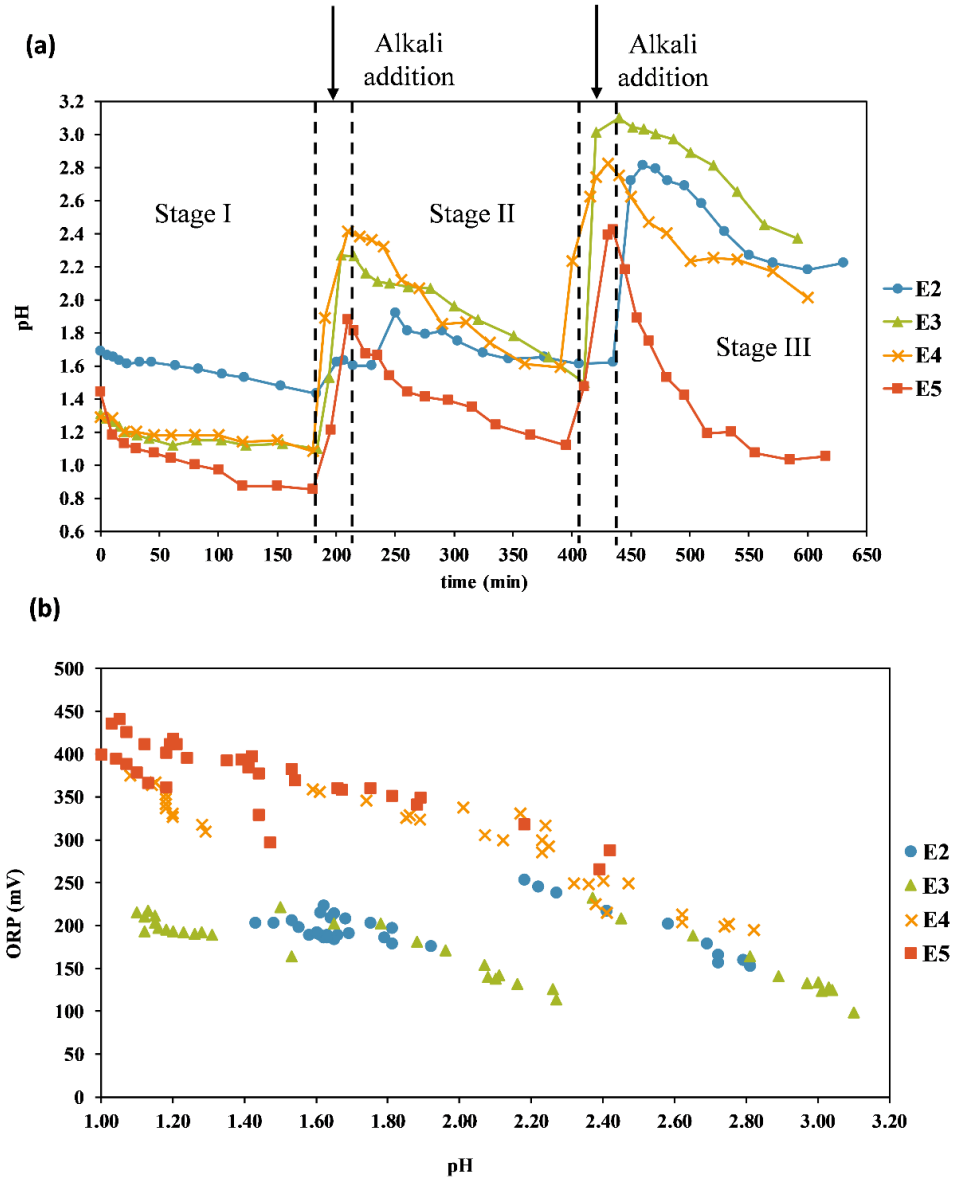

Figure 3.12. *(a) Changes in pH with reaction time and (b) changes in the oxidation–reduction potential (ORP) with the pH of the solution.*

In relation to the change in element concentrations, it is worth noting that Fe and As decreased following the same tendency (Fig. S3.6, Annex I.2), showing that these elements precipitate together. Other major elements such as Cu, Ca, Mg, and S showed different behaviour in each experiment. On the one hand, in experiments E2 and E5, the S concentration decreased due to the addition of $Ca(OH)_2$ since Ca and S precipitate, forming calcium sulphate. On the other hand, in experiment E3, no significant changes were observed in the S concentration, while the concentration of Mg increased, indicating that it does not precipitate (see Fig. S3.6 of the supplementary material, Annex I.2). In experiment E4 (Fig. S3.6 Annex I.2), the Cu, Mg, and S concentrations decreased with time,

suggesting that these elements could co-precipitate. Besides in the experiment E5, the Cu content decreased indicating this could also co-precipitate.

3.2.3.3 Precipitation efficiency (PE)

Fig. 3.13 shows the precipitation efficiency (PE), or the removing efficiency, of the major elements contained in the ES solution as a function of time. It is important to note that this study was not performed in the E1-B experiment (no pH adjustment), but the final As and Fe PEs were calculated, finding that around 65 % of As and 35 % of Fe were removed from the solution.

In experiments E2 and E5, where $Ca(OH)_2$ was used as an alkaline agent, the PE of As and Fe increased with time, removing up to 99.5 % of As and 91 % of Fe in experiment E2 (artificial solution), while for experiment E5 (ES solution) the removal of As and Fe was lower, with around 70 % removal for both elements. This can be due to the high concentrations of Cu and SO_4 ions in the solution, which probably interfere with and inhibit ferric arsenate formation (Fujita et al., 2008c; Gomez et al., 2011a). The PE of Cu was around 50 % in experiment E5, confirming that the Cu co-precipitates with As and Fe, which is a problem for the next Cu recovery stage. Furthermore, the PE for Ca and S in both experiments was higher than 90 %, but it is important to note that in experiment E5 before the As removal stages, a pH adjustment was made to 1.5, where Ca and S precipitated as $CaSO_4 \cdot 2H_2O$, resulting in a PE of greater than 80 % for both elements.

In experiments E3 and E4, where $Mg(OH)_2$ was used as alkalinising agent, the PE of As and Fe increased over time, similar to the observed trend in experiments E2 and E5, precipitating more than 99.5 % of As and 91 % Fe in experiment E3 (artificial solution), while the PE of As and Fe in experiment E4 (ES solution) was about 70 %. This behaviour is similar to the experiment with $Ca(OH)_2$; therefore, the decrease in PE of both elements is probably due to the high content of Cu and SO_4 ions, which could interfere with ferric arsenate formation (Fujita et al., 2008c; Gomez et al., 2011a). In addition, the PE of S in experiments E3 and E4 was about 50 % in both cases, suggesting the co-precipitation of sulphur with the solid $FeAsO_4$.

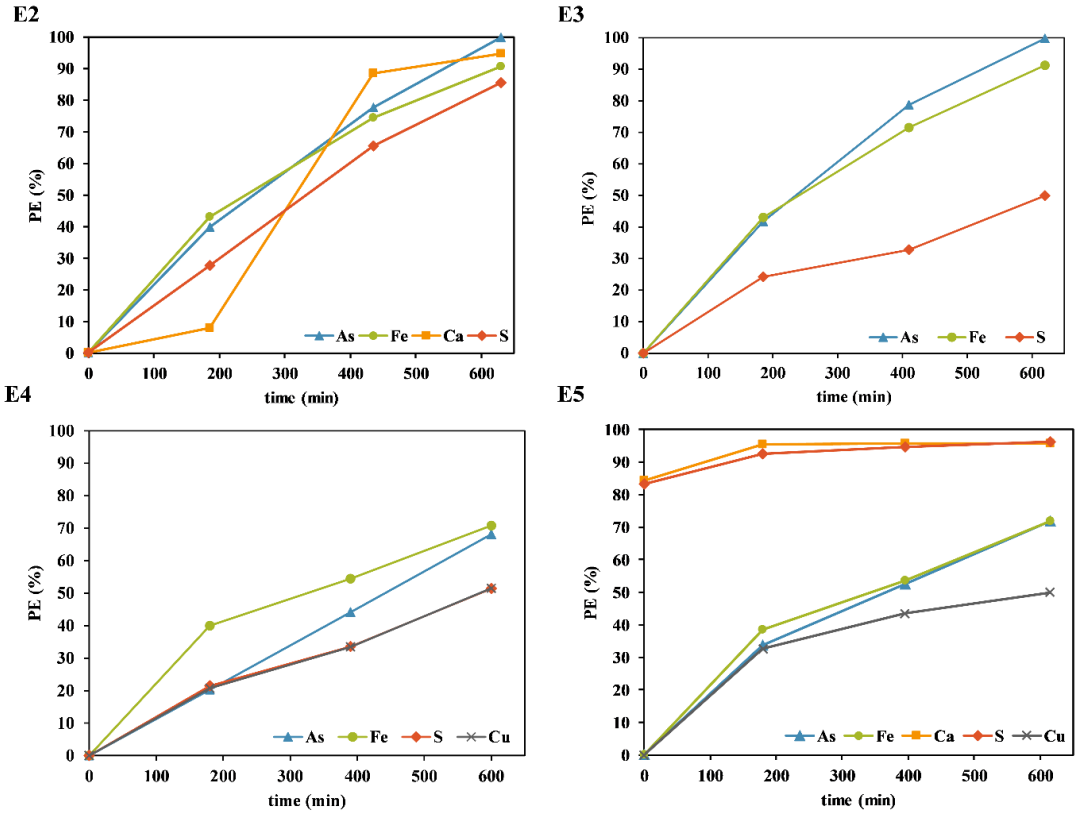

Figure 3.13. *Precipitation efficiency (PE) (%) as a function of time for both types of experiments: E2–E3 for the artificial solution and E4–E5 for the ES solution.*

3.2.3.4 Characterisation of the obtained precipitates

The physicochemical characteristics of the precipitated phases in the As removal experiments using the artificial solution and different Fe^{3+} sources [E1-A1: $FeCl_3$ and E1-A2: $Fe_2(SO_4)_3{\cdot}7H_2O$] are shown in Table S3.5 of the supplementary material (Annex I.2). The solids obtained in these experiments were mainly composed of ≈ 35 % As and ≈ 23 % Fe, which is similar to the composition found in $FeAsO_4$, but the diffraction patterns indicated that these solids were in the amorphous form.

However, scorodite (≈ 96% $FeAsO_4{\cdot}2H_2O$) was synthesised in experiment E1-B, according to the XRD analysis (Fig. S3.7 of the supplementary material, Annex I.2), where Fe^{2+} was used. The concentrations of the major elements of the obtained solid are presented in Table 3.3, showing a high concentration of As (39.0 ± 0.1 %) and Fe (24.0 ± 0.1 %), but also a minor proportion of S (< 0.05 %). In addition, the losses on ignition (around 14 %) agree with the theoretical mass loss (about 15.5 %) associated with the loss of the crystallisation water of $FeAsO_4{\cdot}2H_2O$ (Gomez et al., 2011b; Gonzalez-Contreras et al., 2010; Le Berre et al., 2008). The scorodite was probably formed by arsenic

precipitation with ferrous ions in the presence of oxygen, following Eq. 3.13 (Fujita et al., 2008b, 2008a; Min et al., 2015).

Furthermore, thermogravimetric analysis was performed to determine the thermal behaviour of the formed scorodite. In Fig. S3.8 of the supplementary material, Annex I.2, 2 thermal events were observed at 220 ºC and 960 ºC. Water was detected in the first event due to the dehydration of scorodite, following Eq. 3.14 (Gomez et al., 2011b; Gonzalez-Contreras et al., 2010; Le Berre et al., 2007), while O_2 was detected in the second event, suggesting the decomposition of iron arsenate anhydro (Cervando and Viraca, 2013; Cheng et al., 2019), according the chemical Eq. 3.15.

$$FeAsO_4{\cdot}2H_2O_{(s)} \rightarrow FeAsO_{4(s)} + 2H_2O_{(g)} \qquad \textit{Eq. 3.14}$$

$$2FeAsO_{4\ (s)} \rightarrow Fe_2O_{3(s)} + As_2O_{3(g)} + O_{2(g)} \qquad \textit{Eq. 3.15}$$

According to the amount of mass lost (15.4 %) in the first event, the solid is composed of 99 % $FeAsO_4{\cdot}2H_2O$, corresponding to an As concentration of around 32 %, which is in line with the results obtained from the XRF and XRD analysis. On the other hand, the mass loss in the second event could not be determined because the event did not finish.

Finally, the SEM analysis showed that sample E1-B presents a homogeneous morphology formed by particles mainly composed of As and Fe (point 1 of Fig. S3.9**,** supplementary material in Annex I.2). Its composition (see table, Fig. S3.9) and its bipyramidal octahedral structure confirm that these particles are scorodite, with a size of around 20 µm.

Table 3.3. *Average concentrations (%) of the major elements of the formed precipitates in the As removal experiments. LOI=loss on ignition; Detection limit (DL=0.01%). Standard uncertainty (1 σ) was calculated as the standard deviation of the mean,* $\boldsymbol{\sigma = S_x/(n)^{1/2}}$*, where n=3.*

	Exp. ID	As	Bi	Ca	Cu	Fe	O	Pb	S	Sb	LOI
Artificial solution	E1-B	39.0 ± 0.1	<DL	<DL	<DL	24.0 ± 0.1	22.9 ± 0.1	<DL	0.03 ± 0.01	<DL	14.2 ± 0.2
	E2	20.8 ± 1.1	<DL	11.0 ± 0.6	<DL	15.0 ± 1.0	32.0 ± 1.0	<DL	10.0 ± 1.0	<DL	10.8 ± 1.1
	E3	36.0 ± 1.9	<DL	<DL	<DL	24.0 ± 0.3	24.0 ± 1.0	<DL	1.0 ± 0.8	<DL	15.1 ± 0.1
ES solution	E4	30.2 ± 1.9	2.7 ± 0.5	<DL	7.7 ± 3.4	22.6 ± 1.4	25.3 ± 0.1	0.16 ± 0.03	2.15 ± 0.01	1.23 ± 0.7	7.8 ± 1.2
	E5	10.9 ± 1.2	0.02 ± 0.01	19.0 ± 0.2	0.6 ± 0.2	10.3 ± 0.1	38.8 ± 0.1	<DL	15.4 ± 0.5	0.12 ± 0.02	4.6 ± 1.7

The obtained precipitate of E2 contained As (20.8 ± 1.1 %), Fe (15.0 ± 1.0 %), Ca (11.0 ± 0.6 %), and S (10.0 ± 1.0 %) as major elements (Table 3.3), being gypsum (≈ 50 %, $CaSO_4 \cdot 2H_2O$) and scorodite (≈ 36 %) the main mineral phases presented (Fig. S3.7 of the supplementary material in Annex I.2). The presence of gypsum was expected when calcium hydroxide was used as a neutralising agent due to the precipitation of calcium sulphate dihydrate as a secondary product (Demopoulos, 2005; Droppert, 1996), according to Eq. 3.16. The experimental mass ratio (Ca/S = 1.10) was slightly lower than the theoretical value for gypsum (Ca/S = 1.25), according to the consulted literature (Demopoulos, 2005; Dutrizac and Jambor, 2007; Gomez et al., 2011a), this could be due to small incorporation of S (as SO_4) in the structure of the scorodite as a result of $SO_4 \rightarrow AsO_4$ substitution, forming $Fe(AsO_4)_{1-x}(SO_4)_x \cdot 2H_2O$ (Demopoulos, 2005; Dutrizac and Jambor, 2007; Gomez et al., 2011a; Singhania et al., 2005).

$$Ca(OH)_{2(s)} + H_2SO_{4(aq)} \rightarrow CaSO_4 \cdot 2H_2O_{(s)} \qquad \textit{Eq. 3.16}$$

On the other hand, the proportion of scorodite determined by XRD indicated lower content of As and Fe than that provided by the XRF analysis. This suggests that part of the As and Fe of the sample does not form crystalline scorodite, and therefore that part is associated with the amorphous XRD phase (approximately ≈ 14%) found in this sample.

In Fig. 3.14, it can be seen that the E2 sample presents a heterogeneous morphology formed by two types of particles: large particles (point 1, Fig. 3.14) composed of Ca and S, whose tabular crystals correspond to gypsum, and fines particles (point 2, Fig. 3.14) composed of As and Fe, whose composition and bipyramidal octahedral structure suggest that is scorodite. These results confirm the crystal phases identified by XRD analysis. In addition, the general composition of the E2 sample obtained by EDS analysis showed that this solid is mainly composed of As, Ca, Fe, and S (see table, Fig. 3.14), which is in line with the XRF analysis.

The E3 sample [pH adjustment with $Mg(OH)_2$] contained As (36.0 ± 1.9 %) and Fe (24.0 ± 0.3%) in greater proportions, but it also contained less than 1 % of S, which is analogous to the composition of the E1-B sample. In addition, scorodite (≈ 62 %) was the only mineral phase identified (see Fig. S3.7, Annex I.2), and this compound is consistent with the obtained loss on ignition (LOI ≈ 15.1 %) that is associated with loss of the crystallisation water of $FeAsO_4 \cdot 2H_2O$ (Gomez et al., 2011b; Gonzalez-Contreras et al., 2010; Le Berre et al., 2008). However, the proportion of the mineral phase did not correspond to the composition given by XRF, meaning that part of As and Fe was found in the amorphous phase (≈ 38 %), which is significantly high compared to that obtained in the E1-B (≈ 4 %) and E2 (≈ 14 %) samples.

Moreover, the SEM analysis showed that E3 solid samples presented a homogeneous morphology formed by particles mainly composed of As and Fe (point 2 of Fig. S3.9, supplementary material in Annex I.2). Its composition and bipyramidal octahedral structure confirm that these particles are scorodite. The particle size was less than 10 μm, and aggregates were formed, in contrast to the results obtained for E1-B, where the particle size was around 20 μm and aggregates were not formed.

The major elements of the solid formed in experiment E4 (ES solution) are shown in Table 3.3. The E4 sample contained As (30.2 ± 0.4 %) and Fe (22.6 ± 1.4 %) as major elements and Cu (7.7 ± 3.4 %), Bi (2.7 ± 0.5 %), S (2.15 ± 0.01 %), and Sb (1.2 ± 0.7 %) in minor proportions. The XRD analysis is shown in Fig. S3.10 of the supplementary material (Annes I.2), where it is observed that the solid did not present mineral phases, being formed by poorly crystalline ferric arsenate or amorphous ferric arsenate, similar to the obtained ones by other authors, such as ferric arsenate intermedium [$FeAsO_4 \cdot (2+x)H_2O$ ($0<x<1$)] (Le Berre et al., 2008; Min et al., 2015), ferric arsenate sub-hydrate or Phase 4 [$FeAsO_4 \cdot 3/4H_2O$], and basic ferric arsenate sulphate or Phase 3 [$Fe(AsO_4)_{1-x}(SO_4)_x(OH)_x(1-x)H_2O$ ($0<x<1$)] (Dutrizac and Jambor, 2007; Gomez et al., 2011b; Swash and Monhemius, 1998). The average experimental mass ratio of As/Fe was 1.33, which is similar to the theorical ratio of scorodite (As/Fe = 1.34), within the experimental uncertainties (≤ 10 %). However, the loss on ignition (7.8 ± 1.2 %) was lower than the theoretical mass loss (about 15.5 %) associated with the loss of the crystallisation water of $FeAsO_4 \cdot 2H_2O$.

On the other hand, the thermogravimetry analysis (Fig. S3.11 of the supplementary material in Annex I.2) was performed to identify the compounds obtained in E4 according to its thermal behaviour. Four thermal events can be observed at 155 ºC, 506 ºC, 678 ºC, and 940 ºC. Water was only detected in the first event due to the loss of crystallised water of some hydrated compound. The second and third thermal events were due to the decomposition of sulphates, corroborated by the detection of SO_2 in the ICP-MS system. The thermal behaviour suggests that the compound obtained in E4 is analogous to the ferric arsenate sulphate or Phase 3 found by other authors (Dutrizac and Jambor, 2007; Gomez et al., 2011b) in which the decomposition occurs in three steps: (1) loss of crystallised water at 300–600 ºC; (2) sulphate decomposition at 650–820 ºC; and (3) arsenate decomposition at 820–975 ºC.

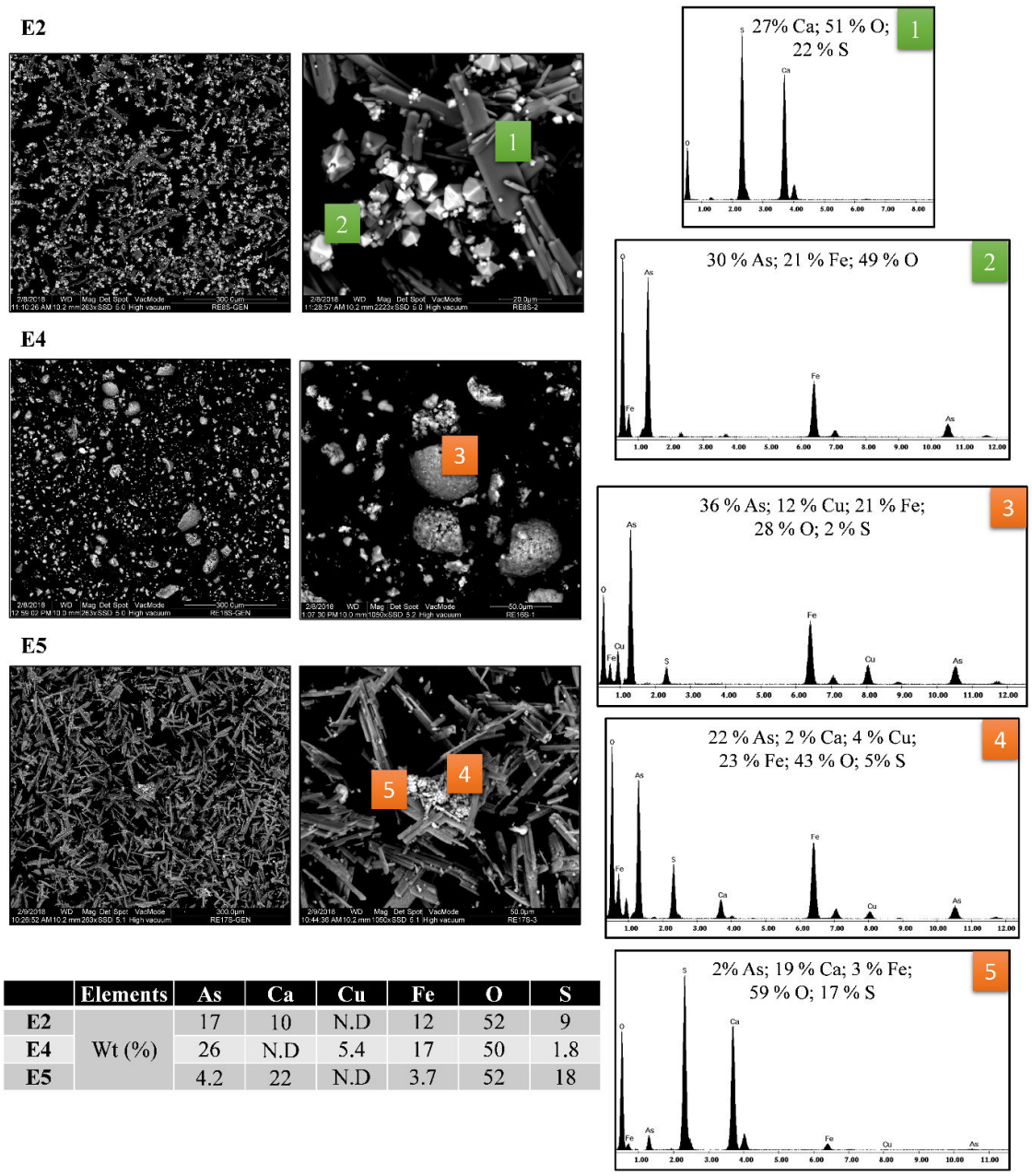

	Elements	As	Ca	Cu	Fe	O	S
E2	Wt (%)	17	10	N.D	12	52	9
E4		26	N.D	5.4	17	50	1.8
E5		4.2	22	N.D	3.7	52	18

***Figure 3.14**. SEM images of the precipitates obtained in experiments E2, E4, and E5. The table also shows the general composition determined by EDS from the image located at the left.*

The SEM analysis (Fig. 3.14) shows that the E4 solid presents an amorphous morphology composed of particle aggregates with sizes of 10–50 µm. These ones are mainly composed of As and Fe and Cu and S in minor proportions (point 3, Fig. 3.14). The obtained elemental composition of this sample by EDS agreed with the XRF results, which showed As, Fe, Cu, and S as the main elements.

The E5 sample is composed of As (10.9 ± 1.2 %), Ca (19.0 ± 0.2 %), Fe (10.3 ± 0.1%), and S (15.4 ± 0.5 %) as main elements, whereas Cu, Sb, and Bi are present in proportion lower than 0.5 %. The presence of Ca and S was expected when the neutralisation was carried out using $Ca(OH)_2$, as previously mentioned, due to gypsum formation (Bluteau et al., 2009; Demopoulos, 2005; Droppert, 1996). In fact, gypsum (≈ 83 % $CaSO_4 \cdot 2H_2O$) was the only mineral phase identified in the E5 sample (Fig. S3.10 of the supplementary material in Annex I.2), which is in agreement with the Ca and S concentrations provided by XRF, and this was confirmed by the mass ratio found (Ca/S = 1.23), which is analogous to the theoretical ratio of gypsum (Ca/S = 1.25). On the other hand, the E5 sample showed a high concentration of As and Fe. The experimental mass ratio (As/Fe = 1.05) found was lower than the theoretical ratio of scorodite (As/Fe = 1.34), and no evidence of its existence was found. Hence, the precipitated As and Fe probably form some type of ferric arsenate (≈ 17 %), as mentioned for the E4 sample, such as ferric arsenate intermedium [$FeAsO_4 \cdot (2+x)H_2O$], ferric arsenate sub-hydrate ($FeAsO_4 \cdot 3/4H_2O$), or basic ferric arsenate sulphate [$Fe(AsO_4)_{1-x}(SO_4)_x(OH)_x(1-x)H_2O$] (Dutrizac and Jambor, 2007; Gomez et al., 2011b; Le Berre et al., 2008).

The SEM analysis of the E5 samples is shown in Fig. 3.14. The obtained elemental composition of these samples by EDS agrees with the results obtained by XRF, where the E5 matrix was mainly composed of As, Ca, Fe, and S. On the other hand, the solid presents a heterogenous morphology, and it is formed by two types of particles: (1) large particles composed of Ca and S, whose tabular structure correspond with gypsum (point 5 Fig. 3.14), verifying the results obtained by XRD, and (2) fine particles composed of As and Fe that do not have a crystalline structure, these form amorphous aggregates (point 4, Fig. 3.14) that are deposited on the gypsum surface.

In agreement with the consulted literature (Fujita et al., 2008c; Gomez et al., 2011a; Singhania et al., 2006), the formation of amorphous or poorly crystalline ferric arsenate in experiments E4 and E5 using the ES solution can be due to the incorporation of more than 5 % SO_4 anions and cations (Cu^{2+}) into the crystal structure.

3.2.4 Practical implications

The removal of As, which is one of the impurities contained in Cu concentrate, has become one of the current challenges of the pyrometallurgical Cu industry since it negatively affects the Cu cathode. Part of the As that flows in the process is dissolved in the Cu electrolyte, and its concentration is reduced when it is subjected to water treatment in which a solid is formed (ES), which is recirculated due to the high Cu content. The process proposed in this work focused on the separation of As and Cu through acid dissolution of the ES and subsequent precipitation of ferric arsenate, obtaining a final liquid effluent with free As and high Cu content. Therefore, the Cu could be returned in the

process without impurities, and the ferric arsenate could be valorised by using it is in commercial applications such as the electrochemical energy storage in Li-battery (Anji Reddy et al., 2009; Gomez et al., 2013).In addition, the formation of scorodite is considered as an alternative for As stabilisation (Rong et al., 2020; Tabelin et al., 2019), keeping its stability under oxidising conditions in the pH range of 2.0–6.0 (KE and LIU, 2019; Riveros et al., 2001). The final wastewater stream, with a low concentration of As and Cu, could be sent to an effluent treatment plant (ETP) for final treatment before its release to the environment.

This procedure could be applied to other acidic liquid effluents that are generated during Cu cathode production; whose current treatment generates As-rich waste that is considered a hazardous material. Therefore, the procedure proposed in this work generates a dual benefit. On the one hand, from an environmental point of view, the decrease in the amount of produced waste and the reduction of the environmental impact due to potential liquid effluent releases, in our case of study into a very impacted environment as the Huelva estuary. On the other hand, from an economic point of view, part of the Cu is recovered, improving the industrial process yield. These facts approach the copper production industrial process to the aim of the circular economy.

3.2.5 Conclusions

The dissolution and subsequent treatment of highly Cu-rich ES with As impurities from the Cu production industry was developed in this work to decrease the As concentration and to recover the remaining Cu. The ES was fully dissolved (> 99 %) in H_2SO_4/HNO_3 medium using a solid-to-liquid ratio of 1:20 for 2.5 h at 50 rpm. During treatment of the obtained solution, amorphous ferric arsenate was obtained, and the obtained PE for As was around 70 %. In addition, around 50 % Cu co-precipitated with the formed solid, suggesting that it would be more appropriate to perform previously Cu recovery as copper sulphate, which will also improve the subsequent PE of As. Therefore, more experiments are required to optimise the As removal process, avoiding Cu co-precipitation, and study the inertisation process and/or the potential applications of the formed solid are required.

SUBCHAPTER 3.3

COPPER RECOVERY FROM SLUDGES GENERATED IN THE ELECTROLYTE TREATMENT PLANT OF A PYROMETALLURGICAL COMPLEX

3.3 COPPER RECOVERY FROM SLUDGES GENERATED IN THE ELECTROLYTE TREATMENT PLANT OF A PYROMETALLURGICAL COMPLEX

D.C. Paz-Gómez, S.M. Pérez-Moreno, I. Ruiz-Oria, G. Ríos and J.P. Bolívar

Hydrometallurgy 206 (2021) 105769

Abstract

Electrolytic sludge is generated in the last stage of the electrolyte decontamination treatment plant in the manufacture of cathodic copper (> 99.99 % Cu). Currently, this sludge is recycled back to the process due to the high concentration of copper, although its recirculation involves a serious problem of arsenic accumulation in the industrial process. This negatively affects the quality of commercial copper. Therefore, the main focus of this study was the recovery of copper contained in the electrolyte sludge as copper (II) sulfate pentahydrate ($CuSO_4 \cdot 5H_2O$) for its return to the industrial process and/or commercialization. The remaining waste, which contains mainly As and other toxic chemical species, were eliminated in a controlled repository. To this end, an exhaustive characterization of the electrolytic sludge was performed to determine its chemical composition, mineral phases, and particle size. The main results indicated that the sludge was composed of very fine particles (~ 99 % < 100 μm), containing mostly Cu (~ 54 %) (Cu_3As, Cu_2O, Cu and $CuSO_4 \cdot xH_2O$), As (~ 10 % as Cu_3As) and S (~ 7 % as $CuSO_4 \cdot xH_2O$). More than 90 % of the Cu contained in the sludge was recovered as very pure copper sulfate (≥ 99.5 %) by an evaporative crystallization process. In addition, around 70 % of the As was removed in the process as a solid (> 99 % in As_2O_3). The rest of pollutants remained in the final solution, which ultimately will be treated in the liquid effluent treatment plant. Therefore, valorization of the electrolytic sludge was achieved by copper recovery as $CuSO_4 \cdot 5H_2O$ using evaporative crystallization; this process was an effective way for both recovering Cu and removing the As contained in the electrolytic sludge generated in the electrolyte treatment plant.

Keywords: Electrolytic sludge; Characterization; Valorization; Copper recovery; Copper sulfate; Crystallization.

3.3.1 Introduction

The growth of global copper demand has increased quickly over the last 50 years, and the same trend is expected for the future. Copper is employed in a wide range of applications, mainly due to its unique electricity conducting properties, which makes it difficult to replace. It will be crucial for future society, given the expected increase of copper-intensive low-carbon energy and electrification

of transport technologies. World refined copper production reached about 23.5 million tonnes in 2017 (ICSC: International Copper Study Group, 2018). This is associated with a large amount of solid waste and wastewater generation. The decrease in the ore grades also intensifies energy use. Thus, copper production has a huge environmental impact (Csavina et al., 2014; D. Dong et al., 2020; S.M. Pérez-Moreno et al., 2018). In the last decades, the industry has tried to achieve a circular economy by recycling, reusing, and valorizing wastes, reducing disposal costs and avoiding risks for the environment and human health (EEA: European Environment Agency, 2017; European Commission, 2015; Liao et al., 2019).

Atlantic Copper SLU, one of the biggest manufacturers of cathodic copper in Europe, is located in Huelva (Spain). This company reduces its waste as much as possible. This company produces around $2.9 \cdot 10^5$ t/y of ultrapure copper (> 99.99 % Cu), and they manage several co-products, intermediate materials, and wastes.

A copper concentrate (~ 30 % Cu) is used as the raw material. This is first smelted in a Flash Smelting Furnace (FSF) to be converted into matte (64 % Cu). It is then oxidized in the Converter Furnaces (CF) to obtain blister copper (> 99 % Cu). The slag from these furnaces is treated in an Electric Furnace (EF), giving a very inert slag that is mainly composed of iron silicates (< 1% Cu), which is used in many civil engineering applications (road bases, concrete, etc.). Finally, the blister copper is introduced into the Refining Furnaces (RF), obtaining copper anodes (99.6 % Cu, 3.3·105 t/y), which are converted to commercial cathodic copper (> 99.99 % Cu) by electrorefining (Atlantic Copper, 2017).

During the electrorefining process, the copper (anode) is electrochemically dissolved in the electrolyte and then electrodeposited onto the cathode. The electrolyte is a solution of copper sulfate and sulfuric acid with around 45 g/L of Cu and 180 g/L of H_2SO_4. Some additives, such as chloride (20–50 mg/L) and organic levelling and grain-refining agents (1–10 mg/L), are added in very low concentrations to improve the morphology and purity of the copper cathode (Schlesinger et al., 2011). In the electrochemical process, elements with lower redox potential than copper, such as arsenic, antimony, bismuth, and nickel, remain in solution, while Cu is deposited onto the cathode. The concentration of these impurities gradually increases in the electrolyte, and this negatively affects the copper cathodic quality. Consequently, they must be reduced to acceptable levels. A conventional process is used for controlling the impurity levels in the electrolyte. This process involves three stages of decopperizing by electrowinning in liberator cells in the Electrolyte Treatment Plant (ETP) (Artzer et al., 2018; Wesstrom and Araujo, 2012). In the first stage, the copper concentration is reduced from 45 g/L to 25 g/L, obtaining a B-grade copper cathode (> 99.97 % Cu), which is used to produce wire rods, tubes, foils, copper-based alloyed products, and chemicals. In the second stage,

the copper concentration is further reduced to around 10 g/L. This anode scrap is used as cathodes in the electrorefining plant. In the third stage, arsenic is removed from the solution by electrowinning onto a cathode, forming an electrolyte sludge (ES), which guarantees a dissolved copper concentration of 1–2 g/L. About 1300 t/y of ES are produced. The final treated electrolyte is sent back to the electrolyte tank house for reuse. Currently, the ES is sent back to the FSF to recover its Cu content (around 60 %), although its recirculation involves serious problems of As accumulation in the industrial process. Figure 3.15 shows the general industrial process and the procedure developed in this study for As-free Cu recovery. This consists in dissolving the ES using acid digestion and then recovering Cu from the obtained solution (ES solution) as copper (II) sulfate pentahydrate ($CuSO_4 \cdot 5H_2O$) by evaporative crystallization. Finally, copper sulfate can be reintroduced into the industrial process or marketed. The resulting solution can be mixed with the industrial wastewater stream and be sent to an effluent treatment plant (ETP) for final treatment before it is released into the environment.

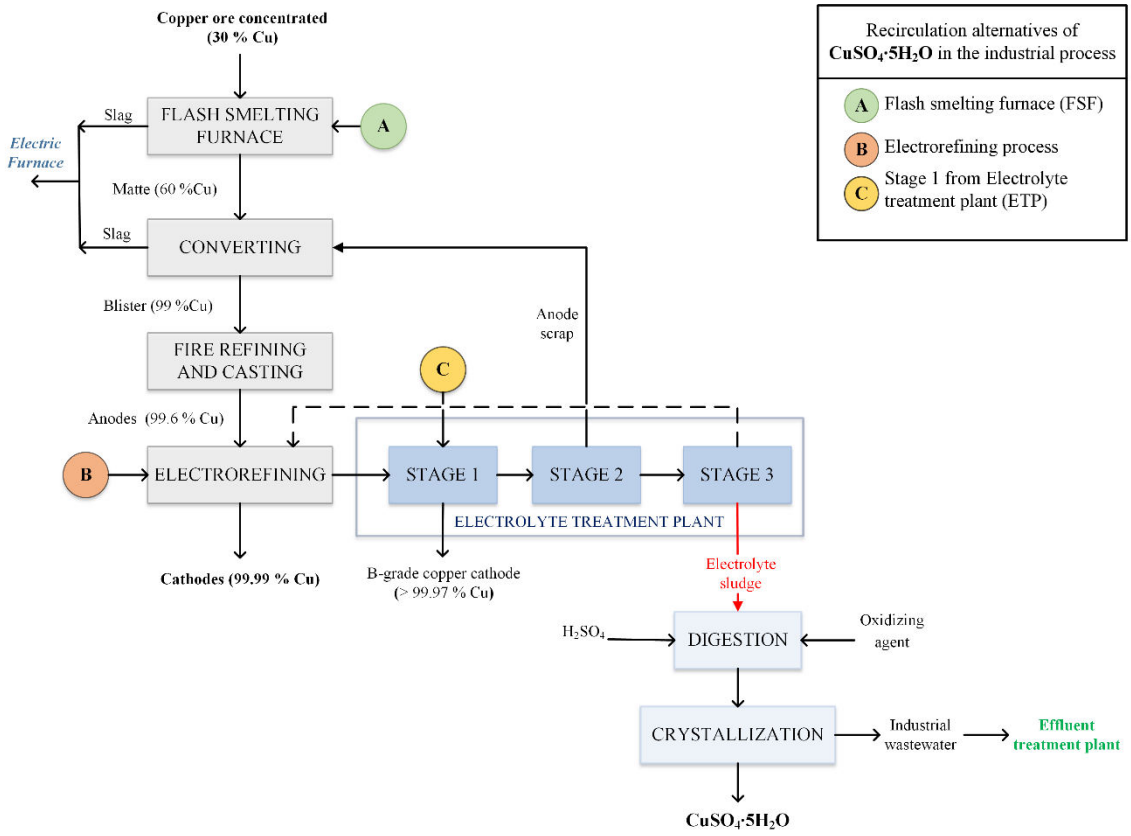

Figure 3.15. *Flowchart of the general industrial process and the ES treatment proposal.*

There are few studies in the literature concerning the characterization and valorization of the copper electrolyte sludge (Chen and Dutrizac, 2009; Marković et al., 2012). Most studies are focused on

alternatives to the conventional process for the purification of the electrolyte (Artzer et al., 2018; Hoffmann, 2004; Navarro and Alguacil, 2002; Sheedy et al., 2006; Wang, 2004; Zhou et al., 2011). Therefore, there are no studies concerning copper recovery from ES by its dissolution and Cu precipitation as $CuSO_4 \cdot 5H_2O$, which is widely used in many areas, such as in agriculture, antiseptic agents, electroplating processes, electronics (as an intermediate), antifungal agents, treatment for copper refining, and even as catalysts in petrochemical processes (Aktas, 2011; Alimohammadizadeh et al., 2018; Ayala and Fernández, 2014; Giulietti et al., 1996).

The copper sulfate pentahydrate or blue vitriol is usually produced by dissolving copper compounds (from scrap copper and/or copper residues in sulfuric acid solution) in the presence of an oxidizing agent such as air, oxygen, peroxide or nitric acid (Z. Dong et al., 2020; Khalid et al., 2019a; Marković et al., 2012; Valera et al., 2003; Yang et al., 2011). $CuSO_4 \cdot 5H_2O$ crystallization is achieved by reducing the solubility of the copper sulfate in solution, i.e., supersaturating the solution of cupric and sulfate ions. This can be performed by different methods, such as cooling, adding an antisolvent (ethanol, methanol, glycol, acetone, etc.), evaporation, or some combination of these methods (Giulietti et al., 1995; Mersmann, 1999; O'Grady, 2014). The method normally used in the industry is based on evaporating and cooling the copper solution (Atoche and Huayta, 2015; Cortes-Egaña, 2009; Marković et al., 2012). Cupric sulfate crystal precipitation by adding an antisolvent is being currently researched (Alimohammadizadeh et al., 2018; Ayala and Fernández, 2014; Kokes et al., 2014; Yazici and Deveci, 2016).

In view of the above considerations, the aim of the present study was to extract the Cu contained in the ES coming from the electrolyte cleaning plant by wet acid leaching and its subsequent recovery as copper (II) sulfate pentahydrate ($CuSO_4 \cdot 5H_2O$) for its return to the industrial process (arsenic-free) and/or commercialization. For that purpose, a secondary general objective was proposed, which was to develop an exhaustive characterization as a preliminary step and to select the most appropriate methodology for dissolving ES and extracting Cu.

3.3.2 Materials and methods

3.3.2.1 Materials

Several sampling campaigns were conducted over a period of three months in the spring of 2017. One sample was collected every eight days to verify the homogeneity of the ES. About 5 kg of sample was collected, dried at 60 °C to constant mass, and homogenized by manual agitation while carefully trying to break the clods of the sample. The homogenization process was verified by measuring three aliquots through inductively coupled plasma optical emission spectrometry (ICP-OES), which indicated that the dispersion of the obtained concentrations was comparable to the RSD (relative

standard deviation) of the individual measurements. Likewise, one aliquot of each homogenized sample was analyzed by X-ray fluorescence (XRF) to study the uniformity and/or possible temporal variability of the samples. The experiments were carried out with a mix of ES samples.

3.3.2.2 Experiments

3.3.2.2.1 Dissolution of electrolytic sludge

The ES dissolution experiments were presented and discussed in a previous article (Paz-Gómez et al., 2021a), where the dissolution of ES was carried out in a solution of sulfuric acid by using three different oxidizing agents (air, oxygen and nitric acid). In the experiments with sulfuric and nitric acid, different conditions were simulated: 1) two solid-to-liquid ratios (1:10 to 1:20 g/mL) were employed; 2) sulfuric acid and nitric acid concentrations used ranged between 0.9 and 2.7 M and between 1.0 and 1.8 M, respectively; 3) the temperature and reaction time were 24 and 50 ºC for 12 and 2.5 h, respectively. The solution was stirred at 500 rpm. The experiments with air used different concentrations of the sulfuric acid solution (2, 4, 6 and 10 M), in which a constant air flow (2 L/min) was introduced. When O_2 (purity > 99.5 %) was used, this experiment was performed under optimal conditions, with a 2 M H_2SO_4 solution and a constant O_2 flow of 8 L/min. In both experiments, the solution was at 80 °C and stirred at 500 rpm for 2.5 h.

3.3.2.2.2 Copper recovery

Copper recovery was carried out by an evaporative crystallization process to obtain copper (II) sulfate pentahydrate. The ES solution was evaporated with continuous stirring (450 rpm) at 80 ± 5 ºC to a final given volume. Then the temperature was reduced at a cooling rate of 0.5 ºC/min until reaching room temperature (~ 20 ºC). The crystal growth stage was carried out for 24 h, and then the solution was filtered to collect the $CuSO_4 \cdot 5H_2O$ crystals, which were rinsed with ethanol and dried at 50 ºC until reaching a constant mass. The experiments were performed by two methods: (a) sequential and (b) non-sequential evaporation, which are explained below.

Prior to the experiments, the theoretical copper recovery percentage (η_{Cu}) curve, as $CuSO_4 \cdot 5H_2O$, was predicted to determine the concentration factor range ($CF = V_0 / V_i$, where V_0 is the initial volume of the solution, and V_i is the final volume of the obtained solution at each evaporation step) that was subsequently used in the experiments. Considering the initial molar concentrations of Cu and S (as SO_4) in the ES initial solution, the solubility product equation under saturated conditions for different final volumes, and reaction 1, the copper recovery percentage as copper sulfate was calculated as a function of *CF*. The theoretical curve (Fig. S3.12, Annex I.3) shows that the range of study should

cover from *CF* = 1.1 (η_{Cu} ~ 18 %) to *CF* = 4 (η_{Cu} ~ 95 %), thus the experiments were designed to cover this range.

$$Cu^{2+} + SO_4^{2-} \leftrightarrow CuSO_4 \qquad \textit{Eq. 3.17}$$

a) Sequential evaporation

An evaporative crystallization process was carried out in five sequential stages by using an initial volume, V_0 = 200 mL, in which approximately a constant volume (about 25 mL) was evaporated every time at 80 ºC. After each evaporation stage, the solution was cooled and filtered to collect the $CuSO_4 \cdot 5H_2O$ crystals formed, until a final step in which the volume of the obtained solution was 50 mL (*CF* = 4).

b) Non-sequential evaporation

In the non-sequential experiments, the same initial volume (V_0= 80 mL) of the ES solution was taken for each experiment, and this was evaporated at 80 °C to final volumes (V_1, V_2, and V_3) of 20, 30, and 50 mL, respectively. The solution was cooled, and the crystals were collected by filtration and preserved for analysis.

3.3.2.3 Characterization techniques

3.3.2.3.1 Granulometry

The particle size distribution of the samples was determined through a granulometric analysis employing a modular analyzer, Mastersizer 2000, with He-Ne laser diffraction technology, at a wavelength of 632.8 nm. A representative amount of each sample was placed in ethanol and subjected to ultrasound for 10 minutes, followed by magnetic stirring for about 30 minutes. Moreover, several certified reference materials were used to verify the measurements: LTX3300C Nanosphere Size Standards; 2009A and 2009B Duke Polymer Microsphere Uniform Standards; 4009, 4009A, and 4009B Duke Standards, Microsphere Size Standards.

3.3.2.3.2 Elemental composition

The major elements were measured by XRF employing a Panalytical sequential spectrometer (AXIOS model) equipped with an X-ray tube of 4 kW, a front window, and an anode of Rh, five analyzing crystals (PX1, PE 002, LIF 200, Ge 111, and LIF 220), and two detectors (flow and scintillation). Prior to the analysis, the samples were prepared as pressed discs of 40 mm in diameter

and 25 mm in thickness. To verify the quality of the result, a gold alloy (FISHER 603-683) was used as certified reference material.

The trace elements were measured by two techniques: inductively coupled plasma mass spectrometry (ICP-MS), Perkin Elmer Sciex ELAN 9000, and inductively coupled plasma optical emission spectrometry (ICP-OES), Varian 735 ES. Prior to the analysis, the samples were digested by mixing with four acids (hydrochloric, nitric, perchloric. and hydrofluoric acid). Some aliquots were dissolved by fusion with sodium peroxide. Quality control (QC) included the use of blanks, replicates, and several certified reference materials (CZN-4, DNC-1a- GXR-1, MP-1b, OREAS-97/98/101a, RGTH, etc.) to ensure that experimental uncertainties were less than 10 %.

3.3.2.3.3 Mineralogy composition

The mineral phases present in the samples were identified through X-ray diffraction (XRD) analysis using a Panalytical X'Pert Pro diffractometer equipped with a Cu X-ray source and an X'celerator detector operating under the following conditions: voltage, 40 kV; current, 10 mA; range 5–70° 2Θ; step size, 0.017° 2Θ; time per step, 50.165 s; divergence slit fixed angle, 0.5˚. The crystalline mineral phases were identified using X'Pert HighScore Plus software along with the PDF-4 Minerals 2013 ICDD database. Quantification of the mineral phases was performed using the Rietveld method, which employed corundum (Standard reference material, SRM 1976a) as an internal standard to determine the amount of amorphous material. In addition, the mineral composition of some samples was performed with a Bruker D8-Advance diffractometer equipped with Göebel mirrors, a high temperature chamber (up to 900 ºC), a KRISTALLOFLEX K 760-80F x-ray generator, and an X-ray tube with a copper anode. Diffractometer settings were 3000 W, 20–60 kV, 5–80 mA. The crystalline mineral phases were identified using the Match! software (Phase Identification from Powder Diffraction) of Crystal Impact using the COD database (Crystallography Open Database). In this case, zincite (ZnO) was added prior to the analysis as an internal standard to determine amorphous material and quantify the mineral phases.

3.3.2.3.4 Thermal properties

Thermogravimetric analysis (TGA) and differential thermal analysis (DTA) were used to study the thermal behavior of the samples using a TG-85E 11 SDTA Mettler thermobalance coupled to the ICP-MS (Pffeifer ThermoStar) equipment to determine the composition of the residual gases. The operating conditions used were 25–1000 °C with a heating rate of 10 °C/min and an inert N_2 atmosphere with a flow rate of 50 mL/min.

3.3.2.3.5 Morphology and microstructure

The morphology and microstructure of the samples were analyzed using a scanning electron microscope (SEM) QUANTA-Fei 200 equipped with an energy dispersive spectrometer (EDS), which enables multi-elemental, semi-quantitative analysis. The mineralogical database was used to determine the mineralogical composition (Mineralogy Database, 2012b).

Spatial distribution of major elements present in the samples was determined using a scanning electron microprobe (EPMA) JEOL JXA-820 model equipped with four wavelength-dispersive X-ray spectrometers and EDS.

3.3.3 Results and discussion

3.3.3.1 Physical-chemical characterization of electrolytic sludge

The particle distribution of the ES sample is shown in Table S3.6 and Fig. S3.13 (Annex I.3). The sludge is mostly composed of silt (86 ± 6%) and a low content of clay (8 ± 2%) and sand (6 ± 3%), obtaining that the median of the particle size distribution d_{50} = 17 µm, percentiles d_{90} = 50 µm, and d_{99} = 100 µm. This granulometry distribution is highly beneficial for metal recovery by the hydrometallurgy route (ASTM D2487, 2006; Hansen et al., 2005; Khalid et al., 2019a).

ES contained mainly Cu (54 ± 1 %), As (10 ± 1 %), and S (7 ± 1 %) as major elements (Fig. 3.16 and Fig S3.14, Annex I.3). Other elements, such as Bi, Fe, Ni, Pb, Sb and Zn, were found at concentrations below 1 %. The average composition of the ES mix was analogous to the average composition of the sludge collected. Student's t-tests were applied for each element, verifying that there were no significant differences between the ES-mix composition and the average of the samples collected at a confidence level of 95 %.

Several mineral phases, such as domeykite (~ 27 % Cu_3As), cuprite (~ 22 % Cu_2O), copper metal (~ 19 % Cu), and poitevinite (~ 5 % $CuSO_4 \cdot H_2O$), were detected (Fig. S3.15, Annex I.3), with a low content of XRD-amorphous phase (about ~27 %).

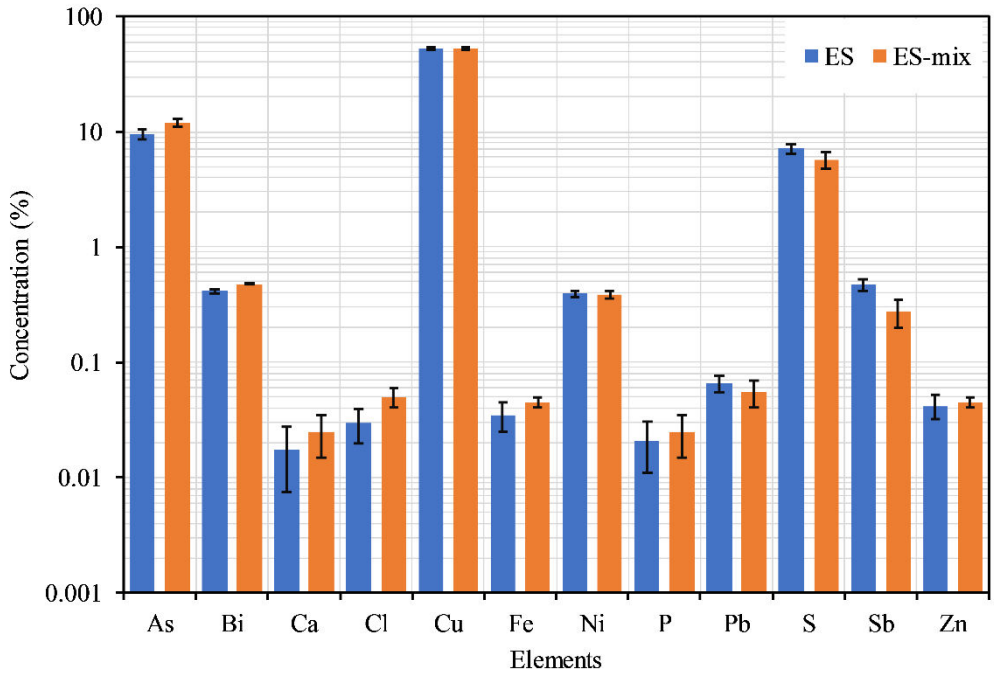

Figure 3.16. *Average composition of major elements present in ES samples. Standard uncertainty (1σ) calculated as the standard deviation of the mean* $\boldsymbol{\sigma = S_x / (n)^{1/2}}$

The thermal analysis data ratified the mineralogical composition. Four thermal events were observed (Fig. S3.16 of the supplementary material in Annex I.3). Water was detected in the two first events at 110 ºC and 277 ºC, thus the mass loss is probably associated with dehydration of different hydrated copper (II) sulfate species, such as $CuSO_4 \cdot 5H_2O$ (10 %) and $CuSO_4 \cdot H_2O$ (18 %), where only 5 % was crystalline, according to the XRD analysis. The third event at 454 ºC can be associated with the decomposition of anhydrous species (14 % $CuSO_4$), verified by the detection of SO_2 in the ICP-MS system (Singh et al., 2010; Földvári, 2011). In the fourth event at 850 ºC, no mass change was detected in the sample, indicating a state change, which could be due to domeykite melting, since the melting point of this species is around 827 ºC (Pereira et al., 2015; Ramsdell, 1929).

The SEM-EDS analysis of ES is shown in Fig. S3.17 and Fig. S3.18, in the Supplementary Material (Annex I.3). The EDS analysis indicated that the elemental composition was similar to that obtained in the XRF analysis, where the sample was mainly composed of Cu, As, and S (see Fig. S3.17). The sample presented particles mainly composed of Cu, S, and O (see point 1 of Fig. S3.17). The composition and morphology suggest that this particle was similar to chalcocyanite ($CuSO_4$). The sludge also contained particles identified as copper metal (point 2, Fig. S3.17). Moreover, the matrix contained particles composed of Cu and O (point 3, Fig. S3.18). The Cu and O proportion and cubic morphology suggest that this particle could be cuprite (Cu_2O). The ES sample also contained

particles mostly composed of Cu and As (point 4, Fig. S3.18), whose composition and dendritic structure correspond to domeykite (Cu_3As). It was also observed that the copper arsenide phase contained Bi-S-rich regions (point 5, Fig. S3.18) which were found in the pores or on the surface of Cu_3As. These results are in agreement with the literature consulted (Chen and Dutrizac, 2009; Hiskey and Maeda, 2003) and with those phases identified by XRD and thermal analysis.

Secondary electron images of the ES region and X-ray mapping of the principal elements (Cu, As, S, Bi, Ni, Pb, Sb and Zn) are shown in Fig. S3.19 (see, Supplementary Material, Annex I.3). The mapping revealed regions with a high content of Cu and As, confirming the presence of copper arsenide. Mapping also showed areas with high contents of Ni and S, suggesting that these elements can be in the form of nickel sulfates (Hoffmann, 2004; Wang, 2004). Likewise, there were also regions where Bi and S were coincident, confirming the presence of Bi-S-rich regions, which could be bismuth sulfate particles.

3.3.3.2 Dissolution of the electrolytic sludge

After this exhaustive characterization was performed, ES dissolution tests were carried out, in which several conditions were studied. A summary of the best results using different oxidizing agents is shown in Table 3.4. ES was successfully dissolved in the following conditions: the leaching agent was a solution composed of 1.4 M H_2SO_4 and 1.8 M HNO_3, the solid-to-liquid ratio was 1:20 g/mL, the stirring speed was 500 rpm at a temperature of 50 ºC, and the reaction time was 2.5 h. ES dissolution tests are reported and discussed extensively in a previous article (Paz-Gómez et al., 2021a).

***Table 3.4**. Summary of the conditions analyzed in the sludge dissolution experiments.*

Exp. ID	Oxidising agent	S:L (g/mL)	[H_2SO_4] (M)	[HNO_3] (M)	Gas flow (L/min)	time (h)	Temperature (°C)	Dissolution efficiency of the ES (%)
N-1.8-1.4	Nitric acid	1:20	1.4	1.8	-	2.5	50	100
A-2-2-C	Air	1:20	2.0	-	2	2.5	80	32
O-8-2-C	Oxygen	1:20	2.0	-	8	2.5	80	66

The composition of the ES solution used in these experiments is shown in Table 3.5.

***Table 3.5.** Elemental concentration of electrolytic sludge solution in mg/L except for elements with (*), which were measured in g/L*

As (*)	Bi	Fe	Cu (*)	Ni	Pb	Sb	S (*)	Zn
5.1	190	9.2	31	140	15	140	44	5.6

3.3.3.3 Copper recovery

In order to study the copper recovery by evaporative crystallization, two types of tests were carried out: 1) sequential experiments in which an initial volume of ES solution was evaporated in five stages until the solution was reduced by about 75 % (*CF* ~ 3.8) and the solids formed were removed at each step by filtration; and 2) non-sequential experiments in which same initial volumes of ES solution were evaporated separately up to different final volumes (V_1, V_2 and V_3) (see Fig. 3.17).

The physicochemical characterization of the solid phase obtained in the Cu recovery experiments is detailed below, as well as recovery efficiencies of the major elements. The composition of the final solutions can be seen in Table S3.7 in the Supplementary Material (Annex I.3).

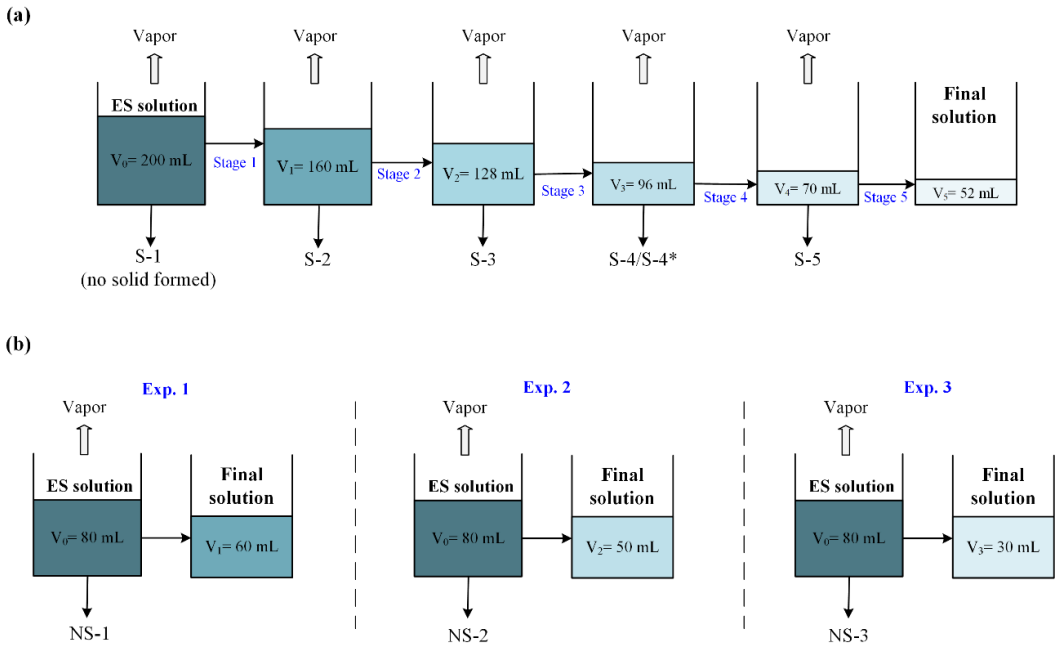

Figure 3.17. *Flowchart of copper recovery experiments: (a) sequential and (b) non-sequential.*

3.3.3.3.1 Characterization of solid phases obtained in Cu recovery

The compositions of the major and trace elements of the obtained solid phases in the sequential and non-sequential experiments are shown in Table 3.6. It is important to highlight that no solid was observed in the first stage of the sequential experiment (S-1, *CF* = 1.25). The obtained solids in the rest of the stages can be observed in Fig. S3.20 and Fig. S3.21 (Supplementary Material, Annex I.3).

***Table 3.6**. Chemical composition of the solids precipitated in the copper recovery experiments. V (mL) is the final volume. Detection limit (DL = 3 mg/L). S-4*= white dust.*

			Major elements (%)			***Trace elements (mg/L)***					
	Exp. ID	*V_i (mL)*	*As*	*Cu*	*S*	*Bi*	*Cr*	*Ni*	*Pb*	*Sb*	*Zn*
Sequential	S-2	128	0.14	25.3	12.8	68	11	45	< DL	9	4
	S-3	96	0.22	25.1	13.8	71	9	61	< DL	28	5
	S-4	70	1.50	24.0	13.7	61	7	113	3	139	10
	S-4*	**70**	**63.0**	**1.93**	**1.08**	**38**	**10**	**15**	**8**	**321**	**3**
	S-5	52	0.38	24.9	13.7	54	7	203	27	16	17
Non-sequential	NS-1	60	0.03	25.3	13.1	56	10	36	< DL	10	6
	NS-2	50	0.49	24.8	13.6	47	8	45	< DL	15	4
	NS-3	**30**	**5.10**	**22.0**	**11.8**	**31**	**8**	**73**	**< DL**	**393**	**7**

Most solids crystallized in the sequential experiments contain a high concentration of Cu (~ 25 %) and S (~ 13 %) and a minor proportion of As (< 0.5 %). The experimental mass ratio (Cu/S = 1.92) is similar to the theoretical ratio of copper sulfate pentahydrate (Cu/S = 1.94). Other elements, such as Bi, Cr, Ni, Pb, Sb, and Zn (< 100 mg/L), were also present in the sample. If the obtained $CuSO_4 \cdot 5H_2O$ is compared with copper sulfate pentahydrate product-type 2 used as private and public health area disinfectants and other biocidal products (see Table S3.8, Supplementary Material in Annex I.3), it can be seen that the blue vitriols formed present high concentrations of impurities, especially Ni and As, and consequently these precipitates cannot be marketed, according to the regulations and report consulted (BPC: Biocidal Product Committee, 2013; Regulation (EU) Nº 528/2012, 2012).

A white dust crystallized with the $CuSO_4 \cdot 5H_2O$ crystals (S-4) in the fourth stage. This dust was manually separated for analysis (S-4*) and was found to contain a very high concentration of As (63 %), while the Cu and S proportions were below 2 %, since their physical separation was not efficient. Furthermore, the dust contained low concentrations of Sb (~300 mg/L), Bi, Cr, Ni, Pb, and Zn (< 50 mg/L), which were their main trace elements. As a result of the presence of the remaining dust in $CuSO_4 \cdot 5H_2O$ crystals, sample S-4 had a concentration of As (1.5 %) ten times higher than that of the rest of the $CuSO_4 \cdot 5H_2O$ samples. This is due to the fact that a physical separation of the two solids could not be fully achieved, and thus contamination was observed in both solid phases.

Solids crystallized in the non-sequential experiments, i.e., NS-1 and NS-2, had compositions similar to those of the first two solids obtained in the sequential process, as expected. In contrast, the NS-3 solid mostly contained Cu (~ 22 %), S (~ 12 %), and As (~ 5 %) with Sb (~ 400 mg/L), Ni (> 50 mg/L), and Bi, Cr, Pb, and Zn (< 50 mg/L) as the main trace elements. In this case, the high As

concentration in NS-3 was due to the fact that both white dust (arsenic) and blue vitriol (copper sulfate crystals) phases could not be separated.

Fig. 3.18 shows the obtained diffraction pattern by XRD for two representative samples (S-2 for sequential experiments and NS-3 for the non-sequential process) as examples of the solids formed in both experiments. The only mineral phase identified in the S-2 sample was chalcanthite (~ 99.8 % $CuSO_4 \cdot 5H_2O$), agreeing with the composition given by the XRF results.

The main mineral phases present in NS-3 were chalcanthite (~ 86 % $CuSO_4 \cdot 5H_2O$) and arsenolite (~ 6.5 % As_2O_3), corresponding to about 80 % of the As removed as arsenic trioxide. The Cu, S, and As concentrations are in line with those obtained in the XRF analysis. The formation of arsenic trioxide can be explained by considering the equilibrium solubility of arsenious acid (H_3AsO_3) (Eq. 3.19), which comes from the dissolution of Cu_3As (Eq. 3.18). Its solubility decreases as the evaporated water increases, favoring the formation of As_2O_3 (Drahota and Filippi, 2009; Nordstrom et al., 2014). Furthermore, NS-3 had a low content of an amorphous phase (about 7 %), which could contain a poorly crystalline phase, which cannot be detected by the equipment.

$$Cu_3As + 3HNO_3 + 3H_2SO_4 \rightarrow 3CuSO_4 + H_3AsO_3 + 3H_2O + 3NO \qquad \textit{Eq. 3.18}$$

$$2H_3AsO_3 \leftrightarrow As_2O_3 + 3H_2O \qquad \textit{Eq. 3.19}$$

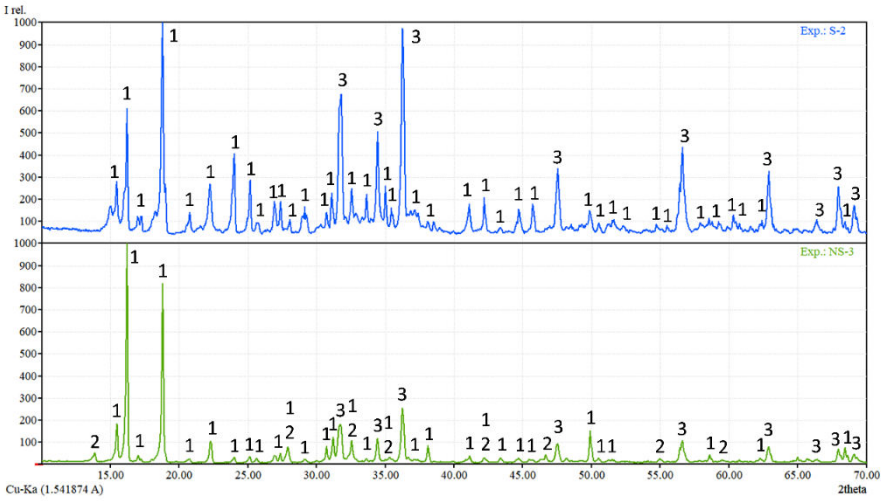

Figure 3.18. *XRD pattern of the obtained precipitate in the S-2 and NS-3 experiments. Mineral phases identified: chalcanthite-$CuSO_4 \cdot 5H_2O$ (1), arsenolite-As_2O_3 (2), and zincite-ZnO (3), which was used as internal standard.*

A thermal analysis was carried out to verify the identity of the white dust (S-4*) that formed along with the copper sulfate pentahydrate. The results are presented in Fig. 3.19, where a single thermal event can be observed at around 301 ºC. According to the literature consulted (Cervando and Viraca, 2013; Helsen et al., 2004; Kercher and Nagle, 2001), and the elemental composition of the sample, this thermal event must be associated with sublimation of the arsenic trioxide (arsenolite, As_2O_3) at around 280 ºC (see reaction 3.20). In addition, the gases detected by the coupled ICP-MS confirmed the presence of As_4O_6. In agreement with the mass loss, the sample contained around 93 % of this compound, corresponding to 70 % of arsenic, which is in line with the content of As given by XRF. Therefore, the white dust was demonstrated to be As_2O_3, meaning that around 70 % of the As contained in the ES solution is removed as arsenic trioxide.

$$2As_2O_{3(s)} \rightarrow As_4O_{6(g)} \qquad \textit{Eq. 3.20}$$

The DTA curve revealed that arsenic trioxide sublimation is an endothermic process. Other peaks were also observed above 400 ºC. These can be associated with the interaction of the remaining sample with the atmosphere (Földvári, 2011).

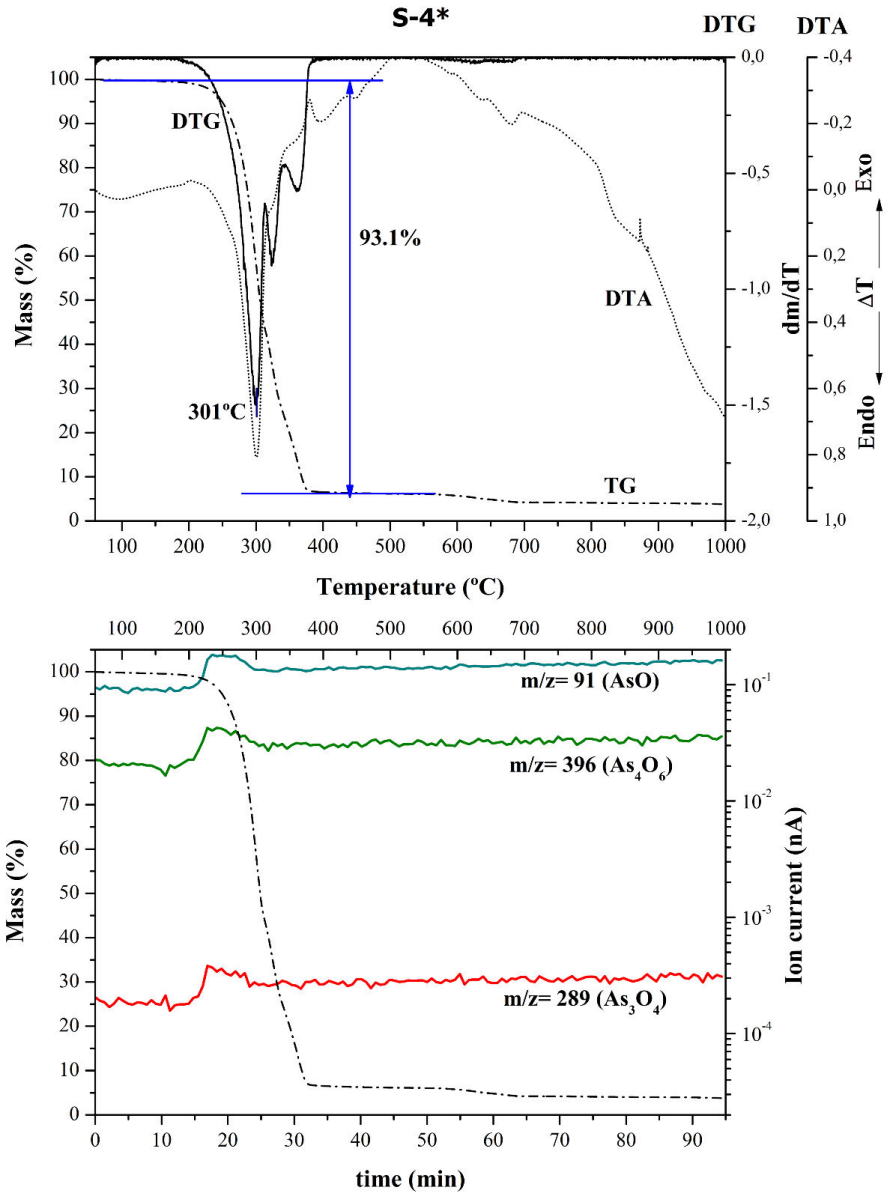

Figure 3.19. *TG-DTG-DTA curves of S-4* (white dust) sample.*

3.3.3.3.2 Copper recovery in the crystallization process

In order to assess the copper recovery (or the fraction of As removed in the case of dissolution cleaning), the recovery efficiency (*E*) was defined as the ratio between the mass of element X in the obtained solid at the end of the stage/experiment i (m_{Xi}) and the mass of X in the initial ES solution (m_{X0}) (see Eq. 3.21):

$$E\ (\%) = \frac{m_{X_i}}{m_{X_0}} \times 100 \qquad \textbf{Eq. 3.21}$$

The results are shown in Fig. 3.20 where the precipitation efficiency of the studied elements is shown as a function of the concentration factor ($CF = V_0/V_i$) for both sequential and non-sequential experiments.

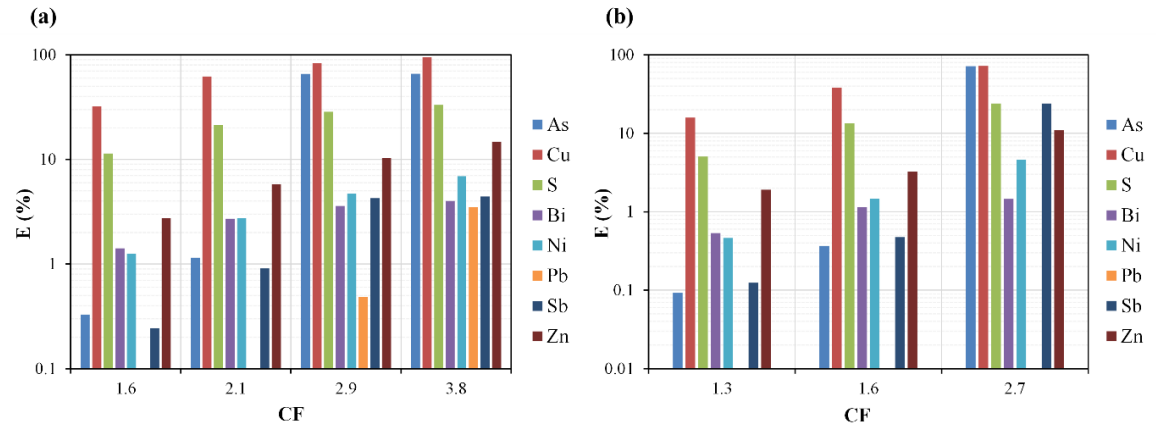

Figure 3.20. *Recovery efficiency (%) as a function of the concentration factor for both types of experiments: (a) sequential, (b) non-sequential.*

In both experiments, the recovery efficiency of Cu and S increased as the volume of the evaporated solution increased. In the sequential experiment, it was observed that more than 80 % of the Cu was crystallized when the *CF* was 2.9. The recovery efficiency of Cu was around 95 % when the solution was evaporated up to 75 % (*CF*= 3.8). On the other hand, in the non-sequential experiments, which were concentrated up to *CF* = 2.7, the *E* for Cu was around 70 %. This is a value similar to that found in the sequential experiment if the experimental uncertainties are taken into account (around 10% at 1 sigma level). Nevertheless, these results must be replicated to improve the control of the variables involved in *E* (temperature, impurity degree, etc.).

The recovery efficiency of As for evaporated fractions ($EF = (V_0\text{-}V)/V_0$) higher than 60 % ($CF = 1/(1\text{-}EF) > 2.5$) was constant, with values of around 70 %, proving that the As mainly crystallized at a specific *CF* (Fig. 3.20). As crystallization was produced at a *CF* of around 2.5, while for *CF* values lower than this critical value, its recovery is less than 1 %. However, further research is needed to determine the range in which arsenious acid (H_3AsO_3) becomes insoluble and forms arsenic trioxide As_2O_3.

In both experiments, the recovery efficiency of Ni and Zn was around 5 % and 10 %, respectively, for both the sequential and non-sequential methods (Fig. 3.20). In contrast, the recovery efficiency of Sb in the non-sequential experiment (NS-3) was around 24 % (Fig. 3.20b), which was higher than that obtained in the fourth step of the sequential experiment (~ 5 %) (Fig. 3.20a). Moreover, elements such as Bi and Pb had an *E* below 5 % in both cases. The formation of As_2O_3 favors the

coprecipitation of other impurities, such as Sb, according to the literature consulted (Peng et al., 2012; Zhou et al., 2011).

Finally, if the experimental data are compared with the theoretical curve for copper recovery as $CuSO_4 \cdot 5H_2O$ (Fig. 3.21), it can be observed that the experimental points have a similar tendency, where the percentage of copper recovery increases with the concentration of the solution, i.e., when the volume of evaporated solution increases.

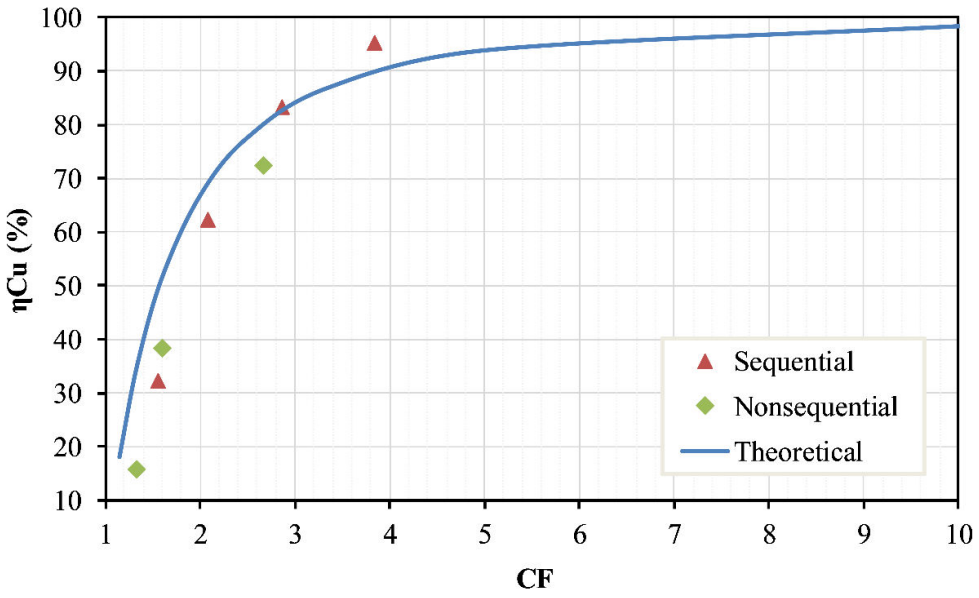

Figure 3.21. *Theoretical curve and experimental points of copper recovery (%) as a function of the concentration factor.*

3.3.4 Practical implications

The recovery of copper from ES (free of arsenic) has become a challenge for the copper industry, since the current way to recover copper from this sludge is by recycling it back to the FSF, which involves serious problems of arsenic accumulation in the industrial process, negatively affecting the quality of the cathodic copper. The process proposed in this study focuses on the recovery of copper from sludge, first by dissolving the ES in an acidic medium and then recovering the copper from the obtained ES solution using evaporative crystallization. Finally, copper recovered as copper (II) sulfate pentahydrate can be returned to the process free of impurities (mainly arsenic) and/or marketed (Fig. 3.15).

The copper sulfate obtained in the recovery experiments contained more than 99.5 % of $CuSO_4 \cdot 5H_2O$ and less than 0.5 % of other impurities (mainly As). This copper sulfate could be reintroduced in several stages of the industrial process. It could be sent back to the FSF, as is currently done with

ES, avoiding the problem of As accumulation when ES is directly recycled (point A, Fig. 3.15). A second more attractive proposal would be dissolving the $CuSO_4 \cdot 5H_2O$ crystals with H_2SO_4 and using it as an electrolyte, which could be introduced in the electrorefining process (point B, Fig. 3.15) or stage 1 of the ETP (point C, Fig. 3.15). Nevertheless, in this case, it must be verified that the obtained electrolyte conditions are suitable and do not affect the quality of cathodic copper. Thirdly, copper sulfate could be marketed for other applications, such as agriculture, antiseptic agents, electroplating processes, electronics, or water treatment. However, the saleable copper sulfate pentahydrate must have a minimum purity of 99.99 %, equivalent to 25.4 % of Cu (BPC: Biocidal Product Committee, 2013; Regulation (EU) Nº 528/2012, 2012). For this reason, the evaporative crystallization process is currently being optimized to reduce impurities to the appropriate level for commercialization.

The process of copper recovery by evaporative crystallization proposed in this work could generate two benefits. On the one hand, arsenic accumulation in the industrial process is decreased, thus the amount of hazardous wastes produced is also reduced, since there is less arsenic in the liquid effluents, which implies a reduction of the environmental impact. On the other hand, arsenic-free copper recovery improves the industrial process yield and could generate economic profit if the copper sulfate is sold or used in the copper refining plant as an electrolyte. This process furthers the aim of circular economy in industrial copper manufacture.

3.3.5 Conclusions

After a detailed characterization of the sludge obtained in the electrolyte treatment plant, experiments for recovering its copper content as copper sulfate pentahydrate by evaporative crystallization were designed and carried out. The main conclusions of this investigation are as follows:

1. The ES sample had a high Cu content, around 54 %, which is mainly present as Cu_3As, Cu_2O, Cu metal, and $CuSO_4 \cdot xH_2O$. ES also contained a high As concentration, around 10 %, mainly as Cu_3As. According to the composition and physicochemical properties found for this sludge, the ES can be an important secondary source of copper, although it is necessary to decrease or remove the As content for reprocessing or valorization.
2. The copper recovery experiments were successful, obtaining that more than 90 % of the Cu was recovered as $CuSO_4 \cdot 5H_2O$ by evaporative crystallization. Nevertheless, the $CuSO_4 \cdot 5H_2O$ obtained had a significant concentration of impurities, mainly As, when compared with the common copper sulfate product. Thus, the $CuSO_4 \cdot 5H_2O$ crystals must be purified to meet the demands of the industry or reintroduced into the industrial process. The impurities can be easily reduced by adding several recrystallization steps until reaching an appropriate level for their commercialization.

3. About 70 % of the As present in the sludge was removed as As_2O_3, according to XRD and thermal analysis. Thus, the As concentration can be drastically reduced from that which is currently returned to the process.
4. The cleaning of As_2O_3 from the traces of $CuSO_4 \cdot 5H_2O$ can be carried out by dissolving this copper sulfate in water, since arsenic trioxide is almost insoluble, although the recrystallization process could be conducted to recover the copper as copper sulfate free of arsenic compounds.
5. More experiments are needed to optimize the copper recovery process, as copper (II) sulfate pentahydrate, for the copper to be suitable as a commercial product, although it can be sent back as raw material in the pyrometallurgical or electrorefining process. In addition, it is necessary to investigate the stabilization of the obtained arsenolite, or convert it to scorodite, which is a very inert mineral of arsenic.

SUBCHAPTER 3.4

IMMOBILIZATION OF HAZARDOUS WASTES ON ONE-PART BLAST FURNACE SLAG BASED GEOPOLYMERS

3.4 IMMOBILIZATION OF HAZARDOUS WASTES ON ONE-PART BLAST FURNACE SLAG BASED GEOPOLYMERS

D.C Paz-Gómez, I.S Vilarinho, S.M Pérez-Moreno, J. Carvalheiras, J.L. Guerrero, Rui M. Novais, Maria P. Seabra, G. Ríos, J.P. Bolívar and João A. Labrincha.

*Sustainability (*under review)

Abstract

The immobilization of hazardous wastes in Ordinary Portland Cement (OPC) based materials has been widely studied and implemented. However, OPC based material production is associated with high carbon footprint and alternative solutions are needed. The geopolymer materials are a sustainable and eco-friendly alternative and can replace the OPC-based materials. Therefore, the main goal of this work was the immobilization of two hazardous wastes: copper wastewater sludge (CWS) and phosphogypsum (PG) in one-part geopolymer pastes and mortars using blast furnace slag (BFS) as the precursor and metasilicate as an activator. For that purpose, BFS was partially substituted by CWS and PG (5, 10 and 20 wt.%) in the geopolymer formulations. The geopolymer fresh and hardened state properties were evaluated, and the immobilisation of pollutants was determined through leaching tests. In the PG-containing pastes (PG5, PG10, PG20) it was observed that the compressive strength decreased with the increase of the PG amount, varying between 67 MPa and 19 MPa. The mortar MPG10 had a compressive strength of 13 MPa which means it can be used in construction sector. In CWS-containing pastes, the compressive strength of the specimens (CWS5, CWS10) was around 50 MPa. The corresponding mortar (MCWSs10) had 21 MPa which can be used in construction sector. Leaching tests showed that pastes and mortars immobilise the hazardous species of the wastes, excepting As from CWS. The best result was found in the highest compact paste (CWSs10) leached 2 mg/kg of As.

Graphical abstract

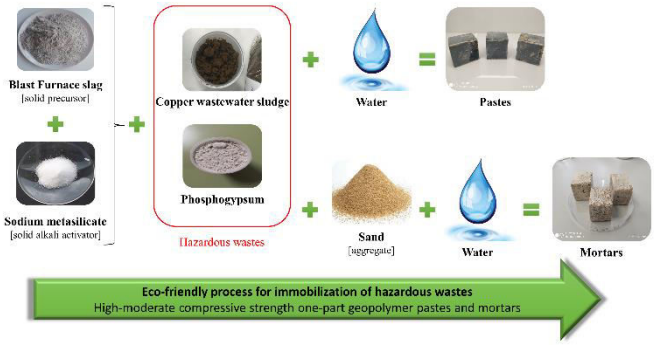

Keywords: One-part geopolymer; Hazardous waste; Immobilization; valorisation; circular economy.

3.4.1 Introduction

The demand for copper (Cu) continues to increase rapidly due to its crucial role in new technologies (Auping et al., 2012; Schipper et al., 2018b). World refinery production reached 24 Mt in 2019 having an increase of 30 % when compared to the reported value in 2009 which in line with the increasing demand of this material. The increase in the copper production also implies that the amount of generated waste (e.g., dust, sludge, and slag) and gas emissions rises (ICSG: International Copper Study Group, 2020). In recent decades, copper manufacturing industries have focused on systems to improve the recycling rate of the wastes and by-products, trying to reduce the environmental impact and achieve economic benefits, in line with the current European Union strategy for Circular Economy (Khan et al., 2020; Liao et al., 2019).

Atlantic Copper S.L.U is a company whose metallurgy complex is in Huelva (Southwestern Spain). This company is one of the biggest copper cathodes manufacturers in Europe. The plant produces about $3 \cdot 10^5$ t/y of high-purity copper cathodes (> 99.99 wt. % Cu) (Atlantic Copper, 2017). The industrial process generates several wastes and by-products, such as slag and effluents that are sent to the liquid effluent treatment plant (LETP), where the heavy metals and other impurities (mainly As) are removed. The treatment process involves four steps: homogenization, pre-treatment, polishing and ultrafiltration. Homogenization is carried out to control the composition and flow that feeds the system. In this stage, the effluents are stored in two tanks, one for acid/neutral effluents and another for alkaline effluents. In the pre-treatment, the effluents are mixed in a lamellar decanter where iron coagulants ($FeCl_3$ and/or $FeSO_4 \cdot 7H_2O$), an oxidizing agent (H_2O_2), and lime slurry (to adjust pH 10–11.5) are added. The stream is sent to the polishing stage where the arsenic is reduced, adding CO_2 to adjust the pH between 8–9, iron coagulant and other reactants in a second lamellar decanter. The outlet effluent is sent to an ultrafiltration (UF) system where fine particles that remain in the liquid effluent are removed. During the pre-treatment and the polishing stages metals precipitation generates sludges that are collected in the underflow of the decanters, mixed in the thickener, and sent to pressure filters. The final sludge is here designated CWS (copper wastewater sludge). About $2 \cdot 10^3$ t/y of CWS are produced and stored in a controlled landfill, located 70 km from Huelva city. This management strategy not only involves high transportation and storage costs but raises environmental concerns.

On another hand, in Huelva was located from 1965 to 2010 year two factories devoted to the phosphoric acid production, generating annually about 2.5 Mt of a waste called phosphogypsum

(PG). This waste was stored in big stacks in the saltmarshes of Tinto River covering a surface of about 1000 ha, and containing around 80–100 Mt of PG. Therefore, efforts are being done for the valorisation of this waste in other applications in order to reduce its environmental impact. This PG in many studies has been characterized, and it is mainly formed by gypsum ($CaSO_4 \cdot 2H_2O$), more than 95 %, and the remaining fraction are impurities containing F^-, P_2O_5, and other pollutants in trace concentrations (Bolívar et al., 2009; Guerrero et al., 2020; S. M. Pérez-Moreno et al., 2018).

The immobilization of hazardous wastes in Ordinary Portland Cement (OPC) based materials (e.g. mortars, concrete) is widely studied and implemented, despite the low effectiveness in several situations (Al-Kindi, 2019; Chen et al., 2009; Provis and Van Deventer, 2014; Shively et al., 1986). The use of geopolymer matrices seem more effective in several cases (Bankowski et al., 2004; Minaříková and Škvára, 2006; Van Jaarsveld et al., 1997), but there are some papers reporting low immobilization effectiveness (Fernández-Jiménez et al., 2005; Provis and Van Deventer, 2014; Vu and Gowripalan, 2018). Anyway, geopolymers show a lower carbon footprint when compared to OPC, namely a reduction in CO_2 emissions of up to 50 % if properly designed (L. Assi et al., 2018; Yang et al., 2013).

The conventional process (two-part) to obtain a geopolymer involves a reaction between a concentrated alkali solution (e.g., sodium hydroxide and sodium silicate), and a solid aluminosilicate precursor (metakaolin, fly ash, blast furnace slag - BFS) (Komnitsas and Zaharaki, 2007; Mobili et al., 2020). The geopolymer materials exhibit excellent physic-chemical properties, including high compressive strength, low shrinkage, controllable setting, acid resistance, fire resistance and low thermal conductivity, consequently, a wide range of potential applications in the construction sector is expected (Duxson et al., 2007; Komnitsas and Zaharaki, 2007). However, the use of corrosive (alkaline) solutions difficult the real manipulation of such solutions. An interesting/realistic alternative to produce these materials is named one-part or “just add water”. In this process, a solid alkaline activator is blended with the solid aluminosilicate precursor (dry mixture), and the reaction begins when water is added. In fact, this process is analogous to the preparation of OPC-based materials (Hajimohammadi and van Deventer, 2017; Luukkonen et al., 2018a).

Consequently, this work is focused on the immobilization of CWS and PG in one-part geopolymer pastes and mortars using blast furnace slag (BFS) as precursor. Geopolymers materials were prepared by substituting 5, 10 and 20 wt.% of BFS by the residues. Fresh and hardened state properties were analysed, and immobilization efficiency was evaluated through water leaching test, to determine the pollutant fixation.

3.4.2 Materials and Methods

3.4.2.1 Materials

Blast Furnace slag (BFS) from Ecocem, Aix-en-Provence, France, was used as the main solid precursor. BFS is a product made by rapidly cooling a slag melt, obtained by smelting iron ore. The precursor was partially replaced by two hazardous wastes, namely phosphogypsum (PG) and wastewater sludge from copper cathodes production (CWS). PG samples were collected from the PG stacks, which are located less than 1 km from Huelva city (Spain). CWS samples were collected in the liquid effluent treatment plant of Atlantic Copper, a copper smelting plant located in Huelva. After collection, both residues were immediately dried at 60 ºC, milled and manually homogenized. CWS residue was further milled in a mill ring (Retsch, RS 100) and then sieved through 63 μm mesh. Granulated anhydrous sodium metasilicate (Na_2O= 47–49.5 %, SiO_2= 50.5–53 %) from Sigma-Aldrich, was used as a solid alkaline activator and, for mortars preparation, commercial natural sand from Weber Saint-Gobain (W), Aveiro, Portugal, was used as aggregate. Sand particles size ranges between 0.5 and 1 mm.

3.4.2.2 Preparation of geopolymer pastes

One-part geopolymer pastes were prepared, and the composition of specimens is shown in Table 3.7. The letters stand for the solid precursor used and the numbers for the substitution (mass %): “R” is the reference geopolymer paste prepared only with BFS; “PG” and “CWS” denote the respectively used residues. The “s” indicates that the waste was sieved at 63 μm. Finally, the letter “M” was used to designate the mortars. For example, PG5 is a paste where PG replaced 5 wt.% of BFS and MPG10 is a mortar where PG replaced 10 wt.% of BFS.

The geopolymers preparation procedure was the following:

1. The solid components (precursor, activator and aggregated, if applied) were mixed and homogenized manually in a plastic bag for about 1–2 min.
2. The solids were mechanically mixed while adding the water for 1 min.
3. The fresh paste was manually mixed for 1 min.
4. The fresh paste was, once more, mechanically mixed for 1.5 min.
5. The fresh paste was cast into pieces (40×40×40 mm), on metallic moulds, and vibrated for 2 min using an electric vibrator.
6. The specimens were covered with a plastic film and kept at ambient temperature during the first 24 h of curing.

7. All the specimens were unmoulded and introduced into the climatic chamber (20 ºC and 65 % RH) until the 7th and 28th curing day.

Table 3.7. *Compositions of specimens and designation.*

Specimen Name	Mixture Proportion (g)				
	BFS	**Waste**	***Sodium metasilicate***	**Sand**	**Water/Binder**
R	100	-	10	-	0.38
PG5	95	5			0.37
PG10	90	10			0.36
PG20	80	20			0.38
CWS5	95	5			0.38
CWS10	90	10			0.39
CWSs10	90	10			0.38
M	100	-	10	400	0.71
MPG10	90	10			0.71
MCWSs10	90	10			0.71

3.4.2.3 Materials characterization

The raw materials used to prepare the geopolymer specimens were analysed by different analytical techniques 1) X-ray fluorescence (XRF), on a Philips Xert PRO MPD spectrometer, used to determine the major elements (as oxides); 2) X-ray diffraction (XRD), with a Panalytical X'Pert PRO^3 diffractometer and X'Pert HighScore Plus software to identify crystalline phases; 3) The particles size distribution was determined by laser diffraction technology using a HORIBA Scientific LA-960V2 analyser, working from 10 nm to 3000 μm; 4) Scanning electron microscopy (SEM, Hitachi S4100), used to study the microstructure and morphology of the samples.

3.4.2.4 Geopolymer characterization tests

The fresh pastes were subjected to three tests: 1) flow table test was used to assess the consistency of the paste, in agreement with the EN 1015-3 standard (CEN: European Committee for Standardization, 1998); 2) setting time (initial and final) was determined using the Vicat apparatus, according to the EN 196-3 standard (CEN: European Committee for Standardization, 2005); 3) The calorimetry test was performed to evaluate the temperature evolution upon the first 24 h of curing. In this test, the relative humidity and temperature were controlled being 65 % and 20 ºC, respectively.

After 7 and 28 days of curing, the compression strength of the samples was determined using a Universal Testing Machine (Shimadzu AG-25TA) with a displacement rate of 0.5 mm/min, according to the EN 1015-11 standard (CEN: European Committee for Standardization, 1999). The

water absorption of specimens was measured by weight variation after total immersion in water for 24 h. The capillary coefficient was determined by immersing one of the faces of each specimen in 5–10 mm water, according to the EN 1015-18 standard (CEN: European Committee for Standardization, 2002c). The apparent density of specimens was also determined, by measuring their mass and volume (cubic regular shape). In all those tests, three replicates were used, and the respective deviation error was calculated.

Further, the geopolymer specimens were characterized after 28 days of curing by some of the previous analytical techniques (XRD and SEM). Additionally, attenuated total reflection Fourier transform infrared spectroscopy (FTIR-ATR), performed on a Perkin Elmer SPECTRUM BX FT-IR apparatus, was used to determine the vibrational-bonds (functional group) formed in the geopolymer. The spectra were obtained over the wavenumber range 4000–400 cm^{-1}, with an 8 cm^{-1} resolution and 128 scans.

Finally, leaching tests were carried out following the EN 12457-2 standard (CEN: European Committee for Standardization, 2002b) to evaluate the pollutants mobility on specimens cured for 28 days. The extraction fluid was distilled water at a liquid/solid ratio of 10 L/kg (± 2 %). The monolithic specimens were submerged in distilled water without agitation for 24 ± 0.5 h. Then, the solution was collected and measured in total reflection x-ray fluorescence spectrometer (TXRF – S2 PICOFOX 50 keV), with detection limit raging in the ppb.

3.4.3 Results and Discussion

3.4.3.1 Raw materials characterization

The chemical composition of the materials used as precursors (BFS, PG and CWS) are presented in Table 3.8. The BFS sample is majorly composed of CaO, SiO_2 and Al_2O_3 (approximately 47 wt.%, 33 wt.% and 9 wt.%, respectively), enabling its use as a solid precursor in the synthesis of geopolymers as reported recently (Gonçalves et al., 2021). MgO and SO_3 are present in lower proportions (approximately 7 wt.% and 2 wt.%, respectively). PG and CWS also presented a high concentration of CaO (about 40 wt.% and 69 wt.%, respectively), but the amount of SiO_2 and Al_2O_3 is very low (around 2.4 wt.% and 0.40 wt.%, respectively). As expected, PG is very rich in SO_3 (around 52 wt.%), while F^- concentration is 3.3 wt.%. In CWS Fe_2O_3, MgO, SO_3 contents exist in proportion between 15–3 wt.%. Furthermore, CWS contains As (around 3.4 wt.%) as the main trace (and hazardous) element, and others such as Ba, Cu, Pb, Sb, Sr, and Zn in a concentration less than 1 %. The EN 197-1 standard does not specify the admissible amount of these elements.

Due to the lack of standards for geopolymers, the EN 197-1 standard (CEN: European Committee for Standardization, 2000) was used to define the composition, specification and conformity criteria. The loss on ignition (LOI) of a mixture must be lower than 5 %, and this limits the maximum admissible level (14 wt.%) of CWS that shows LOI of 35 %. This limit assures that chlorides content is below 0.10 wt.%. SO_3 content can vary between 3.5–5 % depending on the application. SO_3 content was acceptable in BFS and CWS, but is much higher in PG, limiting its admissible incorporation amount to 10 wt.%.

Table 3.8. *Chemical composition of the materials used in the preparation of geopolymers, estimated by XRF (major components represented as oxides).*

	BFS	**PG**	**CWS**		**BFS**	**PG**	**CWS**
Major Components		wt. %		Minor Components		wt. %	
Al_2O_3	9.1	0.40	0.40	As	-	-	3.4
CaO	47	40	69	Ba	0.06	0.02	0.80
Fe_2O_3	0.33	0.23	15	Ce	0.04	-	-
K_2O	0.58	0.03	-	Cl	0.02	-	0.36
MgO	6.7	0.04	3.6	Cu	-	0.01	0.65
MnO	0.21	-	0.09	F-	-	3.3	-
Na_2O	0.23	0.13	0.24	Pb	-	-	0.29
P_2O_5	0.01	0.95	0.14	Sb	-	-	0.06
SiO_2	33	2.4	2.3	Sr	0.06	0.08	0.05
SO_3	1.7	52	3.8	Zn	-	-	0.34
TiO_2	0.80	0.04	-	Zr	0.02	0.01	-
				LOI	**0.20**	**2.4**	**36**

X-ray diffractogram of BFS, PG and CWS are shown in Fig.3.22. BFS is highly amorphous, as indicated by the broad peak between 20º and 40º (2θ). Gypsum ($CaSO_4 \cdot 2H_2O$) and calcite ($CaCO_3$) were the identified crystalline phases. Intense peaks of gypsum are observed in PG. The crystalline phases present in the CWS sample are calcite, gypsum, iron oxide hydroxide ($Fe_{21}O_{31}(OH)$), and portlandite ($Ca(OH)_2$).

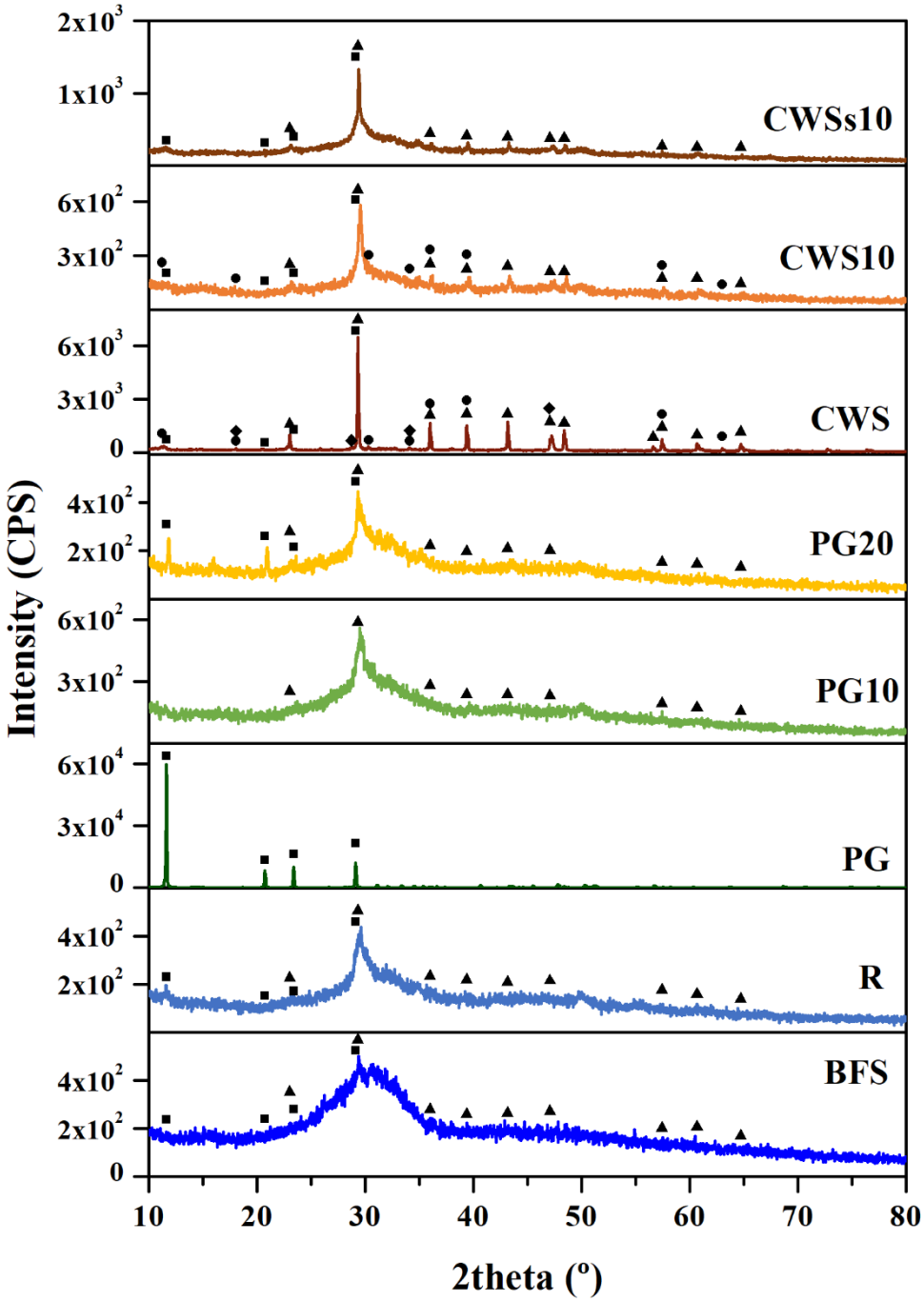

Figure 3.22. *XRD patterns of the raw materials (BFS, PG and CWS) and the R2, PG10, PG20, SW10 and SWs10 specimens. Minerals phases identified: Gypsum-$CaSO_4 \cdot 2H_2O$ (■), calcite-$CaCO_3$ (▲),iron oxide hydroxide-$Fe_{21}O_{31}(OH)$ (●) and portlandite-$Ca(OH)_2$ (♦).*

The particle size distributions of precursor and wastes are shown in Fig. 3.23. The median particles size (D_{50}) is 6.7 µm, 10.8 µm and 10.9 µm, respectively, for BFS, PG and CWSs, being naturally superior (34.7 µm) for CWS. The milling of this waste adjusted the size distribution to the one of PG. BFS shows a broader distribution, including finer particles than the wastes. The observed

fineness assures high reactivity in the geopolymerization process. At the same time, fine particles fill the existing space and assure high compactness (L. N. Assi et al., 2018; Sambucci et al., 2021).

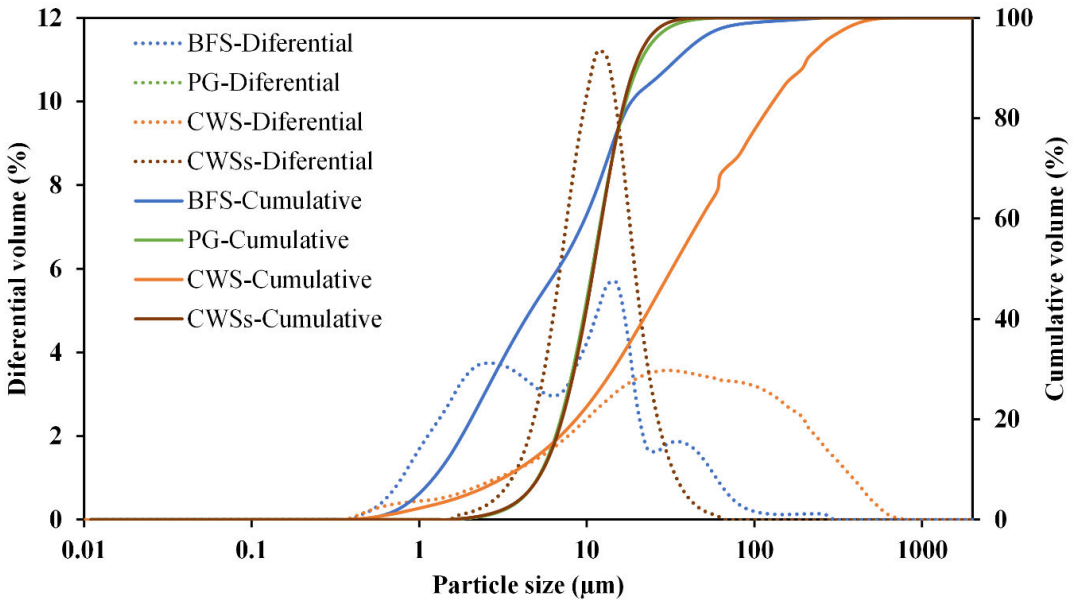

	d_{10} (µm)	d_{50} (µm)	d_{90} (µm)
BFS	1.3	6.7	30.3
PG	5.4	10.8	20.0
CWS	4.0	34.8	192
CWSs	5.5	10.9	19.3

Figure 3.23. *Particle size distribution of BFS and wastes: PG and CWS.*

SEM images of the wastes (PG and CWS) are shown in Fig 3.24. Gypsum particles in PG are easily denoted by their typical tabular shape. By contrast, CWS particles have irregular shapes and tend to form agglomerates.

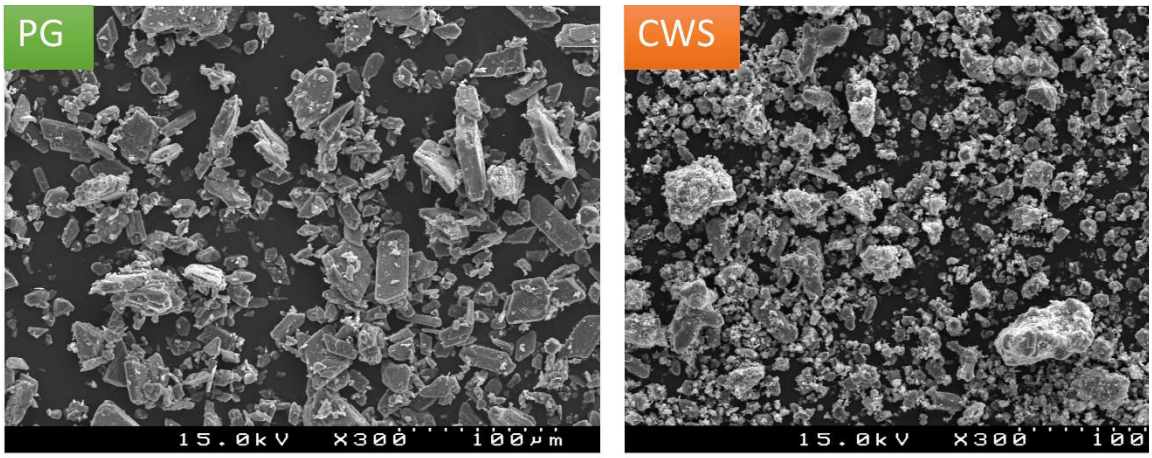

Figure 3.24. *SEM images of PG and CWS.*

3.4.3.2 Geopolymers characterization

3.4.3.2.1 Fresh state

Values of spread in the flow table for pastes and mortars are illustrated in Fig 3.25. The increasing proportion of PG in the mixture (PG5, PG10 and PG20 with water-to-binder ratio (W/B) of 0.37, 0.36 and 0.38, respectively) enhances the flowability. This behaviour can be associated with the calcium sulphate content of the residue since gypsum spreads easily. Additionally, free-sulphate anions (SO_4^{2-}) can react and consume the alkaline activator and hinder the geopolymerization process (Lancellotti et al., 2015; Rattanasak et al., 2011). Although, the differences in flowability can also be associated with the decrease of the amount of reactive precursors. The reactivity loss is also denoted by the increase of the setting time (Fig. 3.26), again expected for a gypsum-rich component. Spread values also tend to enhance with increasing amounts of CWS, denoting reactivity retarding (Luukkonen et al., 2018a; Zhang et al., 2018). The setting time is, coherently, longer. These differences are equally observed on mortars but seem less expressive than in pastes since effects are attenuated by the presence of sand and the use of a larger W/B ratio (0.71).

According to EN 197-1 (CEN: European Committee for Standardization, 2000), the initial setting values of the MPG10 and MSWs10 specimens seem appropriate for real applications without requiring the use of setting retarders or accelerators. Common types of cement (CEM I to CEM V or CEMI-SR 0 to 3) have an initial setting time between 40–60 min.

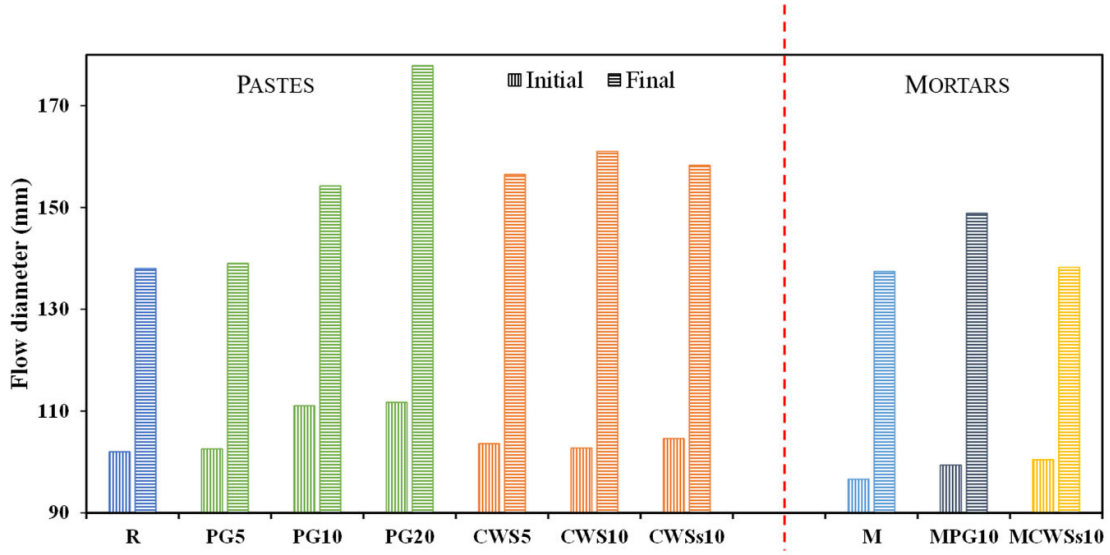

Figure 3.25. *Flow diameters of the specimens (pastes and mortars).*

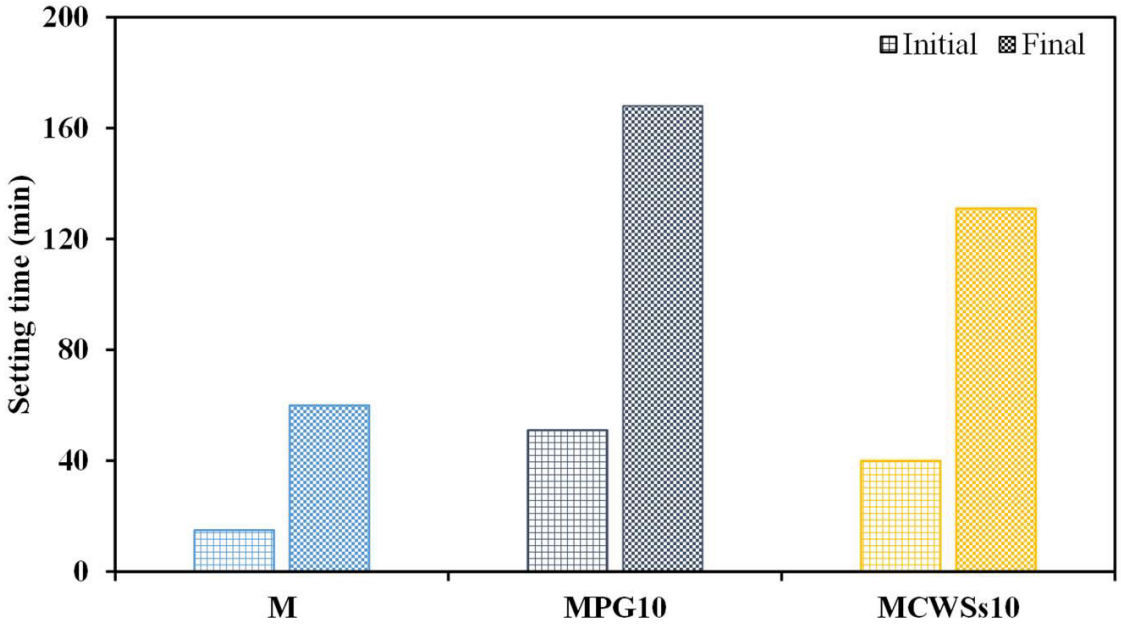

Figure 3.26. *Setting times of prepared mortars.*

Fig. 3.27 shows the temperature evolution of selected pastes during the first 24 h of curing. Two exothermic peaks can be seen in all samples. For R specimen, the first peak occurred at about 15 min after the mixing with water and is named pre-induction period. It corresponds to the wetting and dissolution of the activator (metasilicate). On CWSs10 sample this peak has a similar magnitude but

its maximum is observed after 30 min. On PG10 sample the peak has a much lower intensity, confirming the reactivity decrease of the mixture caused by the presence of $CaSO_4 \cdot 2H_2O$ and due to a change in the alkalinity of the paste (Criado et al., 2018; Provis and Van Deventer, 2014).

On R sample a second peak is observed around 7 h after water addition, corresponding to acceleration and deceleration periods that are associated with polymerization and condensation reactions (Criado et al., 2018; Luukkonen et al., 2018b). SWs10 shows a similar peak, again slightly delayed with respect to R. On PG10 sample this peak is again much less intense and the delay is more expressive (about 5 h). These observations are in line with the discussed differences in the setting behaviour of the various mixes.

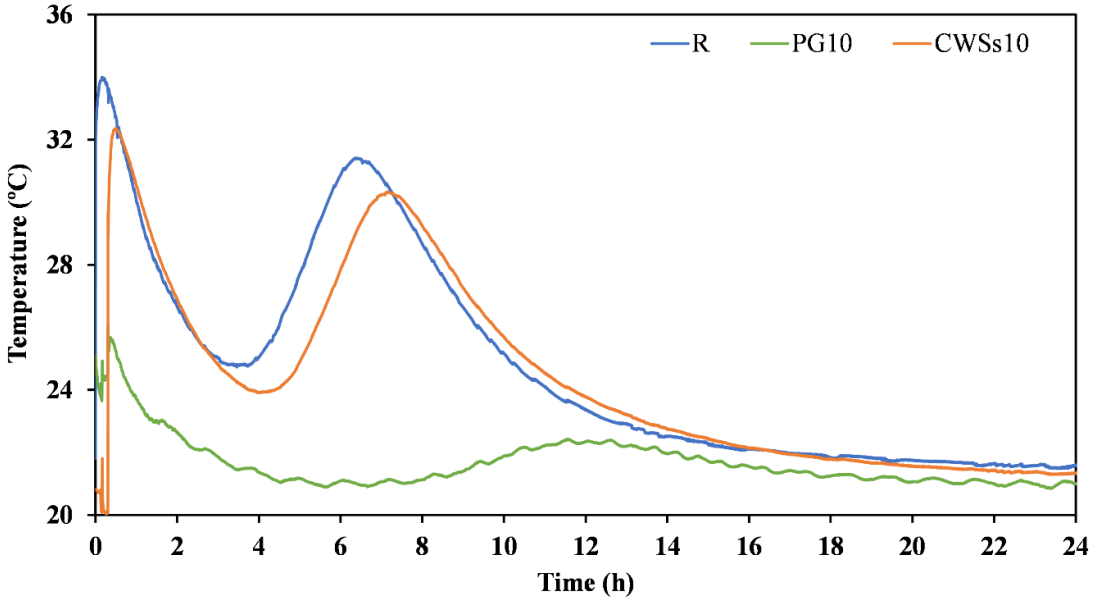

Figure 3.27. *Calorimetry curves upon the first 24 h of curing for selected specimens: R, PG10 and CWSs10.*

3.4.3.2.2 Hardened samples

Fig. 3.28 shows the compressive strength of the studied specimens cured for 7 and 28 days. Pastes presented higher mechanical resistance (3x more in general) than the corresponding mortars, an expectable behaviour since aggregates are not reactive and binder: aggregates ratio used was 1:4. In general, there is a strength gain from 7 to 28 days, only the CWSs10 paste reveals an unexpected drop.

R specimens show a compressive strength of about 79 MPa after 28 days of curing. The substitution of BFS by the two wastes induces a decrease of the mechanical resistance that tends to be intensified when their amount rises. The strength of the geopolymer is associated with the solubility of alumina

and silica from precursor (BFS). PG contains calcium sulphate that decreases the dissolution of BFS and alters the gel formation. PG5 shows 67 MPa while PG20 reached only 19 MPa after 28 days of curing. Looking at the specimens with CWS, relatively high compressive strength is observed for CWS5 and CWS10 samples, over 50 MPa. However, the CWSs10 specimen, prepared with sieved (< 63µm) sludge, shows a drop from 56 MPa to 31 MPa between the 7th and 28th curing days. Microcracking was observed in these samples (see Fig. S3.22, in supplementary materials, Annex I.4) upon curing/drying between the two mentioned dates, as a result of the higher compactness of the material that might difficult the microstructural evolution during the polycondensation process (Lee et al., 2016; Luukkonen et al., 2018a). This paste also required a higher amount of water to achieve the desirable flowability, as a consequence of the higher fineness of sieved sludge particles. More water will then be removed upon drying, causing higher shrinkage.

Compressive strength values of 26 MPa, 21 MPa, and 13 MPa were obtained for M, MCWSs10 and MP10 mortars, respectively. These values are admissible for applications in construction. Following the EN-1992-1-1 (CEN: European Committee for Standardization, 2004) mortar can be used in structural applications, while the others (strength values between 10–25 MPa) could be employed as non-structural material. These values can be improved in further trials, by playing with the binder: aggregates ratio and adjusting the particle size distributions. The mortars can be seen in Fig. S3.23, in the supplementary material, Annex I.4.

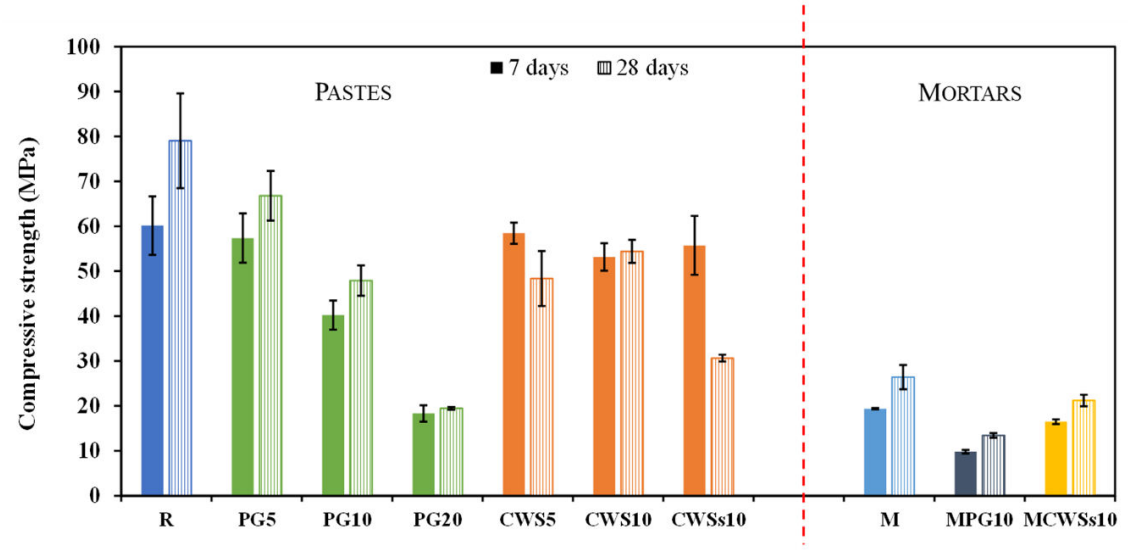

Figure 3.28. *Compressive strength at 7 and 28 days of curing of geopolymer: pastes and mortars.*

The apparent density of the studied specimens, as well as their water absorption by total immersion are shown in Fig 3.29.

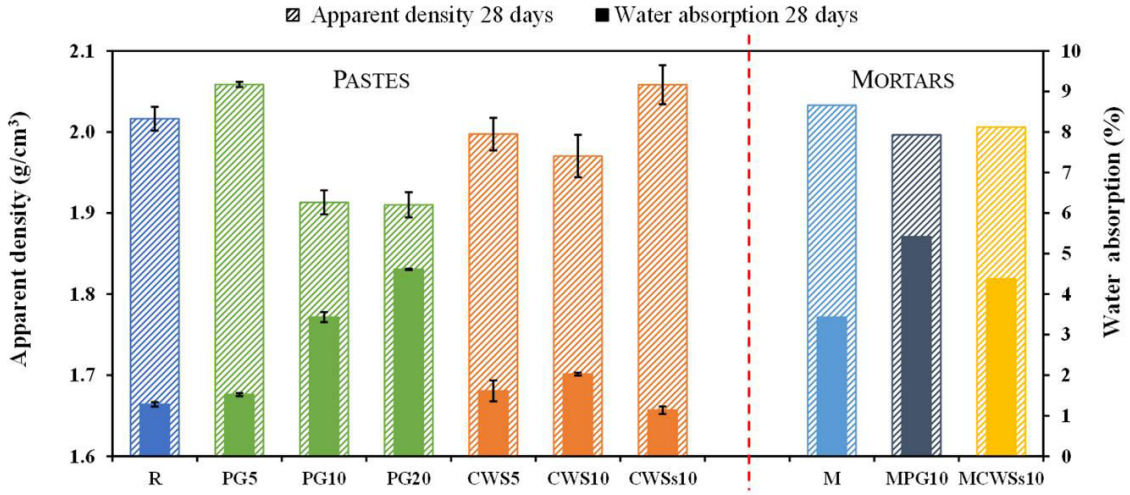

Figure 3.29. *Apparent density and water absorption by total immersion of samples cured for 28 days.*

The apparent density of pastes and mortars varied between 1.9–2.1 g/cm^3. The apparent density of R is 2.02 g/cm^3. Looking at the specimens with PG, the incorporation of 5 wt.% of PG (PG5) slightly increased the apparent density (2.06 g/cm^3) in comparison with R, but when 10 wt.% and 20 wt.% (PG10 and PG20) was incorporated apparent density decreased to 1.91 g/cm^3. For samples with CWS, the density slightly decreased from 2.00 to 1.97 g/cm^3 when 5 wt.% and 10 wt.% of sludge was incorporated. CWSs10 specimen (sieved at 63 μm) is slightly denser (2.06 g/cm^3), confirming its higher compactness. Differences between the prepared mortars (M, MPG10 and MCWSs10) are coherent with the variations of the respective pastes.

Water absorption is directly related to the open porosity of the samples. In general, denser pastes tend to absorb less water. The only exception is the CWSs10 sample, due to the above-mentioned formation of microcracks. All mortars show more expressive water absorption values since the use of coarser aggregates tend to create porosity. This also explains their lower mechanical resistance, as already discussed in Fig 3.28.

Most of the prepared specimens show good quality since the water absorption is less than 3 %. Only those specimens that exhibit water absorption values greater than 5 % might have notorious compressive strength deterioration (Vilarinho et al., 2021; Yahya et al., 2017). For conventional (two-part) geopolymers, reported water absorption values are between 5 and 11%. (Mermerdaş et al., 2017; Novais et al., 2018).

Fig. 3.30 illustrates the data of the performed capillarity tests. The capillarity coefficient of the specimens was determined through the slope of the straight line linking the representative points of

the measurements done at 10 min and 90 min. The capillarity coefficient of M, MPG10 and MCWSs10 is 0.08 kg/m^{2}min$^{0.5}$, 0.09 kg/m^{2}min$^{0.5}$ and 0.10 kg/m^{2}min$^{0.5}$, respectively. These results agree with the ones reported in a previous work (Gonçalves et al., 2021) and are lower than those reported for OPC mortars (0.5–0.9 kg/m^{2}min$^{0.5}$) (Deboucha et al., 2017; Mobili et al., 2020), and for conventional geopolymers (0.3–0.5 kg/m^{2}min$^{0.5}$) (Mobili et al., 2020; Novais et al., 2018; Saeli et al., 2019).

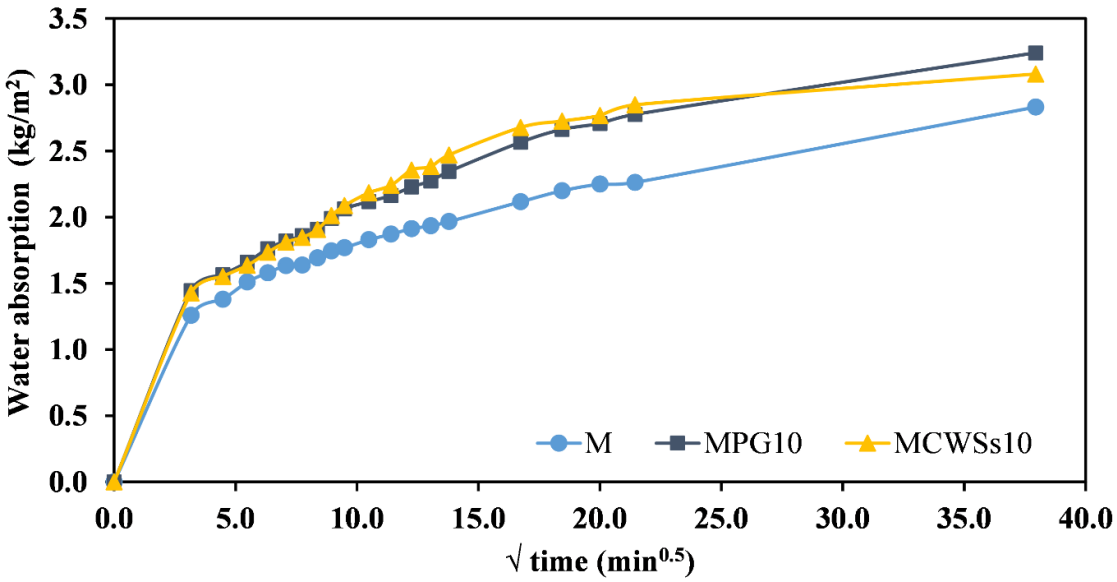

Figure 3.30. *Capillarity of mortars after 28 days of curing.*

The X-ray diffraction patterns for the most representative specimens are shown in Fig.3.22. Gypsum ($CaSO_4 \cdot 2H_2O$) and calcite ($CaCO_3$) were the only two crystalline phases identified in the R, agreeing with the crystalline phases identified in BFS. In PG10 specimen calcite has the only detected crystalline phase, while in PG20 $CaSO_4 \cdot 2H_2O$ was also detected. In CWS10 sample gypsum, calcite and bernalite ($Fe(OH)_3$) were detected, but this last phase was not identified in CWSs10. These data suggested that identified crystalline phases can be inherited from raw materials (that remain partially unreacted), or might result from recrystallization after the geopolymerization process (Luukkonen et al., 2018b; Mádai et al., 2015; Novais et al., 2018).

Geopolymerization products are mainly amorphous, like cement hydrates. FTIR-ATR spectra of the most representative specimens after 28 days of curing are shown in Fig. 3.31. Absorption bands located between 3000–1647 cm^{-1} correspond to stretching vibrations of O-H and O-H-O groups, indicating the presence of water molecules (Abdollahnejad et al., 2015; Qiu et al., 2019). The peak observed around 1398 cm^{-1} is probably due to the asymmetric stretching of the O-C-O bonds,

suggesting the presence of calcite from the raw materials (BFS or CWS) or superficial carbonation of the specimens during curing (Bernal et al., 2011; Buruberri et al., 2019; Qiu et al., 2019). Absorption bands located between 1130–1040 cm^{-1} are attributed to the asymmetric stretching vibrations of the Si-O-T bonds (T = Si or Al tetrahedral units), indicating the formation of a geopolymeric structure (Bernal et al., 2011; Buruberri et al., 2019; Gonçalves et al., 2021; Hakem Aziz et al., 2020; Qiu et al., 2019). The absorption bands between 803–761cm^{-1} are related to the Al-O and Si-O symmetric stretching vibrations and the bands around 626–523 cm^{-1} are assigned to the symmetric stretching vibrations of Si–O–Si and Al–O–Si group, corresponding to the formation of a geopolymeric network (Kumar and Kumar, 2011; Panias et al., 2007; Qiu et al., 2019). The change in the peaks intensity is probably associated with the structural reorganization of geopolymer matrix, giving information on the polymerization degree (Kumar and Kumar, 2011; Qiu et al., 2019). In Fig.3.31 can be seen that the polymerization degree of the PG10 and PG20 specimens is smaller than in SW10 and SWs10 specimens. Whereas R samples had a greater polymerization degree. Observing the peaks intensity, it can be concluded that water content decreased R< CWS10< CWSs10< PG10 < PG20.

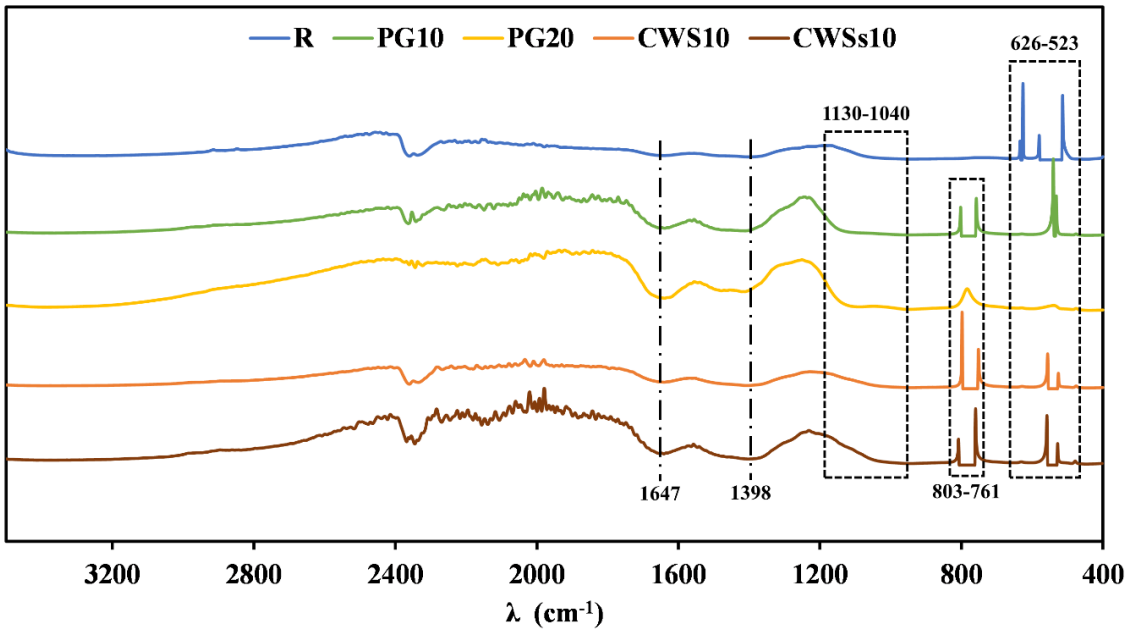

***Figure 3.31**. FTIR-ATR spectra of specimens without sand: R, PG10, PG20, CWS10 and CWSs10*

Fig. 3.32 shows the microstructure of the most representative specimens after 28 days of curing. In general, crystalline phases were not observed in geopolymeric materials. All specimens presented a heterogeneous microstructure composed of geopolymerization gel and partially reacted or unreacted particles. The relative volume of unreacted particles rises with the increase of PG content

(PG20>PG10) and decreases with the use of finer/sieved CWS (CWS10>CWSs10). Also, a smaller volume of unreacted particles was observed in the reference material (R). A large amount of unreacted particles implies a lower polymerization degree, which affects the compressive strength (Qiu et al., 2019; Yousefi Oderji et al., 2019). Furthermore, there are microcracks present in the specimens, deserving a future change of the curing conditions (Luukkonen et al., 2018b).

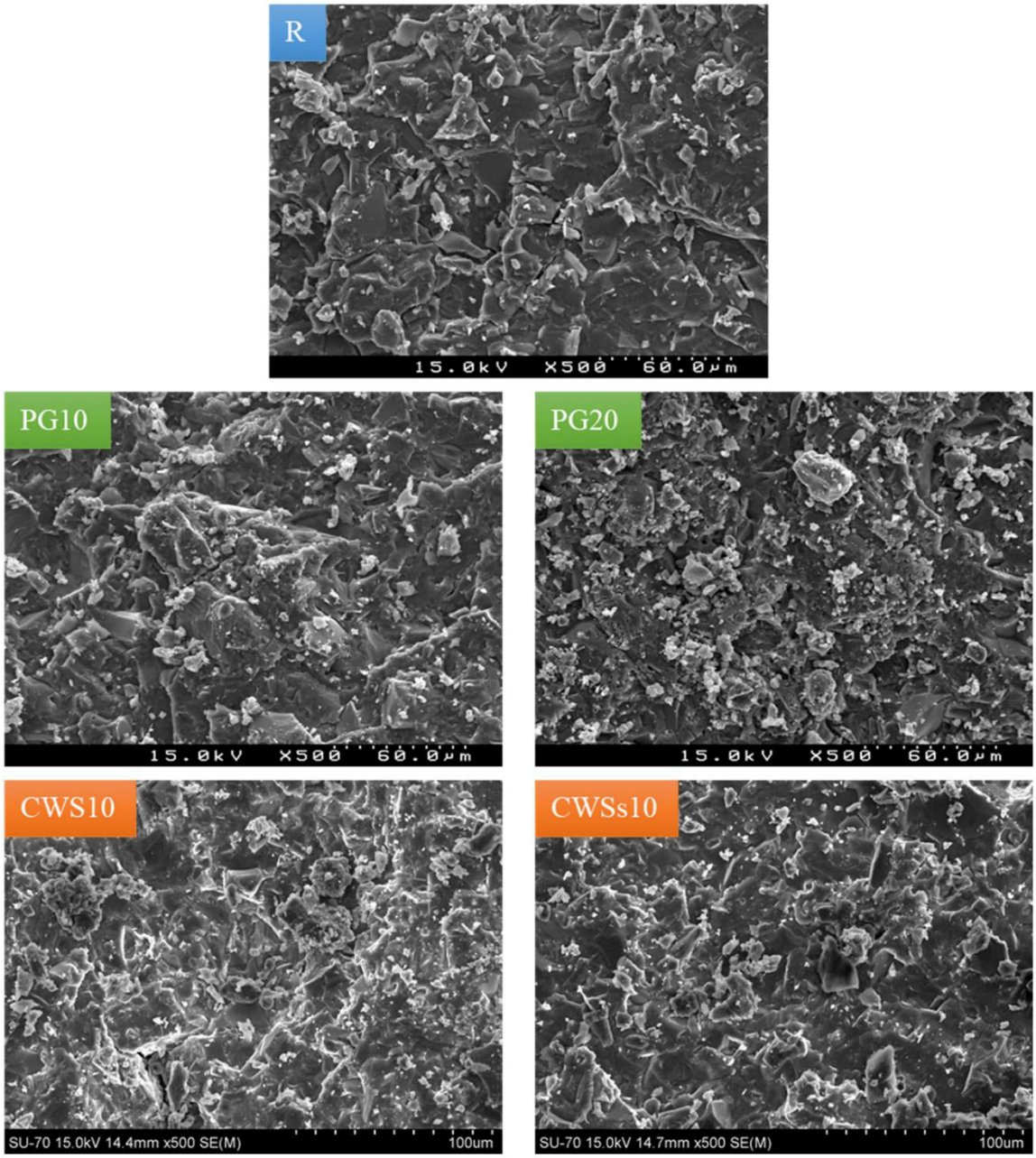

Figure 3.32. *SEM images of the specimens: R, PG10, PG20, CWS10 and CWSs10.*

3.4.3.3 Leaching test

The leaching test results are shown in Table 3.9. The leaching test determined that the reference specimens (R and M) and PG specimens (PG5, PG10 and WPG10) produce leachates with low contents of pollutants, according to the thresholds established in the Directive 2003/33/EC (Council of the European Union, 2003), which defines the threshold concentration for non-hazardous (NHM) and hazardous materials (HM). In PG specimens, the leached amount of S (as SO_4^{2-}) is moderately high but does not exceed the established thresholds. CWS-containing samples can be considered hazardous since the leached concentration of As exceeds 2 mg/kg. Only the CWSs10 sample is in the limit, certainly because of its higher compactness. This occurs despite the identification of microcracks in the sample. However, the higher porosity of the mortar formulated with that paste (MCWSs10) responds for the high leached amount from this sample. Consequently, the immobilization of As in such geopolymer matrixes may be possible, but further studies are necessary to determine the optimal processing conditions (e.g., fineness of components, curing conditions, etc).

Fernández-Jiménez et al. (Fernández-Jiménez et al., 2005) studied the fixation of arsenic in cementitious material activated by alkali, also obtaining a high content of leached As (50–90 mg/L). These values are higher than the content of leached As for all the specimens studied. However, it is essential to note that they used the TCLP method (U.S, 1992). Álvarez-Ayuso et al. (Álvarez-Ayuso et al., 2008) obtained that elements, such as Ni, Cu, Zn and Pb, had low leaching (< 0.2 mg/kg) and oxyanions (As, Se, Sb) had higher leaching (> 0.2 mg/kg), especially high release increases were found for As. These results are in agreement with the data found in this work. In addition, some studies confirmed that a low porosity one favours the immobilization of oxyanions, which is in line with As leaching (Álvarez-Ayuso et al., 2008; Provis and Van Deventer, 2014; Vu and Gowripalan, 2018).

***Table 3.9**. Leaching results for all specimens. The concentration is expressed in mg of element leached per kg of original material, according with Directive 2003/33/EC. Colour system: elements that are below established thresholds (green), close (yellow), above (red) and other elements leached (blue).*

Element	R	PG5	PG10	PG20	CWS5	CWS10	CWSs10	M	MPG10	MCWSs10	NHM	HM
	mg/kg											
As	-	-	-	-	13	40	2.0	-	-	35	2	25
Ba	-	-	-	-	-	-	-	-	-	-	100	300
Br	0.10	0.21	0.19	0.11	-	-	-	0.11	0.04	-	-	-
Ca	25	49	12	117	27	22	19	9.2	45	11	-	-
Cd	-	-	-	-	-	-	-	-	-	-	1	5
Cl	6.7	14	-	-	17	24	8.8	-	-	1.5	15000	25000
Cr	0.05	-	-	-	-	-	-	-	-	-	10	70
Cu	-	-	-	-	0.07	0.14	0.03	-	-	0.42	50	100
Fe	0.68	0.27	0.25	1.21	0.32	0.20	0.26	0.13	0.11	0.49	-	-
Hg	-	0.09	0.10	0.14	-	-	-	-	-	-	0.2	2
K	105	98	51	51	103	106	74	18	32	12	-	-
Mo	-	-	-	-	-	-	-	-	-	-	10	30
Ni	0.03	0.06	0.03	0.02	-	0.02	-	-	-	-	10	40
Pb	-	-	-	-	-	0.11	-	-	-	-	10	50
Rb	0.35	0.35	0.30	0.42	0.44	0.45	0.33	0.13	0.10	0.06	-	-
S	-	372	880	853	83	90	23	-	647	70	-	-
SO_4^{2-}	-	1100	2600	2500	250	270	70	-	1900	210	20000	50000
Sb	-	-	-	-	-	-	-	-	-	-	0.7	5
Se	0.01	0.01	0.02	-	0.08	0.21	0.01	-	-	0.2	0.5	7
Sr	0.08	0.17	0.08	1.51	-	-	-	-	0.16	-	-	-
Ti	0.99	0.11	0.17	0.16	0.10	0.13	0.14	-	-	-	-	-
V	0.14	0.13	0.14	-	0.06	0.19	0.00	-	-	-	-	-
Zn	0.01	-	-	-	0.01	0.03	0.02	-	-	0.1	50	200

3.4.4 Conclusions

Blast furnace slag-based one-part geopolymers were successfully processed showing interesting mechanical properties. Two hazardous wastes, copper wastewater sludge (CWS) and phosphogypsum (PG), partially substituted BFS in the geopolymer formulations, aiming to immobilize the hazardous species of the wastes. In particular, As from CWS is a challenging element.

PG-containing pastes (PG5, PG10, PG20) denote an expressive compressive strength reduction, from 67 MPa to 19 MPa, due to the presence/role of calcium sulphate in the waste. The setting is delayed and spread increases with PG amount. The MPG10 mortar also shows a large reduction (50 %) in the mechanical resistance when compared with the reference mortar (26 MPa). In this case, constructions applications are envisaged.

In CWS-containing pastes, the increase of sludge content from 5 to 10 wt.% did not alter the compressive strength of the specimens (value around 50 MPa). The attempt to improve the compactness of the samples by using sieved sludge (CWSs10) generated microcracks upon drying/curing, and the mechanical strength reduced to 31 MPa. The corresponding mortar has 21 MPa which can be applied for contractions sector. In the fresh state, samples show properties (setting time and spread on flow table) similar to the reference, being the calorimetric behaviour also close.

The leaching tests showed that pastes and mortars immobilize the hazardous species of the wastes, excepting As from CWS. Only the highest compact paste (CWSs10) leached 2 mg/kg of As, a value that coincides with the threshold limit for non-hazardous materials. Further studies are necessary to determine the optimal processing conditions (e.g., fineness of components, curing conditions, etc.) to increase the immobilization efficiency.

CHAPTER 4.
CONCLUSIONS

4.1 CONCLUSIONS

This chapter presents a summary of the main conclusions obtained in this doctoral thesis. The central objective has been to evaluate and develop possible valorisation lines for different wastes and/or secondary materials from a copper metallurgical complex. The studied materials were sludge scrubber (SS), sludge from converters (SC), electrolyte sludge (ES), and copper wastewater sludge (CWS).

The main conclusions are the following:

1. The physical, chemical, mineralogical, and microstructural characterisation of the sludges under the study, as well as the evaluation of mobility of pollutants, provided essential knowledge to identify possible applications and valorisations lines.

2. SS and SC had a high Pb content (> 20 % w/w), mainly as anglesite ($PbSO_4$), and SS also presented a high Se content (> 30 % w/w) as metallic selenium. Therefore, SS could be an important secondary source of selenium, while both sludges can be considered a significant secondary source of lead. The treatment proposed for Se-Pb recovery consists of Se extraction from SS by a roasting process, and the calcined Pb-rich residue is mixed with SC to recover Pb by hydrometallurgy route. Thus, the procedure proposed for Se-Pb recovery could be an attractive option for managing these hazardous wastes, which could have remarkable economic and environmental benefits compared to their disposal in landfills.

3. Electrolyte sludge (ES) had a high Cu content (≈ 50 % w/w) as domeykite (Cu_3As), cuprite (Cu_2O), Cu metal and copper sulphate hydrate ($CuSO_4 \cdot xH_2O$). ES also contained a high As content (≈ 10 % w/w), mainly as Cu_3As. Therefore, ES could be an important secondary source of Cu, but As content should be removed to avoid reprocessing and valorisation problems.

4. For the Cu recovery, ES dissolution was chosen, which was achieved using an acid medium, H_2SO_4 (1.4 M)/HNO_3 (1.8 M), and a solid-to-liquid ratio of 1:20 g/mL. Subsequently, two lines of research were carried out: a) Arsenic removal from the ES solution by precipitation with iron, and then copper recovery from the arsenic-free solution; b) Copper recovery from the ES solution by an evaporative crystallisation, and then arsenic precipitation.

5. In arsenic removal experiments, about 70 % of As is removed from the ES solution by precipitation as ferric arsenate. However, about 50 % of Cu was also co-precipitated, suggesting copper should be previously recovered. Furthermore, the ferric arsenate formed

leached a high As and Cu concentration, which exceeded the thresholds established for their disposal as hazardous material in a controlled landfill (25 mg/kg of As and 100 mg/kg of Cu). Thus, inertization and/or valorisation of the formed solid are needed.

6. In the copper recovery experiments, more than 90 % of the copper was recovered as copper (II) sulphate pentahydrate ($CuSO_4 \cdot 5H_2O$) by a traditional evaporative crystallisation. However, the copper sulphate obtained had a significant concentration of impurities, mainly As. The crystals of $CuSO_4 \cdot 5H_2O$ can be recycled back to the smelting or electrorefining process or commercialised for other applications (agriculture, antiseptic agent, electroplating processes, etc.). In this case, the copper sulphates must be purified to reduce their impurities to the level suitable for commercialisation (> 99.99 % w/w). Moreover, 70 % of As precipitated as As_2O_3, getting a drastically As reduction from that which is currently returned to the process. Nevertheless, further research on the stabilisation and/or valorisation of As_2O_3 are needed.

7. As_2O_3 was formed with the $CuSO_4 \cdot 5HO$ crystals during the evaporative crystallization process. These were separated by a mechanical method. However, this separation was not efficient because traces of As_2O_3 remained in copper sulphate crystals and was impossible when the particles of As_2O_3 and $CuSO_4 \cdot 5H_2O$ had a similar size. Thus, a purification process should be designed in order to achieve a high purity of $CuSO_4 \cdot 5H_2O$.

8. Copper wastewater sludge (CWS) presented a high concentration of CaO (≈ 70 % w/w) and, in a minor proportion, contained SiO_2, Fe_2O_3, MgO, SO_3 (15–1 % w/w) and Al_2O_3 (≈ 0.4 % w/w). In addition, CWS presented As (≈ 3.4 % w/w) and other elements such as Ba, Cu, Pb, Sb, Sr, and Zn in traces concentration (< 1 % w/w). This material contained several mineral phases: calcite ($CaCO_3$), gypsum ($CaSO_4 \cdot 2H_2O$), portlandite ($Ca(OH)_2$), and iron oxide hydroxide ($Fe_{21}O_{31}(OH)$). For CWS, the proposed valorisation and/or immobilisation line was to use it as raw material in geopolymer materials, which are currently recognized as a potential alternative to ordinary Portland cement (OPC) based materials since it has a lower carbon footprint.

9. The geopolymers obtained (pastes and mortars) had an excellent compressive strength (50–20 Mpa), considering admissible for construction application. Only the most compact paste (CWSs10) leached 2 mg/kg of As, a value that coincides with the threshold limit for non-hazardous materials landfill disposal. But further studies are necessary to determine the optimal processing conditions (e.g., fineness of components, curing conditions, etc.) to increase the immobilization efficiency.

4.2 CONCLUSIONES

En esta sección se presentan un resumen de las principales conclusiones obtenidas en esta tesis doctoral. El objetivo principal ha sido evaluar y desarrollar posibles líneas de valorización para diferentes residuos y/o materiales secundarios procedentes de un complejo metalúrgicos de obtención de cobre. Los materiales estudiados fueron: torta del lavado de gases (TLG), finos de convertidores (FC), torta del electrolito (TE), y lodos de la planta de tratamiento de efluentes líquidos (LPTEL).

Las principales conclusiones son la siguientes:

1. Las caracterización física, química, mineralógica y microestructural de los materiales en estudio, así como la evaluación de la movilidad de los contaminantes, proporciona una información esencial para identificar las posibles aplicaciones y líneas de valorización.

2. TLG y FC tuvo un alto contenido en Pb (> 20 % p/p) principalmente en forma de anglesita, y la TLG presento además un alto contenido en Se (> 30 % p/p) en forma metálica. Por lo tanto, TLG podría ser una importante fuente secundaria de selenio, mientras que ambos residuos pueden considerar una importante fuente secundarias de plomo. El tratamiento propuesto para la recuperación de Se-Pb consiste en una extracción de selenio mediante un proceso de tostado y luego el residuo calcinado rico en Pb se mezcla con FC para recuperar el Pb por un proceso hidrometalúrgico. El procedimiento propuesto para la recuperación de Se-Pb podría ser una alternativa atractiva para la gestión de estos residuos peligrosos, la cual podrían suponer notables beneficios económicos y ambientales en comparación con su disposición en vertederos.

3. TE tuvo un alto contenido en Cu (≈ 50 % p/p) en forma de domeiquita (Cu_3As), cuprita (Cu_2O), Cu metálico y sulfato de cobre hidratado ($CuSO_4 \cdot xH_2O$), y una alta concentración de As (≈ 10 % p/p), principalmente como Cu_3As. Por lo tanto, dicho material podría ser una importante fuente secundaria de Cu. Sin embargo, el contenido de As debería ser eliminado para evitar problemas durante su reprocesamiento o valorización.

4. Para la recuperación de cobre, se decidió disolver TE, la cual se logró usando un medio ácido, H_2SO_4 (1.4 M)/HNO_3 (1.8 M), y una relación sólido-líquido 1:20 g/mL. Posteriormente, se llevaron a cabo dos líneas de investigación: a) Eliminar el As de la disolución de TE mediante una precipitación con hierro y luego recuperar el Cu de disolución libre de arsénico; y b) Recuperar el cobre de la disolución de TE mediante una cristalización evaporativa y luego precipitar el arsénico.

5. En los experimentos de eliminación del arsénico, en torno a un 70 % del As presente en la disolución de TE se eliminó como arseniato de hierro (III) mediante una precipitación con hierro. Sin embargo, alrededor del 50 % del Cu también co-precipitó junto al As, sugiriendo que el cobre debería recuperarse previamente. Además, el arseniato férrico formado lixivia altas concentraciones de As y Cu, la cuales superan los límites establecidos para su depósito en vertedero controlados de materiales peligrosos (25 mg/kg de As and 100 mg/kg de Cu). Por lo que, la inertización y valorización de los sólidos formados son necesaria.

6. En los experimentos de recuperación del cobre, más del 90 % del Cu contenido en la disolución de la TE se recuperó como sulfato de cobre (II) pentahidratado ($CuSO_4 \cdot 5H_2O$) mediante un proceso de cristalización evaporativa. Sin embargo, los cristales de sulfato de cobre obtenido contienen una significativa concentración de impurezas, principalmente As. Estos pueden ser recirculados a la fundición o al proceso de refino electrolítico, o ser comercializado para otras aplicaciones (agricultura, agente antiséptico, procesos galvanoplásticos, etc.). En este caso, el sulfato de cobre debería ser purificado hasta reducir sus impurezas a un nivel adecuado para su comercialización (> 99,99 % p/p). Además, alrededor del 70 % del As se eliminó durante dicho proceso, en forma de As_2O_3, obteniéndose una reducción considerable del As que actualmente se devuelve al proceso. No obstante, se necesitan más investigaciones sobre la estabilización y/o valorización del As_2O_3.

7. As_2O_3 se formó junto a los cristales de $CuSO_4 \cdot 5H_2O$ durante el proceso de cristalización evaporativa. Estos fueron separados por un método mecánico. Sin embargo, la separación no fue efectiva y quedaron trazas de As_2O_3 en los cristales de $CuSO_4 \cdot 5H_2O$. Además, la separación fue imposible cuando las partículas de As_2O_3 y $CuSO_4 \cdot 5H_2O$ tenían un tamaño similar. Por lo tanto, se debe estudiarse un proceso de purificación más efectivo para lograr una alta pureza de $CuSO_4 \cdot 5H_2O$.

8. LPTEL presentó una alta concentración de CaO (≈ 70 % p/p) y en menor proporción contenía SiO_2, Fe_2O_3, MgO, SO_3 (15–1 % p/p) y Al_2O_3 (≈ 0.4 % p/p). Además, presentó As (≈ 3.4 % p/p) y otros elementos como Ba, Cu, Pb, Sb, Sr y Zn en concentraciones traza (< 1 % p/p). Este material contenía varias fases minerales: calcita ($CaCO_3$), yeso ($CaSO_4 \cdot 2H_2O$), y portlandita ($Ca(OH)_2$) y oxihidróxido de hierro (III) ($Fe_{21}O_{31}(OH)$). Para LPTEL, la línea de valorización y/o inmovilización propuesta fue usarlo como materia prima en la fabricación de geopolímeros, materiales que actualmente son considerados como una potencial alternativa a los materiales basados en cemento Portland ordinario (OPC), ya que tiene una huella de carbono más baja.

9. Los geopolímeros obtenidos (pastas y morteros) tuvieron una excelente resistencia a la compresión (50–20 Mpa), considerándolos admisibles para aplicaciones de construcción. Sólo la pasta más compacta (CSWs10) lixivió 2 mg/kg de As, valor que se encuentra en el límite establecido para la admisión de materiales en vertederos de residuos no peligrosos. Sin embargo, son necesarios más estudios para determinar las condiciones óptimas (ej. tamaño de partícula de lo componentes, condiciones de fraguado, etc.) con el fin de incrementar la eficiencia de inmovilización.

4.3 FUTURE RESEARCH LINES

The findings of this doctoral thesis point out the future research lines, such as:

1. To design and develop experiments to evaluate the proposed alternative to reuse the SC and SS residues as secondary sources of Se and Pb.
2. To perform optimization experiments of the copper recovery process, such as $CuSO_4 \cdot 5H_2O$, focusing on obtaining a copper sulphate pentahydrate with high purity (≥ 99.99%) for commercialization. For that purpose, first As_2O_3 and $CuSO_4 \cdot 5H_2O$ should be separated by dissolving copper sulphate in water since arsenic trioxide is almost insoluble, and then the dissolution should be conducted to several recrystallization steps until reaching the desired purity.
3. To conduct experiments of stabilization of As_2O_3 by iron precipitation as scorodite ($FeAsO_4 \cdot 2H_2O$) after Cu recover.
4. To determine the optimal conditions (e.g., fineness of components, curing conditions, etc.) to increase the immobilization efficiency in the geopolymer specimens. In addition, study the mobility of pollutants in the short and long time.

REFERENCES

REFERENCES

Abdollahnejad, Z., Pacheco-Torgal, F., Aguiar, J.B., Jesus, C., 2015. Durability performance of fly ash based one-part geopolymer mortars. Key Eng. Mater. 634, 113–120. https://doi.org/10.4028/www.scientific.net/KEM.634.113

Aktas, S., 2011. A novel purification method for copper sulfate using ethanol. Hydrometallurgy 106, 175–178. https://doi.org/10.1016/j.hydromet.2011.01.001

Al-Jabri, K.S., Al-Saidy, A.H., Taha, R., 2011. Effect of copper slag as a fine aggregate on the properties of cement mortars and concrete. Constr. Build. Mater. 25, 933–938. https://doi.org/10.1016/j.conbuildmat.2010.06.090

Al-Kindi, G.Y., 2019. Evaluation the solidification/stabilization of heavy metals by Portland Cement. J. Ecol. Eng. 20, 91–100. https://doi.org/10.12911/22998993/99739

Ali, S., Sajadi, A., 2011. A Comparative Investigation of Lead Sulfate and Lead Oxide Sulfate Study of Morphology and Thermal Decomposition. Am. J. Anal. Chem. 2, 206–211. https://doi.org/10.4236/ajac.2011.22024

Alimohammadizadeh, H., Behrad-Vakylabad, A., Ghader, S., 2018. On the optimization of the crystallization related to an aqueous copper sulfate (CuSO4.5H2O). Miner. Process. Extr. Metall. Trans. Inst. Min. Metall. 0, 1–9. https://doi.org/10.1080/25726641.2018.1521575

Álvarez-Ayuso, E., Querol, X., Plana, F., Alastuey, A., Moreno, N., Izquierdo, M., Font, O., Moreno, T., Diez, S., Vázquez, E., Barra, M., 2008. Environmental, physical and structural characterisation of geopolymer matrixes synthesised from coal (co-)combustion fly ashes. J. Hazard. Mater. 154, 175–183. https://doi.org/10.1016/j.jhazmat.2007.10.008

Angelov, A., Groudev, S., 2002. Treatment of gold-bearing solutions by cementation with metallic zinc. Min. Miner. Process. 44–45, 117–121.

Anji Reddy, M., Pralong, V., Caignaert, V., Varadaraju, U. V., Raveau, B., 2009. Monoclinic iron hydroxy sulphate: A new route to electrode materials. Electrochem. commun. 11, 1807–1810. https://doi.org/10.1016/j.elecom.2009.07.024

Artzer, A., Moats, M., Bender, J., 2018. Removal of Antimony and Bismuth from Copper Electrorefining Electrolyte: Part I—A Review. Jom 70, 2033–2040. https://doi.org/10.1007/s11837-018-3075-x

Assi, L., Carter, K., Deaver, E. (Eddie), Anay, R., Ziehl, P., 2018. Sustainable concrete: Building a greener future. J. Clean. Prod. 198, 1641–1651. https://doi.org/10.1016/j.jclepro.2018.07.123

Assi, L.N., Eddie Deaver, E., Ziehl, P., 2018. Effect of source and particle size distribution on the mechanical and microstructural properties of fly Ash-Based geopolymer concrete. Constr. Build. Mater. 167, 372–380. https://doi.org/10.1016/j.conbuildmat.2018.01.193

ASTM D2487, 2006. Standard Practice for Classification of Soils for Engineering Purposes (Unified Soil Classification System), ASTM Standard Guide. https://doi.org/10.1520/D2487-11.

Atlantic Copper, 2017. Annual Environmental Report. Huelva, Spain.

Atoche, W., Huayta, F., 2015. Simulación de Control de Mermas en el Proceso de Producción de Sulfato de Cobre Pentahidratado, in: Proceedings of the 13th Latin American and Caribbean Conference for Engineering and Technology Engineering Education Facing the Grand Challenges What Are We Doing? LACCEI, Santo Domingo, Dominican Repluclic, pp. 0–6. https://doi.org/10.18687/LACCEI2015.1.1.102

Auping, W.L., Pruyt, E., Kwakkel, J.H., 2012. Analysing the Uncertain Future of Copper with Three Exploratory System Dynamics Models, in: International System Dynamics Conference. Delft, The Netherlands, pp. 1–25.

Ayala, J., Fernández, B., 2014. Synthesis of commercial products from copper wire-drawing waste. Jom 66, 1099–1105. https://doi.org/10.1007/s11837-014-0920-4

Bacedoni, M., Moreno-Ventas, I., Ríos, G., 2020. Copper flash smelting process balance modeling. Metals (Basel). 10, 1–19. https://doi.org/10.3390/met10091229

BăDănoiu, G., Buzatu, T., Ghica, V.G., Buzatu, M., Iacob, G., Petrescu, I.M., 2014. Study of PbSO4 solubilisation in NaOH solution, for the treatment of oxide-sulphate pastes obtained from dismembered lead-acid batteries. UPB Sci. Bull. Ser. B Chem. Mater. Sci. 76, 209–218.

Balaji, T., Yokoyama, T., Matsunaga, H., 2005. Adsorption and removal of As(V) and As(III) using Zr-loaded lysine diacetic acid chelating resin. Chemosphere 59, 1169–1174. https://doi.org/10.1016/j.chemosphere.2004.12.007

Balladares, E., Kelm, U., Helle, S., Parra, R., Araneda, E., 2014. Chemical-mineralogical characterization of copper smelting flue dust. Dyna 81, 11. https://doi.org/10.15446/dyna.v81n186.32852

Bankowski, P., Zou, L., Hodges, R., 2004. Using inorganic polymer to reduce leach rates of metals from brown coal fly ash. Miner. Eng. 17, 159–166. https://doi.org/10.1016/j.mineng.2003.10.024

Bernal, S.A., Provis, J.L., Rose, V., Mejía De Gutierrez, R., 2011. Evolution of binder structure in sodium silicate-activated slag-metakaolin blends. Cem. Concr. Compos. 33, 46–54. https://doi.org/10.1016/j.cemconcomp.2010.09.004

Bluteau, M.C., Becze, L., Demopoulos, G.P., 2009. The dissolution of scorodite in gypsum-saturated waters: Evidence of Ca-Fe-AsO4 mineral formation and its impact on arsenic retention. Hydrometallurgy 97, 221–227. https://doi.org/10.1016/j.hydromet.2009.03.009

Bolívar, J.P., Martín, J.E., García-Tenorio, R., Pérez-Moreno, J.P., Mas, J.L., 2009. Behaviour and fluxes of natural radionuclides in the production process of a phosphoric acid plant. Appl. Radiat. Isot. 67, 345–356. https://doi.org/10.1016/j.apradiso.2008.10.012

BPC: Biocidal Product Committee, 2013. Assessment Report: Copper sulfate pentahydrate Product-type 2 (Disinfectants and algaecides not intended for direct application to humans or animals). https://echa.europa.eu/documents/10162/b49e17b8-7402-434e-245b-4e539c3bebbd.

Buruberri, L.H., Tobaldi, D.M., Caetano, A., Seabra, M.P., Labrincha, J.A., 2019. Evaluation of reactive Si and Al amounts in various geopolymer precursors by a simple method. J. Build. Eng. 22, 48–55. https://doi.org/10.1016/j.jobe.2018.11.017

Cao, Q., Chen, C., Li, K., Sun, T., Shen, Z., Jia, J., 2021. Arsenic(V) removal behavior of schwertmannite synthesized by KMnO4 rapid oxidation with high adsorption capacity and Fe utilization. Chemosphere 264, 128398. https://doi.org/10.1016/j.chemosphere.2020.128398

Caruso, B.S., Cox, T.J., Runkel, R.L., Velleux, M.L., Bencala, K.E., Nordstrom, D.K., Julien, P.Y., Butler, B.A., Alpers, C.N., Marion, A., Smith, K.S., 2008. Metals fate and transport modelling in streams and watersheds: state of the science and USEPA workshop review B. Hydrol. Process. 22, 4011–4021. https://doi.org/10.1002/hyp

CEN: European Committee for Standardization, 2005. EN 196-3 Methods of Testing Cement Part 3—Determination of Setting Times and Soundness. Brussels.

CEN: European Committee for Standardization, 2004. EN 1992-1-1 Eurocode 2: Design of concrete structures - Part 1-1 : General rules and rules for buildings.

CEN: European Committee for Standardization, 2002a. UNE-EN- 12457-4 Characterisation of waste - Leaching - Compliance test for leaching of granular waste materials and sludges - Part 4: One stage batch test at a liquid to solid ratio of 10 l/kg for materials with particle size below 10 mm (without or with . Spain.

CEN: European Committee for Standardization, 2002b. EN 12457-2 Leaching - Compliance test for leaching of granular waste materials and sludges — Part 2: One stage batch test at a liquid to solid ratio of 10 l/kg for materials with particle size below 4 mm (without or with size reduction), British Standards Institution.

CEN: European Committee for Standardization, 2002c. EN 1015-18 Methods of Test for Mortar for Masonry Part 18—Determination of water- Absorption Coefficient Due to Capillary Action of Hardened Mortar. Brussels.

CEN: European Committee for Standardization, 2000. EN 197-1 Cement- Part 1: Composition, specifications and conformity criteria for common cements.

CEN: European Committee for Standardization, 1999. EN 1015-11 Methods of test for mortar for masonry - Part 11: Determination of flexural and compressive strength of hardened mortar. Belgium, Brussels.

CEN: European Committee for Standardization, 1998. EN 1015-3 Methods of test for mortar for masonry - Part 3: Determination of consistence of fresh mortar (by flow table), Brussels. Brussels.

Cervando, L., Viraca, C., 2013. Termodinámica de la estabilización del arsénico. Rev. Met. UTO 34, 3–12.

Chen, M.L., Sun, Y., Huo, C.B., Liu, C., Wang, J.H., 2015. Akaganeite decorated graphene oxide composite for arsenic adsorption/removal and its proconcentration at ultra-trace level. Chemosphere 130, 52–58. https://doi.org/10.1016/j.chemosphere.2015.02.046

Chen, Q.Y., Tyrer, M., Hills, C.D., Yang, X.M., Carey, P., 2009. Immobilisation of heavy metal in cement-based solidification/stabilisation: A review. Waste Manag. 29, 390–403. https://doi.org/10.1016/j.wasman.2008.01.019

Chen, T.T., Dutrizac, J.E., 2009. Characterization of the liberator cell sludges from three copper electrorefineries. Can. Metall. Q. 48, 61–68. https://doi.org/10.1179/cmq.2009.48.1.61

Chen, Y., Liao, T., Li, G., Chen, B., Shi, X., 2012. Recovery of bismuth and arsenic from copper smelter flue dusts after copper and zinc extraction. Miner. Eng. 39, 23–28. https://doi.org/10.1016/j.mineng.2012.06.008

Cheng, R., Zhang, H., Ni, H., 2019. Arsenic removal from arsenopyrite-bearing iron ore and arsenic recovery from dust ash by roasting method. Processes 7. https://doi.org/10.3390/pr7100754

Cortes-Egaña, C.M., 2009. Evaluación del Negocio del Barro Anódico en Codelco. http://repositorio.uchile.cl/handle/2250/102032.

Council of the European Union, 2003. Directive 2003/33/EC of 19 December 2002 establishing criteria and procedures for the acceptance of waste at landfills pursuant to Article 16 of and Annex II to Directive 1999/31/EC. Off. J. Eur. Communities 11, 27–49.

Criado, M., Walkley, B., Ke, X., Provis, J.L., Bernal, S.A., 2018. Slag and activator chemistry control the reaction kinetics of sodium metasilicate-activated slag cements. Sustain. 10. https://doi.org/10.3390/su10124709

Csavina, J., Landázuri, A., Wonaschütz, A., Rine, K., Rheinheimer, P., Barbaris, B., Conant, W., Sáez, A.E., Betterton, E.A., 2011. Metal and metalloid contaminants in atmospheric aerosols from mining operations. Water. Air. Soil Pollut. 221, 145–157. https://doi.org/10.1007/s11270-011-0777-x

Csavina, J., Taylor, M.P., Félix, O., Rine, K.P., Eduardo Sáez, A., Betterton, E.A., 2014. Size-resolved dust and aerosol contaminants associated with copper and lead smelting emissions: Implications for emission management and human health. Sci. Total Environ. 493, 750–756. https://doi.org/10.1016/j.scitotenv.2014.06.031

Dabekaussen, R., Droppert, D., Demopoulos, G.P., 2001. Ambient pressure hydrometallurgical conversion of arsenic trioxide to crystalline scorodite. CIM Bull. 94, 116–122.

Deboucha, W., Leklou, N., Khelidj, A., Oudjit, M.N., 2017. Natural pozzolana addition effect on compressive strength and capillary water absorption of Mortar. Energy Procedia 139, 689–695. https://doi.org/10.1016/j.egypro.2017.11.273

Demopoulos, G.P., 2014. Arsenic immobilization research advances: past, present and future, in: Conference of Metallurgists Proceedings (COM). Canadian Institute of Mining, Metallurgy and Petroleum, Vancouver, Canada.

Demopoulos, G.P., 2005. On the preparation and stability of scorodite, in: Reddy, R.G., Ramachandran, V. (Eds.), Proceedings of Arsenic Metallurgy. The Minerals, Metals & Materials Society (TMS), Warrendale, PA., pp. 25–50.

Deselnicu, D.C., Militaru, G., Deselnicu, V., Zainescu, G., Albu, L., 2018. Towards a Circular Economy– a Zero Waste Programme for Europe, in: ICAMS. pp. 563–568. https://doi.org/10.24264/icams-2018.XI.4

Directive 1999/31/EC, 1999. of the European Parliament and of the Council of 26 April 1999 on the landfill of waste.

Directive 2008/98/EC, 2008. Directive 2008/98/EC of the European Parliament and of the Council of 19 November 2008 on waste and repealing certain Directives (Text with EEA relevance), Official Journal of the European Union. https://doi.org/10.5040/9781782258674.0028

Dong, D., van Oers, L., Tukker, A., van der Voet, E., 2020. Assessing the future environmental impacts of copper production in China: Implications of the energy transition. J. Clean. Prod. 274, 122825. https://doi.org/10.1016/j.jclepro.2020.122825

Dong, Z., Jiang, T., Xu, B., Yang, J., Chen, Y., Li, Q., Yang, Y., 2020. Comprehensive recoveries of selenium, copper, gold, silver and lead from a copper anode slime with a clean and economical hydrometallurgical process. Chem. Eng. J. 393, 124762. https://doi.org/10.1016/j.cej.2020.124762

Drahota, P., Filippi, M., 2009. Secondary arsenic minerals in the environment: A review. Environ. Int. 35, 1243–1255. https://doi.org/10.1016/j.envint.2009.07.004

Droppert, D.J., 1996. The ambient pressure precipitation of crytalline scorodite (FeAsO4 .2H2O) from sulphate solutions. McGill University Montreal, Canada.

Droppert, D.J., Demopoulos, G.., Harris, G.., 1996. Ambient pressure production of crystalline scorodite from arsenic-rich metallurgical effluent solutions, in: EPD Congress 1996, Warren, G.W. (Eds.), . The Minerals, Metals & Materials Society, 1996, pp. 227–239.

Dunn, J.G., Muzenda, C., 2001. Thermal oxidation of covellite (CuS). Thermochim. Acta 369, 117–113.

Dutrizac, J.E., Jambor, J.L., 2007. Characterization of the iron arsenate–sulphate compounds precipitated at elevated temperatures. Hydrometallurgy 86, 147–163.

https://doi.org/10.1016/j.hydromet.2006.11.011

Duxson, P., Fernández-Jiménez, A., Provis, J.L., Lukey, G.C., Palomo, A., Van Deventer, J.S.J., 2007. Geopolymer technology: The current state of the art. J. Mater. Sci. 42, 2917–2933. https://doi.org/10.1007/s10853-006-0637-z

EEA: European Environment Agency, 2017. Circular by design: Products in the circular economy, European Environment Agency. https://doi.org/10.1002/14651858.CD004884.pub3

EEA: European Environment Agency, 2016. Circular economy in Europe. Developing the knowledge base, European Environment agency. https://doi.org/10.2800/51444

European Commission, 2015. Closing the loop - An EU action plan for the Circular Economy. https://doi.org/10.1017/CBO9781107415324.004

European Copper Institute, 2018. Benefits of Copper: contributions to sustainability-driven trends [WWW Document]. URL https://copperalliance.eu/benefits-of-copper/ (accessed 8.5.21).

Fernández-Jiménez, A., Palomo, A., Macphee, D.E., Lachowski, E.E., 2005. Fixing arsenic in alkali-activated cementitious matrices. J. Am. Ceram. Soc. 88, 1122–1126. https://doi.org/10.1111/j.1551-2916.2005.00224.x

Földvári, M., 2011. Handbook of Thermogravimetric System of Minerals and Its Use in Geological Practice. Cent. Eur. Geol. 213, 180. https://doi.org/10.1556/CEuGeol.56.2013.4.6

Font, O., Moreno, N., González, A., Querol, X., Navia, R., 2011. Copper Smelting Flue Dust: A Potential Source Of Germanium. Macla, Rev. la Soc. española Mineral. 15, 87–88.

Fujita, T., Taguchi, R., Abumiya, M., Matsumoto, M., Shibata, E., Nakamura, T., 2009a. Effect of pH on atmospheric scorodite synthesis by oxidation of ferrous ions: Physical properties and stability of the scorodite. Hydrometallurgy 96, 189–198. https://doi.org/10.1016/j.hydromet.2008.10.003

Fujita, T., Taguchi, R., Abumiya, M., Matsumoto, M., Shibata, E., Nakamura, T., 2009b. Effect of pH on atmospheric scorodite synthesis by oxidation of ferrous ions: Physical properties and stability of the scorodite. Hydrometallurgy 96, 189–198. https://doi.org/10.1016/j.hydromet.2008.10.003

Fujita, T., Taguchi, R., Abumiya, M., Matsumoto, M., Shibata, E., Nakamura, T., 2008a. Novel

atmospheric scorodite synthesis by oxidation of ferrous sulfate solution. Part I. Hydrometallurgy 90, 92–102. https://doi.org/10.1016/j.hydromet.2007.09.012

Fujita, T., Taguchi, R., Abumiya, M., Matsumoto, M., Shibata, E., Nakamura, T., 2008b. Novel atmospheric scorodite synthesis by oxidation of ferrous sulfate solution. Part II. Effect of temperature and air. Hydrometallurgy 90, 85–91. https://doi.org/10.1016/j.hydromet.2007.09.011

Fujita, T., Taguchi, R., Abumiya, M., Matsumoto, M., Shibata, E., Nakamura, T., 2008c. Effects of zinc, copper and sodium ions on ferric arsenate precipitation in a novel atmospheric scorodite process. Hydrometallurgy 93, 30–38. https://doi.org/10.1016/j.hydromet.2008.02.016

Giulietti, M., Derenzo, S., Nývlt, J., Ishida, L.K., 1995. Crystallization of copper sulphate. Cryst. Res. Technol. 30, 177–183. https://doi.org/10.1002/crat.2170300206

Giulietti, M., Seckler, M.M., Derenzo, S., Valarelli, J.V., 1996. Changes in copper sulfate crystal habit during cooling crystallization. J. Cryst. Growth 166, 1089–1093. https://doi.org/10.1016/0022-0248(95)00941-8

Gomez, M.A., Becze, L., Celikin, M., Demopoulos, G.P., 2011a. The effect of copper on the precipitation of scorodite (FeAsO4·2H2O) under hydrothermal conditions: Evidence for a hydrated copper containing ferric arsenate sulfate-short lived intermediate. J. Colloid Interface Sci. 360, 508–518. https://doi.org/10.1016/j.jcis.2011.05.010

Gomez, M.A., Becze, L., Cutler, J.N., Demopoulos, G.P., 2011b. Hydrothermal reaction chemistry and characterization of ferric arsenate phases precipitated from Fe2(SO4)3-As 2O5-H2SO4 solutions. Hydrometallurgy 107, 74–90. https://doi.org/10.1016/j.hydromet.2011.01.007

Gomez, M.A., Ventruti, G., Celikin, M., Assaaoudi, H., Putz, H., Becze, L., Lee, K.E., Demopoulos, G.P., 2013. The nature of synthetic basic ferric arsenate sulfate (Fe(AsO 4)1-x(SO4)x(OH)x) and basic ferric sulfate (FeOHSO4): Their crystallographic, molecular and electronic structure with applications in the environment and energy. RSC Adv. 3, 16840–16849. https://doi.org/10.1039/c3ra42235f

Gonçalves, M., Vilarinho, I.S., Capela, M., Caetano, A., Novais, R.M., Labrincha, J.A., Seabra, M.P., 2021. Waste-Based One-Part Alkali Activated Materials. Materials (Basel). 14, 2911. https://doi.org/10.3390/ma14112911

Gonzalez-Contreras, P., Weijma, J., Van Der Weijden, R., Buisman, C.J.N., 2010. Biogenic scorodite crystallization by Acidianus sulfidivorans for arsenic removal. Environ. Sci. Technol. https://doi.org/10.1021/es902063t

González, A., Font, O., Moreno, N., Querol, X., Arancibia, N., Navia, R., 2017. Copper Flash Smelting Flue Dust as a Source of Germanium. Waste and Biomass Valorization 8, 2121–2129. https://doi.org/10.1007/s12649-016-9725-8

Gouvea, L.R., Morais, C.A., 2007. Recovery of zinc and cadmium from industrial waste by leaching/cementation. Miner. Eng. 20, 956–958. https://doi.org/10.1016/j.mineng.2007.04.016

Guerrero, J.L., Gutiérrez-Álvarez, I., Mosqueda, F., Gázquez, M.J., García-Tenorio, R., Olías, M., Bolívar, J.P., 2020. Evaluation of the radioactive pollution in the salt-marshes under a phosphogypsum stack system. Environ. Pollut. 258. https://doi.org/10.1016/j.envpol.2019.113729

Ha, T.K., Kwon, B.H., Park, K.S., Mohapatra, D., 2015. Selective leaching and recovery of bismuth as Bi2O3 from copper smelter converter dust. Sep. Purif. Technol. 142, 116–122. https://doi.org/10.1016/j.seppur.2015.01.004

Hait, J., Jana, R.K., Sanyal, S.K., 2009. Processing of copper electrorefining anode slime: a review. Miner. Process. Extr. Metall. 118, 240–252. https://doi.org/10.1179/174328509x431463

Hajimohammadi, A., van Deventer, J.S.J., 2017. Characterisation of One-Part Geopolymer Binders Made from Fly Ash. Waste and Biomass Valorization 8, 225–233. https://doi.org/10.1007/s12649-016-9582-5

Hakem Aziz, I., Mustafa Al Bakri Abdullah, M., Arif Anuar Mohd Salleh, M., Victor Sandu, A., 2020. The Incorporation of Sodium Hydroxide (NaOH) Concentration and CaO-Si Components on Ground Granulated Blast Furnace Slag Geopolymers. IOP Conf. Ser. Mater. Sci. Eng. 864. https://doi.org/10.1088/1757-899X/864/1/012005

Hansen, H.K., Yianatos, J.B., Ottosen, L.M., 2005. Speciation and leachability of copper in mine tailings from porphyry copper mining: Influence of particle size. Chemosphere 60, 1497–1503. https://doi.org/10.1016/j.chemosphere.2005.01.086

Hao, L., Liu, M., Wang, N., Li, G., 2018. A critical review on arsenic removal from water using iron-based adsorbents. RSC Adv. https://doi.org/10.1039/c8ra08512a

Helsen, L., Van Den Bulck, E., Van Bael, M.K., Vanhoyland, G., Mullens, J., 2004. Thermal behaviour of arsenic oxides (As2O5 and As2O3) and the influence of reducing agents (glucose and activated carbon). Thermochim. Acta 414, 145–153. https://doi.org/10.1016/j.tca.2003.12.016

Hiskey, J.B., Maeda, Y., 2003. A study of copper deposition in the presence of Group-15 elements by cyclic voltammetry and Auger-electron spectroscopy. J. Appl. Electrochem. 33, 393–401. https://doi.org/10.1023/A:1024445210550

Hoffmann, J.E., 2004. The Purification of Copper Refinery Electrolyte. JOM 56, 30–33.

Hoffmann, J.E., 1989. Recovering selenium and tellurium from copper refinery slimes. Jom 41, 33–38. https://doi.org/10.1007/BF03220269

Hoffmann, J.E., King, M.J., 2000. Selenium and Selenium Compounds, Kiik Othmer Encyclopedia of Chemical Technology. https://doi.org/10.1002/0471238961.1905120508150606. a01.pub2.

Hu, Z., Gao, S., 2008. Upper crustal abundances of trace elements: A revision and update. Chem. Geol. 253, 205–221. https://doi.org/10.1016/j.chemgeo.2008.05.010

ICSC: International Copper Study Group, 2018. The World Copper Factbook. Lisbon, Portugal.

ICSG: International Copper Study Group, 2020. The World Copper Factbook 2020. Lisbon, Portugal.

Izydorczyk, G., Mikula, K., Skrzypczak, D., Moustakas, K., Witek-Krowiak, A., Chojnacka, K., 2021. Potential environmental pollution from copper metallurgy and methods of management. Environ. Res. 197, 111050. https://doi.org/10.1016/j.envres.2021.111050

Jain, C.K., Singh, R.D., 2012. Technological options for the removal of arsenic with special reference to South East Asia. J. Environ. Manage. 107, 1–18. https://doi.org/10.1016/j.jenvman.2012.04.016

KE, P. chao, LIU, Z. hong, 2019. Synthesis, in-situ coating and characterization of scorodite with high leaching stability. Trans. Nonferrous Met. Soc. China (English Ed. 29, 876–892. https://doi.org/10.1016/S1003-6326(19)64998-8

Kercher, A.K., Nagle, D.C., 2001. TGA modeling of the thermal decomposition of CCA treated lumber waste. Wood Sci. Technol. 35, 325–341. https://doi.org/10.1007/s002260100094

Khalid, M.K., Hamuyuni, J., Agarwal, V., Pihlasalo, J., Haapalainen, M., Lundström, M., 2019a. Sulfuric acid leaching for capturing value from copper rich converter slag. J. Clean. Prod. 215, 1005–1013. https://doi.org/10.1016/j.jclepro.2019.01.083

Khalid, M.K., Hamuyuni, J., Agarwal, V., Pihlasalo, J., Haapalainen, M., Lundström, M., 2019b. Sulfuric acid leaching for capturing value from copper rich converter slag. J. Clean. Prod. 215, 1005–1013. https://doi.org/10.1016/j.jclepro.2019.01.083

Khan, S.A.R., Yu, Z., Golpira, H., Sharif, A., Mardani, A., 2021. A state-of-the-art review and meta-analysis on sustainable supply chain management: Future research directions. J. Clean. Prod. 278, 123357. https://doi.org/10.1016/j.jclepro.2020.123357

Khan, S.A.R., Yu, Z., Sharif, A., Golpîra, H., 2020. Determinants of economic growth and environmental sustainability in South Asian Association for Regional Cooperation: evidence from panel ARDL. Environ. Sci. Pollut. Res. 27, 45675–45687. https://doi.org/10.1007/s11356-020-10410-1

Kilic, Y., Kartal, G., Timur, S., 2013. An investigation of copper and selenium recovery from copper anode slimes. Int. J. Miner. Process. 124, 75–82. https://doi.org/10.1016/j.minpro.2013.04.006

Kokes, H., Morcali, M.., Acma, E., 2014. Dissolution of copper and iron from malachite ore and precipitation of copper sulfate pentahydrate by chemical process. Eng. Sci. Technol. , Int. J. 17, 39–44.

Kolta, G.A., Askar, M.H., 1975. Thermal decomposition of some metal sulphates. Thermochim. Acta 11, 65–72. https://doi.org/10.1016/0040-6031(75)80038-4

Komnitsas, K., Zaharaki, D., 2007. Geopolymerisation: A review and prospects for the minerals industry. Miner. Eng. 20, 1261–1277. https://doi.org/10.1016/j.mineng.2007.07.011

Król, A., Mizerna, K., Bożym, M., 2020. An assessment of pH-dependent release and mobility of heavy metals from metallurgical slag. J. Hazard. Mater. 384. https://doi.org/10.1016/j.jhazmat.2019.121502

Kumar, S., Kumar, R., 2011. Mechanical activation of fly ash: Effect on reaction, structure and properties of resulting geopolymer. Ceram. Int. 37, 533–541. https://doi.org/10.1016/j.ceramint.2010.09.038

Lancellotti, I., Barbieri, L., Leonelli, C., 2015. Use of alkali-activated concrete binders for toxic

waste immobilization, Handbook of Alkali-Activated Cements, Mortars and Concretes. Woodhead Publishing Limited. https://doi.org/10.1533/9781782422884.4.539

Lastra-Quintero, R., Rowlands, N., Rao, S.R., Finch, J.A., 2014. Characterization and Separation of a Copper Smelter Dust Residue. Can. Metall. Q. 26, 85–90. https://doi.org/10.1179/cmq.1987.26.2.85

Le Berre, J.F., Gauvin, R., Demopoulos, G.P., 2008. A study of the crystallization kinetics of scorodite via the transformation of poorly crystalline ferric arsenate in weakly acidic solution. Colloids Surfaces A Physicochem. Eng. Asp. 315, 117–129. https://doi.org/10.1016/j.colsurfa.2007.07.028

Le Berre, J.F., Gauvin, R., Demopoulos, G.P., 2007. Characterization of Poorly-Crystalline Ferric Arsenate Precipitated from Equimolar Fe(III)-As(V) Solutions in the pH Range 2 to 8. Metall. Mater. Trans. B 38, 751–762. https://doi.org/10.1007/s11663-007-9081-y

Lee, S., van Riessen, A., Chon, C.M., 2016. Benefits of sealed-curing on compressive strength of fly ash-based geopolymers. Materials (Basel). 9. https://doi.org/10.3390/MA9070598

Lee, W.R., Eom, Y., Lee, T.G., 2017. Mercury recovery from mercury-containing wastes using a vacuum thermal desorption system. Waste Manag. https://doi.org/10.1016/j.wasman.2016.12.017

Lenoble, V., Chabroullet, C., Al Shukry, R., Serpaud, B., Deluchat, V., Bollinger, J.C., 2004. Dynamic arsenic removal on a MnO 2-loaded resin. J. Colloid Interface Sci. 280, 62–67. https://doi.org/10.1016/j.jcis.2004.07.034

Liao, M.I., Shih, X.H., Ma, H. wen, 2019. Secondary copper resource recycling and reuse: A waste input–output model. J. Clean. Prod. 239, 118142. https://doi.org/10.1016/j.jclepro.2019.118142

Lin, X., Peng, Z., Yan, J., Li, Z., Hwang, J.Y., Zhang, Y., Li, G., Jiang, T., 2017. Pyrometallurgical recycling of electric arc furnace dust. J. Clean. Prod. 149, 1079–1100. https://doi.org/10.1016/j.jclepro.2017.02.128

Litter, M.I., Morgada, M.E., Bundschuh, J., 2010. Possible treatments for arsenic removal in Latin American waters for human consumption. Environ. Pollut. 158, 1105–1118. https://doi.org/10.1016/j.envpol.2010.01.028

LME: London Metal Exchange, 2019. LME Lead [WWW Document]. URL https://www.lme.com/Metals/Non-ferrous/Lead#tabIndex=0 (accessed 8.1.19).

Lucheva, B., ILiev, P., Kolev, D., 2017. Hydro - pyrometallurgical treatment of copper converter flue dust. J. Chem. Technol. Metall. 52, 320–325.

Luukkonen, T., Abdollahnejad, Z., Yliniemi, J., Kinnunen, P., Illikainen, M., 2018a. One-part alkali-activated materials: A review. Cem. Concr. Res. 103, 21–34. https://doi.org/10.1016/j.cemconres.2017.10.001

Luukkonen, T., Abdollahnejad, Z., Yliniemi, J., Kinnunen, P., Illikainen, M., 2018b. Comparison of alkali and silica sources in one-part alkali-activated blast furnace slag mortar. J. Clean. Prod. 187, 171–179. https://doi.org/10.1016/j.jclepro.2018.03.202

Mádai, F., Kristály, F., Mucsi, G., 2015. Microstructure, mineralogy and physical properties of ground fly ash based geopolymers. Ceram. - Silikaty 59, 70–79.

Marković, R., Stevanović, J., Avramović, L., Nedeljković, D., Jugović, B., Stajić-Trošić, J., Gvozdenović, M., 2012. Copper-sulfate pentahydrate as a product of the waste sulfuric acid solution treatment. Metall. Mater. Trans. B Process Metall. Mater. Process. Sci. 43, 1388–1392. https://doi.org/10.1007/s11663-012-9721-8

Martínez Roca, J., 2007. Influencia de variables experimentales seleccionadas en la descomposición térmica de CaC2O4· H2O y CuSO4· 5H2O.

Mermerdaş, K., Manguri, S., Nassani, D.E., Oleiwi, S.M., 2017. Effect of aggregate properties on the mechanical and absorption characteristics of geopolymer mortar. Eng. Sci. Technol. an Int. J. 20, 1642–1652. https://doi.org/10.1016/j.jestch.2017.11.009

Mersmann, A., 1999. Crystallization and precipitation. Chem. Eng. Process. Process Intensif. 38, 345–353. https://doi.org/10.1016/S0255-2701(99)00025-2

Min, X.B., Liao, Y.P., Chai, L.Y., Yang, Z.H., Xiong, S., Liu, L., Li, Q.Z., 2015. Removal and stabilization of arsenic from anode slime by forming crystal scorodite. Trans. Nonferrous Met. Soc. China (English Ed. 25, 1298–1306. https://doi.org/10.1016/S1003-6326(15)63728-1

Minaříková, M., Škvára, F., 2006. Fixation of heavy metals in geopolymeric materials based on brown coal fly ash. Ceram. - Silikaty 50, 200–207.

Mineralogy Database, 2012a. Mineral Database [WWW Document]. URL http://webmineral.com/data/Anglesite.shtml#.XO_Hm4gzaUk (accessed 5.30.19).

Mineralogy Database, 2012b. Chalcanthite [WWW Document]. URL http://www.webmineral.com/data/Chalcanthite.shtml#.XoI2TIgzZPY (accessed 3.30.20).

Mobili, A., Telesca, A., Marroccoli, M., Tittarelli, F., 2020. Calcium sulfoaluminate and alkali-activated fly ash cements as alternative to Portland cement: study on chemical, physical-mechanical, and durability properties of mortars with the same strength class. Constr. Build. Mater. 246, 118436. https://doi.org/10.1016/j.conbuildmat.2020.118436

Mocellin, J., Mercier, G., Morel, J.L., Charbonnier, P., Blais, J.F., Simonnot, M.O., 2017. Recovery of zinc and manganese from pyrometallurgy sludge by hydrometallurgical processing. J. Clean. Prod. 168, 311–321. https://doi.org/10.1016/j.jclepro.2017.09.003

Montenegro, V., Sano, H., Fujisawa, T., 2013. Recirculation of high arsenic content copper smelting dust to smelting and converting processes. Miner. Eng. 49, 184–189. https://doi.org/10.1016/J.MINENG.2010.03.020

Morales, A., Cruells, M., Roca, A., Bergó, R., 2010. Treatment of copper flash smelter flue dusts for copper and zinc extraction and arsenic stabilization. Hydrometallurgy 105, 148–154. https://doi.org/10.1016/j.hydromet.2010.09.001

Mu, J., Perlmutter, D.D., 1981. Thermal Decomposition of Inorganic Sulfates and Their Hydrates. Ind. Eng. Chem. Process Des. Dev. 20, 640–646. https://doi.org/10.1021/i200015a010

Murari, K., Siddique, R., Jain, K.K., 2014. Use of waste copper slag, a sustainable material. J. Mater. Cycles Waste Manag. 17, 13–26. https://doi.org/10.1007/s10163-014-0254-x

Navarro, P., Alguacil, F.J., 2002. Adsorption of antimony and arsenic from a copper electrorefining solution onto activated carbon. Hydrometallurgy 66, 101–105. https://doi.org/10.1016/S0304-386X(02)00108-1

Newhook, R., Hirtle, H., Byrne, K., Meek, M.E., 2003. Releases from copper smelters and refineries and zinc plants in Canada: Human health exposure and risk characterization. Sci. Total Environ. 301, 23–41. https://doi.org/10.1016/S0048-9697(02)00229-2

Nidheesh, P. V., Singh, T.S.A., 2017. Arsenic removal by electrocoagulation process: Recent trends and removal mechanism. Chemosphere. https://doi.org/10.1016/j.chemosphere.2017.04.082

Nordstrom, D.K., Majzlan, J., Königsberger, E., 2014. Thermodynamic properties for arsenic minerals and aqueous species. Rev. Mineral. Geochemistry 79, 217–255. https://doi.org/10.2138/rmg.2014.79.4

Novais, R.M., Carvalheiras, J., Senff, L., Labrincha, J.A., 2018. Upcycling unexplored dregs and biomass fly ash from the paper and pulp industry in the production of eco-friendly geopolymer mortars: A preliminary assessment. Constr. Build. Mater. 184, 464–472. https://doi.org/10.1016/j.conbuildmat.2018.07.017

Nuñez, C., Espiell, F., Roca, A., 1985. Recovery of copper, silver and zinc from Huelva (Spain) copper smelter flue dust by a chloride leach process. Hydrometallurgy 14, 93–103. https://doi.org/10.1016/0304-386X(85)90008-8

O'Grady, D., 2014. Crystallization and Precipitation. Guide to effective process development, Crystallization Guide. www.mt.com/Crystallization.

Öhrlund, I., 2012. Future Metal Demand from Photovoltaic Cells and Wind Turbines - Investigating the Potential Risk of Disabling a Shift to Renewable Energy Science and Technology Options Future Metal Demand from Photovoltaic Cells and Wind Turbines Investigating the Potent. https://doi.org/10.13140/RG.2.1.4524.9049

Okanigbe, D.O., Popoola, A.P.I., Adeleke, A.A., 2017. Characterization of Copper Smelter Dust for Copper Recovery. Procedia Manuf. 7, 121–126. https://doi.org/10.1016/j.promfg.2016.12.032

Olin, Å., Noläng, B., Osadchii, E.G., Öhman, L.-O., Rosén, E., 2010. Chemical Thermodynamics of Selenium.

Orhan, G., 2005. Leaching and cementation of heavy metals from electric arc furnace dust in alkaline medium. Hydrometallurgy 78, 236–245. https://doi.org/10.1016/J.HYDROMET.2005.03.002

Panias, D., Giannopoulou, I.P., Perraki, T., 2007. Effect of synthesis parameters on the mechanical properties of fly ash-based geopolymers. Colloids Surfaces A Physicochem. Eng. Asp. 301, 246–254. https://doi.org/10.1016/j.colsurfa.2006.12.064

Paz-Gómez, D.C., Pérez-Moreno, S.M., Gázquez, M.J., Guerrero, J.L., Ruiz-Oria, I., Ríos, G., Bolívar, J.P., 2021a. Arsenic removal procedure for the electrolyte from a hydro-pyrometallurgical complex. Chemosphere 281, 130651. https://doi.org/10.1016/j.chemosphere.2021.130651

Paz-Gómez, D.C., Pérez-Moreno, S.M., Ruiz-Oria, I., Ríos, G., Bolívar, J.P., 2021b. Copper recovery from sludges generated in the electrolyte treatment plant of a pyrometallurgical complex. Hydrometallurgy 206, 105769. https://doi.org/10.1016/j.hydromet.2021.105769

Paz-Gómez, D.C., Pérez-Moreno, S.M., Ruiz-Oria, I., Ríos, G., Bolívar, J.P., 2020. Characterization of Two Sludges from a Pyrometallurgical Copper Smelting Complex for Designing a Se and Pb Recovery Proposal. Waste and Biomass Valorization. https://doi.org/10.1007/s12649-020-01197-w

Peng, Y.L., Zheng, Y.J., Zhou, W.K., Chen, W.M., 2012. Separation and recovery of Cu and As during purification of copper electrolyte. Trans. Nonferrous Met. Soc. China (English Ed. 22, 2268–2273. https://doi.org/10.1016/S1003-6326(11)61459-3

Pereira, F., Silva, R.J.C., Soares, A.M.M., Araújo, M.F., Oliveira, M.J., Martins, R.M.S., Schell, N., 2015. Effects of long-term aging in arsenical copper alloys. Microsc. Microanal. 21, 1413–1419. https://doi.org/10.1017/S1431927615015263

Pérez-Moreno, S.M., 2018. CARACTERIZACIÓN Y VALORIZACIÓN DE RESIDUOS INORGÁNICOS PROCEDENTES DE INDUSTRIAS QUÍMICAS DE HUELVA. Universidad de Huelva.

Pérez-Moreno, S. M., Gázquez, M.J., Pérez-López, R., Vioque, I., Bolívar, J.P., 2018. Assessment of natural radionuclides mobility in a phosphogypsum disposal area. Chemosphere 211, 775–783. https://doi.org/10.1016/j.chemosphere.2018.07.193

Pérez-Moreno, S.M., Gázquez, M.J., Ruiz-Oria, I., Ríos, G., Bolívar, J.P., 2018. Diagnose for valorisation of reprocessed slag cleaning furnace flue dust from copper smelting. J. Clean. Prod. 194, 383–395. https://doi.org/10.1016/j.jclepro.2018.05.090

Pérez, I., Moreno-Ventas, I., Parra, R., Ríos, G., 2019. Post-mortem study of magnesia-chromiterefractory used in the gas area of a Submerged ArcFurnace for the copper-making process. Bol. la Soc. Esp. Ceram. y Vidr. 1–11. https://doi.org/10.1016/j.bsecv.2018.12.001

Pérez, I., Moreno-Ventas, I., Parra, R., Ríos, G., 2018a. Post-mortem Study of Magnesia–Chromite Refractory Used in a Submerged Arc Furnace in the Copper-Making Process. Jom 70, 2435–2442. https://doi.org/10.1007/s11837-018-3090-y

Pérez, I., Moreno-Ventas, I., Ríos, G., 2018b. Chemical degradation of magnesia-chromite refractory

used in the conversion step of the pyrometallurgical copper-making process: A thermochemical approach. Ceram. Int. 44, 18363–18375. https://doi.org/10.1016/j.ceramint.2018.07.052

Provis, J.L., Van Deventer, J.S.J., 2014. Alkali Activated Materials, 1st ed, RILEM State-of-the-Art Reports, RILEM State-of-the-Art Reports. Springer Netherlands, Dordrecht. https://doi.org/10.1007/978-94-007-7672-2

Qiu, J., Zhao, Y., Xing, J., Sun, X., 2019. Fly Ash/Blast Furnace Slag-Based Geopolymer as a Potential Binder for Mine Backfilling: Effect of Binder Type and Activator Concentration. Adv. Mater. Sci. Eng. 2019. https://doi.org/10.1155/2019/2028109

Ramachandra Rao, S., 2006. Chapter 10 Resource recovery from process wastes, in: Resource Recovery and Recycling from Metallurgical Wastes. pp. 375–457. https://doi.org/10.1016/S0713-2743(06)80095-4

Ramsdell, L.S., 1929. An X-ray study of the domeykite grou [WWW Document]. Am. Mineral. URL http://www.minsocam.org/msa/collectors_corner/arc/domeykite.htm (accessed 6.30.20).

Rattanasak, U., Pankhet, K., Chindaprasirt, P., 2011. Effect of chemical admixtures on properties of high-calcium fly ash geopolymer. Int. J. Miner. Metall. Mater. 18, 364–369. https://doi.org/10.1007/s12613-011-0448-3

RD 1481/2001, 2013. Real Decreto 1481/2001 , de 27 de diciembre , por el que se regula la eliminación de residuos mediante depósito en vertedero., Boletin Oficial Del Estado.

Regulation (EU) Nº 528/2012, 2012. Regulation (EU) No 528/2012 of the European parliament and of the countil of 22 May 2012 concerning the making available on the market and use of biocidal products, Official Journal of the European Union.

Riveros, P.A., Dutrizac, J.E., Spencer, P., 2001. Arsenic Disposal Practices in the Metallurgical Industry. Can. Metall. Q. 40, 395–420. https://doi.org/10.1179/cmq.2001.40.4.395

Rong, Z., Tang, X., Wu, L., Chen, X., Dang, W., Li, X., Huang, L., Wang, Y., 2020. The effect of precursor speciation on the growth of scorodite in an atmospheric scorodite synthesis. R. Soc. Open Sci. 7. https://doi.org/10.1098/rsos.191619

Rosengrant, L., Fargo, L., 1990. Final Best Demonstrated Available Technology (BDTA) Background Document for K031, K084, K101, K102, Characterization As Wastes (D004), Characteristic Se Wastes (D010), and P and U Wastes Containing As and Se Listing

Constituents.

Rumayor, M., Diaz-Somoano, M., Lopez-Anton, M.A., Martinez-Tarazona, M.R., 2013. Mercury compounds characterization by thermal desorption. Talanta 114, 318–322. https://doi.org/10.1016/j.talanta.2013.05.059

Ruşen, A., Sunkar, A.S., Topkaya, Y.A., 2008. Zinc and lead extraction from Çinkur leach residues by using hydrometallurgical method. Hydrometallurgy 93, 45–50. https://doi.org/10.1016/j.hydromet.2008.02.018

Rzymski, P., Klimaszyk, P., Marszelewski, W., Borowiak, D., Mleczek, M., Nowiński, K., Pius, B., Niedzielski, P., Poniedziałek, B., 2017. The chemistry and toxicity of discharge waters from copper mine tailing impoundment in the valley of the Apuseni Mountains in Romania. Environ. Sci. Pollut. Res. 24, 21445–21458. https://doi.org/10.1007/s11356-017-9782-y

Saeli, M., Senff, L., Seabra, M.P., Labrincha, J.A., 2019. Alkali-activated Fly Ash-based Mortars for Green Applications in Architecture and Civil Engineering. Int. J. Struct. Civ. Eng. Res. 8, 1–9. https://doi.org/10.18178/ijscer.8.1.1-9

Şahin, M., Erdem, M., 2015. Cleaning of high lead-bearing zinc leaching residue by recovery of lead with alkaline leaching. Hydrometallurgy 153, 170–178. https://doi.org/10.1016/J.HYDROMET.2015.03.003

Sambucci, M., Sibai, A., Valente, M., 2021. Recent advances in geopolymer technology. A potential eco-friendly solution in the construction materials industry: A review. J. Compos. Sci. 5. https://doi.org/10.3390/jcs5040109

Schipper, B.W., Lin, H.C., Meloni, M.A., Wansleeben, K., Heijungs, R., van der Voet, E., 2018a. Estimating global copper demand until 2100 with regression and stock dynamics. Resour. Conserv. Recycl. 132, 28–36. https://doi.org/10.1016/j.resconrec.2018.01.004

Schipper, B.W., Lin, H.C., Meloni, M.A., Wansleeben, K., Heijungs, R., van der Voet, E., 2018b. Estimating global copper demand until 2100 with regression and stock dynamics. Resour. Conserv. Recycl. 132, 28–36. https://doi.org/10.1016/j.resconrec.2018.01.004

Schlesinger, M.E., King, M.J., Sole, K.C., Davenport, W.G., 2011. Extractive Metallurgy of Copper, Fifth. ed. Elsevier. https://doi.org/10.1016/C2010-0-64841-3

Schwartz, D.M., Omaynikova, V.Y., Stocker, S.K., 2017. Environmental benefits of the CESL

Process for the treatment of high-arsenic copper-gold concentrates, in: Hydroprocess-ICMSE. pp. 1–10.

Seetharaman, S., Adri, McLean, A., Guthrie, R., Sridhar, S., 2014. Treatise on Process Metallurgy, Treatise on Process Metallurgy. Elsevier. https://doi.org/10.1016/C2010-0-67120-3

Sheedy, M., Pajunen, P., Pickering, O., Wesstrom, B., 2006. Control of Copper Electrolyte Impurities-Overview of the Short Bed Ion Exchange Technique and Phelps Dodge El Paso Case Study, Eco-Tec Inc. - Technical Paper 183.

Shen, H., Forssberg, E., 2003. An overview of recovery of metals from slags. Waste Manag. 23, 933–949. https://doi.org/10.1016/S0956-053X(02)00164-2

Shively, W., Bishop, P., Gress, D., Brown, T., 1986. Leaching tests of heavy metals stabilized with Portland cement. J. Water Pollut. Control Fed. 58, 234–241.

Singh, M., Kumar, D., Thomas, J., Ramanan, A., 2010. Crystallization of copper(II) sulfate based minerals and MOF from solution: Chemical insights into the supramolecular interactions. J. Chem. Sci. 122, 757–769. https://doi.org/10.1007/s12039-010-0064-1

Singhania, S., Wang, Q., Filippou, D., Demopoulos, G.P., 2006. Acidity, valency and third-ion effects on the precipitation of scorodite from mixed sulfate solutions under atmospheric-pressure conditions. Metall. Mater. Trans. B Process Metall. Mater. Process. Sci. 37, 189–197. https://doi.org/10.1007/BF02693148

Singhania, S., Wang, Q., Filippou, D., Demopoulos, G.P., 2005. Temperature and seeding effects on the precipitation of scorodite from sulfate solutions under atmospheric-pressure conditions. Metall. Mater. Trans. B Process Metall. Mater. Process. Sci. 36, 327–333. https://doi.org/10.1007/s11663-005-0062-8

Siriwardane, R. V., Poston, J.A., Fisher, E.P., Shen, M.S., Miltz, A.L., 1999. Decomposition of the sulfates of copper, iron (II), iron (III), nickel, and zinc: XPS, SEM, DRIFTS, XRD, and TGA study. Appl. Surf. Sci. 152, 219–236. https://doi.org/10.1016/S0169-4332(99)00319-0

Song, P., Yang, Z., Zeng, G., Yang, X., Xu, H., Wang, L., Xu, R., Xiong, W., Ahmad, K., 2017. Electrocoagulation treatment of arsenic in wastewaters: A comprehensive review. Chem. Eng. J. 317, 707–725. https://doi.org/10.1016/j.cej.2017.02.086

Statista, 2019. Copper consumption distribution by world region 2018 [WWW Document]. Statista.

URL https://www.statista.com/statistics/693466/distribution-of-global-refined-copper-consumption-by-region/ (accessed 9.30.21).

Svens, K., 1985. Outokumpu Mercury Recovery. Met. News 7.

Swash, P.M., Monhemius, J., 1998. The Scorodite Process: a technology for the disposal of arsenic in the 21st century., Effluent Treatment in the Mining Industry. University of Concepción.

Tabelin, C.B., Corpuz, R.D., Igarashi, T., Villacorte-Tabelin, M., Ito, M., Hiroyoshi, N., 2019. Hematite-catalysed scorodite formation as a novel arsenic immobilisation strategy under ambient conditions. Chemosphere 233, 946–953. https://doi.org/10.1016/j.chemosphere.2019.06.020

Tagawa, H., 1984. Thermal decomposition temperatures of metal sulfates. Thermochim. Acta 80, 23–33. https://doi.org/10.1016/0040-6031(84)87181-6

The World Bank, 2017. The Growing Role of Minerals and Metals for a Low Carbon Future, The Growing Role of Minerals and Metals for a Low Carbon Future. https://doi.org/10.1596/28312

U.S. Geological Survey, 2019. Mineral Commodity Summaries 2019. https://doi.org/https://doi.org/10.3133/70202434

U.S, E.P.A., 1992. SW-846 Test Method 1311: Toxicity Characteristic Leaching Procedure, Environmental Health.

Valera, A.E., Arias, A., Reyes, Y., 2003. Cinética de la producción de sulfato de cot pentahidratado a partir de chatarra de cobre. Rev. Tec. la Fac. Ing. Univ. del Zulia 26, 101–108.

Van Jaarsveld, J.G.S., Van Deventer, J.S.J., Lorenzeni, L., 1997. the Potential Use of Geopolymeric Materials To Immobilise Toxic Metals: Part I. Theory and Applications. Miner. Eng. 10, 659–669.

Vilarinho, I.S., Carneiro, J., Pinto, C., Labrincha, J.A., Seabra, M.P., 2021. Development of coloured stoneware bodies through the incorporation of industrial Cr/Ni electroplating sludge. Sustain. 13, 1–13. https://doi.org/10.3390/su13041999

Vircikova, E., Havlik, M., 1999. Removing As from converter dust by a hydrometallurgical method. Jom 51, 20–23. https://doi.org/10.1007/s11837-999-0152-1

Vítková, M., Ettler, V., Hyks, J., Astrup, T., Kříbek, B., 2011. Leaching of metals from copper smelter flue dust (Mufulira, Zambian Copperbelt). Appl. Geochemistry 26, 263–266. https://doi.org/10.1016/j.apgeochem.2011.03.120

Vu, T.H., Gowripalan, N., 2018. Mechanisms of heavy metal immobilisation using geopolymerisation techniques – A review. J. Adv. Concr. Technol. 16, 124–135. https://doi.org/10.3151/jact.16.124

Wang, C., Li, S., Wang, H., Fu, J., 2016. Selenium minerals and the recovery of selenium from copper refinery anode slimes. J. South. African Inst. Min. Metall. 116, 593–600. https://doi.org/10.17159/2411-9717/2016/v116n6a16

Wang, P.Z., Trettin, R., Rudert, V., 2005. Effect of fineness and particle size distribution of granulated blast-furnace slag on the hydraulic reactivity in cement systems. Adv. Cem. Res. 17, 161–166. https://doi.org/10.1680/adcr.2005.17.4.161

Wang, Q., Guo, X., Tian, Q., Jiang, T., Chen, M., Zhao, B., 2017. Effects of matte grade on the distribution of minor elements (Pb, Zn, As, Sb, and Bi) in the bottom blown copper smelting process. Metals (Basel). 7. https://doi.org/10.3390/met7110502

Wang, S., 2004. Impurity control and removal in copper tankhouse operations. JOM 56, 34–37. https://doi.org/10.1007/s11837-004-0089-3

Wang, T., Berrill, P., Zimmerman, J.B., Hertwich, E.G., 2021. Copper Recycling Flow Model for the United States Economy: Impact of Scrap Quality on Potential Energy Benefit. Environ. Sci. Technol. 55, 5485–5495. https://doi.org/10.1021/acs.est.0c08227

Wesstrom, B.C., Araujo, O., 2012. Optimizing a cascading liberator. T.T. Chen Honor. Symp. Hydrometall. Electrometall. Mater. Charact. 01, 151–156. https://doi.org/10.1002/9781118364833.ch13

Xiao, L., Wang, Y., Yu, Y., Fu, G., Liu, Y., Sun, Z., Ye, S., 2019. Enhanced selective recovery of selenium from anode slime using MnO 2 in dilute H 2 SO 4 solution as oxidant. J. Clean. Prod. 209, 494–504. https://doi.org/10.1016/j.jclepro.2018.10.144

Xing, P., Ma, B., Wang, C., Chen, Y., 2018. Cleaning of lead smelting flue gas scrubber sludge and recovery of lead, selenium and mercury by the hydrometallurgical route. Environ. Technol. (United Kingdom) 39, 1461–1469. https://doi.org/10.1080/09593330.2017.1332102

Yahya, Z., Abdullah, M.M.A.B., Talib, S.Z.A., Razak, R.A., 2017. Comparative study on early strength of sodium hydroxide (NaOH) activated fly ash based geopolymer. AIP Conf. Proc. 1887, 6–11. https://doi.org/10.1063/1.5003542

Yang, H., Liu, J., Yang, J., 2011. Leaching copper from shredded particles of waste printed circuit boards. J. Hazard. Mater. 187, 393–400. https://doi.org/10.1016/j.jhazmat.2011.01.051

Yang, K.H., Song, J.K., Song, K. Il, 2013. Assessment of CO 2 reduction of alkali-activated concrete. J. Clean. Prod. 39, 265–272. https://doi.org/10.1016/j.jclepro.2012.08.001

Yang, Z., Rui-Lin, M., Wang-Dong, N., Hui, W., 2010. Selective leaching of base metals from copper smelter slag. Hydrometallurgy 103, 25–29. https://doi.org/10.1016/j.hydromet.2010.02.009

Yazici, E.Y., Deveci, H., 2016. Recovery of copper sulphate from sulphuric acid leach solutions via solvent displacement crystallisation using acetone, in: Aydiner, K., Yasar, S., Yasar, O. (Eds.), International Black Sea Mining and Tunnelling Symposium. Trabzon, Turkey, pp. 455–460.

Yousefi Oderji, S., Chen, B., Ahmad, M.R., Shah, S.F.A., 2019. Fresh and hardened properties of one-part fly ash-based geopolymer binders cured at room temperature: Effect of slag and alkali activators. J. Clean. Prod. 225, 1–10. https://doi.org/10.1016/j.jclepro.2019.03.290

Zhang, P., Zheng, Y., Wang, K., Zhang, J., 2018. A review on properties of fresh and hardened geopolymer mortar. Compos. Part B Eng. 152, 79–95. https://doi.org/10.1016/j.compositesb.2018.06.031

Zhang, T., Zhao, Y., Bai, H., Wang, W., Zhang, Q., 2019. Enhanced arsenic removal from water and easy handling of the precipitate sludge by using FeSO4 with CaCO3 to Ca(OH)2. Chemosphere 231, 134–139. https://doi.org/10.1016/j.chemosphere.2019.05.117

Zhao, H., Xiao, Q., Huang, D., Zhang, S., 2014. Influence of Pore Structure on Compressive Strength of Cement Mortar. Sci. World J. 2014, 1–12. https://doi.org/10.1155/2014/247058

Zhou, W.K., Peng, Y.L., Zheng, Y.J., Ma, Y.T., Cui, T., 2011. Reduction and deposition of arsenic in copper electrolyte. Trans. Nonferrous Met. Soc. China (English Ed. 21, 2772–2777. https://doi.org/10.1016/S1003-6326(11)61122-9

Zouboulis, A.I., Katsoyiannis, I.A., 2018. Recent advances in water and wastewater treatment with emphasis in membrane treatment operations. Water (Switzerland). https://doi.org/10.3390/w11010045

ANNEX I

SUPPLEMENTARY MATERIAL

ANNEX I.1. SUPPLEMENTARY MATERIAL OF SUBCHAPTER 3.1

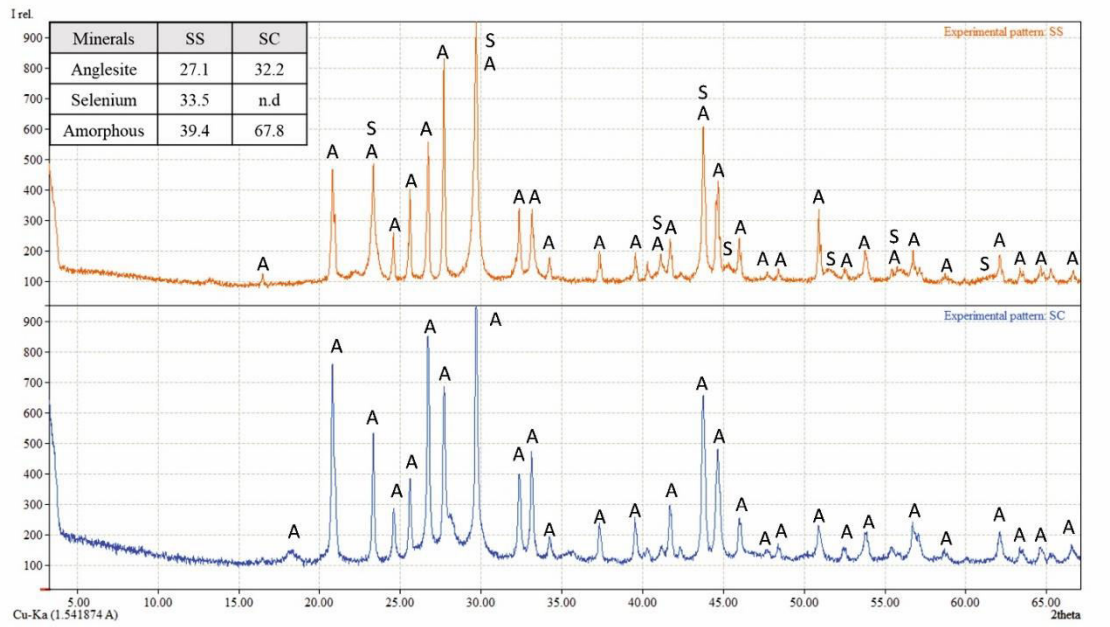

Fig. S3.1. *X-ray diffraction (XRD) pattern of sludges. Mineral phases identified: Anglesite- $PbSO_4$ (A) and Selenium- Se (S). n. d= no detect.*

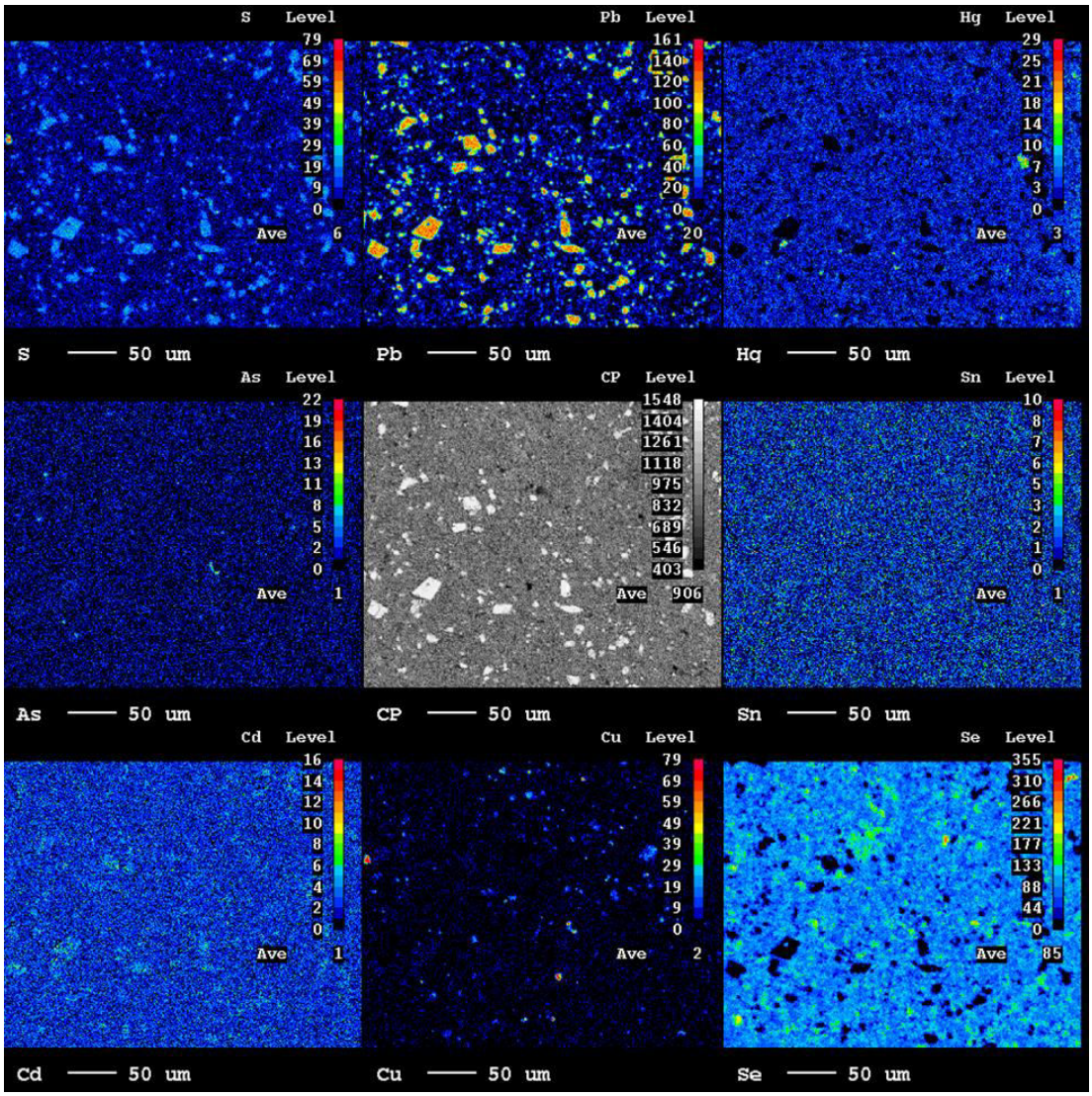

***Fig. S3.2**. Secondary electron image of SS region and distribution of Se, Pb, S, Hg, As, Cu, Sn and Cd.*

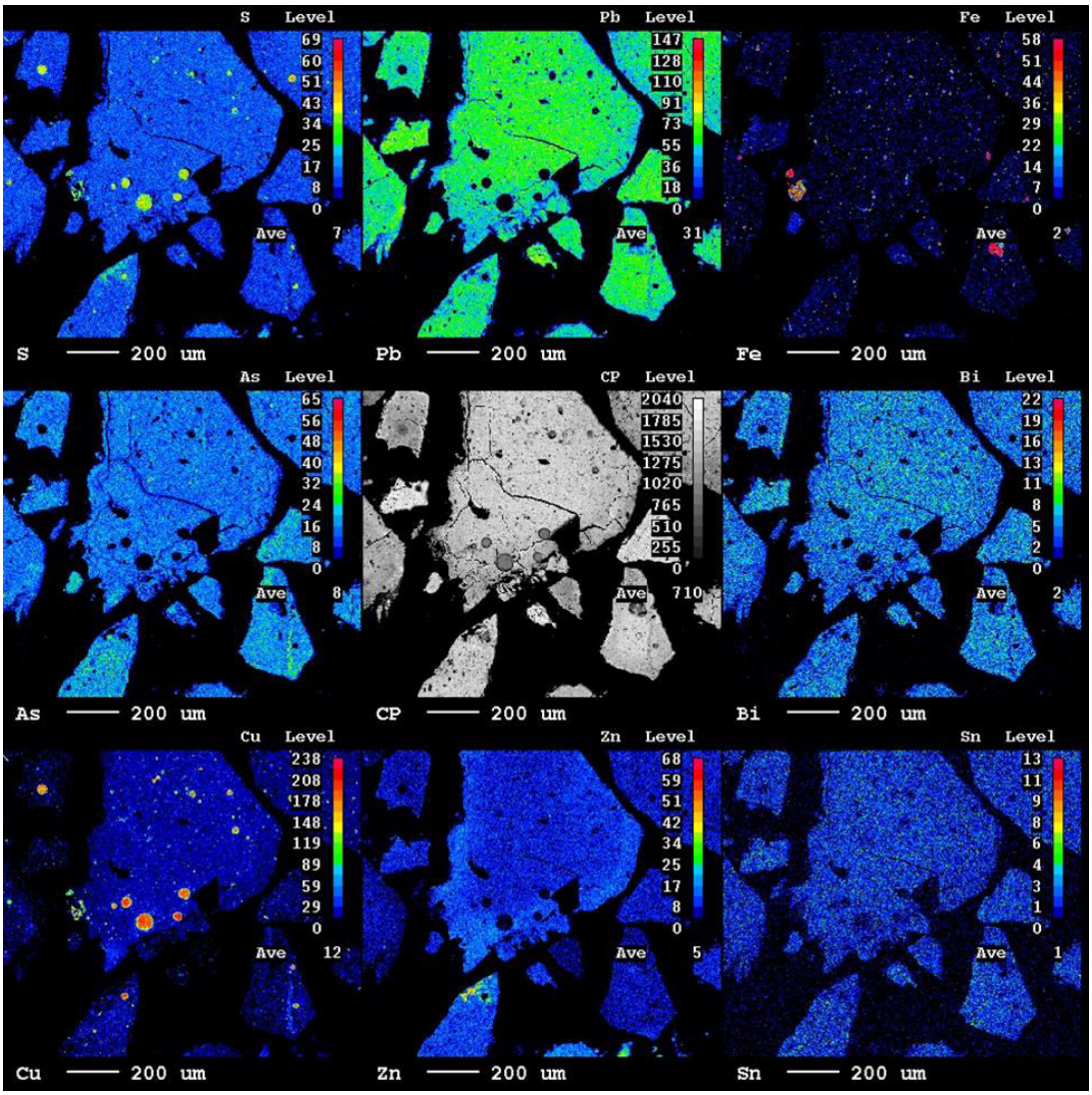

Fig. S3.3. Secondary electron image of a SC region and distribution of S, Pb, Fe, As, Bi, Cu, Zn and Sn.

Size (µm)	Type	SS (%)			SC (%)		
		Average concentration	Cumulative	Global	Average concentration	Cumulative	Global
<4	Clay	11 ± 4	11 ± 4	11 ± 4	34 ± 4	34 ± 3	34 ± 3
4-8	Silt	35 ± 6	46 ± 7	87 ± 8	20.1 ± 1.3	54.1 ± 3.1	62 ± 3
8-16		38 ± 3	84 ± 8		12.8 ± 0.8	66.9 ± 3.2	
16-32		11 ± 4	95 ± 9		15.6 ± 0.8	82.5 ± 3.3	
32-62	Sand	2.1 ± 0.9	97.1 ± 9.2	2.4 ± 1.3	13 ± 3	95.5 ± 4.3	4.6 ± 1.5
62-125		1.9 ± 1.3	99.0 ± 9.3		4.2 ± 1.5	99.7 ± 4.5	
125-250		0.36 ± 0.36	99.4 ± 9.3		0.33 ± 0.14	100.0 ± 4.6	
250-500		0.13 ± 0.13	99.5 ± 9.3		0.13 ± 0.13	100.0 ± 4.6	
500-1000		0.07 ± 0.07	100.0 ± 9.3		0.03 ± 0.04	100.0 ± 4.6	
1000-2000		-	-		-	-	

Table S3.1. *Average grain-size and cumulative distribution (%V) of the studied samples.* ***Note:*** *Standard uncertainty (1 σ) calculated as the standard deviation of the mean* $\sigma = S_x / (n)^{1/2}$*, where "n=3" is the number of samples analysed.*

Process	Advantages	Disadvantages
Soda Roasting	No volatilization of Se Recycling of much of the solution Acceptable efficiency of Se recovery	High or moderate* energy consumption Large number of stages Large liquid effluents Long reaction time Extremely corrosive solutions*
Alkaline Autoclaving	No volatilization of Se Lower number of stages Low corrosiveness Acceptable efficiency of Se recovery	High energy consumption High oxygen consumption High NaOH consumption Large liquid effluents Reacts with all metal sulphates Long reaction time
Sulphating Roasting	High efficiency of Se recovery Lower number of stages Highly pure (> 99.5 %) Uses only H_2SO_4 as reagent Regeneration of sulphuric acid	Moderate energy consumption Long reaction time Large gaseous effluents Modest sulphuric acid consumption
Oxidizing Roasting	High efficiency of Se recovery Lower number of stages Highly pure (> 99.5 %)	Moderate energy consumption Long reaction time High oxygen consumption Moderate gaseous effluents Requires Se reduction stage
Chlorination Process	No volatilization of Se High efficiency of Se recovery Modest reagent consumption Short reaction time	Moderate energy consumption Large number of stages Losses of Se Moderate gaseous and liquid effluents Requires a purification stage

Table S3.2. *Advantages and disadvantages of currently applied processes in primary copper refineries to recover of selenium. Note: Soda roasting uses two processes for Se recovery: process 1 by crystallization, and process 2 (*) by precipitation.*

ANNEX I.2. SUPPLEMENTARY MATERIAL OF SUBCHAPTER 3.2

Exp. ID	Oxidising agent	S/L (g mL^{-1})	$[H_2SO_4]$ (M)	$[HNO_3]$ (M)	Gas flow (L min^{-1})	time (h)	Temperature (ºC)	Dissolution efficiency of the ES (%)	Note
N-1.0-1.8-A	Nitric acid	1/20	1.8	1.0	-	12	24	65.13	Low dissolution efficiency of the ES.
N-1.2-1.8-A	Nitric acid	1/20	1.8	1.2	-	12	24	98.85	Total dissolution of ES. Additionally, precipitation of copper sulphate was observed
N-1.2-1.8-A-R	Nitric acid	1/20	1.8	1.2	-	12	24	98.88	
N-1.4-1.8-A	Nitric acid	1/20	1.8	1.4	-	12	24	100.0	
N-1.6-1.8-A	Nitric acid	1/20	1.8	1.6	-	12	24	100.0	
N-1.4-1.6-A	Nitric acid	1/20	1.6	1.4	-	12	24	91.77	High dissolution efficiency of the ES.
N-1.6-1.6-A	Nitric acid	1/20	1.6	1.6	-	12	24	99.36	Total dissolution of ES. Additionally, precipitation of copper sulphated was observed
N-1.6-1.6-A-R	Nitric acid	1/20	1.6	1.6	-	12	24	99.81	
N-1.2-1.4-A	Nitric acid	1/20	1.4	1.2	-	12	24	37.12	Low dissolution efficiency of the ES.
N-1.4-1.4-A	Nitric acid	1/20	1.4	1.4	-	12	24	87.75	High dissolution efficiency of the ES.
N-1.6-1.4-A	Nitric acid	1/20	1.4	1.6	-	12	24	90.16	
N-1.8-1.4-A	Nitric acid	1/20	1.4	1.8	-	12	24	99.40	Total dissolution without precipitation of the copper sulphate was observed.
N-1.8-1.4-A-R	Nitric acid	1/20	1.4	1.8	-	12	24	98.94	
N-1.8-1.4-B	**Nitric acid**	**1/20**	**1.4**	**1.8**	**-**	**2.5**	**50**	**99.97**	**Optimization experiment**
N-1.8-1.4-B-R	**Nitric acid**	**1/20**	**1.4**	**1.8**	**-**	**2.5**	**50**	**99.95**	
N-1.8-1.4-B-RR	**Nitric acid**	**1/20**	**1.4**	**1.8**	**-**	**2.5**	**50**	**99.96**	
A-2-2-C	**Air**	**1/20**	**2.0**	**-**	**2**	**2.5**	**80**	**32.02**	The change of sulfuric acid concentration did not influence in the dissolution of electrolyte sludge
A-2-2-C-R	**Air**	**1/20**	**2.0**	**-**	**2**	**2.5**	**80**	**31.93**	
A-2-4-C	Air	1/20	4.0	-	2	2.5	80	32.87	
A-2-4-C-R	Air	1/20	4.0	-	2	2.5	80	33.93	
A-2-6-C	Air	1/20	6.0	-	2	2.5	80	32.90	
A-2-6-C-R	Air	1/20	6.0	-	2	2.5	80	32.96	
A-2-10-C	Air	1/20	10.0	-	2	2.5	80	28.45	
O-8-2-C	**Oxygen**	**1/20**	**2.0**	**-**	**8**	**2.5**	**80**	**64.29**	Increasing oxygen flow increased the dissolution efficiency of the electrolyte sludge, but it did not dissolve completely
O-8-2-C-R	**Oxygen**	**1/20**	**2.0**	**-**	**8**	**2.5**	**80**	**67.04**	

Table S3.3. *Summary of ES dissolution experiments.*

Artificial solution							
	Exp. ID	***Fe/As mole ratio***	***Iron source***	***Oxidizing Agent***	***Basic Agent***	***Stage***	***Reaction time by stage***
Non-adjust of pH	E1-A	1.5	Fe^{3+}	-	-	1	6 h
	E1-B	1.5	Fe^{2+}	Air	-	1	8 h
Adjust of pH	E2	1.5	Fe^{2+}	Air	$Ca(OH)_2$	3	3 h
	E3	1.5	Fe^{2+}	Air	$Mg(OH)_2$	3	3 h
Electrolyte sludge solution							
Adjust of pH	E4	1.7	Fe^{2+}	Air	$Mg(OH)_2$	4	3 h
	E5	1.7	Fe^{2+}	Air	$Ca(OH)_2$	4	3 h

Table S3.4*. Experimental conditions for arsenic removal.*

				Major element (%)				**XRD**	**Precipitation (%)**	
Exp. ID	**Fe^{3+} source**	**Colour**	**Method**	**As**	**Cl**	**Fe**	**S**		**As**	**Fe**
E1-A1	$FeCl_3$	Yellow brown (After drying of the solid at 60 ºC change to dark brown)	Reproducible	33	21	24	-	No scorodite	120	78
E1-A2	$Fe_2(SO_4)_3{\cdot}7H_2O$	Beige (After drying of the solid at 60 ºC change to brown)	Reproducible	36	-	22	1.1	No scorodite	53	43

Table S3.5*.. Summary results of Fe^{3+} experiments.*

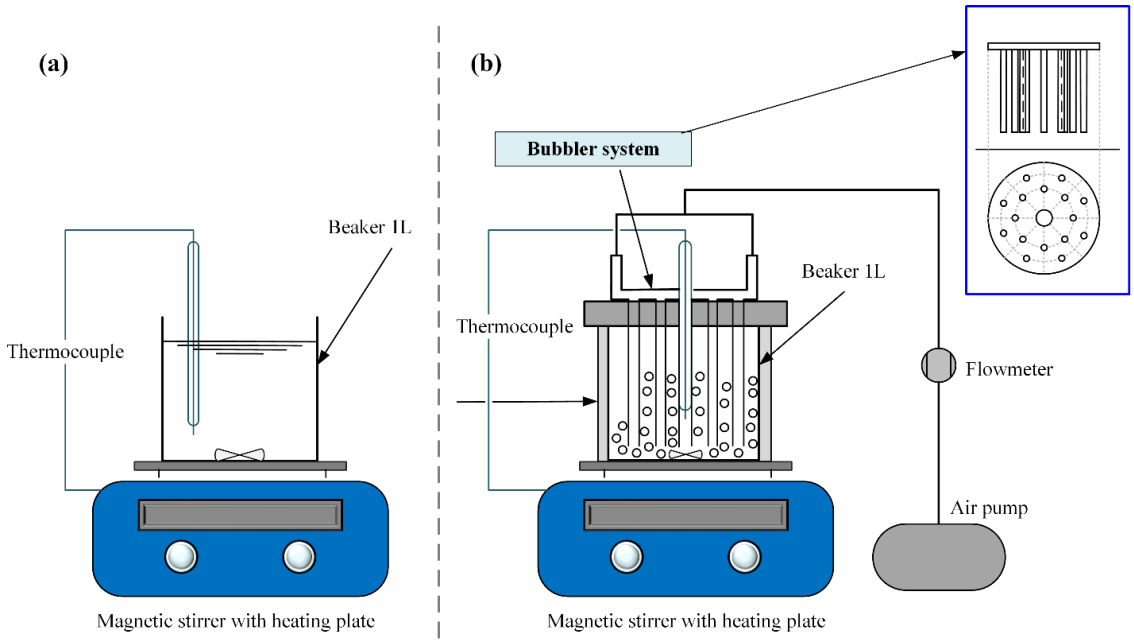

Fig. S3.4. *Experimental equipment using dissolution of ES. (a) With HNO_3 and (b) with Air or O_2. Bubbler system consists of a lid with holes through which 16 equidistant glass tubes are inserted for a homogeneous distribution of the air/O_2. The O_2 is injected from oxygen bottles.*

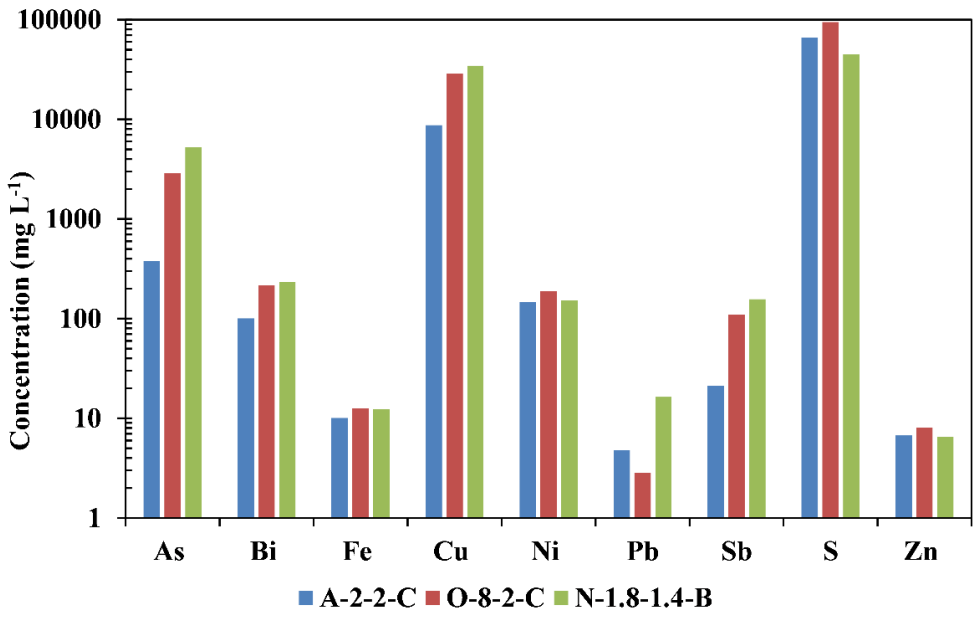

Fig. S3.5. *Chemical composition (mg L^{-1}) of the ES solutions obtained in each representative experiment.*

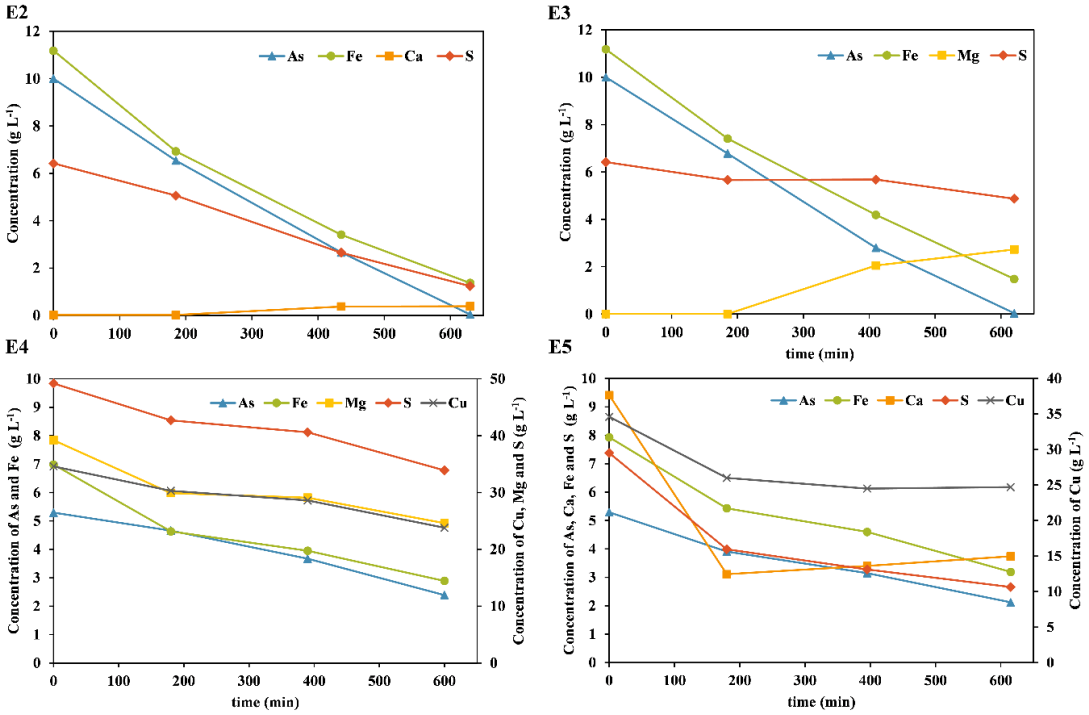

***Fig. S3.6**. Concentration of major elements in solution as a function of time for both types of experiments: E2-E3, artificial solution, and E4-E5, ES solution.*

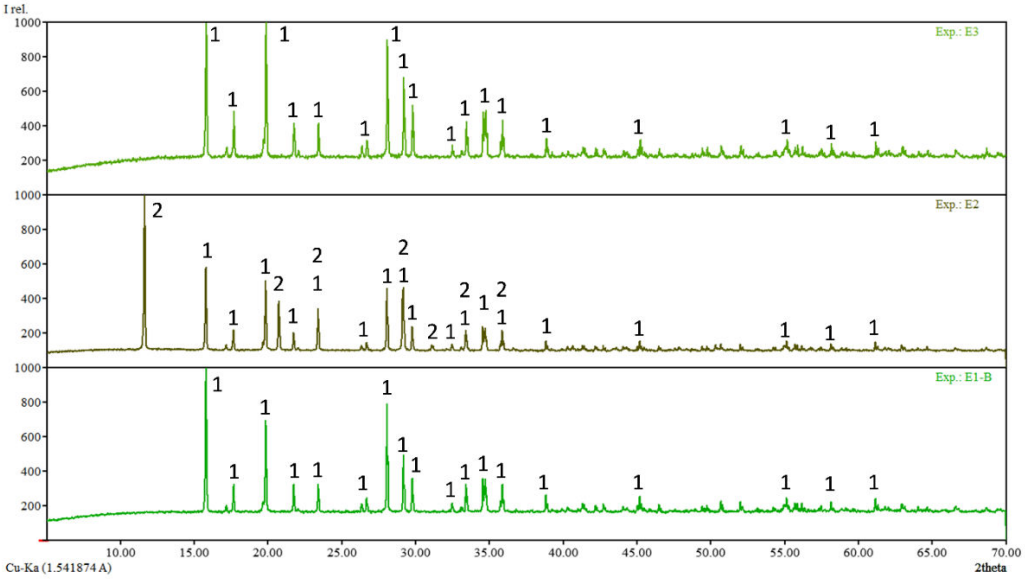

***Fig. S3.7.** XRD pattern of ES. Mineral phases identified: Scorodite-$FeAsO_4{\cdot}2H_2O$ (1)a and Gypsum-$CaSO_4{\cdot}2H_2O$ (2).*

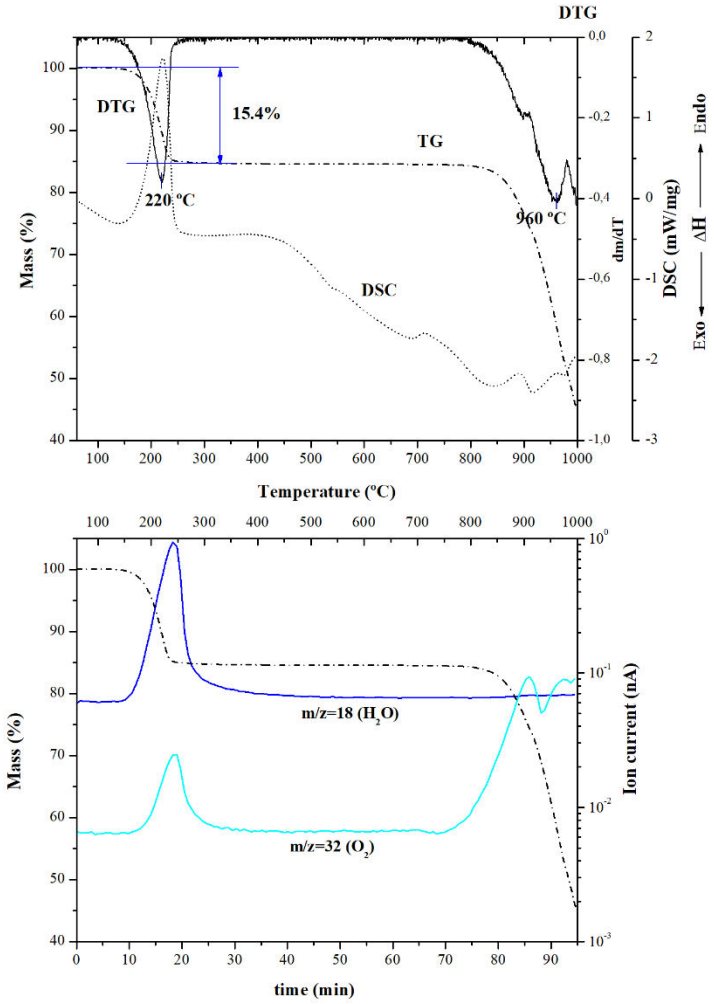

Fig. S3.8. *TG-DTG-DSC curve and gases detected in the precipitate obtained at the E1-B.*

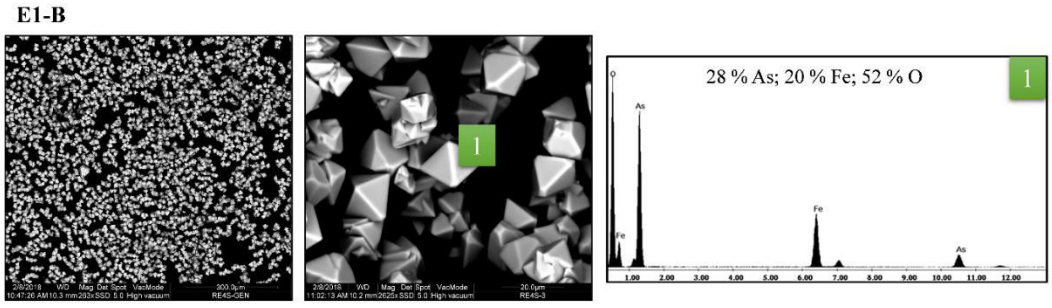

	Elements	As	Ca	Fe	O
E1-B	Wt (%)	35	N.D	24	41
E3		30	N.D	21	49

Fig. S3.9. *SEM images of precipitates obtained in E1-B and E3. The table also shows the general composition determined by EDS from the image located at the left.*

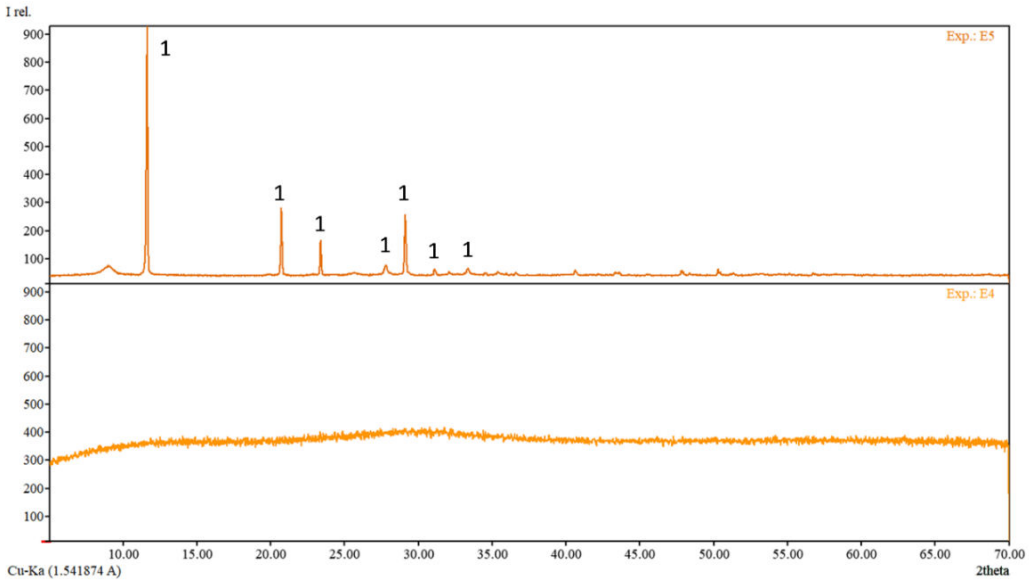

Fig. S3.10. *XRD pattern of the experiments using ES solution. Mineral phases identified in E5: Gypsum-$CaSO_4{\cdot}2H_2O$ (1). No mineral phases identified in E4.*

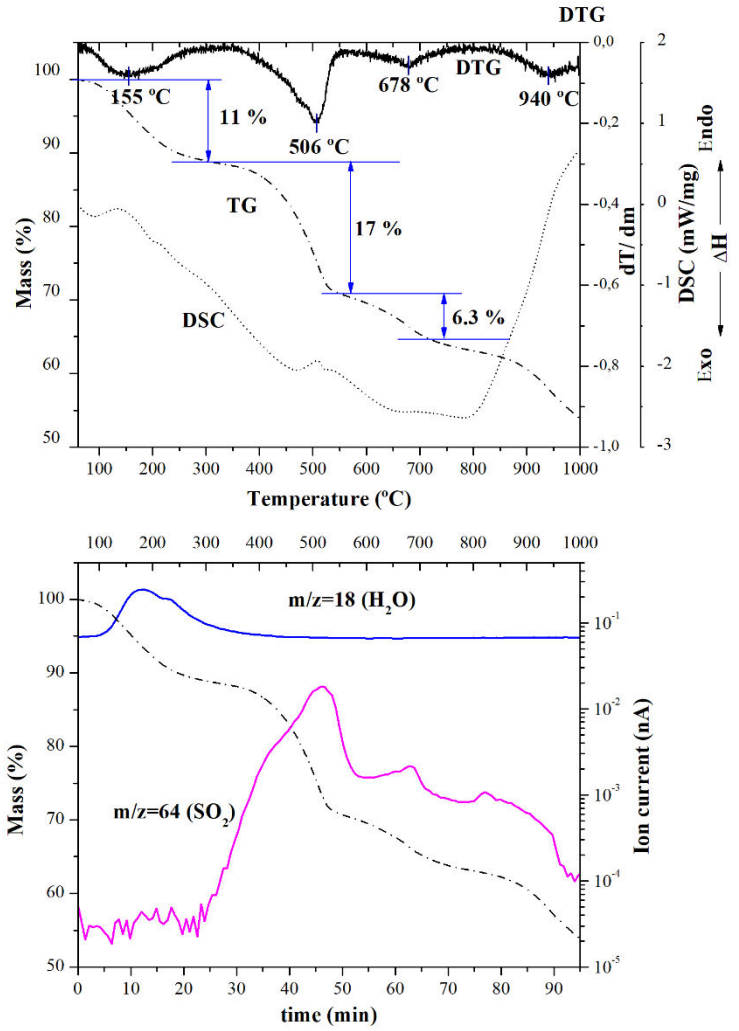

Fig. S3.11. *TG-DTG-DSC curve and gases detected in the precipitate obtained at the E4.*

ANNEX I.3. SUPPLEMENTARY MATERIAL OF SUBCHAPTER 3.3

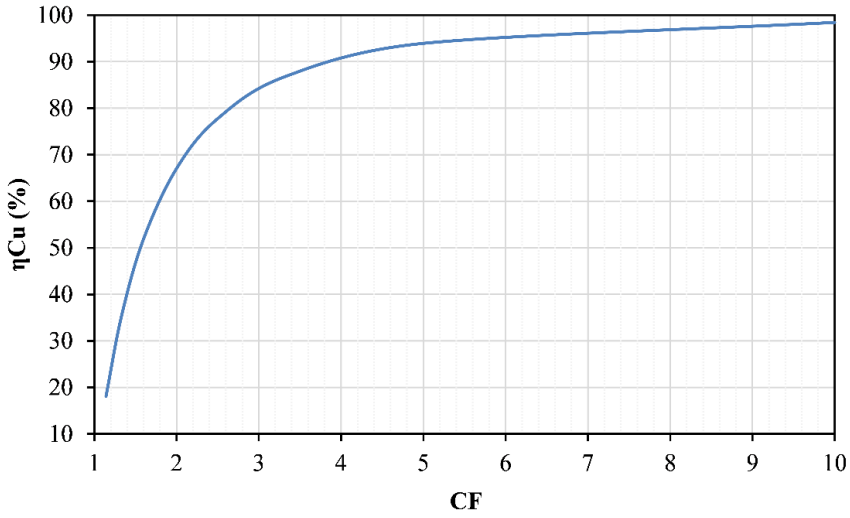

***Fig. S3.12**. Theoretical curve of copper recovery (%) as a function of the concentration factor.*

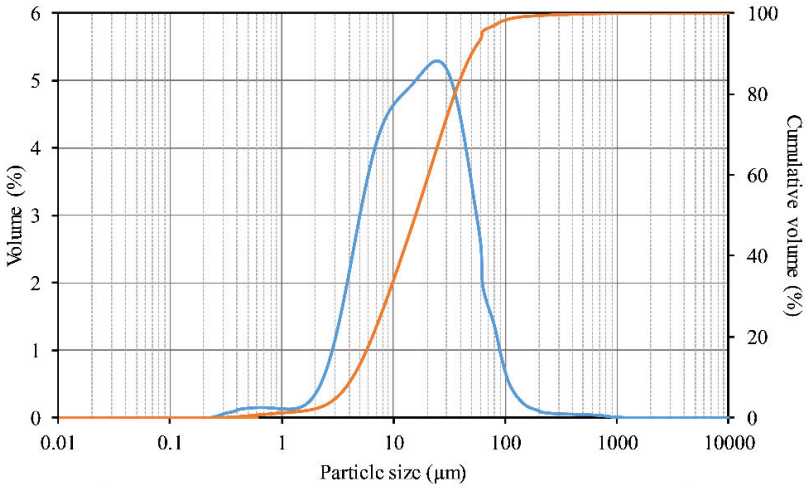

Type	Clay	Silt	Sand
ES (%)	8 ± 2	86 ± 6	6 ± 3

***Fig. S3.13.** Particle size distribution of the ES.*

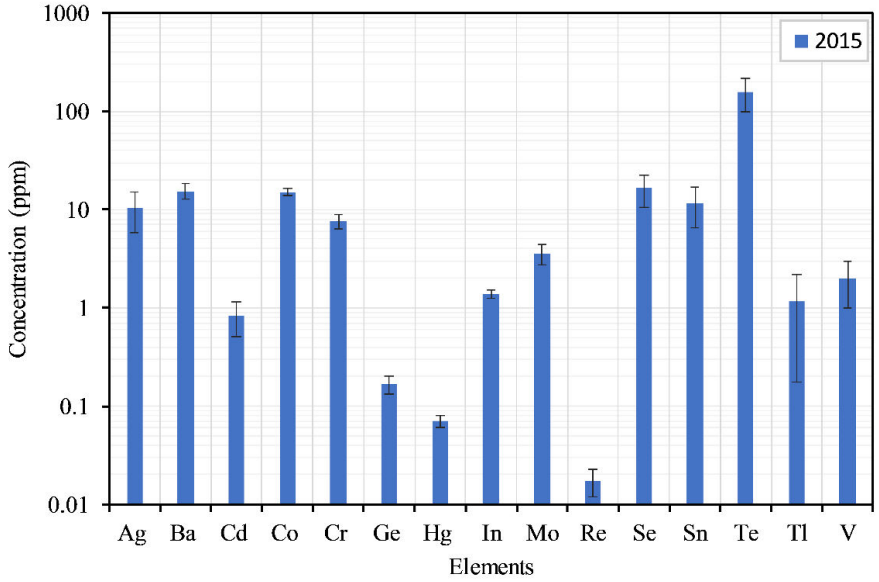

Fig. S3.14*. Trace elements in the ES. Standard uncertainty (1 σ) calculated as the standard deviation of the mean* $\boldsymbol{\sigma = S_x/(n)^{1/2}}$*, where "n=3" is the number of samples analysed.*

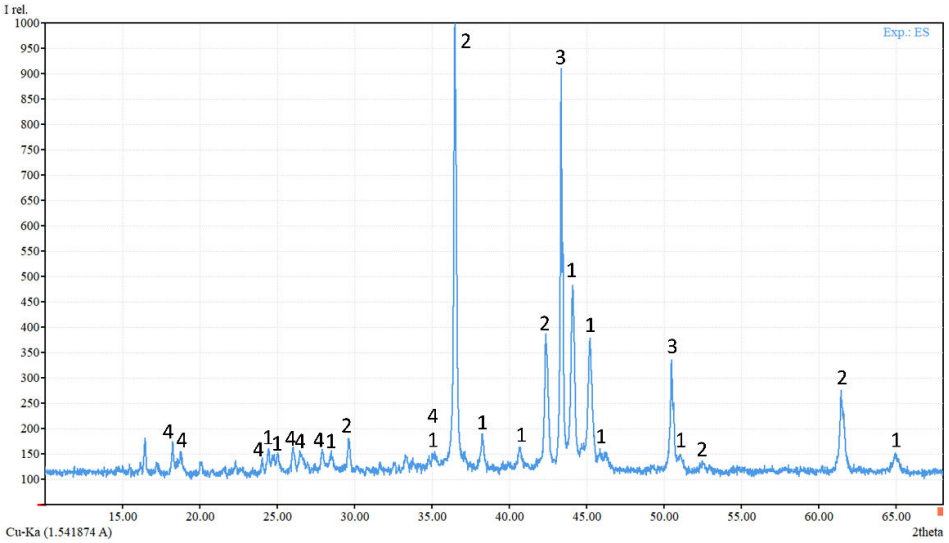

Fig. S3.15.*. X-ray diffraction (XRD) pattern of ES. Mineral phases identified: Domeykite-*Cu_3As *(1), Cuprite-*Cu_2O *(2), Copper metal-Cu (3) and Poitevinite-*$CuSO_4 \cdot H_2O$ *(4).*

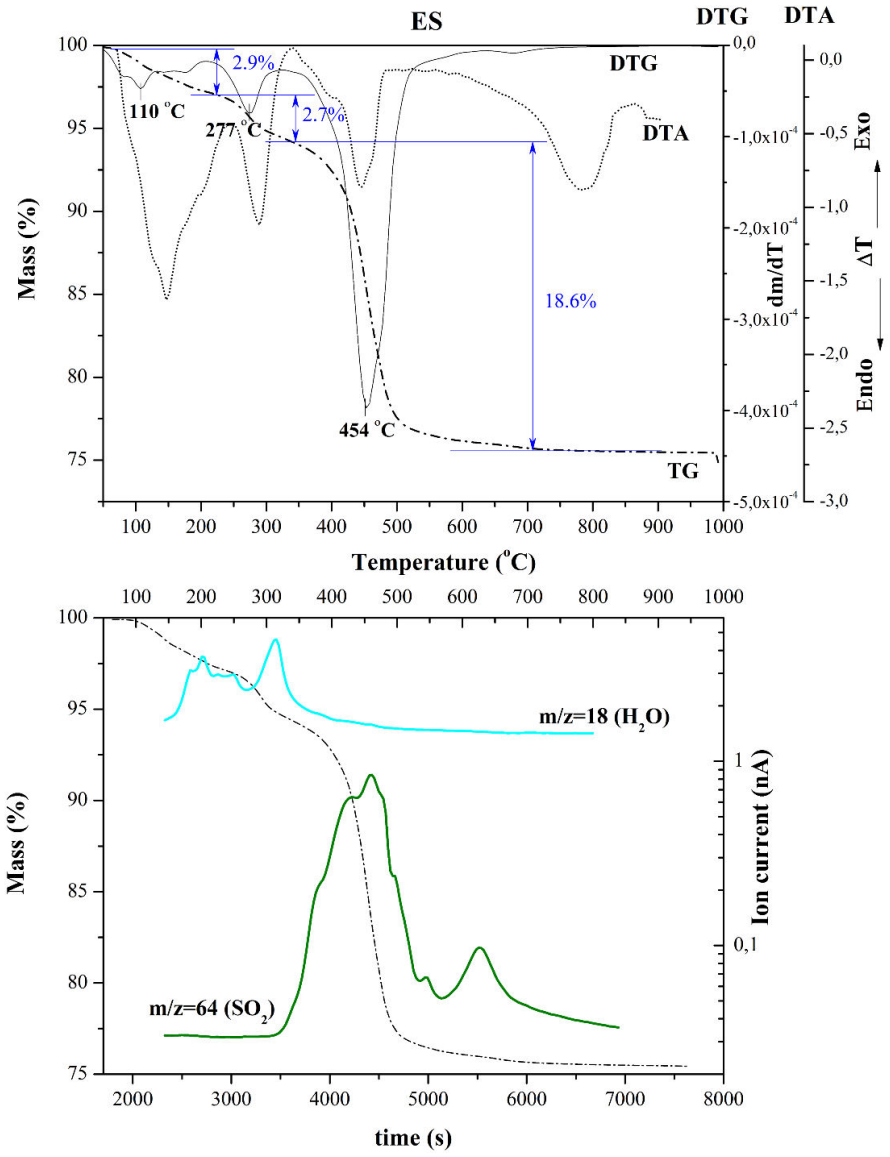

Fig. S3.16. *TG-DTG-DTA curve and gases detected in the ES.*

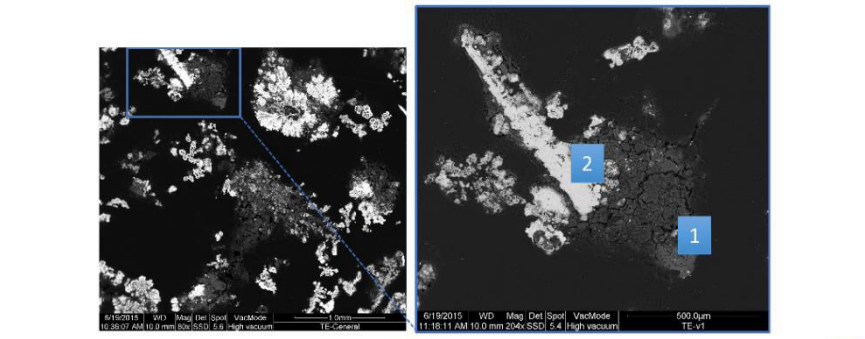

Elements	As	Cu	Fe	O	S	Si
Wt (%)	10	56	2.6	27	3.2	2.2

Fig. S3.17. *Scanning electron micrograph of ES general and specific particles. The table also shows the general composition determined by EDS from the image located at the top left.*

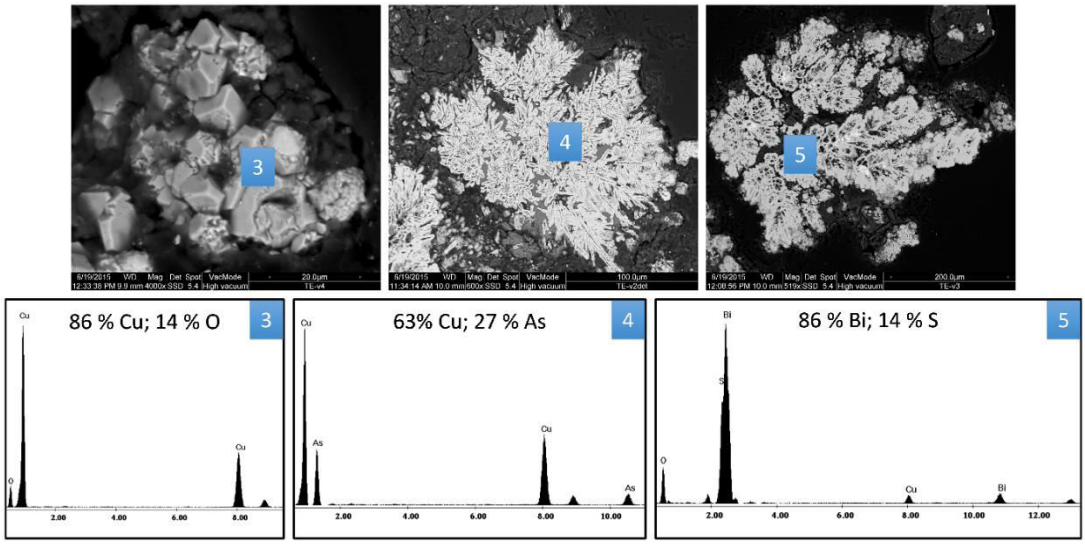

Fig. S3.18. *Scanning electron micrograph of ES specific particles.*

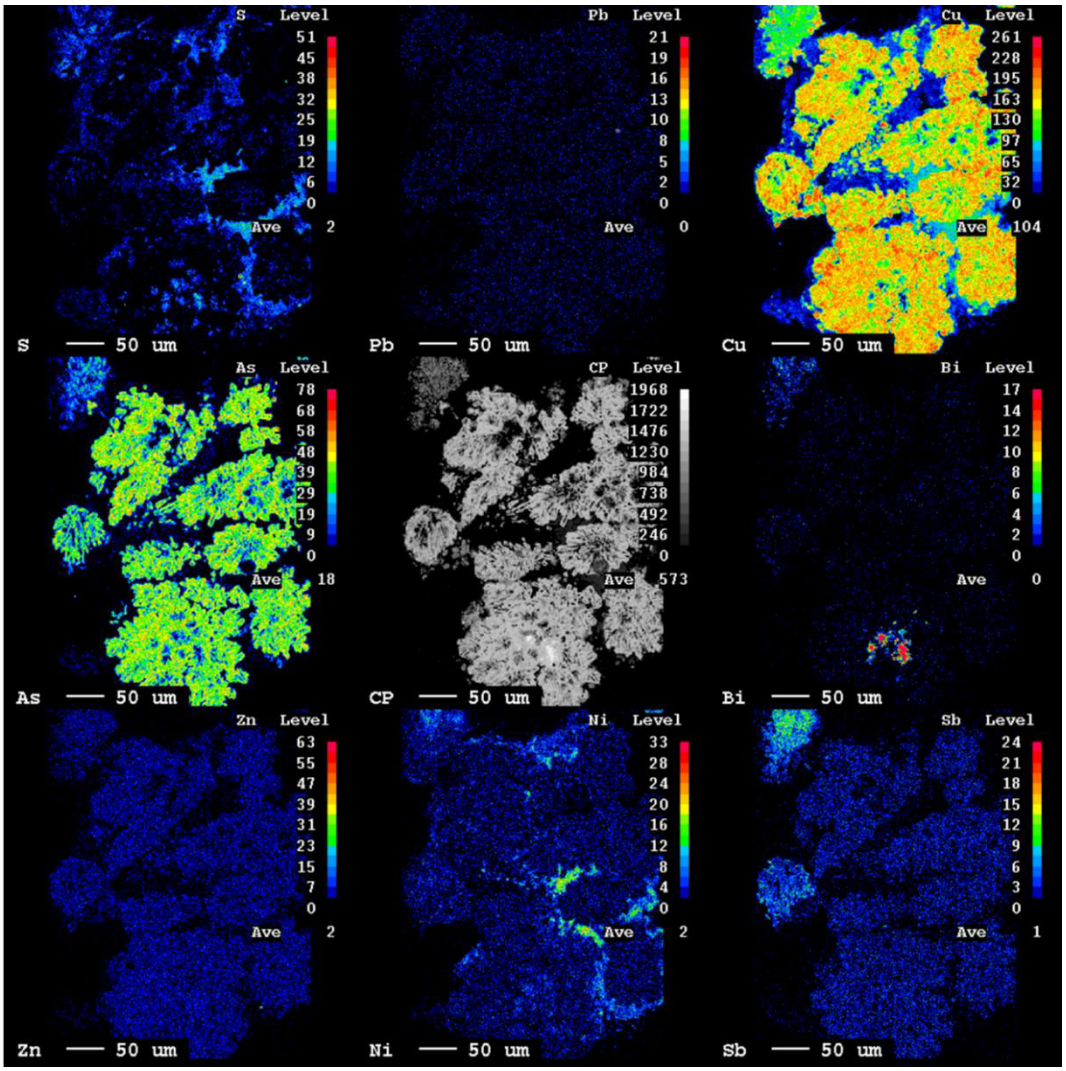

Fig. S3.19. *Secondary electron image of ES region and distribution of As, Bi, Cu, Ni, Pb, S, Sb and Zn.*

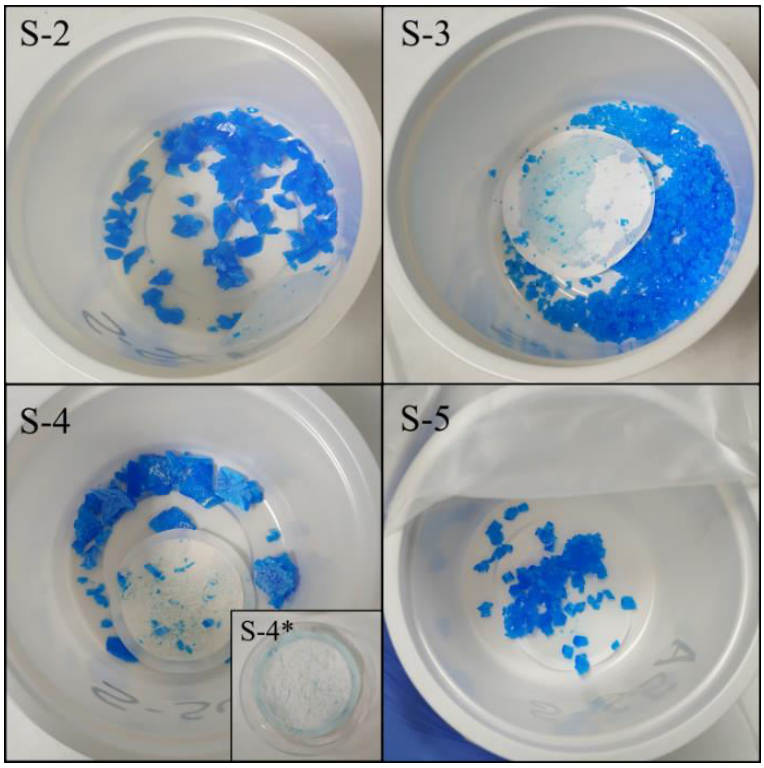

Fig. S3.20. *The solid precipitated in the sequential experiment.*

Fig. S3.21. *The solid precipitated in the non-sequential experiments.*

Size (µm)	Type	ES (%)		
		Average concentration	Cumulative	Global
<4	Clay	7.9 ± 2.1	7.9 ± 2.1	7.9 ± 2.1
4-8	Silt	17.2 ± 3.1	25.1 ± 3.8	85.9 ± 5.8
8-16		23.7 ± 2.8	48.8 ± 4.7	
16-32		26.0 ± 0.7	74.8 ± 4.7	
32-62		18.9 ± 3.9	93.7 ± 6.1	
62-125	Sand	5.2 ± 3.0	98.9 ± 6.8	6.3 ± 3.1
125-250		0.7 ± 0.7	99.6 ± 6.9	
250-500		0.3 ± 0.3	99.9 ± 6.9	
500-1000		0.1 ± 0.1	100.0 ± 6.9	
1000-2000		-	-	-

Table S3.6. *Average grain-size and cumulative distribution (% V) of the studied samples. Note: Standard uncertainty (1 σ) calculated as the standard deviation of the mean* $\sigma = S_x / (n)^{1/2}$*, where "n=3" is the number of samples analysed.*

			Major elements (g/L)			***Trace elements (ppm)***					
	Exp. ID	*V (mL)*	*As*	*Cu*	*S*	*Bi*	*Cr*	*Ni*	*Pb*	*Sb*	*Zn*
Sequential	S-5	52	8.2	15	97	720	< DL	430	20	330	16
No sequential	NS-1	60	6.6	38	56	330	< DL	180	19	190	7.0
	NS-2	50	7.5	28	56	360	< DL	210	22	220	8.1
	NS-3	30	2.5	9.2	35	260	< DL	150	17	120	6.3

Table S3.7. *Chemical composition of the final solutions in the copper recovery experiments. V (mL) is the final volume. Detection Limit (DL= 0.2 ppm).*

Impurities	$CuSO_4 \cdot 5H_2O$ Product-type 2 (≥ 99.9 %)
As	0.00017
Cd	0.00017
Ni	0.00033
Pb	0.001
Zn	0.0006

Table S3.8. *Impurity levels (%) in the copper sulphate pentahydrate for products-type 2 (BPC: Biocidal Product Committee, 2013).*

ANNEX I.4. SUPPLEMENTARY MATERIAL OF SUBCHAPTER 3.4

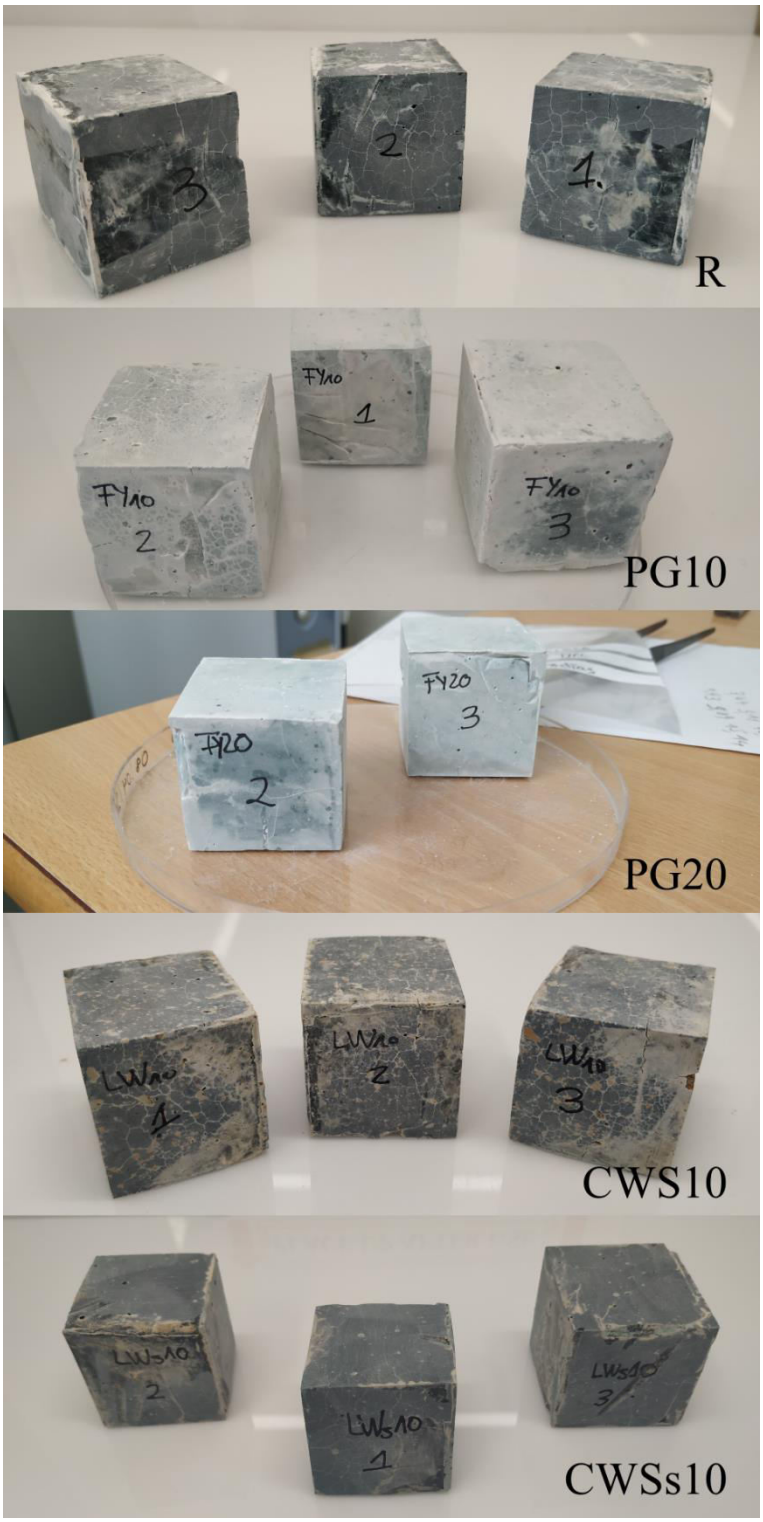

Fig. S3.22. *Paste specimens.*

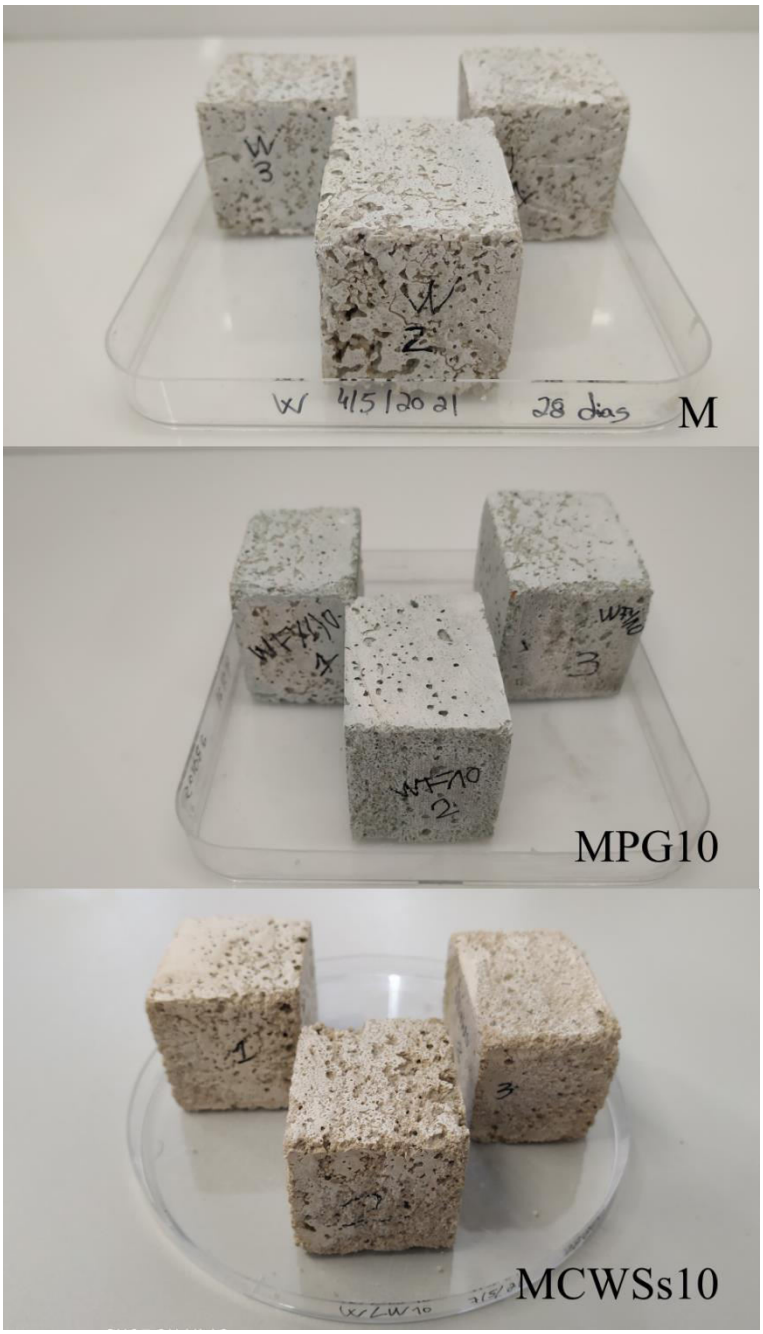

Fig. S3.23. *Mortar specimens.*

ANNEX II

PUBLICATIONS

Waste and Biomass Valorization (2021) 12:2739–2755
https://doi.org/10.1007/s12649-020-01197-w

ORIGINAL PAPER

Characterization of Two Sludges from a Pyrometallurgical Copper Smelting Complex for Designing a Se and Pb Recovery Proposal

D. C. Paz-Gómez[1] · S. M. Pérez-Moreno[1] · I. Ruiz-Oria[2] · G. Ríos[2] · J. P. Bolívar[1]

Received: 10 January 2020 / Accepted: 3 August 2020 / Published online: 13 August 2020
© Springer Nature B.V. 2020

Abstract

Gas scrubbing sludge (SS) and fine dust of converters (SC) are wastes generated in the off-gas cleaning system of smelting and converting processes. Both wastes are considered hazardous materials due to their high metal contents and leaching characteristics. The main purpose of this study was to gain essential knowledge on the recovery of valuable elements contained in these wastes. Thus, an exhaustive characterization was carried out to determine the composition, mineral phases, particle size, and leachability of both wastes (SS and SC) as a preliminary step to select the most appropriate applications and treatment for them. These wastes are composed of fine particles (~95% < 63 µm), mainly containing Pb (> 20%) as anglesite ($PbSO_4$), while SS presents a high concentration of Se (34%), which is mainly identified as metallic selenium. Therefore, these residues could be used as secondary sources of Pb and Se. The recovery of Se by roasting process and Pb recovery by hydrometallurgical route seem to be the best options for the management of these wastes.

Graphic Abstract

Keywords Converter dust · Gas scrubbing sludge · Selenium recovery · Copper smelting · Sludge characterization

Statement of Novelty

This study is new to Waste & Biomass Valorization, because it is the first time that these two wastes from copper smelting are deeply characterized and proposed a viable pathway for their valorization.

Electronic supplementary material The online version of this article (https://doi.org/10.1007/s12649-020-01197-w) contains supplementary material, which is available to authorized users.

✉ D. C. Paz-Gómez
daniela.paz@dci.uhu.es

[1] Department of Integrated Sciences. Center for Natural Resources, Health and Environment (RENSMA), University of Huelva, Huelva, Spain

[2] R&D Department, Atlantic Copper S.L.U, Huelva, Spain

Chemosphere 281 (2021) 130651

Contents lists available at ScienceDirect

Chemosphere

journal homepage: www.elsevier.com/locate/chemosphere

Arsenic removal procedure for the electrolyte from a hydro-pyrometallurgical complex

D.C. Paz-Gómez [a], S.M. Pérez-Moreno [a], M.J. Gázquez [b,*], J.L. Guerrero [a], I. Ruiz-Oria [c], G. Ríos [c], J.P. Bolívar [a]

[a] Department of Integrated Sciences, Research Centre on Natural Resources, Health and the Environment (RENSMA), University of Huelva, 21007, Huelva, Spain
[b] Department of Applied Physics, Marine Research Institute (INMAR), University of Cadiz, 11510, Cádiz, Spain
[c] Atlantic Copper S.L.U., 21001, Huelva, Spain

ARTICLE INFO

Handling Editor: Derek Muir

Keywords:
Electrolyte sludge
Ferric arsenate
Scorodite
Arsenic removal
Copper–arsenic solution

ABSTRACT

Commercial copper (Cu) is obtained by a hydro-pyrometallurgical process, where the Cu anodes obtained in the furnaces (Cu > 99.5%) are enriched up to 99.99% in "cathodes" by electrorefining at an electrolysis plant. During this process, some impurities accumulate in the electrolyte, mainly arsenic (As), which decrease the quality of the Cu cathode. For this reason, the electrolyte is sent to an electrolyte cleaning plant (ECP) for its purification. Electrolyte sludge (ES) is produced in the last stage of purification and is recirculated back to the furnace due to the high Cu content. This recirculation involves a severe problem of As accumulation in the industrial process. The objective of this work was to develop a procedure to fully dissolve the ES, removing the As and recovering its Cu content. The ES dissolution process was optimised (dissolution efficiency > 99%) in H_2SO_4 (1.4 M)/HNO_3 (1.8 M) medium using a 1:20 g mL^{-1} solid-to-liquid ratio. As was removed from the ES solution by its precipitation as iron (III) arsenate, with high efficiency (more than 70%). After As removal, the Cu can be precipitated as copper sulphate, which is used in several applications.

1. Introduction

The demand for copper (Cu) minerals has increased quickly over the last 50 years, and it is expected to keep growing due to the essential role of Cu in modern technologies. Worldwide refined Cu production reached 24 Mt in 2019, and it involves a large amount of waste and wastewater generation (ICSG, 2020). In recent decades, the manufacturing industry has tried to develop policies to reduce the environmental impact and to achieve sustained economic growth, following the current strategic lines aimed at ensuring the implementation and development of the "Circular Economy" through the efficient use of raw materials and residues. Therefore, policies on waste management must be directed apply the hierarchy established by normative: prevention, reduction, reuse, and recycle. A proper waste valorisation represents an excellent management alternative producing economic and environmental benefits. For this, industries have introduced effective resource management consisting of recycling, reusing, and valorisation of these ones, reducing the production cost and decreasing risks for the environment and human health (Khan et al, 2020, 2021, 2020; Liao et al., 2019).

Atlantic Copper S.L.U, located in Huelva (Spain), is one of the biggest manufacturers of ultrapure Cu cathodes (>99.99% Cu) in Europe, producing more than $3{\cdot}10^5$ t y^{-1} (Atlantic Copper, 2017). During Cu electrorefining, the concentrations of the raw material impurities, such as As, Sb, Bi, Ni, etc., gradually increase in the electrolyte, which negatively affects the quality of the Cu cathode; therefore, the impurities must be removed. For this, a fraction of the electrolyte is continuously sent to an electrolyte cleaning plant (ECP) to reduce the level of impurities, especially As, and to recover a significant fraction of the Cu that is not electrodeposited in the cathode ("decopperising").

The electrolyte cleaning process involves three stages by electrowinning in liberator cells (Artzer et al., 2018; Wesstrom and Araujo, 2012). Firstly, the Cu concentration is reduced from 45 g L^{-1} to 25 g L^{-1}, providing a B-grade Cu cathode (>99.97% Cu), which is commercialised. Secondly, the Cu concentration is further reduced to around 10 g L^{-1}. Finally, in the third step, the remaining Cu, and most of the As, is removed from the solution in the electrolyte sludge (ES). In the Huelva factory, about 1300 t of ES are produced annually. The final treated electrolyte is returned to the electrolyte tank for reuse.

* Corresponding author.
E-mail address: manuel.gazquez@dfa.uhu.es (M.J. Gázquez).

https://doi.org/10.1016/j.chemosphere.2021.130651
Received 10 December 2020; Received in revised form 7 April 2021; Accepted 21 April 2021
Available online 4 May 2021
0045-6535/© 2021 Elsevier Ltd. All rights reserved.

Hydrometallurgy 206 (2021) 105769

Contents lists available at ScienceDirect

Hydrometallurgy

journal homepage: www.elsevier.com/locate/hydromet

Copper recovery from sludges generated in the electrolyte treatment plant of a pyrometallurgical complex

D.C. Paz-Gómez [a,*], S.M. Pérez-Moreno [a], I. Ruiz-Oria [b], G. Ríos [b], J.P. Bolívar [a]

[a] Department of Integrated Sciences, Research Centre on Natural Resources, Health and the Environment (RENSMA), University of Huelva, 21007 Huelva, Spain
[b] Atlantic Copper S.L.U., 21001 Huelva, Spain

ARTICLE INFO

Keywords:
Electrolytic sludge
Characterization
Valorization
Copper recovery
Copper sulfate
Crystallization

ABSTRACT

Electrolytic sludge is generated in the last stage of the electrolyte decontamination treatment plant in the manufacture of cathodic copper (> 99.99 % Cu). Currently, this sludge is recycled back to the process due to the high concentration of copper, although its recirculation involves a serious problem of arsenic accumulation in the industrial process. This negatively affects the quality of commercial copper. Therefore, the main focus of this study was the recovery of copper contained in the electrolyte sludge as copper (II) sulfate pentahydrate ($CuSO_4 \cdot 5H_2O$) for its return to the industrial process and/or commercialization. The remaining waste, which contains mainly As and other toxic chemical species, were eliminated in a controlled repository. To this end, an exhaustive characterization of the electrolytic sludge was performed to determine its chemical composition, mineral phases, and particle size. The main results indicated that the sludge was composed of very fine particles (~ 99 % < 100 μm), containing mostly Cu (~ 54 %) (Cu_3As, Cu_2O, Cu and $CuSO_4 \cdot xH_2O$), As (~ 10 % as Cu_3As) and S (~ 7 % as $CuSO_4 \cdot xH_2O$). More than 90 % of the Cu contained in the sludge was recovered as very pure copper sulfate (≥ 99.5 %) by an evaporative crystallization process. In addition, around 70 % of the As was removed in the process as a solid (> 99 % in As_2O_3). The rest of pollutants remained in the final solution, which ultimately will be treated in the liquid effluent treatment plant. Therefore, valorization of the electrolytic sludge was achieved by copper recovery as $CuSO_4 \cdot 5H_2O$ using evaporative crystallization; this process was an effective way for both recovering Cu and removing the As contained in the electrolytic sludge generated in the electrolyte treatment plant.

1. Introduction

The growth of global copper demand has increased quickly over the last 50 years, and the same trend is expected for the future. Copper is employed in a wide range of applications, mainly due to its unique electricity conducting properties, which makes it difficult to replace. It will be crucial for future society, given the expected increase of copper-intensive low-carbon energy and electrification of transport technologies. World refined copper production reached about 23.5 million tonnes in 2017 (ICSC: International Copper Study Group, 2018). This is associated with a large amount of solid waste and wastewater generation. The decrease in the ore grades also intensifies energy use. Thus, copper production has a huge environmental impact (Csavina et al., 2014; Dong et al., 2020a; Pérez-Moreno et al., 2018). In the last decades, the industry has tried to achieve a circular economy by recycling, reusing, and valorizing wastes, reducing disposal costs and avoiding risks for the environment and human health (EEA: European Environment Agency, 2017; European Commission, 2015; Liao et al., 2019).

Atlantic Copper SLU, one of the biggest manufacturers of cathodic copper in Europe, is located in Huelva (Spain). This company reduces its waste as much as possible. This company produces around $2.9 \cdot 10^5$ t/y of ultrapure copper (> 99.99 % Cu), and they manage several co-products, intermediate materials, and wastes.

A copper concentrate (~ 30 % Cu) is used as the raw material. This is first smelted in a Flash Smelting Furnace (FSF) to be converted into matte (64 % Cu). It is then oxidized in the Converter Furnaces (CF) to obtain blister copper (> 99 % Cu). The slag from these furnaces is treated in an Electric Furnace (EF), giving a very inert slag that is mainly composed of iron silicates (< 1% Cu), which is used in many civil engineering applications (road bases, concrete, etc.). Finally, the blister copper is introduced into the Refining Furnaces (RF), obtaining copper anodes (99.6 % Cu, 3.3•105 t/y), which are converted to commercial

* Corresponding author.
E-mail address: daniela.paz@dci.uhu.es (D.C. Paz-Gómez).

https://doi.org/10.1016/j.hydromet.2021.105769
Received 1 November 2020; Received in revised form 10 October 2021; Accepted 14 October 2021
Available online 19 October 2021
0304-386X/© 2021 Elsevier B.V. All rights reserved.